UNIVERSITÄT HAMBURG

DISSERTATION WITH THE AIM OF ACHIEVING A DOCTORAL
DEGREE AT THE FACULTY OF MATHEMATICS, INFORMATICS AND
NATURAL SCIENCES

Departement of Physics

Mitochondrial networks

Daniel Mellem

Beiersdorf AG

Institut für Nanostruktur- und Festkörperphysik

August 9, 2017

Declaration of Authorship

I hereby declare, on oath, that I have written the present dissertation by my own and have not used other than the acknowledged resources and aids.

Signed:

_____

Date:

_____

Erstgutachter der Dissertation

Prof. Dr. Michael A. Rübhausen

Zweitgutachter der Dissertation

Dr. Frank Fischer

Disputation - 29.09.2016

Vorsitzende des Prüfungsausschusses

Prof. Dr. Daniela Pfannkuche

Gutachter der Disputation

Prof. Dr. Arwen Pearson, Prof. Dr. Nils Huse

"Weil, man kann zwar nicht ewig die Luft anhalten. Aber doch ziemlich lange."

Tschick (Wolfgang Herrndorf)

Abstract

Mitochondria produce the molecule adenosine triphosphate (ATP), in order to supply different cell functions with energy. In the cytoplasm of eukaryotic cells they form a highly dynamic network. In this theses, the behavior of the mitochondrial network within the energy demanding structure of cells was investigated.

Biological processes, such as networking, recycling, oxidative stress and repair mechanisms act on mitochondria and alter their qualities in terms of the integrity of their DNA, their metabolic supply and their ability to produce ATP. A biophysical model was created, that simulates mitochondrial qualities represented by virtual quality states in a discrete-time Markov chain. Simulations show an increase of isolated, damaged mitochondria during the aging of the cell. The coupling of networking processes and recycling helps mitochondria to establish high qualities. A decreasing repair ability of mitochondria during cell aging drives the recycling process and helps to sustain mitochondrial qualities.

A spatially resolved model combines the qualitative behavior of mitochondria with morphological alterations depending on the energy demand of the cell. Consumers of ATP are modeled as oscillating Mie potentials, determining the mitochondrial network structure over time. In simulations, the morphological and qualitative parameters of the mitochondrial network couple to the global energy states of the cell. During phases of high energy demands mitochondrial structures condensate around the cell's nucleus. Increases of mitochondrial masses and mitochondrial velocities lead to growing mitochondrial qualities. During the aging of the cell the mitochondrial network fragments.

The mitochondrial network was investigated experimentally in keratinocytes in the epidermis of volunteers via in-vivo measurements with multiphoton microscopy. Both, the comparison of mitochondrial structures in the stratum granulosum of a young and an old age group and the differentiation process of keratinocytes during the epidermal turnover reveal a fragmentation of the mitochondrial network.

Zusammenfassung

Mitochondrien produzieren das Molekül Adenosintriphosphat (ATP), um die Zelle mit Energie zu versorgen. Im Zytoplasma von eukaryotischen Zellen bilden sie ein dynamisches Netzwerk. In dieser Doktorarbeit wurde das Verhalten des mitochondrialen Netzwerks in der energetischen Struktur der Zelle untersucht.

Biologische Prozesse, wie das Netzwerken, das Recycling, oxidativer Stress und Reparaturmechanismen wirken auf Mitochondrien und ändern ihre Qualitäten in Bezug auf die Integrität ihrer DNA, ihre Versorgung mit Metaboliten und ihre Fähigkeit ATP zu produzieren. Ein biophysikalisches Modell wurde entwickelt, das mitochondriale Qualitäten über die Zeit als virtuelle Zustände einer diskreten Markov-Kette simuliert. In Simulationen zeigt sich eine Zunahme geschädigter Mitochondrien während der Zellalterung. In der Kopplung von Netzwerkprozessen und Recycling offenbart sich ein qualitätssteigernder Mechanismus. Die sinkende Reparaturfähigkeit von Mitochondrien während der Zellalterung fördert das Recycling und sorgt so für einen Qualitätserhalt in gealterten Zellen.

Ein ortsaufgelöstes Modell kombiniert das qualitative Verhalten von Mitochondrien mit morphologischen Änderungen in Abhängigkeit von der energetischen Struktur der Zelle. Verbraucher von Adenosintriphosphat werden als oszillierende Mie-Potentiale modelliert, innerhalb derer Mitochondrien ihre Netzwerkstruktur anpassen. In Simulationen koppeln die morphologischen und qualitativen Parameter des mitochondrialen Netzwerks an die globalen Energiezustände der Zelle. In Phasen hohen Energiebedarfs kondensieren mitochondriale Strukturen um den Zellkern. Die Erhöhung mitochondrialer Massen und Geschwindigkeiten führen zu einer Steigerung mitochondrialer Qualitäten. Während der Zellalterung zeigt sich eine Fragmentierung des mitochondrialen Netzwerks.

Das mitochondriale Netzwerk wurde experimentell in den Keratinozyten der Epidermis von Probanden mit Hilfe von Multiphotonenmikroskopie untersucht. Sowohl im Vergleich mitochondrialer Strukturen im Stratum Granulosum einer jungen und einer alten Alterskohorte als auch im Differenzierungsprozess der Keratinozyten während des epidermalen Turnovers zeigt sich die Fragmentierung des mitochondrialen Netzwerks.

Contents

List of Figures

List of Tables

Chapter 1

Introduction

Skin is one of the most sophisticated organs of the human body. In order to protect the internal environment, it serves as a barrier against the penetration of germs and ultraviolet (UV) radiation of the sun and provides immune surveillance. It prevents the loss of proteins, fluids or electrolytes, helps to establish a homeostatic regulation of the body and maintains its average temperature. Furthermore, it enables sensual perception. However, extrinsic influences as e.g. air pollution, smoking, UV radiation and internal factors such as hormonal changes and oxidative stress make the skin age. [1] In order to engage against these aging processes, skin is treated with cosmetic products. Examples are given by fighting the free radicals produced by oxidative stress due to UV radiation with antioxidants. [2]

Keratinocytes are a very important cell type in skin, as they form its most outer layer, the epidermis. The epidermis consists of four sublayers, that are constantly regenerated. In the deepest layer, the stratum basale, stem cells generate new keratinocytes. Subsequently, cells move to the upper layers, the stratum spinosum and the stratum granulosum, and perform a differentiation process. At the outermost layer, the stratum corneum, keratinocytes finally transform to corneocytes, which build an effective barrier against the penetration of germs and other substances and prevent the loss of water by evaporation. [3]

Keratinocytes rely on a sufficient amount of energy in form of the molecule adenosintriphosphate (ATP) in order to perform the various processes of differentiation. [4] One possibility of cells to produce ATP molecules are glycolytic procedures. In these processes, two ATP molecules are gained out of a single glucose molecule uptaken by diet. A more efficient way for the cell to produce ATP molecules is oxidative phosphorylation. It transforms the pyruvate molecules, that are side products of glycolysis, to acetyl-CoA.

The energy of this molecule is released during the Krebs cycle and the respiratory chain in order to gain 32 ATP molecules in total. The process of oxidative phosphorylation takes place within mitochondria. Mitochondria are mobile organelles in the cytoplasm of a cell, that have their own genotype. [5] Many cell types, such as fibroblasts, neurons and keratinocytes possess hundreds of mitochondria. [6] Mitochondria do not remain at fixed positions in the cell, but move within the cytoplasm [7] and fuse and divide to form a dynamic, interconnected network. [8] By this means, mitochondria are able to exchange metabolites among each other, that are necessary for the production of ATP. [9] Furthermore, they compensate for each others failures in their mitochondrial DNA sequences [10], which are used to produce enzymes and proteins involved in Krebs cycle and respiratory chain.

A treatment of the cells by actives, that improve mitochondrial behavior could help to strengthen the production of ATP and control the production of oxidative stress that harms the mitochondrial DNA. [11] Since the loss of mitochondrial integrity is connected to the aging of cells [12], actives that treat mitochondria could fight aging issues.

However, so far the various dynamics of the mitochondrial network are not yet fully understood. In this thesis, morphological and qualitative characteristics of mitochondrial networks are investigated by creating biophysical, computational models and by experimentally examining mitochondrial networks in vivo.

In chapter 2, a computational model is presented, that simulates mitochondrial qualities over time. In a probabilistic approach, mitochondrial qualities q are discrete values in a Markov chain. A mitochondrion establishes every quality q with a certain probability. These probabilities change their value depending on biological processes acting on mitochondria. By changing the probability of these processes over time, an aging procedure is included in the model. Thus, the change of mitochondrial qualities during aging is simulated and corresponding quality saving mechanisms of the mitochondrial network are disclosed.

A second biophysical, computational model including mitochondrial morphologies is introduced in chapter 3. There, small mitochondrial units move within a two-dimensional virtual cell and connect with each other by inelastic collisions. As a result, mitochondria form complex network structures. Additionally, quality parameters for the health of the mitochondrial DNA and the supply with metabolites are included. The quality parameters change upon fusion and fission procedures and biologicial processes. Thus, the model allows to correlate mitochondrial qualities with mitochondrial morphologies. In a further step, ATP consumers within the virtual cell representing energy consuming

organelles and other cell functions are modeled by Mie potentials. This opens up the possibility to not only investigate the internal dynamics among mitochondria but also the interaction between the mitochondrial network and the energy demands of the cell.

In chapter 4, multiphoton microscopy is utilized to image the mitochondrial network experimentally in vivo in the epidermis. Excitation of the autofluorescence of the coenzyme nicotinamide adenine dinucleotide (NADH) within mitochondrial clusters with femtosecond laser pulses allows to visualize the morphologies of mitochondrial networks in keratinocytes of volunteers' skin. Studies on mitochondrial morphologies during epidermal differentiation of keratinocytes and differences between mitochondrial networks of young and old volunteers are performed.

Chapter 2

Mitochondrial Quality Model

A computational model was created, in order to interpret the behavior of mitochondrial qualities during cell aging. The model presented in this chapter simulates mitochondrial qualities under the influence of various biological processes acting on mitochondria over time. The biological processes include mitochondrial networking, mitochondrial recycling, the production of ATP, oxidative stress by external factors and repair mechanisms.

2.1   Master Equation

The quality of a mitochondrion depends on different aspects such as a sufficient supply with metabolites as ADP [13], the integrity of the mitochondrial DNA (mtDNA) [14, 15] or the health of protein complexes in the electron transport chain. [16] In the mitochondrial quality model, all these factors are merged into one quality parameter q. [17] The quality q is a discrete value between a minimum quality of $q_{min} = 0$ and a maximum quality of $q_{max} = Q$. Mitochondria with $q = 0$ are considered to be inactive. They are drastically harmed and carry an insufficient amount of metabolites and enzymes. In contrast, qualities $q = Q$ represent completely healthy mitochondria, saturated with metabolites and equipped with an error-free mtDNA.

The system of whole-numbered quality states is modeled as a discrete-time Markov chain, in which a mitochondrion exhibits each quality state with a certain probability. The presented model simulates the change of the probabilities for all quality states q over time, depending on all biological processes that act on mitochondrial qualities (Figure 2.1). Consequently, a probability distribution $P(q, t)$ between $q_{min} = 0$ and $q_{max} = Q$ is formed. The corresponding master equation (2.1) describes the time-dependent change of this distribution:

$$\frac{\partial}{\partial t}P(q,t) = \sum_{q \neq q'}(R_{q'q}P(q',t) - R_{qq'}P(q,t)) \tag{2.1}$$

In formula 2.1, all elements R_{ij} of matrix $\mathbf{R}$ represent specific rates with which distinct biological processes alter probabilities P of quality states q and q' over time t. While $R_{q'q} \in \mathbf{R}$ derives the probabilistic gain of quality state q from all other quality states q', the rate $R_{qq'} \in \mathbf{R}$ takes into account the probabilistic losses from q to q'.

During all points in time the overall probability of the quality chain is conserved and normalized:

$$N_{\mathrm{prob}} = \sum_{q=0}^{Q} P(q,t) = 1 \tag{2.2}$$

2.2 Model Design

To date, interconnections between biological processes acting on mitochondrial qualities are not yet fully experimentally investigated. Hence, the master equation (2.1) is modeled without any coupling of the rates R_{ij}, but is intended to be a superposition of the individual impacts of all biological processes included:

$$\frac{\partial}{\partial t}P(q,t) = \frac{\partial}{\partial t}P_{\mathrm{FF}}(q,t) + \frac{\partial}{\partial t}P_{\mathrm{MB}}(q,t) + \frac{\partial}{\partial t}P_{\mathrm{REP}}(q,t) + \frac{\partial}{\partial t}P_{\mathrm{EC}}(q,t) + \frac{\partial}{\partial t}P_{\mathrm{ED}}(q,t) \tag{2.3}$$

In formula (2.3), each term on the right-hand side of the differential equation represents the contribution of one single biological process on the probability distribution $P(q,t)$. Biological processes involve the networking dynamics of mitochondrial fission and fusion (FF) [8], the recycling procedure of mitophagy and biogenesis (MB) [18, 19], the ability of mitochondria to repair failures in mtDNA sequences and reproduce proteins and enzymes (REP) [20], the quality loss due to energy consumption of cell functions (EC) [21, 22], and the oxidative stress produced by other cell organelles (ED). [23]

During aging, biological processes change their frequency of occurrence. In the model, this is taken into account by introducing individual process probabilities $\rho_i(t)$, that either increase or decrease over time depending on the effect of aging on the biological process. As many biological procedures depend on the number of enzymes, proteins or other molecules involved as, e.g., in drug usage [24], the time-dependence of each biological processes is modeled by a homogeneous differential equation of first order,

FIGURE 2.1: Mitochondrial processes as discrete-state Markov chain
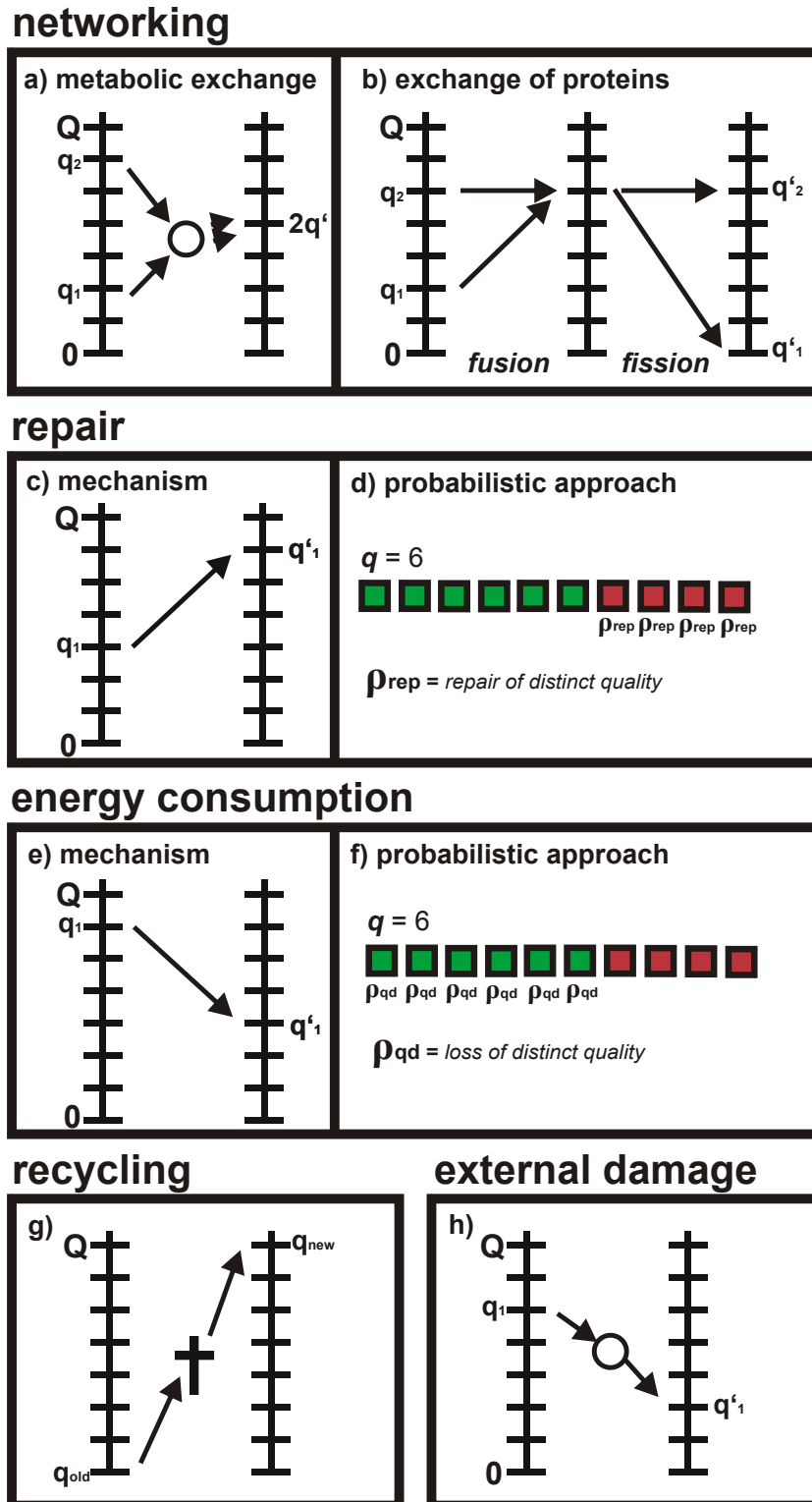
Networking is divided in to a metabolic (a) and an inner membrane (b) part. Modeling of mitochondrial repair ((c) and (d)) and energy consumption ((e) and (f)) follows an approach, in which every quality q is gained and lost with the same probability ρ_{rep} and ρ_{qd}, respectively. In (d) and (f) red squares represent lost qualities, green squares stand for existing qualities. In (g) and (h) the schemes of recycling and external damage are depicted.

$$A_i = \pm \frac{dN_i}{dt}, \tag{2.4}$$

with N_i being the number of particles involved and $A_i = \lambda_i N_i$ being the activity of the corresponding process i. Here, λ_i is a constant for normalization between particle numbers N and activity A_i. By solving differential equation (2.4) with an exponential function, the change of the frequency of a biological process during aging is either modeled by a decay or by a growth law depending on the underlying physiology:

$$\rho_\mathrm{i}(t) = \rho_{0,\mathrm{i}} \cdot \exp(\pm \frac{t}{\tau_\mathrm{i}}), \tag{2.5}$$

Here, $\rho_\mathrm{i}(t) = c \cdot N_i(t)$ is the probability of the corresponding process at a specific point in time and $\rho_{0,\mathrm{i}} = c \cdot N_{0,i}$ is the probability of the process at the beginning of the simulation, with c being a constant for normalization between probabilities and particle numbers. By altering the starting probabilities $\rho_{0,\mathrm{i}}$, the magnitude of the influence of biological processes on the quality distribution $P(q,t)$ can be weighted relatively to each other. The lifetime $\tau_i = 1/\lambda_i$ represents the degree of change of a biological process during cell aging. The higher the value of τ_i, the slower alters the probability $\rho_i(t)$ of a biological process over time.

The biophysical definitions of all processes acting on mitochondria during the aging of the cell are presented in the following.

2.2.1 Biological Processes

2.2.1.1 Networking

The morphological shape of the mitochondrial network alters dynamically over time due to ongoing fission and fusion processes among mitochondrial clusters. [8] Mitochondria merge their outer membrane in order to exchange unattached substances such as metabolites and enzymes [9] or, additionally, connect their inner mitochondrial membrane to share mtDNA sequences. [10] Consequently, the impact of mitochondrial networking on the probability distribution is separated into an outer membrane and an inner membrane part:

$$\frac{\partial}{\partial t} P_{\mathrm{FF}}(q,t) = \frac{\partial}{\partial t} P_{\mathrm{FF}_{\mathrm{outer}}}(q,t) + \gamma \cdot \frac{\partial}{\partial t} P_{\mathrm{FF}_{\mathrm{inner}}}(q,t) \tag{2.6}$$

As, so far, there is no experimental evidence if one of both fusion processes occurs more frequently than the other, the proportion parameter is assumed to be $\gamma = 1$ according

to Laplace's principle of indifference. [25]

In case of a metabolic exchange (Figure 2.1a) by merging only the outer mitochondrial membrane, the following assumptions are made in the model:

- The exchange of metabolites does not gain any total quality, but redistributes unattached substances between involved mitochondria. This leads to the following conservation law: $q_1 + q_2 = q_1' + q_2'$, where q_1 and q_2 represent mitochondrial qualities before and q_1' and q_2' after the process.

- Due to entropic considerations, redistribution of qualities leads to two mitochondria of the same quality after the fusion event: $q_1' = q_2'$. If the sum of qualities is uneven, the redistribution leads to $q_1' = q_2' + 1$, with the first assumption still being fulfilled.

The model's mathematical definition of fusion processes involving also the inner mitochondrial membrane (Figure 2.1b) relies on the following experimental insights and biophysical ideas:

- While fusion events involving the outer mitochondrial membrane experimentally appear as fast "kiss-and-run" patterns, fusion of inner membrane parts endures for longer periods of time. [9] Therefore, networking processes involving the inner mitochondrial membrane are separated into two terms representing a single fission and a single fusion process.

- Experiments revealed, that fusing inner membrane parts enables mitochondria to utilize the mtDNA sequences [10] of their fusion partner. So far, there is no evidence, in which capacity mitochondria benefit from each other during this process. In the framework of the model the daughter mitochondrion with the lower quality level is raised to the quality level of its partner. Thus, fusion of inner membrane parts is a quality gaining process: $q_1 + q_2 \rightarrow 2 \cdot q_1$, with $q_1 \geq q_2$

- Recent research discovered, that a fission process constitutes one daughter mitochondrion keeping its mitochondrial membrane potential, while the other daughter mitochondrion becomes metabolically inactive. [18] Thus, in the model, a fission process produces a mitochondrion with a quality of 0 and a mitochondrion with the quality prior to the fission process: $2 \cdot q_1 \rightarrow q_1 + 0_2$

With these rules, the change of the quality distribution by outer membrane fusion of mitochondria $\frac{\partial}{\partial t} P_{\mathrm{FF_{outer}}}(q, t)$ and the quality gain by merging the inner membrane $\frac{\partial}{\partial t} P_{\mathrm{FF_{inner}}}(q, t)$ read as:

$$\frac{\partial}{\partial t} P_{\text{FF}_{\text{outer}}}(q,t) = \rho_{\text{Fus}}(t) \cdot \sum_{q_1,q_2>0}^{Q} P(q_1,t)P(q_2,t)R_{\text{Fus}}(\|q_1 - q_2\|,t) \cdot$$
$$\delta_{(q_1+q_2),(q_1'+q_2')}\delta_{q_1',q_2'}(\delta_{q,q_1'} + \delta_{q,q_2'} - \delta_{q,q_1} - \delta_{q,q_2}) \tag{2.7}$$

and

$$\frac{\partial}{\partial t} P_{\text{FF}_{\text{inner}}}(q,t) = \rho_{\text{Fus}}(t) \cdot \sum_{q_1,q_2>0}^{Q} P(q_1,t)P(q_2,t)R_{\text{Fus}}(\|q_1 - q_2\|,t) \cdot$$
$$\delta_{q_1,q_1'}\delta_{q_1',q_2'}(\delta_{q,q_2'} - \delta_{q,q_2}) +$$
$$\rho_{\text{Fis}}(t) \cdot \sum_{q_1,q_2>0}^{Q} P(q_1,t)P(q_2,t)R_{\text{Fis}}(\|Q - q_2\|,t) \cdot$$
$$\delta_{q_1,q_2}\delta_{q_1,q_1'}\delta_{q_2',0}(\delta_{q,0} - \delta_{q,q_2}) \tag{2.8}$$

Here, all δ_{ij} act as Kronecker's delta. The terms $\rho_{\text{Fus}}(t)$ and $\rho_{\text{Fis}}(t)$ represent the general time-dependent probabilities of fission and fusion processes, respectively. The rates R_{Fus} and R_{Fis} indicate the probabilities of two mitochondria of different qualities, q_1 and q_2, to perform networking procedures. These rates are modeled with Hill's equation, that describes the biochemical binding of a ligand to a macromolecule. [26] Due to the lack of experimental insights, it is assumed, that the probability of a fusion process increases with the discrepancy between the qualities of involved mitochondria in order to apply a more effective redistribution of metabolites at the outer membrane and a stronger quality gain at the inner membrane:

$$R_{\text{Fus}}(\|q_1 - q_2\|,t) = \frac{\|q_1 - q_2\|^{\text{FF}_1}}{\text{FF}_2^{\text{FF}_1} + \|q_1 - q_2\|^{\text{FF}_1}} \tag{2.9}$$

On the contrary, with decreasing qualities, a fission process becomes more likely:

$$R_{\text{Fis}}(\|q_1 - q_2\|,t) = \frac{\|Q - q_1\|^{\text{FF1}}}{\text{FF2}^{\text{FF1}} + \|Q - q_1\|^{\text{FF1}}} \tag{2.10}$$

In both equations, the Hill coefficients FF1 and FF2 are considered to be free parameters. During the aging of the cell, networking dynamics among mitochondria are disturbed. [27] For that reason, the probability of a fusion process over time is modeled as a decay law. In contrast, the fission process over time is represented by a growth law. Hence, the alterations over time of probabilities of fission and fusion read as

$$\rho_{\mathrm{Fus}}(t) = \rho_{0,\mathrm{FF_m}} \cdot \exp(-\frac{t}{\tau_{\mathrm{FF_m}}}) \tag{2.11}$$

and

$$\rho_{\mathrm{Fis}}(t) = \rho_{0,\mathrm{FF_m}} \cdot \exp(+\frac{t}{\tau_{\mathrm{FF_m}}}) \tag{2.12}$$

The parameter $\rho_{0,\mathrm{FF_m}}$ represents the starting probability of networking processes in the model, $\tau_{\mathrm{FF_m}}$ the corresponding lifetimes.

2.2.1.2 Recycling

Aggressively harmed mitochondria in terms of many failures in mitochondrial DNA sequences and broken matrix protein complexes are removed from the cell by mitophagy. [18] In order to keep the mitochondrial mass at a constant level, after autophagic processes biogenesis substitutes removed mitochondria by producing fresh mitochondria of high qualities. [19] In the model, these procedures are taken into account by including a recycling mechanism. As primarily metabolically inactive mitochondria are removed from the cell, in the model mitophagy only deletes mitochondria with a quality of $q = 0$. Correspondingly, biogenesis adds mitochondria with the maximum quality of $q = Q$. Due to the conservation norm 2.2, mitophagy and biogenesis are coupled processes in the model: The same probability fraction, that is substracted from quality state $q = 0$ by mitophagy is parallel added by biogenesis to the probability mass of $q = Q$, so that $N_{\mathrm{prob}} = 1$ for all points in time (Figure 2.1g). This ansatz leads to the following formula:

$$\frac{\partial}{\partial t} P_{\mathrm{mb}}(q,t) = \rho_{\mathrm{mb}}(t) \cdot (-\delta_{q,0} P(q,t) + \delta_{q,Q} P(0,t)) \tag{2.13}$$

Recent research revealed, that autophagy of mitochondria increases during the aging of the cell. [28] Hence, the corresponding process probability over time $\rho_{\mathrm{mb}}(t)$ is modeled as a growth law:

$$\rho_{\mathrm{mb}}(t) = \rho_{0,\mathrm{mb}} \cdot \exp(\frac{t}{\tau_{\mathrm{mb}}}) \tag{2.14}$$

Here, parameters $\rho_{0,\mathrm{mb}}$ and τ_{mb} are the starting probability and the lifetime of the recycling process, respectively.

2.2.1.3 Energy Consumption

During the production of ATP by oxidative phosphorylation, mitochondria consume enzymes and metabolites [5] and harm their own mtDNA by generating oxidative stress in processes within the electron transport chain. [21, 22] Hence, mitochondria loose their quality during energy production. As metabolically active mitochondria have a higher chance of generating oxidative stress, mitochondria of high qualities are more likely to impair themselves. Assuming that a single quality is always lost with the same probability ρ_{ec} (Figure 2.1e-f), the activity-dependent quality decay is modeled with a binomial approach:

$$\frac{\partial}{\partial t}P_{ec}(q,t) = \sum_{q'>q}^{Q} \binom{q'}{q'-q} \rho_{ec}(t)^{q'-q}(1-\rho_{ec}(t))^q \cdot P(q',t)$$
$$- \sum_{q''=0}^{q''<q} \binom{q}{q-q''} \rho_{ec}(t)^{q-q''}(1-\rho_{ec}(t))^{q''} \cdot P(q,t) \tag{2.15}$$

The first term on the right-hand side of equation (2.15) refers to the gain of quality state q by the decay of all higher quality states q', while the second term takes into account the loss of q to lower qualities q''.

During the aging of the cell the number of failures in the mitochondrial DNA increases. [21] As a result, the generation of oxidative stress in energy production becomes more likely. Thus, the probability of loosing a specific quality ρ_{ec} in a mitochondrion grows over time:

$$\rho_{ec}(t) = \rho_{0,ec} \cdot \exp(\frac{t}{\tau_{ec}}) \tag{2.16}$$

Again, $\rho_{0,ec}$ and τ_{ec} denote the starting probability and the lifetime of the process.

2.2.1.4 External Oxidative Stress

In addition to the oxidative stress created by mitochondria themselves, other cell organelles, such as the endoplasmatic reticulum and peroxisomes [23] or external factors (e.g. the radiation by the sunlight [29]) generate reactive oxygen species in a random manner. Reflecting this behavior, the model picks random pairs of quality states and subtracts random fractions of probability mass from a higher quality state to assign it to a lower quality state (Figure 2.1h):

$$\frac{\partial}{\partial t}P_{\mathrm{ed}}(q,t) = \rho_{\mathrm{ed}}(t) \cdot \sum_{q'=q+1}^{Q} P(q',t)R_{\mathrm{ed}}(q' \to q,t) - P(q,t)\sum_{q''=0}^{q-1} R_{\mathrm{ed}}(q \to q'',t) \quad (2.17)$$

In formula (2.17), rate $R_{\mathrm{ed}}(q' \to q,t)$ represents the gain of a lower quality state q by the loss of probability fraction of a higher quality state q', while $R_{\mathrm{ed}}(q \to q'',t)$ indicates the loss of q to lower qualities q''. The subtracted fraction has a maximum value of f_{rd}. Hence, the exchange of probability mass between two quality states q and q' reads as

$$P(q',t) = P(q',t)(1 - f_{\mathrm{rd}}) \quad (2.18)$$

for the lost fraction of a higher quality state q' and

$$P(q,t) = P(q,t) + P(q',t)f_{\mathrm{rd}} \quad (2.19)$$

for the gained fraction of a lower quality state q.

Similar to reactive oxygen species produced by mitochondria themselves, external oxidative stress increases during the aging of the cell [30]:

$$\rho_{\mathrm{ed}}(t) = \rho_{0,\mathrm{ed}} \cdot \exp(\frac{t}{\tau_{\mathrm{ed}}}) \quad (2.20)$$

In this formula, parameters $\rho_{0,\mathrm{ed}}$ and τ_{ed} represent the starting probability and the lifetime of this process.

2.2.1.5   Repair mechanisms

In order to fix impairments in the mitochondrial DNA induced by oxidative stress, mitochondria hold repair mechanisms which are similar to the cell's strategies to eliminate failures in the nuclear DNA. [20] Furthermore, mitochondria are able to produce and import protein complexes and enzymes necessary for the Krebs cycle and the respiratory chain. [31] To date, there is a lack of experimental insight about the probabilities for mitochondria to repair specific qualities, that are impaired. Therefore, the model follows the approach of the mathematical definition of the energy consumption and assumes, that every quality is repaired with the same probability $\rho_{\mathrm{rep}}(t)$ (Figure 2.1c-d). With a binomial approach this means, that the lower the quality of a mitochondrion is, the more

likely is the repair of at least one of the missing qualities. The mathematical definition
of this biophysical process then reads as:

$$
\frac{\partial}{\partial t} P_{\text{rep}}(q,t) = \sum_{q'=0}^{q'<q} \binom{Q-q'}{q-q'} \rho_{\text{rep}}(t)^{q-q'} (1-\rho_{\text{rep}}(t))^{Q-q} \cdot P(q',t)
$$
$$
- \sum_{q''>q}^{q''<q} \binom{Q-q}{q''-q} \rho_{\text{rep}}(t)^{q''-q} (1-\rho_{\text{rep}}(t))^{Q-q''} \cdot P(q,t)
$$

$$(2.21)$$

The positive term on the right-hand side of equation (2.21) represents the gain of quality
state q by the repair of lower quality states q', while the negative term derives the loss
of q to higher qualities q'' by mitochondrial repair.

During aging, the cell's ability to repair defective sequences in the DNA decreases. [32]
Hence, the probability of repairing a single quality $\rho_{\text{rep}}(t)$ within the mtDNA is modeled
as a decay law:

$$
\rho_{\text{rep}}(t) = \rho_{0,\text{rep}} \cdot \exp(-\frac{t}{\tau_{\text{rep}}})
$$

$$(2.22)$$

Here, $\rho_{0,\text{rep}}$ represents the starting probability of mitochondrial repair, while τ_{rep} is the
corresponding lifetime.

2.3   Model Validation

For computational realization of the presented model, its mathematical definitions were
implemented in the programming language Java SE [33] under usage of the packages
java.util.* [34] and *java.io.**. [35] All programming scripts are attached to Appendix A.
For validation of the model, its two most important physiological parameters were in-
vestigated. The average quality

$$
\bar{q}(t) = \sum_{q=0}^{Q} q \cdot P(q,t)
$$

$$(2.23)$$

represents the general well-being of mitochondria in the cell. The fraction of inactive
states $P(0,t)$ gives the amount of mitochondria that are not involved in any networking
processes. These mitochondria lie isolated in the cytoplasm of the cell and thereby
represent the degree of fragmentation of the mitochondrial network.

2.3.1 Euler Method

Due to the complexity of the homogeneous differential equation of first order (2.3), simulations of the quality distribution $P(q,t)$ are not solved analytically, but numerically. Similar to the ansatz of Figge et al. [17] for that purpose the simplest form of the classical Runge-Kutta method (**RK4**), the so called Euler method, is utilized. An ordinary differential equation of the form

$$\frac{dP}{dt} = f(P(t), t) \tag{2.24}$$

the is solved by the Euler method using:

$$P(t_{n+1}) = P(t_n) + h \cdot f(P(t_n), t_n) \tag{2.25}$$

with $P(t)$ being the differential equation and h representing the step size in time dimension t of the numerical solution.

In order to find the appropriate step size for both, a preferable exact solution of the differential equation (2.3) and a acceptable running time of simulations, numerical solutions (2.3) for step sizes $h = 10000$, $h = 1000$, $h = 100$, $h = 10$ and $h = 1$ were derived. For these simulations, the maximum quality Q was defined as 10, so that in total eleven quality states (including $q = 0$) were investigated. The free parameters in the model were set to the values given in Table 2.1. As the starting condition, the uniform distribution of $P(q,0)_1$ in Table 2.2 was used.

Simulations presented in Figure 2.2 reveal, that decreasing the step size from $h = 10000$ to $h = 10$ leads to both, a qualitative and quantitative improvement of the accuracy of numerical solutions of the average quality $\bar{q}(t)$ and the fraction of inactive states $P(0,t)$. A further lowering of the step size from $h = 10$ to $h = 1$ results only in marginal aberrations during the setting process in the first few time steps of parameter $\bar{q}(t)$ and then establishes qualitatively and quantitatively same level for both parameters, $\bar{q}(t)$ and $P(0,t)$.

The discrepancy in values in both parameters are lower than 1%. This remaining difference can be explained by fluctuations due to the randomness of external oxidative stress. Hence, $h = 1$ is a reasonable step size for the numerical solution of the differential equation (2.3) regarding an accetable quantitative and qualitative accuracy. In the following, the results of all simulations based on equation (2.3) are solved with minimal time steps of $h = 1$.

FIGURE 2.2: Simulations on the Euler method in the quality model
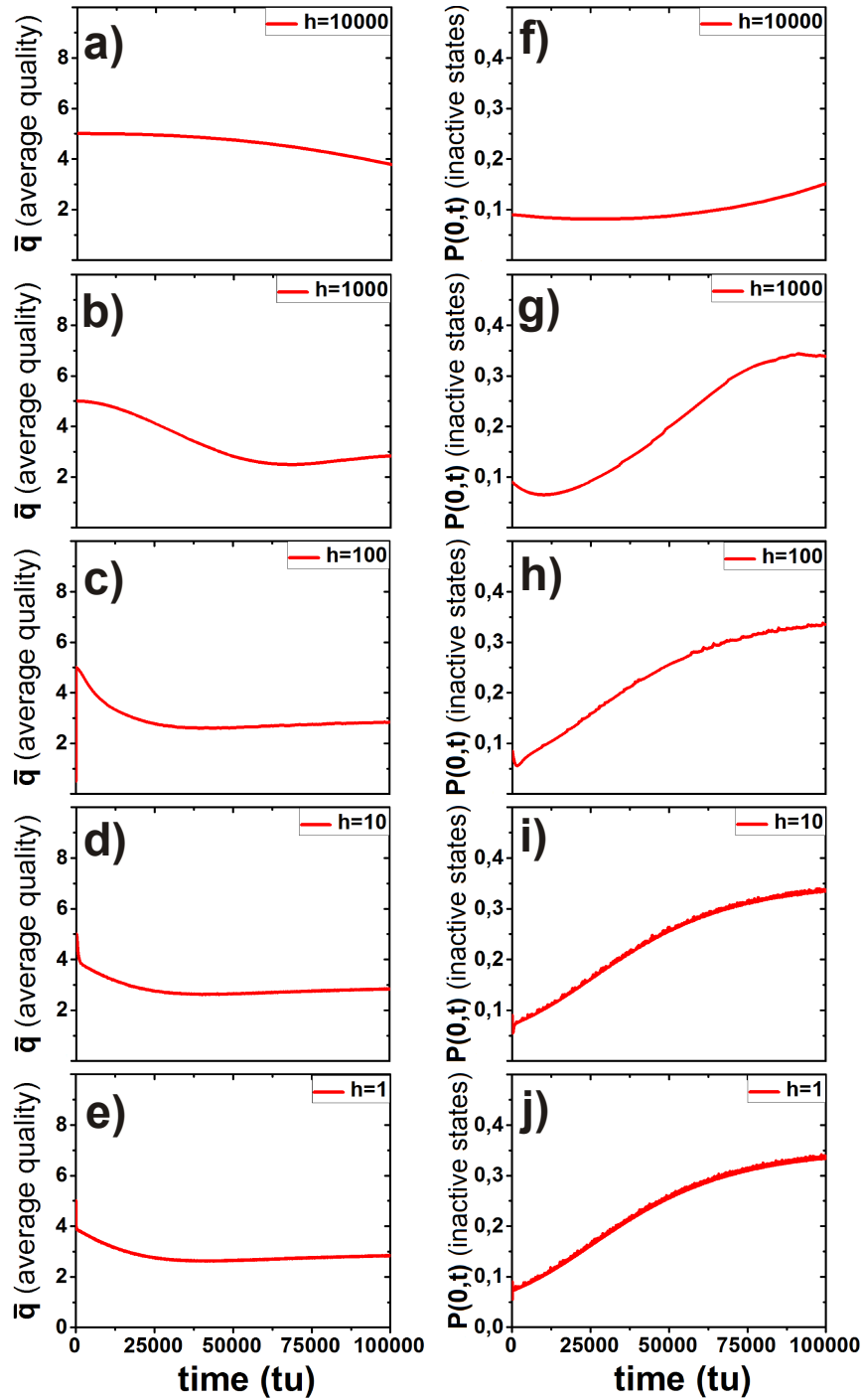
The average quality $\overline{q}(t)$ and the fraction of inactive states $P(0,t)$ over time for a numerical solution of equation (2.3) solved with the Euler method for step sizes h=10000 (a,f), h=1000 (b,g), h=100 (c,h), h=10 (d,i) and h=1 (e,j).

parameter	value
γ	1
$\rho_{0,\mathrm{FF_m}}$	0.05
$\tau_{\mathrm{FF_m}}$	50000 tu
$\rho_{0,\mathrm{FF_p}}$	0.05
$\tau_{\mathrm{FF_p}}$	50000 tu
$\mathrm{FF_1}$	2
$\mathrm{FF_2}$	3
$\rho_{0,\mathrm{mb}}$	0.01
τ_{mb}	50000 tu
$\rho_{0,\mathrm{rep}}$	0.01
τ_{rep}	50000 tu
$\rho_{0,\mathrm{ec}}$	0.01
τ_{ec}	50000 tu
$\rho_{0,\mathrm{ed}}$	0.01
τ_{ed}	50000 tu
f_{rd}	0.03

TABLE 2.1: Values of free parameters in validation simulations of quality model

2.3.2 Starting distribution

Prior starting the simulations, the algorithm has to be fed with a starting condition in form of a probability distribution $P(q,0)$. Since in this model the mitochondrial network during the aging of the cell is investigated, $P(q,0)$ represents the state of the mitochondrial network before it enters the biological aging processes. However, as cells, by definition, start to age in the moment of their existence, the qualitative state of the mitochondrial network before cell birth remains unknown. Therefore, the starting distribution $P(q,0)$ can not be determined. In order to find out, if $P(q,0)$ actually influences the results of the model, simulations with five very different starting distributions were performed (see Table 2.2). Again, as example parameters, $\overline{q}(t)$ and $P(0,t)$ were investigated. Free parameters in the model were set as in Table 2.1, the maximum quality Q was defined as 10.

In Figure 2.3, depictions of the simulations disclose, that after a short period of about 200 tu (0.2 % of usual simulation duration of 100000 tu) at the beginning of the simulations, all different starting distributions $P(q,0)_i$ quantitatively and qualitatively establish the same level for both investigated parameters, $\overline{q}(t)$ and $P(0,t)$.

Therefore, the outcomes of the simulations with the presented model seem to be independent from the starting distribution. In all simulations presented in the following sections, the starting distribution is a uniform distribution as $P(q,0)_1$ in Table 2.2.

quality q	$P(q,0)_1$	$P(q,0)_2$	$P(q,0)_3$	$P(q,0)_4$	$P(q,0)_5$
0	0.090	0.9	0.01	0.01	0.455
1	0.091	0.01	0.01	0.01	0.01
2	0.091	0.01	0.01	0.01	0.01
3	0.091	0.01	0.01	0.01	0.01
4	0.091	0.01	0.01	0.01	0.01
5	0.091	0.01	0.01	0.9	0.01
6	0.091	0.01	0.01	0.01	0.01
7	0.091	0.01	0.01	0.01	0.01
8	0.091	0.01	0.01	0.01	0.01
9	0.091	0.01	0.01	0.01	0.01
10	0.091	0.01	0.9	0.01	0.455

TABLE 2.2: Different starting distributions for $Q = 10$ in quality model

FIGURE 2.3: Simulations with different starting distributions in the quality model
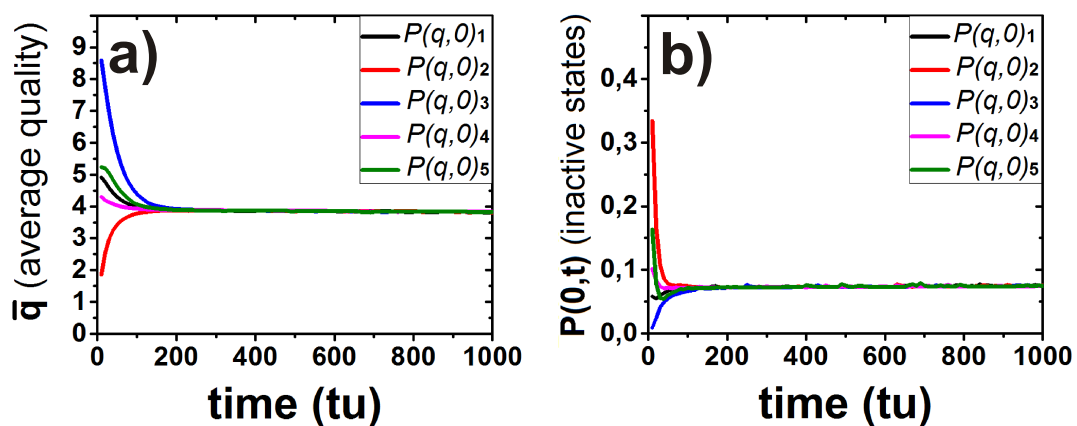
The average quality $\overline{q}(t)$ and the fraction of inactive states $P(0,t)$ over time for starting distributions $P(q,0)_1$ (black), $P(q,0)_2$ (red), $P(q,0)_3$ (blue), $P(q,0)_4$ (pink) and $P(q,0)_5$ (green) corresponding with Table 2.2.

Physiologically, one can conclude from these results, that the balance of biological processes acting on mitochondria during aging is very robust and that, if the processes are still functioning well, this balance is able to establish robust qualities levels among mitochondria in every cell independent from its prior state.

2.3.3 Parameter Setting

The presented model includes several free parameters. Due to simplifications in the model, as for example, the combination of the integrity of the mitochondrial DNA and the supply with metabolites to an artificial quality parameter q, the free parameters introduced in the mathematical definitions of the biological processes are of artificial

nature as well. Thus, it is not possible to measure the values of these free parameters directly by experiments. Correspondingly, to date experimental publications do not quantitatively determine neither frequencies nor power of mitochondrial processes relatively to each other regarding specific cell types. As, in the model, the quantitative progression of quality parameters, such as $\bar{q}(t)$ and $P(0,t)$ over time depends on process probabilities $\rho_{i,0}$ and lifetimes τ_i, it is, so far, not possible to apply an absolute time scale to the model. Therefore, all presented simulations deal with artifical time units (tu).

Due to the lack of experimental input on the quantitative change of biological processes acting on mitochondria during aging, it is intricate to estimate process probabilities $\rho_{i,0}$ and lifetimes τ_i relatively to each other. Corresponding with Table 2.3, in Figure 2.4 different settings of free parameters are compared regarding their impact on the average quality $\bar{q}(t)$ and the fraction of inactive states $P(0,t)$. For all biological processes i, simulations with three different values of corresponding parameters $\rho_{i,0}$ and τ_i were performed.

Simulations (Figure 2.4) reveal, that different parameter sets lead to similar qualitative outcomes. The average quality of mitochondria declines during over time, while the number of inactive mitochondria grows. However, different values for $\rho_{i,0}$ and τ_i modify the slope of the investigated quality parameters.

parameter	value 1	value 2	value 3
$\rho_{0,\mathrm{FF_m}}$	0.05	0.025	0.1
$\tau_{\mathrm{FF_m}}$	50000 tu	25000 tu	100000 tu
$\rho_{0,\mathrm{FF_p}}$	0.05	0.025	0.1
$\tau_{\mathrm{FF_p}}$	50000 tu	25000 tu	100000 tu
$\rho_{0,\mathrm{mb}}$	0.01	0.005	0.02
τ_{mb}	50000 tu	25000 tu	100000 tu
$\rho_{0,\mathrm{rep}}$	0.01	0.005	0.02
τ_{rep}	50000 tu	25000 tu	100000 tu
$\rho_{0,\mathrm{ec}}$	0.01	0.005	0.02
τ_{ec}	50000 tu	25000 tu	100000 tu
$\rho_{0,\mathrm{ed}}$	0.01	0.005	0.02
τ_{ed}	50000 tu	25000 tu	100000 tu

TABLE 2.3: Different values of free parameters for process probabilities

Raising the starting probability of recycling from $\rho_{i,0} = 0.005$ to $\rho_{i,0} = 0.02$ leads to higher mitochondrial qualities and lower fraction of inactive states. Contrarily, an increase of the corresponding lifetime τ_{mb} from 50000 tu to 100000 tu delays the growth of biogenetic activity during aging and hence prevents its stabilizing effect of mitochondrial qualities. A very short lifetime of the process of $\tau_{\mathrm{mb}} = 25000$ tu induces a surprising increase of mitochondrial qualities at the end of the simulations. This rather unphysiological behavior is explained in section 4.3.4.

FIGURE 2.4: Simulations with different process parameters in the quality model
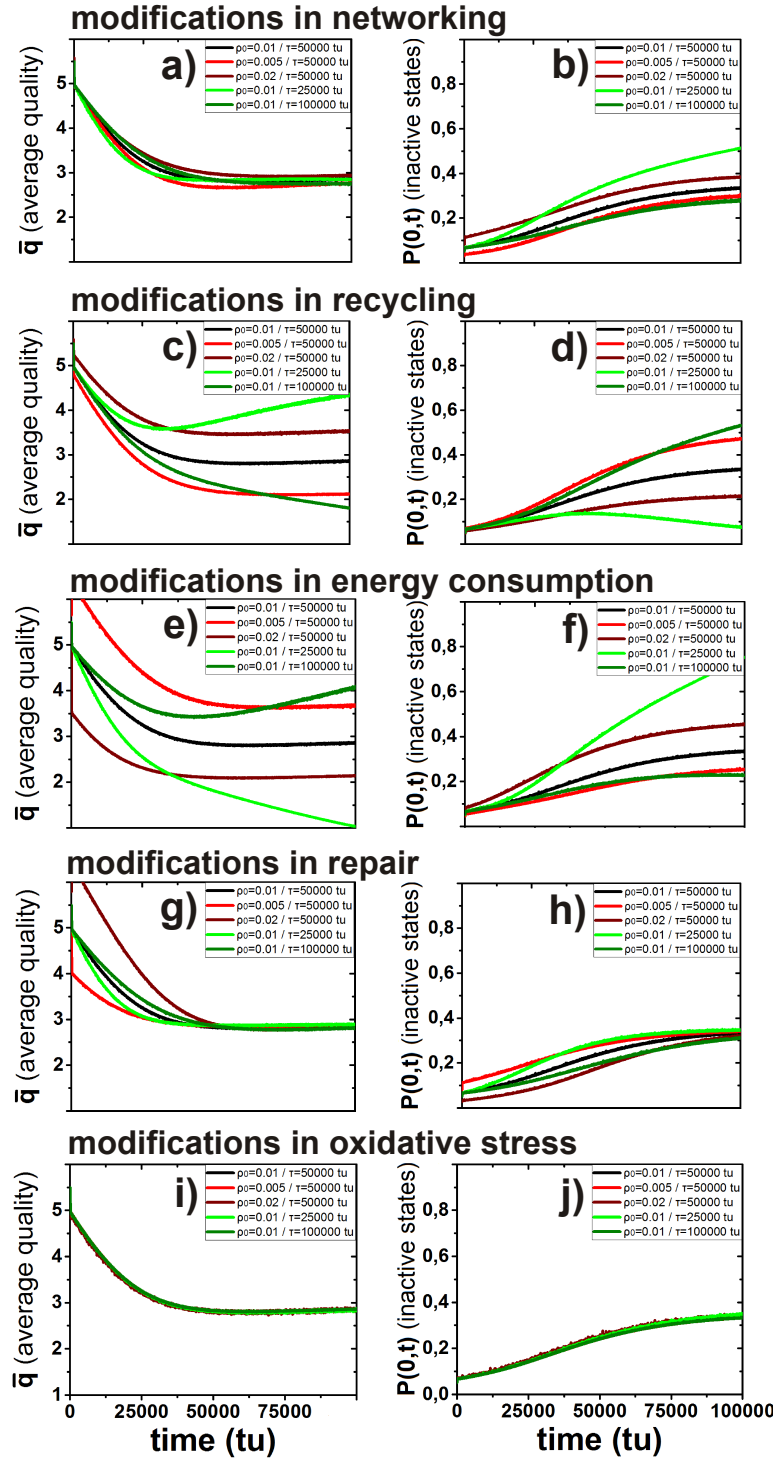
The average quality $\overline{q}(t)$ and the fraction of inactive states $P(0,t)$ over time for different values of free process parameters in networking (a,b), recycling (d,c), energy consumption (e,f), repair (g,h) and oxidative stress (i,j). Variations in the starting probability are depicted in red color, modifications in lifetimes are indicated by green color. The black graph in each plot represents a simulation with parameters given in Table 2.1.

Modifications of lifetimes τ_{FF} and starting probabilities ρ_{FF} of the networking process have only a marginal impact on average qualities of mitochondria. However, a shortening of the lifetime to $\tau_{mb} = 25000\,\mathrm{tu}$ leads to an increase of the fraction of inactive states to over $P(0,t) = 0.5$. This reflects an accelerated disturbance of the equal distribution of qualities among the mitochondrial network by decelerated fission and fusion.

Modifications in lifetimes and starting probabilities of mitochondrial repair and energy consumption lead to intuitive results. A temporal stabilization of the repair mechanism by an increase of τ_{rep} induces higher average qualities and less inactive mitochondria. Moreover, higher starting probabilities $\rho_{rep,0}$ of the repairing process and thereby a delay of the loss of repair functionality in mitochondria leads to higher values of $\bar{q}(t)$ and lower values of $P(0,t)$. In contrast, extended impairments of mitochondria due to increased energy production represented by high starting probabilities $\rho_{0,EC}$ and low lifetimes τ_{EC} decrease mitochondrial qualities and increase the fraction of inactive mitochondria.

Alterations in the starting probability $\rho_{0,ED}$ and the lifetime $\rho_{0,ED}$ of the process of external oxidative stress and other damage lead only to a hardly recognizable quantitative change in both, the average quality $\bar{q}(t)$ and the fraction of inactive mitochondria $P(0,t)$. This behavior reveals, that in the model, external damage has a less significant effect on mitochondrial qualities than the other quality wasting process of energy production.

Although so far it is not possible to perform quantitative comparison between experimental investigations and simulations of different starting probabilities ρ_i and liftimes τ_i, the model helps to understand the effects of a qualitative change of the frequencies of all included processes. Thus, for example, the model might be utilized to investigate the effect of actives, that influence distinct biological processes, on the overall quality state of the mitochondrial network.

In following simulations the parameter values of processes are set as presented in Table 2.1. The starting probability of networking ρ_{0,FF_m} has a higher value than the other processes as it was found that mitochondria fuse and divide frequently in the range of minutes. [18] The values of the three other free parameters FF_1, FF_2 and f_{rd} were adopted from the model of Figge et al. [17] and set as in Table 2.1. In further investigations of the model, particularly the harmed fraction of mitochondria by external oxidative stress f_{rd} should be altered.

2.3.4   Duration of simulations

As depicted in Figure 2.5 there is, with the parameter setting given in Table 2.1, a maximum duration of simulations with 11 quality states (Q=11). The simulation in Figure 2.5 reveals, that after about $223500\,\mathrm{tu}$ both parameters, the average quality $\bar{q}(t)$ and the fraction of inactive states $P(0,t)$, begin to oscillate with high amplitudes and high

frequencies for a short period of time. Subsequently, the model does not deliver real numbers any longer for both parameters. Instead, the Java code prints out the message NaN (Not a Number). The reason for that behavior are the growth laws, that model the change of the recycling mechanism and the quality decay due to energy consumption during aging. The probability $\rho_{\mathrm{mb}}(t)$ of removing mitochondria by mitophagy and replacing them by healthy mitochondria during biogenesis and the probability of damage due to oxidative stress grow exponentially over time. Consequently, at a distinct point in time (depending on the setting of the free parameters in Table 2.1), the corresponding terms in the mathematical definitions of both processes exceed the actually existing probability fraction of a quality state q that shall be altered. As a result, the probability mass is not maintained according to the probability norm (2.2). Hence, the differential equation (2.3) can not be solved in the following time steps. This behavior occurs after over $220\,\%$ of the usual time scale of the simulation, so that it does not affect the qualitative outcomes of the model.

FIGURE 2.5: Simulations in the quality model over $300000\,\mathrm{tu}$
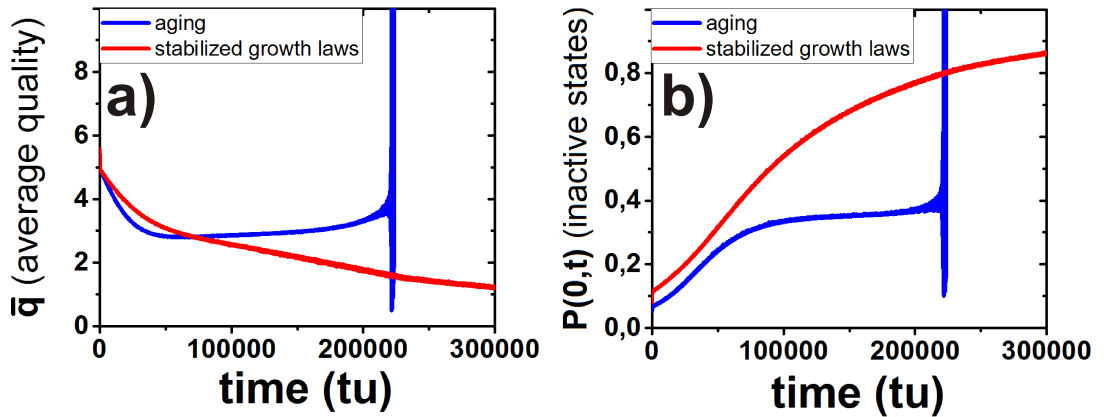
The average quality $\bar{q}(t)$ and the fraction of inactive states $P(0,t)$ over $300000\,\mathrm{tu}$ in an unmodified aging simulation (blue) and in aging without growth laws for recycling and energy consumption (red).

However, in future versions of the model one might be interested in the evaluation of longer time scales. Then, in order to prevent this mathematical dysfunction of the model, instead of an exponential growth law, the change of the recycling probability $\rho_{\mathrm{mb}}(t)$ and the damage due to energy consumption $\rho_{\mathrm{ed}}(t)$ could be modeled by a logistic function:

$$\rho_{\mathrm{mb/ec}}(t) = \rho_{0,\mathrm{mb/ec}} \cdot \frac{S}{1 + \exp(-k(t - t_0))} \tag{2.26}$$

Parameters k and t_0 determine the degree of change of $\rho_{0,\mathrm{mb/ec}}(t)$ and by that substitute the lifetime $\tau_{\mathrm{ec/mb}}$. With a logistic growth law, the recycling probability at first grows exponentially until, after a deflection point, it approaches a saturation value S asymptotically.

Another physiologically anomaly observed in simulations longer than 150000 tu, is the significant growth of the average quality $\overline{q}(t)$ after reaching a minimum. While a slight increase of $\overline{q}(t)$ starting at about 100000 tu is explained by a higher number of inactive mitochondria that are recycled, the significant quality gain observed at the end of quite long simulations representing very old cells is not biologically plausible. This behavior was also observed in Figure 2.4c when the lifetime of the recycling process was shortenend to 50000 tu. These characteristics are the result of the quantitative coupling of biogenesis and mitophagy in the model in order to sustain the probability mass in equation (2.2). In the model, the probability of biogenesis increases with mitophagy, so that even in very old cells all inactive mitochondria are replaced with fresh ones. Hence, mitochondrial qualities in average increase in old cells due to the great amount of inactive mitochondria. According to experiments, the mitochondrial mass grows during aging [36], so that actually harmed mitochondria aggregate in the cytoplasm of a cell. In order to include this mechanism in the model, biogenesis has to be decoupled from mitophagy. As a result, the probability mass would not be fixed to a value of 1, but would increase. Hence, rather than applying probabilities to each quality state q, the model could function with absolute values representing numbers of mitochondria instead of probability fractions.

2.3.5 Quality Resolution

The maximum quality Q determines the number of discrete quality states in the model. Hence, the higher the value of Q is, the more quality states q can be established by mitochondria and the higher is the quality resolution. In order to test the model's scalability of the number of quality states, simulations going from $Q = 1$ to $Q = 14$ and numbers of quality states from 2 to 15 (including the quality state $q = 0$), respectively, were performed. Again, as example parameters the average quality $\overline{q}(t)$ and the fraction of inactive mitochondria $P(0, t)$ were investigated. Values for free parameters were taken from Table 2.1. The results of all simulations are presented in Figure 2.6.

For comparison, both, $\overline{q}(t)$ and $P(0, t)$ are normed to the maximum value of the corresponding simulation.

For all simulations with Q being between 1 and 13 the average quality $\overline{q}(t)$ decreases exponentially during aging. The degree of the decline grows with Q except for $Q = 13$, where the exponential decay is less pronounced than in simulations from $Q = 1$ to

FIGURE 2.6: Simulations in the quality model for different numbers of quality states
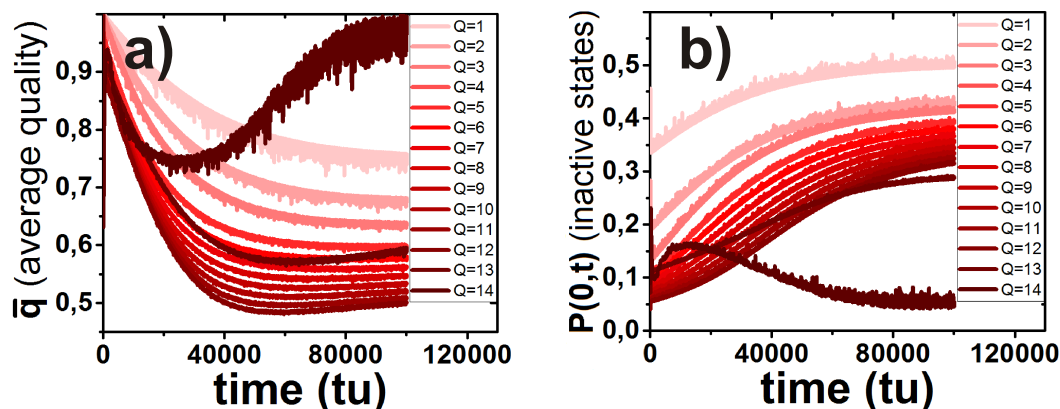
The average quality $\bar{q}(t)$ and the fraction of inactive states $P(0,t)$ over $100000\,\text{tu}$ for simulations going from $Q = 1$ (bright red) to $Q = 14$ (dark red). For better comparison, $\bar{q}(t)$ is normalized to 1 in every simulation.

$Q = 12$. In simulations from $Q = 1$ to $Q = 13$ the fraction of inactive states $P(0,t)$ monotonously increases with time. In the simulation with $Q = 14$ and 15 quality states, respectively, the model experiences a turnover. The average quality $\bar{q}(t)$ falls to a minimum at about $25000\,\text{tu}$, from which it increases again to approach the maximum quality in an asymptotic manner after an inflection point. Additionally, the fraction of inactive states $P(0,t)$ increases for a short period at the beginning of the simulation, reaching a maximum to decline in an exponential manner.

This behavior is not in line with the simulations with lower values than $Q = 14$ and seems rather unphysiological as during aging mitochondrial qualities decrease and the number of inactive mitochondria grows resulting in a fragmentation of the mitochondrial network. Thus, the model in its present form is not able to perform biological plausible simulations with mitochondrial quality state numbers higher than 14.

By raising the number of quality states the impact of both, mitochondrial quality decay due to energy consumption and mitochondrial quality regain by repair mechanisms, decreases. The reason for this is, that the influence of these processes on mitochondrial qualities is fixed to absolute values and therefore does not raise or fall relatively to the maximum quality Q. Moreover, the recycling mechanism becomes more powerful as the quality gained $\Delta q = Q - q$ by replacing harmed mitochondria of $q = 0$ with healthy mitochondria of $q = Q$ increases with growing maximum qualities. To solve this problem the model could be modified by designing energy consumption, oxidative stress and mitochondrial repair as processes that depend on the maximum quality of Q. Consequently, their influence on mitochondrial qualities would not alter with the number of states, but would be stable relatively to Q.

In the following simulations, for better comparison with the model of Figge et al. the maximum quality is set to $Q = 10$.

2.4 Results

After validating the design of the model, various simulations have been performed in order to investigate mitochondrial qualities during the aging of the cell. The free parameters in the model were set to the values in Table 2.1. The results of all simulations are presented and discussed in detail in the following publication in PLoS ONE. [37]

Being in line with recently published experiments *in vitro* [38, 39], simulations illustrate decreasing mitochondrial qualities during the aging of the cell, accompanied by a growing fraction of inactive, isolated mitochondria leading to a fragmented mitochondrial network in old cells.

Investigating the interplay of both kinds of fusion processes, merging of the outer and of the inner mitochondrial membrane, respectively, simulations reveal that fusion processes exchanging only metabolites prevent the quality gain generated by fusing the inner membrane. Hence, if both processes act parallel on mitochondria, mitochondrial qualites are kept at a medium level. However, metabolic fusion in combination with fusion involving the mitochondrial matrix significantly increases the number of inactive mitochondria while maintaining the overall quality level of the mitochondrial network. As mitophagy and biogenesis rely on inactive mitochondria in order to keep their recycling process running, the generation of mitochondria of the lowest quality state $q = 0$ by the collaboration of both kinds of networking, metabolic and proteinaceous, is a very powerful mechanism.

As a consequence the combination of both processes, networking and recycling, leads to a drastic increase of mitochondrial qualities to the maximum value if other processes such as the quality decreasing oxidative stress and energy consumption are neglected. Thus, simulations disclose that mitochondrial networking induces recycling by the generation of metabolically inactive mitochondria. This strategy was proposed in recent experimental publications [40] and is confirmed in the framework of the model.

Simulations with a stabilized ability of mitochondria to repair themselves during aging reveal a lower quality level and a smaller fraction of inactive states among mitochondria in old cells compared to unmodified aging simulations. The explanation for this seemingly paradoxical behavior lies in the thwarting of the recycling process: In old cells, mitochondrial repair works very efficient if it is stabilized. It prevents numerous mitochondria with low quality levels from becoming inactive. As a result, a high amount of harmed mitochondria aggregates without being removed from the cell by mitophagy and being replaced with fresh, high quality mitochondria by biogenesis. Hence, the declining

ability of mitochondria to repair themselves might be a quality saving mechanism during aging.

Several strategies were tested that could help cells establishing high quality levels within the mitochondrial network. For that purpose, two processes controlled by the cell, networking and recycling, were modified by increasing starting probabilities ρ_i and by stabilizing the processes temporally by increasing lifetimes τ_i. Simulations reveal for modifications in recycling parameters, that an increase of the starting probability $\rho_{0,\mathrm{mb}}$ is drastically quality increasing while a temporal stabilization leads to dramatically declining quality states over time. Regarding mitochondrial networking, mitochondrial qualities benefit from parallel modifications in both parameters, meaning an increase of its starting probability $\rho_{0,\mathrm{ff}}$ and a stabilization of the process during cell aging. As a result, the most efficient concept of mitochondria to maintain their qualities over time is a combination of the best single strategies concerning networking and recycling: An increase of both starting probabilities $\rho_{0,\mathrm{mb}}$ and $\rho_{0,\mathrm{ff}}$ and a temporal stabilization of the networking mechanism.

2.5 Discussion

Several of the qualitative outcomes of the mitochondrial quality model are either directly validated by experiments, as, e.g. the morphological behavior of mitochondria during aging, or are experimentally indirectly supported as the efficient induction of mitochondrial recycling by mitochondrial networking. Aging simulations of the model reveal a mitochondrial network fragmentation with growing number of isolated mitochondrial clusters over time. These results agree very well with the experiments [38, 39] and can now be explained by the increasing fission activity in the mitochondrial network due to the growing amount of reactive oxygen species during aging generated by mitochondria themselves and by other cell organelles. Other results, such as the quality saving effect of decreasing mitochondrial repair during aging are not yet experimentally investigated. In this case, the model suggests future experiments on mitochondria.

So far, the results of all simulations are of qualitative value. For a quantitative comparison between computational simulations and experimental measurements precise experimental determination of the values of the free parameters included in the model is required. Many parameters such as the starting probabilities $\rho_{0,i}$ and the lifetimes τ_i are of artificial nature. Hence, they can only be measured indirectly. To date, there is a lack of experimental data to exactly determine these parameters.

Since the rates of mitochondrial dynamics vary among different cell types, experiments have to establish distinct parameter sets for cells types of interest, as, e.g., for epidermal

keratinocytes examined in chapter 4. As a first step, measurements of the frequencies of different biological processes could help, to determine the lifetimes τ_i of all involved processes relatively to each other, in order to integrate an absolute time scale to the model. This would qualify the model for further quantitative investigation of the mitochondrial network in the epidermis during skin aging.

Moreover, the mitochondrial quality q is an artificial parameter, which has no direct counterpart in reality. For quantitative analysis, this parameter has either to be translated to a measurable dimension as the mitochondrial membrane potential or it has to be split up into several subparameters as, e.g., the integrity of the mitochondrial DNA, the amount of metabolites and enzymes available during oxidative phosphorylation or the health of protein complexes in the mitochondrial matrix.

Furthermore, the exact procedures of some biological processes included in the model are experimentally still unclear. Although it is experimentally confirmed that mitochondria share metabolites, mtDNA sequences, and protein complexes during outer and inner mitochondrial membrane fusion, the quantitative extend of this exchange was not yet determined. Additionally, the assumption that every quality is lost by oxidative stress and regained by mitochondrial repair with the same probability depending on the process, is a simplification due to the lack of experimental insights.

So far, the model does not simulate an absolute amount of mitochondria, but each quality state is represented by the probability of one mitochondrion establishing it. Due to the conservation norm (2.2) the probability mass has to remain at a stable value of $N = 1$ for all points in time. However, in reality the number of mitochondria changes over time and increases during cell aging. [36] In order to take into account the effect of an altering mitochondrial mass on mitochondrial qualities, the model could be detached from the probabilistic approach and calculate absolute numbers of mitochondria for each quality state. The coupling between biogenesis and mitophagy, which is necessary to maintain the conservation norm, but which is physiologically not valid, could be decomposed. Biogenesis would not have to increase in the same manner as mitophagy, but could, in line with several experiments [41], decrease over time. Furthermore, some experiments point into the direction, that mitophagic processes decrease during the aging of the cell. [42]

In the current version of the model, the overall change of mitochondrial qualities over time is given by the superposition of the single biophysical definitions of all biological processes, as there are networking, recycling, energy consumption, external damage and mitochondrial repair. This ansatz suggests that there is no direct coupling between some of the processes acting on mitochondria. In reality, there might be interconnections, for example, between the process of energy production and the repair mechanism, mitochondrial recycling and mitochondrial networking, since these processes consume energy in order to perform their tasks. However, so far, there is no experimental evidence

about any quality-dependent interaction among mitochondrial processes. To include corresponding coupling terms in future, further experimental input is necessary.

2.6 Publication

CrossMark
click for updates

RESEARCH ARTICLE

Quality Saving Mechanisms of Mitochondria during Aging in a Fully Time-Dependent Computational Biophysical Model

Daniel Mellem[1,2], Frank Fischer[2]*, Sören Jaspers[2], Horst Wenck[2], Michael Rübhausen[1]

1 Center for Free-Electron Laser Science (CFEL), University of Hamburg, Hamburg, Germany, **2** Beiersdorf AG, Applied Biophysics, Hamburg, Germany

* frank.fischer@beiersdorf.com

Abstract

Mitochondria are essential for the energy production of eukaryotic cells. During aging mitochondria run through various processes which change their quality in terms of activity, health and metabolic supply. In recent years, many of these processes such as fission and fusion of mitochondria, mitophagy, mitochondrial biogenesis and energy consumption have been subject of research. Based on numerous experimental insights, it was possible to qualify mitochondrial behaviour in computational simulations. Here, we present a new biophysical model based on the approach of Figge et al. in 2012. We introduce exponential decay and growth laws for each mitochondrial process to derive its time-dependent probability during the aging of cells. All mitochondrial processes of the original model are mathematically and biophysically redefined and additional processes are implemented: Mitochondrial fission and fusion is separated into a metabolic outer-membrane part and a protein-related inner-membrane part, a quality-dependent threshold for mitophagy and mitochondrial biogenesis is introduced and processes for activity-dependent internal oxidative stress as well as mitochondrial repair mechanisms are newly included. Our findings reveal a decrease of mitochondrial quality and a fragmentation of the mitochondrial network during aging. Additionally, the model discloses a quality increasing mechanism due to the interplay of the mitophagy and biogenesis cycle and the fission and fusion cycle of mitochondria. It is revealed that decreased mitochondrial repair can be a quality saving process in aged cells. Furthermore, the model finds strategies to sustain the quality of the mitochondrial network in cells with high production rates of reactive oxygen species due to large energy demands. Hence, the model adds new insights to biophysical mechanisms of mitochondrial aging and provides novel understandings of the interdependency of mitochondrial processes.

Introduction

A detailed comprehension of the functioning of mitochondria is of great concern in miscellaneous scientific disciplines and plays an important role in aging. [2], [3]

The main task of mitochondria is to provide a cell with energy in form of adenosintriphosphate (ATP). In the cytoplasm of the cell glycolysis decomposes glucose in order to gain pyruvate molecules. These molecules are transported into mitochondria where they enter the Krebs cycle [4]. There, the pyruvate reduces NAD+ molecules to the coenzyme NADH. The NADH molecules arrive at the respiration chain where their energy is released gradually by carrying its reducing electrons to lower potentials. The resulting free energy is employed to establish a proton motive force along the inner membrane of the mitochondrium in order to finally transform adenosindisphosphate (ADP) to ATP.

The efficiency of these processes strongly depends on the quality of mitochondria. Their activity can be tracked by the polarization of their mitochondrial membrane potential (MMP). [5] In order to sustain a high membrane potential, Krebs cycle and respiration chain have to be supplied with a sufficient amount of metabolites such as NAD+, ADP or pyruvate. Additionally, the number of defects within the mitochondrial DNA (mtDNA) should be kept at a low level so that newly generated protein complexes involved in the respiration chain or enzymes involved in the Krebs cycle are of high quality. [6, 7]

During the aging of cells mitochondria suffer from self-generated internal reactive oxygen species (ROS) and external oxidative stress produced by other organelles, eventually leading to the death of cells.[8] In order to retain their reliability in energy production mitochondria behave as a very dynamic network that utilizes numerous processes to remain in a state of high quality. [9] Fission and fusion help mitochondria to compensate for rare metabolites, defect mtDNA sequences or damaged protein complexes. [10], [11] Irreversibly damaged mitochondria are excluded from the network by fission processes and afterwards removed and regenerated by a permanent cycle of mitochondrial autophagy (mitophagy) [12] and mitochondrial biogenesis. [13] Repair mechanisms similar to repair procedures of nuclear DNA defects help to maintain the integrity of the mtDNA. [14]

In recent years various experiments provided a better understanding of the processes within the mitochondrial network. [15] Based on this knowledge several *in silico* models have been developed which are considered to generally simulate mitochondrial dynamics. [16, 17] An established model to describe the mitochondrial development during the aging of cells was introduced by Figge et al. in 2012. [1] In this contribution, the probabilistic change of discrete mitochondrial quality states was described by one differential equation which integrated several dynamic mitochondrial processes. Biophysical simulations revealed a decreasing mitochondrial quality and an increasing fragmentation of the mitochondrial network with time. These findings are in good agreement with experimental results *in vitro*. [18, 19] Furthermore, the simulations predicted a deceleration of fission and fusion cycles as a quality saving mechanism in the presence of infectious molecular damage among mitochondria.

Here, we present a new mitochondrial quality model based on the approach of Figge et al. in 2012. We introduce a universal biophysical decay and growth law that defines a time-dependent probability for every mitochondrial process. Furthermore, we adjust and append the mathematical definitions of all mitochondrial processes in the existing model to explicitly adapt them to latest findings in experimental research on mitochondrial networking, recycling, repair and energy consumption [20], [21], [22], [23]. We present and discuss simulations of the mitochondrial quality model.

Models

Mitochondrial quality depends on the supply with metabolites, the energetic activity and the health of mtDNA and mitochondrial protein complexes. In this model these variables are represented by a single parameter q that defines the state of quality of a mitochondrium. The quality q is a discrete integer of a value between 0 and Q, with Q being the maximal quality. A mitochondrium exhibits each quality state with a time-dependent probability $P(q, t)$. For every point in time the sum of the probabilities of all quality states is normalized to 1:

$$N_{\mathrm{prob}} = \sum_{q=0}^{Q} P(q, t) = 1 \tag{1}$$

This system can be described as a homogeneous Markovian model where mitochondrial processes i represent the transitions between discrete quality states q of a Markov chain. Then, the time-dependence of the probability P of quality states can be derived by a Master equation [24]:

$$\frac{dP}{dt} = \mathbf{R}(t)P, \tag{2}$$

where $\mathbf{R}(t)$ is the time-dependent transition matrix with its elements representing all possible transitions between quality states by mitochondrial processes. Due to the conservation norm Eq (1) the probability P in total is not altered. Solving the one-dimensional Master equation the change of the probability of a single state q can be described with:

$$\frac{\partial}{\partial t} P(q, t) = \sum_{q \neq q'} (R_{q'q} P(q', t) - R_{qq'} P(q, t)) \tag{3}$$

Here, $R_{q'q}$ and $R_{qq'}$ are transition rates of $\mathbf{R}$ that represent the impact of different mitochondrial processes. The rate $R_{q'q}$ represents the probability q gains by transitions from states q' to q, while rate $R_{qq'}$ depicts the loss of probability from q to other states q'.

Neglecting possible coupling terms between arbitrary mitochondrial processes i and j, $\frac{\partial P(q,t)}{\partial t}$ and its corresponding rates R_{ij} of $\mathbf{R}$ can be split up into a sum of several terms, each depicting the change in probabilities of q by a single mitochondrial process:

$$\frac{\partial}{\partial t} P(q, t) = \frac{\partial}{\partial t} P_{\mathrm{FF}}(q, t) + \frac{\partial}{\partial t} P_{\mathrm{MB}}(q, t) + \frac{\partial}{\partial t} P_{\mathrm{REP}}(q, t) + \frac{\partial}{\partial t} P_{\mathrm{EC}}(q, t) + \frac{\partial}{\partial t} P_{\mathrm{ED}}(q, t) \tag{4}$$

The single terms represent mitochondrial quality changing processes which were observed and described in experimental publications in recent years: mitophagy and biogenesis $\frac{\partial}{\partial t} P_{\mathrm{MB}}(q, t)$, fission and fusion $\frac{\partial}{\partial t} P_{\mathrm{FF}}(q, t)$, mitochondrial repair $\frac{\partial}{\partial t} P_{\mathrm{REP}}(q, t)$, energy consumption $\frac{\partial}{\partial t} P_{\mathrm{EC}}(q, t)$ and external mitochondrial damage $\frac{\partial}{\partial t} P_{\mathrm{ED}}(q, t)$ (Fig 1).

During aging the number of enzymes, proteins and metabolites alters. As the impact of biological processes depends on the number of corresponding particles or rather molecules involved, the time-dependence of a process i can be described by homogeneous differential equation of first order. In biology this approach is chosen, e.g. to derive the effect of a drug over time [25]. The differential equation reads:

$$A_i = \pm \frac{dN_i}{dt}, \tag{5}$$

where $A_i = \lambda N_i$ denotes the activity of the process and N_i the number of particles involved in the process. This decay law or growth law, depending on the sign, can be solved with an
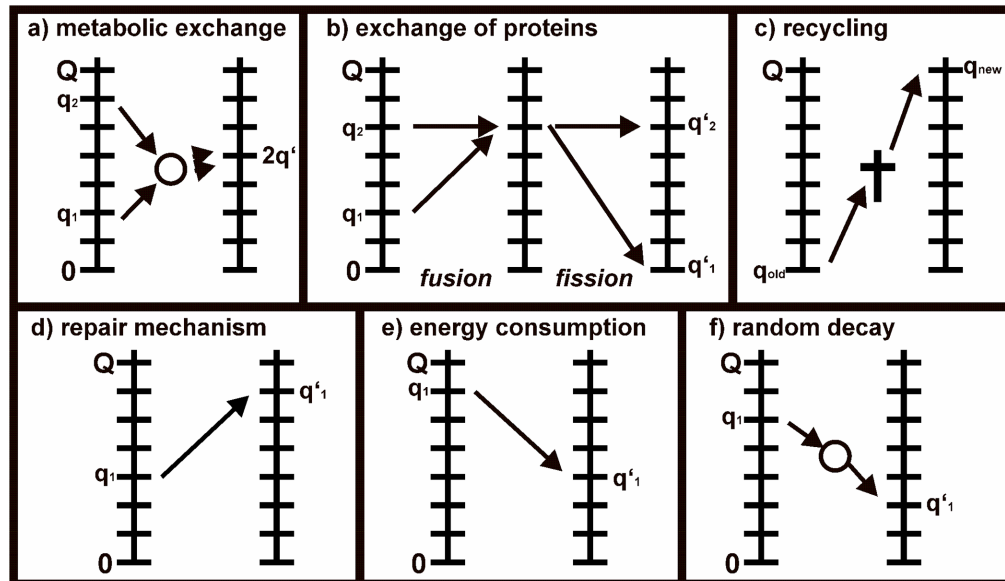
Fig 1. Quality changing processes of the mitochondrial quality model. a) Metabolic fission and fusion process leads to two mitochondria of the same quality. b) Fusion of inner matrix components raises the lower mitochondrium to the quality level of the partner. Fission leads to an inactive mitochondrium while the partner maintains its quality. c) Mitophagy removes inactive mitochondria, biogenesis generates mitochondria of the highest quality. d) Mitochondrial repair renews the quality of mitochondria. e) Energy consumption lowers the quality of highly active mitochondria. f) External damage randomly decreases quality of mitochondria.

exponential function:

$$\rho_i(t) = \rho_{0,i} \cdot \exp\left(\pm \frac{t}{\tau_i}\right), \qquad (6)$$

with $\rho_i(t) = c \cdot N_i(t)$, $\rho_{0,i} = c \cdot N_{0,i}$, $\tau_i = 1/\lambda$ and c being a constant for normalization. This ansatz leads to an decoupling of the mathematical definition f_i of a process and its time-dependent probability $\rho_i(t)$:

$$\frac{\partial}{\partial t} P_i(q, t) = \rho_i(t) \cdot f(P_i(q, t), q, q', \ldots). \qquad (7)$$

Hence, $\rho_{0,i}$ are independent factors that balance the processes relatively to each other, while τ_i determines the slope of their time-evolutions. The decoupling is true for the processes of mitochondrial fission and fusion, mitophagy and biogenesis and external oxidative stress (see corresponding sections). For the mitochondrial repair mechanism and the process of energy consumption it is coupled to the mathematical definition of the process i itself:

$$\frac{\partial}{\partial t} P_i(q, t) = f(\rho_i(t), P_i(q, t), q, q', \ldots). \qquad (8)$$

In the following the parameters $\rho_{0,\,i}$ and τ_i represent the starting probability and the lifetime of the process i, respectively. The sign of τ_i depends on either the increase or the decrease of i with the aging of cells.

Fission and Fusion

The dynamics in a network strongly depend on the mobility of its components. Mitochondria are very motile in the cytoplasm of cells. They are not only transported to different locations [26] but also fuse and divide among each other. [15, 27] These fusion and fission processes exhibit two different patterns. On the one hand there are very quick connections between mitochondria in which only the outer mitochondrial membrane is connected. These so called "kiss and run" patterns are associated with the exchange of rare metabolites among mitochondria. On the other hand more time consuming states of fusion of mitochondria have been found to not only include the outer membrane but also the inner membrane and mitochondrial matrix components. [20] In these fusion states mitochondria are considered to share and compensate for defect protein complexes or DNA sequences which are crucial for the production of ATP. [28] Subsequent fission events lead to one mitochondrium with a still polarized MMP and one mitochondrium with a depolarized MMP. [21]

Considering the two different types of connections among mitochondria we decided to separate the biophysical definition for fission and fusion processes in the model into two parts: metabolic fission and fusion $\frac{\partial}{\partial t} P_{\text{FF}_{\text{m}}}(q, t)$ and a proteinaceous fission and fusion $\frac{\partial}{\partial t} P_{\text{FF}_{\text{p}}}(q, t)$, leading to

$$\frac{\partial}{\partial t} P_{\text{FF}}(q, t) = \frac{\partial}{\partial t} P_{\text{FF}_{\text{m}}}(q, t) + \gamma \cdot \frac{\partial}{\partial t} P_{\text{FF}_{\text{p}}}(q, t), \tag{9}$$

where γ denotes a constant to balance both kinds of fission and fusion relatively to each other.

Metabolic fission and fusion. To biophysically define the metabolic fission and fusion process (Fig 1a) within our model we make the following assumptions according to literature or biophysical considerations.

1. When two mitochondria with different qualities exchange metabolites no quality can be gained or lost in total: The amount of metabolites remains the same. Thus, for a metabolic fission and fusion event, we suggest a conservation law: $q_1 + q_2 \rightarrow q_1' + q_2'$, with q_i being the incoming qualities and q_i' the outcoming qualities.

2. For entropic reasons the mixing of metabolites in mitochondria leads to two mitochondria of the same quality: $q_1' = q_2'$

3. The larger the discrepancy between the qualities of two mitochondria the more valuable is the exchange of metabolites. Hence, the probability of the process raises with $\Delta q = \|q_1 - q_2\|$. Inactive Mitochondria ($q = 0$) are not involved in any fission and fusion exchange of metabolites.

The fission and fusion process of metabolites in the model reads then as follows:

$$\frac{\partial}{\partial t} P_{\text{FF}_{\text{m}}}(q, t) = \rho_{\text{FF}_{\text{m}}}(t) \cdot \sum_{q_1, q_2 > 0}^{Q} P(q_1, t) P(q_2, t) R_{\text{FF}_{\text{m}}}(\| q_1 - q_2 \|, t) \cdot$$
$$\delta_{(q_1 + q_2),(q_1' + q_2')} \delta_{q_1', q_2'} \left(\delta_{q, q_1'} + \delta_{q, q_2'} - \delta_{q, q_1} - \delta_{q, q_2} \right) \tag{10}$$

Here and in the following equations $\delta_{i,\,j}$ refers to Kronecker's delta. The two conditions outside the brackets take into account assumption 1 and 2. The positive and negative terms inside

the brackets represent the gain and loss of probability of quality state q. Assumption 3 is represented by $R_{FF_m}(\|q_1 - q_2\|, t)$. This rate is modeled by Hill's equation, which describes the biochemical process of the binding of a ligand to a macromolecule [29]:

$$R_{FF_m}(\| q_1 - q_2 \|, t) = \frac{\| q_1 - q_2 \|^{FF_1}}{FF_2{}^{FF_1} + \| q_1 - q_2 \|^{FF_1}} \qquad (11)$$

FF_1 and FF_2 are the hill coefficients. They are free parameters that cannot be determined by literature. Later on, we assign them the same values as Figge et al. in their model. The factor $\rho_{FFm}(t)$ represents the time-dependent probability of the process. As the proper balance of fission and fusion is disturbed during the aging of cells [30], the probability of the process decreases with time:

$$\rho_{FF_m}(t) = \rho_{0,FF_m} \cdot \exp\left(-\frac{t}{\tau_{FF_m}}\right) \qquad (12)$$

Fission and fusion of proteins. Concerning the fission and fusion of mitochondrial inner matrix components (Fig 1b) we assume according to literature and biophysical considerations the following:

1. As fusion events involving inner matrix components last longer than the exchange of metabolites fission and fusion are seperated into two independent terms

2. When two mitochondria with different qualities share protein complexes after a fusion event both mitochondria have the same capacities to produce energy via oxidative phosphorylation. Hence, the mitochondrium with the lower quality gains the level of quality of the other mitochondrium: $q_1 + q_2 \rightarrow 2 \cdot q_1$. Thus, sharing of matrix components is a quality gaining process.

3. The larger the discrepancy between the qualities of two mitochondria the more valuable is the compensation for defect proteins. Hence, similar to the metabolic exchange the probability of a fusion process raises with $\Delta q = \|q_1 - q_2\|$. Again, inactive mitochondria ($q = 0$) are not involved in any fusion event.

4. As experimentally observed, after a fission event one mitochondrium keeps the polarization of its MMP while the MMP of the other mitochondrium gets depolarized. [21] In the model, the quality of one mitochondrium remains stable, while the other mitochondrium looses its quality in total: $2 \cdot q_1 \rightarrow q_1 + 0_2$

5. The probability of a fission process increases with lower quality states.

The equation reads as:

$$\frac{\partial}{\partial t} P_{FF_p}(q, t) = \rho_{Fu_p}(t) \cdot \sum_{q_1, q_2 > 0}^{Q} P(q_1, t) P(q_2, t) R_{Fu_p}(\| q_1 - q_2 \|, t) \cdot \delta_{q_1, q_1'} \delta_{q_1', q_2'} (\delta_{q, q_2'} - \delta_{q, q_2})$$

$$+ \rho_{Fi_p}(t) \cdot \sum_{q_1, q_2 > 0}^{Q} P(q_1, t) P(q_2, t) R_{Fi_p}(\| Q - q_2 \|, t) \cdot \delta_{q_1, q_2} \delta_{q_1, q_1'} \delta_{q_2', 0} (\delta_{q, 0} - \delta_{q, q_2})$$

$$(13)$$

The first term represents the fusion of inner matrix components and the second term the correspondend fission process. The Kronecker deltas before the brackets refer to the conditions 2 and 3 for fusion and 4 and 5 for fission, respectively. The rates for fusion $R_{Fu_p}(\|q_1 - q_2\|, t)$ and

fission $R_{\text{Fi}_\text{p}}(\|Q-q_1\|, t)$ are:

$$R_{\text{Fu}_\text{p}}(\| q_1 - q_2 \|, t) = \frac{\| q_1 - q_2 \|^{\text{FF}_1}}{\text{FF}_2^{\text{FF}_1} + \| q_1 - q_2 \|^{\text{FF}_1}} \tag{14}$$

and

$$R_{\text{Fi}_\text{p}}(\| q_1 - q_2 \|, t) = \frac{\| Q - q_1 \|^{\text{FF}_1}}{\text{FF}_2^{\text{FF}_1} + \| Q - q_1 \|^{\text{FF}_1}} \tag{15}$$

Similarly to metabolic fission and fusion, the frequency of networking processes $\rho_{\text{Fu}_\text{p}}(t)$ decreases and the number of fission events $\rho_{\text{Fi}_\text{p}}(t)$ increases with the aging of the cell, representing perturbations of networking among mitochondria:

$$\rho_{\text{Fu}_\text{p}}(t) = \rho_{0,\text{FF}_\text{p}} \cdot \exp\left(-\frac{t}{\tau_{\text{FF}_\text{p}}}\right) \tag{16}$$

$$\rho_{\text{Fi}_\text{p}}(t) = \rho_{0,\text{FF}_\text{p}} \cdot \exp\left(+\frac{t}{\tau_{\text{FF}_\text{p}}}\right) \tag{17}$$

Mitophagy and Biogenesis

Mitophagy and mitochondrial biogenesis represent the mitochondrial recycling mechanism of the cell (Fig 1c). Mitochondria that are heavily damaged in terms of their mtDNA or inner and outer mitochondrial membrane components become inactive and establish a depolarized MMP, before they are removed by mitophagy. [31] The removed mitochondrial mass is substituted by new mitochondrial material generated by mitochondrial biogenesis. [32]

Biophysically we define the following rules for mitophagy and biogenesis:

1. To keep the total probability mass at a value of 1 it is required that mitophagy and mitochondrial biogenesis are coupled processes. The equal amount of probability that is subtracted by mitophagy is added by mitochondrial biogenesis:
   $-\sum_{q=0}^{Q} \frac{\partial}{\partial t} P_{\text{Mitophagy}}(q, t) = \sum_{q=0}^{Q} \frac{\partial}{\partial t} P_{\text{Biogenesis}}(q, t)$

2. As mitophagy removes heavily damaged mitochondria with a depolarized MMP from the system we introduce a threshold: Only the probability of the inactive state ($q = 0$) is reduced by mitophagy.

3. Mitochondrial biogenesis generates only mitochondria with the highest possible quality Q.

Following these assumptions the probabilistic change by mitophagy and mitochondrial biogenesis is modeled as:

$$\frac{\partial}{\partial t} P_{\text{mb}}(q, t) = \rho_{\text{mb}}(t) \cdot (-\delta_{q,0} P(q, t) + \delta_{q,Q} P(0, t)) \tag{18}$$

According to literature mitophagy increases during the aging of cells. [33] Correspondingly, the probability of the processes $\rho_{\text{mb}}(t)$ raises with time:

$$\rho_{\text{mb}}(t) = \rho_{0,\text{mb}} \cdot \exp\left(\frac{t}{\tau_{\text{mb}}}\right) \tag{19}$$

Repair

For a long time it was not clear whether mitochondria exhibit any strategies to fix damages within their own DNA. Although mitochondria possess a reduced ability to fix DNA damage compared to the nucleus [22], they still have mechanisms to repair defects of the mtDNA, many of them being similar to repair procedures of nuclear DNA. [14] These mechanisms help mitochondria to regain the high production grades of enzymes involved in the Krebs cycle and the integrity of respiration proteins. Due to this background we add a repair process to the model (Fig 1d). The repair algorithm increases the state of quality of mitochondria, thus representing an improvement of the quality of the mtDNA and the production of mitochondrial protein complexes. Despite the evidence that mitochondria utilize repair mechanisms, so far little is known about the selection criteria and the frequency of repair. Therefore, we have to make the following assumption according to biophysical considerations for modeling a repair process:

1. Repair is a stochastic process: Every missing quality is repaired with the same probability. Pursuing this idea with a binomial approach leads to a higher probability of an increase of quality of low quality states.

With a binomial approach, the repair process is biophysically defined as:

$$
\begin{aligned}
\frac{\partial}{\partial t} P_{\mathrm{rep}}(q,t) \quad &= \sum_{q'=0}^{q'<q} \binom{Q-q'}{q-q'} \rho_{\mathrm{rep}}(t)^{q-q'} (1-\rho_{\mathrm{rep}}(t))^{Q-q} \cdot P(q',t) \\
&- \sum_{q''>q}^{q''<q} \binom{Q-q}{q''-q} \rho_{\mathrm{rep}}(t)^{q''-q} (1-\rho_{\mathrm{rep}}(t))^{Q-q''} \cdot P(q,t)
\end{aligned}
\tag{20}
$$

The positive term on the right side of the equation refers to all mitochondria with low qualities q' which are repaired to quality state q. The negative term takes into account the repair of q to higher qualities q''. As the quality of repair can not be conserved during the aging of cells, the probability of repairing a single quality $\rho_{\mathrm{rep}}(t)$ decreases with time.

$$
\rho_{\mathrm{rep}}(t) = \rho_{0,\mathrm{rep}} \cdot \exp\left(-\frac{t}{\tau_{\mathrm{rep}}}\right)
\tag{21}
$$

Energy consumption

Mitochondria produce ATP via oxidative phosphorylation including the respiration chain. The protein complexes of the respiration chain are located at the inner mitochondrial membrane and are responsible for releasing the energy of NADH molecules in order to establish the proton motive force to transform ADP to ATP. During this process reactive oxygen species (ROS) are generated which harm intramitochondrial structures including the mtDNA. As highly active mitochondria run through the process of oxidative phosphorylation more frequently they suffer more from oxidative stress generated by the electron transport chain than less active mitochondria. [34] We translate this fact to an activity dependent quality decay. Higher mitochondrial quality states which represent more active mitochondria possess a higher probability of loosing quality due to self-generated oxidative stress. With the premise that every mitochondrial quality is lost with the same probability, the probability of quality decay during energy consumption can be modeled with a binomial distribution similar to the repair mechanism

([Fig 1e](#)). The quality decay term for energy consumption reads:

$$
\frac{\partial}{\partial t} P_{ec}(q,t) = \sum_{q'>q}^{Q} \binom{q'}{q'-q} \rho_{ec}(t)^{q'-q} (1-\rho_{ec}(t))^{q} \cdot P(q',t)
$$

$$
- \sum_{q''=0}^{q''<q} \binom{q}{q-q''} \rho_{ec}(t)^{q-q''} (1-\rho_{ec}(t))^{q''} \cdot P(q,t)
$$

(22)

The positive part of the equation refers to a gain of probability of quality q by the decrease of the probabilities of higher quality states q' due to internal oxidative stress. Equivalently in the second term quality state q looses probability to lower quality states q''. As quality decay by internal ROS damage increases with age due to an increasing amount of mutations in the mtDNA [34], the probability of loosing a specific quality $\rho_{ec}(t)$ increases with time:

$$
\rho_{ec}(t) = \rho_{0,ec} \cdot \exp\left(\frac{t}{\tau_{ec}}\right)
$$

(23)

External Damage

Mitochondria do not only damage themselves by oxidative stress, but their mtDNA is also damaged by externally produced ROS from endoplasmatic reticulum, peroxisomes and other organelles in the cell. [35] Moreover, the quality of protein complexes and enzymes involved in the Krebs cycle and the respiration chain is decreased by other externalities leading to the loss of mitochondrial functionalities. These processes affect mitochondria basically in a random manner which is not dependent on the state of metabolic activity of the involved mitochondria. Therefore, we introduce this kind of damage as a quality decreasing process which randomly decreases the quality states of mitochondria to randomly lower levels ([Fig 1f](#)).

$$
\frac{\partial}{\partial t} P_{ed}(q,t) = \rho_{ed}(t) \cdot \sum_{q'=q+1}^{Q} P(q',t) R_{ed}(q' \to q, t) - P(q,t) \sum_{q''=0}^{q-1} R_{ed}(q \to q'', t)
$$

(24)

Here, $R_{ed}(q' \to q, t)$ represents the gain term whereas $R_{ed}(q \to q'', t)$ represents the loss term of the quality state q. In order to assure the randomness of the process the algorithm picks random pairs of quality states q and q' (and q'', respectively) which exchange a distinct fraction of their probability mass:

$$
P(q',t) = P(q',t)(1-f_{rd})
$$

(25)

and

$$
P(q,t) = P(q,t) + P(q',t)f_{rd}
$$

(26)

with $q' > q$ and f_{rd} being the lost fraction of q' and $\rho_{ed}(t)$ being the probability of the process. As the production of oxidative stress by other organelles and the impact of external pathogens increase during the aging of the cell, we increase the external damage with time:

$$
\rho_{ed}(t) = \rho_{0,ed} \cdot \exp\left(\frac{t}{\tau_{ed}}\right)
$$

(27)

Results

In the following section we present simulations based on the new model on mitochondrial quality states. The differential equation [Eq (4)](#) for $P(q, t)$ is numerically solved using Euler's method for minimal time steps of $\Delta t = 1$ tu (tu = time units). Every simulation runs over 100000 tu. At each time step the integrity of the simulation is evaluated by calculating the probability conservation norm. N_{prob} has to establish a stable value of 1 to at least the twelfth decimal.

In the original model by Figge et al. the time-dependent change of 11 quality states $q_i \in \{0, 10\}$ with $Q = 10$ was investigated. We choose the same number of states for our simulations. The qualitative results are robust for quality state numbers between 5 ($Q = 4$) and 15 ($Q = 14$). A higher number of states impairs the balance of mitochondrial processes.

The qualitative results of the simulations do not depend on the distribution of probabilities which is fed to the algorithm at the beginning of the simulation. The simulations presented here start with a uniform distribution assigning the same probability to each quality state ($q_i = 0, \overline{0909}$).

For every point in time t we investigate three parameters:

1. average quality: $\overline{q}(t) = \frac{\sum_{q=0}^{Q} q \cdot P(q,t)}{Q+1}$

2. deviation of quality: $\sigma_q(t) = \sum_{q=0}^{Q} \| q - \overline{q}(t) \| \cdot P(q,t)$

3. fraction of inactive states: $P(0, t)$

The model exhibits free parameters which cannot be taken from literature but which have to be estimated. The starting probabilities represent the intrinsic frequency of a specific process, the lifetimes the degree of change of the process during the aging of the cell. These parameters are suitable to descriptively evaluate the consequence of relative changes of mitochondrial processes. In [Table 1](#) we present the values for free parameters in the following simulations. As

Table 1. Values of free parameters in simulations.

parameter	value
γ	1
$\rho_{0,\ FF_m}$	0.05
τ_{FF_m}	50000 tu
$\rho_{0,\ FF_p}$	0.05
τ_{FF_p}	50000 tu
FF_1	2
FF_2	3
$\rho_{0,\ mb}$	0.01
τ_{mb}	50000 tu
$\rho_{0,\ rep}$	0.01
τ_{rep}	50000 tu
$\rho_{0,\ ec}$	0.01
τ_{ec}	50000 tu
$\rho_{0,\ ed}$	0.01
τ_{ed}	50000 tu
f_{rd}	0.03

The values were estimated relatively to each other based on literature (see text).

mitochondrial fission and fusion is a very dynamic process it occurs more frequently than the other processes such as the mitochondrial turnover.[31][36][37][38] Thus, its starting probabilities $\rho_{0, \text{FF}_{\text{m, p}}}$ are set to values five times higher than the starting probabilities of the other processes. This is in line with the parameter setting in the publication of Figge et al. in 2012. Overall, the parameter values that are taken from the original model are: $\rho_{0, \text{FF}_{\text{m}}}$, $\rho_{0, \text{FF}_{\text{p}}}$, FF_1, FF_2, f_{rd}. There is evidence in literature whether the modeled mitochondrial processes rise or fall during the aging of cells as cited in the previous section. However, the frequency of these processes relatively to each other can hardly be determined. In the following we assume that all processes but fission and fusion have the same starting probability to avoid overestimation of a single process according to Laplace's principle of indifference. This approach concerns all values for the lifetimes τ_i and the starting probabilities $\rho_{0, \text{mb}}$, $\rho_{0, \text{rep}}$, $\rho_{0, \text{ec}}$, $\rho_{0, \text{ed}}$. Experiments *in vitro* could help to establish distinct parameter sets for different cell types in order to exactly quantify mitochondrial behavior. The normalization of all lifetimes τ_0 by the lifetime τ_i of a particularly suitable process would integrate time scalability in the model. Nevertheless, even without experimental determination of the parameter values the simulations remain qualitatively stable as long as the values are not increased or decreased drastically relatively to each other. Even a doubling of starting probabilities and lifetimes does not change the qualitative outcomes in this model (see S1 Fig for examples).

Single processes

In Fig 2a and 2c the exclusive impacts of the single processes of Eqs 9, 18, 20, 22 and 24 on average quality $\overline{q}(t)$, the deviation of quality $\sigma_q(t)$ and the fraction of inactive states $P(0, t)$ are depicted. In terms of $\overline{q}(t)$ mitochondrial repair is the only quality increasing mechanism while external oxidative stress and energy consumption lead to a decrease of the average quality. Fission and fusion and mitophagy and biogenesis approximately conserve the start value of $\overline{q}(t)$. The fraction of inactive states vanishes in the presence of only either mitochondrial repair or mitophagy and biogenesis and grows to 1 if either energy consumption and external oxidative stress act exclusively on mitochondria. The fission and fusion process leads to a stable fraction of 0.445 of inactive mitochondria. For logical reasons, $\sigma_q(t)$ falls to 0 in the presence of repair, energy consumption or external oxidative stress. Fission and Fusion increases the deviation of quality to about 4.940 while mitophagy and biogenesis keep the value at 2.644 after 30000 tu.

Fission and fusion

In the mitochondrial quality model presented in this paper the process of fission and fusion is separated into a metabolic and a protein part. In Fig 2d–2f the severed influence of both processes on the quality of mitochondria is presented. The metabolic part changes neither the average quality $\overline{q}(t)$ nor the number of inactive mitochondria $P(0, t)$ but decreases the deviation of quality $\sigma_q(t)$ to about 0.905. Fission and fusion involving mitochondrial proteins increases all three parameters. The average quality $\overline{q}(t)$ is raised to 7.441, the number of inactive states $P(0, t)$ to 0.256 and the deviation of quality $\sigma_q(t)$ to 3.808 after 30000 tu.

Interplay of recycling and networking

In the following mitophagy and biogenesis is refered to as 'recycling' and to fission and fusion as 'networking'. Fig 2a depicts that mitochondrial networking on the one hand and mitochondrial recycling on the other hand are quality conserving processes. In Fig 2g–2i the interplay of both processes in absence of other processes is depicted. A coupling of recycling and networking leads to a drastic increase of the average quality $\overline{q}(t)$ to 10, and a decrease of both, $\sigma_q(t)$ and $P(0, t)$ to 0 after 30000 tu.
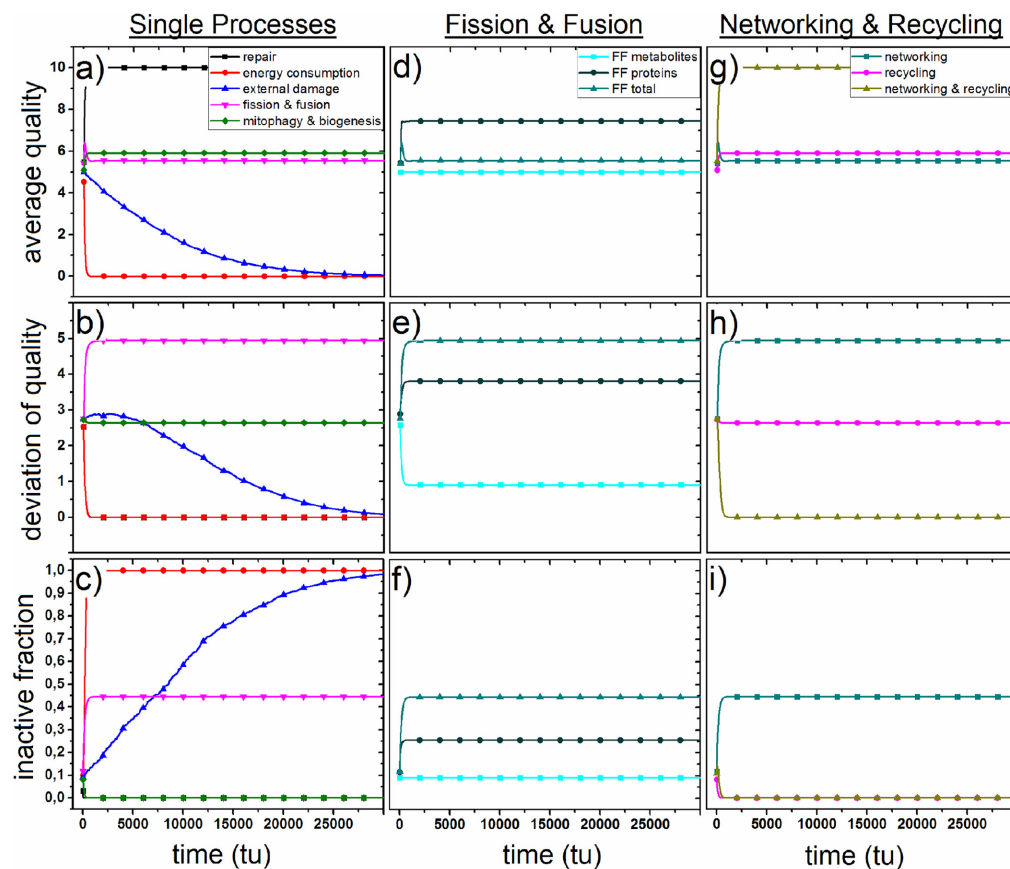
Fig 2. a–c: impact of mitochondrial repair (black), energy consumption (red), external damage (blue), fission and fusion (turquoise) and mitophagy and biogenesis (violett) on the average quality, the deviation of quality and the fraction of inactive states of mitochondria. d–f: impact of metabolic fission and fusion (light turquoise) and proteinaceous fission and fusion (dark turquoise) on average quality, deviation of quality and the inactive fraction compared to the fission and fusion process in total (turquoise). g–h: influence of interplay of networking and recycling (yellow) compared to fission and fusion (turquoise) and mitophagy and biogenesis (violett) on average quality, deviation of quality and inactive fraction.

doi:10.1371/journal.pone.0146973.g002

Mitochondria during cell aging

Fig 3a–3c depicts the time-dependence of mitochondrial qualities if all processes act parallel on mitochondria. This simulation represents the evolvement of the mitochondrial network during the aging of cells. For comparison a non-aging cell with stable, time-independenct processes is depicted. To simulate stability in time the lifetimes of all processes were set to τ_i = 500000000. During aging the average quality $\overline{q}(t)$ falls to a value of about 2.813 at 6900 tu. Then, $\overline{q}(t)$ slightly increases again to about 2.869 at 100000 tu. The number of inactive states $P(0,t)$ increases monotonously to fraction of 0.334 at 100000 tu. After a short period of fluctuation the deviation of quality $\sigma_q(t)$ starts at about 1450 tu to increase monotonously to
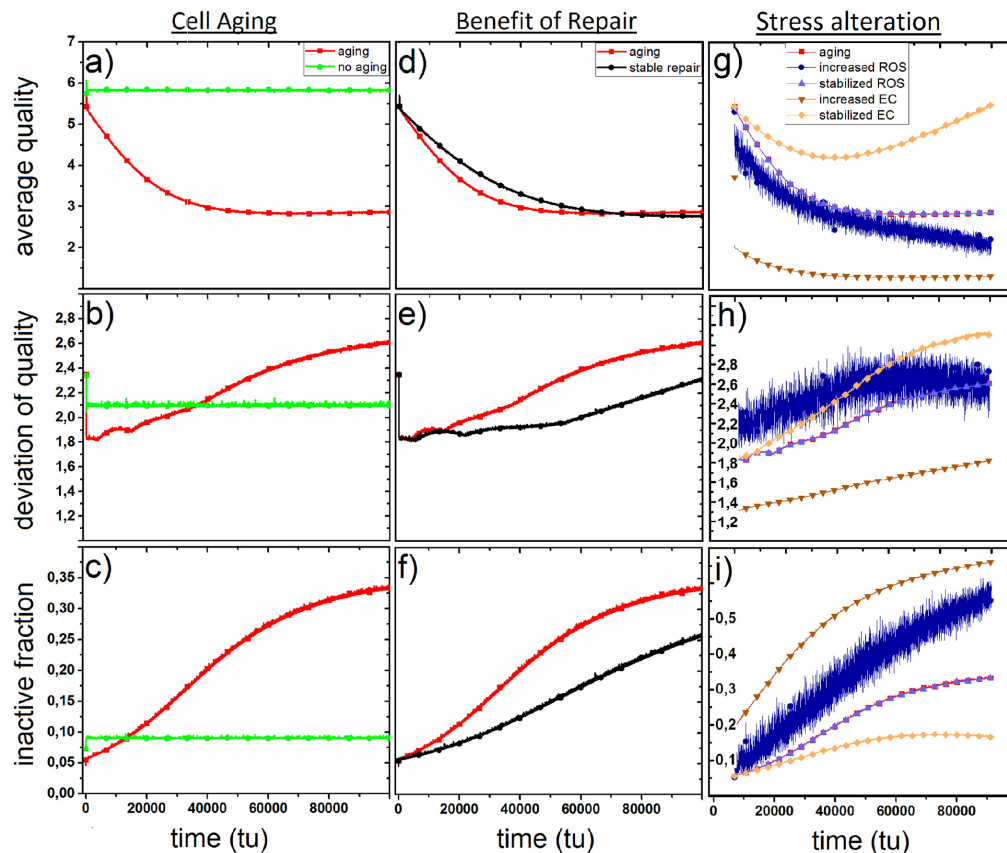
Fig 3. a–c: Comparison of impact of a aging (red) and non-aging (green) of mitochondrial processes on average quality, deviation of quality and fraction of inactive mitochondria with values for free parameters given in Table 1. d–f: Comparison of an aging process with physiologically decreasing repair (red) and an aging process with physiologically stable repair (black) concerning average quality, deviation of quality and fraction of inactive states. g–i: Alteration of parameters in energy consumption (increase of $\rho_{0, ec}$ in dark brown, temporal stabilization in light brown) and external damage (increase of $\rho_{0, ed}$ in dark blue, temporal stabilization in light blue) concerning average quality, deviation of quality and fraction of inactive states compared to aging (red).

doi:10.1371/journal.pone.0146973.g003

2.611 at 100000 tu. The non-aging process leads to stable values over time for all parameters: $\overline{q}(t) = 5.850$, $\sigma_q(t) = 2.134$ and $P(0, t) = 0,095$.

Stable repair

We compare the physiologically decreasing repair mechanism with a theoretically stable repair. In order to simulate a stable repair mechanism the lifetime $\tau_{0, rep}$ is set to 500000000 tu. A comparison of these two simulations (Fig 3d–3f) reveals that only until about 70000 tu a stable repair mechanism is superior to decreasing mitochondrial repair in terms of the average quality $\overline{q}(t)$. From that point in time on a decreasing repair mechanism leads to a higher average

quality than stable mitochondrial repair. The fraction of inactive states $P(0, t)$ and the deviation of quality $\sigma_q(t)$ is lower for stable mitochondrial repair at all points in time.

Change of ROS production and metabolic activity

In these simulations we investigate the behavior of mitochondrial quality if the conditions of external ROS production and metabolic activity of mitochondria alter. For that purpose, the starting probabilities of the energy consumption is increased to $\rho_{0,\,ec} = 0.05$, while $\rho_{0,\,ed}$ and f_{rd} are set to 0.1 and 0.3, respectively. Furthermore, we simulate a stabilization of both processes over time by setting the lifetimes τ_{ec} and τ_{ed} to 500000000 tu. Simulations show that an increase of production of oxidative stress as well as a higher metabolic activity (3g-i) leads to a faster loss of quality of mitochondria over time. The increased fluctuation of the dark blue plot is the result of the increased randomization of the production of ROS by externalities. Stabilizing the energy consumption process helps the network to sustain its integrity and even increase it in aged cells. Stabilizing the external damage has no effect on mitochondrial qualities.

High energy demanding cells

Here, we present different strategies cells with high energy demands could apply to sustain their mitochondrial quality. High energy demanding cells (hec) establish an increased oxidative phosphorylation in order to cope with their high demands for ATP. This mechanism leads to a higher production of reactive oxygen species in mitochondria.

Therefore, we raise the starting probability $\rho_{0,\,ec}$ to 0.05, representing an increased mitochondrial damage induced by internal oxidative stress. The black graphs in Fig 4a–4i indicate the time-dependence of the three quality parameters in high energy demanding cells. The average quality $\overline{q}(t)$ rapidly decreases with time and asymptotically approaches a value of about 1.650, the deviation of quality $\sigma_q(t)$ increases during the aging of the cell to about 1.800 and the inactive fraction $P(0, t)$ grows to 0.650 after 100000 tu. We simulated several possible alterations of the networking and recycling processes in order to compensate for the loss of quality. The starting probabilities $\rho_{0,\,mb}$ and/or $\rho_{0,\,FF_{m,\,p}}$ of were raised by five times and/or the temporal change was prohibited by increasing the lifetimes τ_{mb} and/or $\tau_{FF_{mathrmm,\,p}}$ to 500000000 tu. In the plots of Fig 4 these changes are indicated by green arrows (increase of starting probabilities) and a red arrows (increase of lifetimes).

In Fig 4a–4c alterations of the parameters of the networking process in high energy demanding cells are presented. The single increase of the starting probability and the single temporal stabilization of the process leads only to marginal changes in the three quality parameters. The single raise of the starting probability induces only a slight increase of the average quality and a bigger increase of the deviation of quality at the beginning of the simulations. A change of both, $\rho_{0,\,FF_{m,\,p}}$ and $\tau_{FF_{m,\,p}}$ leads to bigger increases of $\overline{q}(t)$ and $\sigma_q(t)$ at the beginning of the simulation which decline over time and a slight decrease of the inactive fraction of mitochondria $P(0, t)$ compared to an unmodified high energy demanding cell.

Fig 4d–4f depicts modifications of the parameters of the recycling process in high energy demanding cells. An increase of the starting probability raises drastically the average quality and the deviation of quality. Additionally, the inactive fraction of mitochondria decreases. These changes are stable in time. A temporal stabilization of the recycling process results in a very low average quality and an increase of $P(0, t)$ to about 0.9 after 100000 tu. A combination of the alterations in both parameters leads to a increase of $\overline{q}(t)$ at the beginning of the simulation which then drastically falls to lower values. In the same drastic manner the inactive fraction $P(0, t)$ climbs to about 0.7 at 100000 tu.
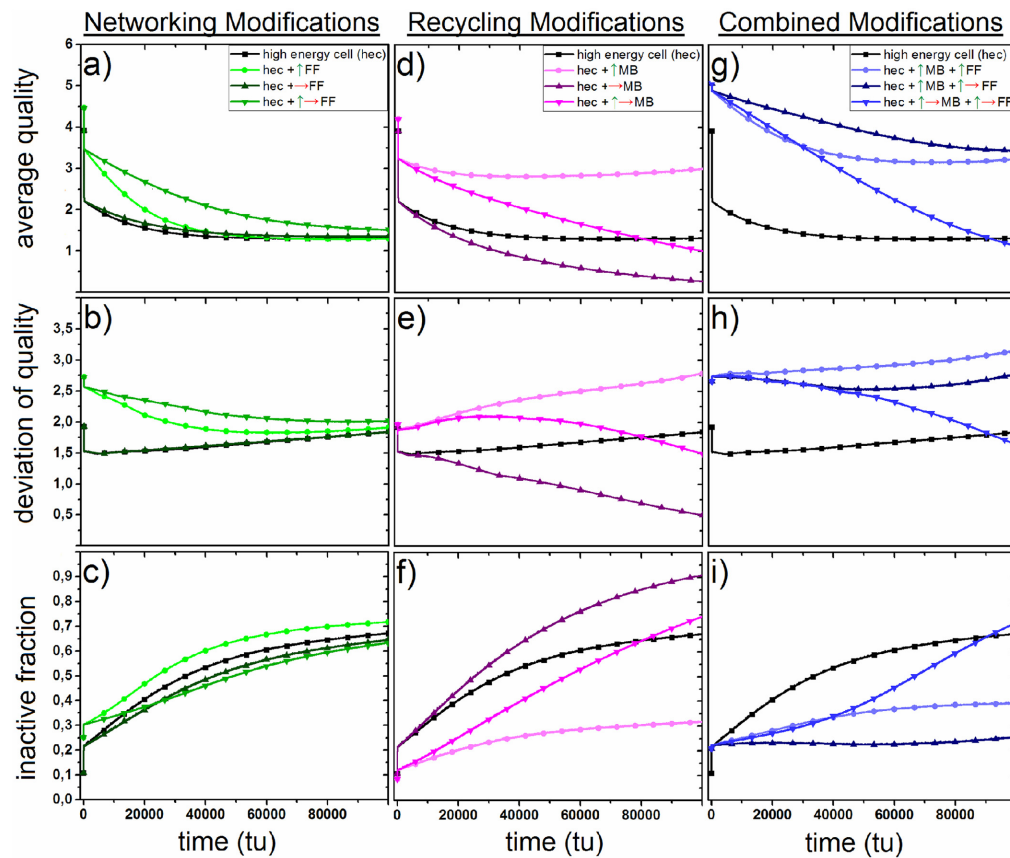
Fig 4. a–c: Development of mitochondrial average quality, deviation of mitochondrial quality and fraction of inactive mitochondria during the aging of a cell with high energy demand ($\rho_{0,\,ec} = 0.05$, black). The turquoise graphs represent modifications in fission and fusion parameters in high energy demanding cells. (green arrow: ρ_0, $FF_{m,\,p} = 0.5$, red arrow: $\tau FF = 500000000$). d–f: The violet graphs represent modifications in mitophagy and biogenesis parameters in high energy demanding cells. (green arrow: ρ_0, mb = 0.05, red arrow: τmb = 500000000). g–i: The blue graphs depict simulations with modifications in both, mitochondrial networking and mitochondrial recycling with same parameter alterations as above.

In Fig 4g–4i simulations with alterations of parameters in both processes are presented. Increases of starting probabilities of both networking and recycling lead to an increase of the average quality as well as the deviation of quality. Moreover, the inactive fraction of mitochondria is lower than in a unmodified high energy demanding cell. For simulations with a change of starting probabilities and lifetimes in both processes, networking and recycling, simulations show a high increase in average quality and few inactive mitochondria at the beginning of the simulations. However, the average quality decreases with time while the inactive fraction increase. This decrease of quality is attenuated in simulations with no temporal stabilization of the recycling process but only changes of $\rho_{0,\,FF_{m,\,p}}$, $\rho_{0,\,mb}$ and $\tau_{FF_{m,\,p}}$. In these simulations the

average quality establishes the highest values and the inactive fraction the lowest values during all points in time compared to all other simulations. The deviation of quality develops a moderate level compared to other modifications.

Discussion

During the aging of cells mitochondria run through various mitochondrial dynamics. In recent years simulations based on biophysical models of mitochondrial network structures have been performed in order to detect underlying mechanisms behind perfunctory mitochondrial processes. In the new mitochondrial model presented in this publication, five distinct mitochondrial processes were taken into account: A recycling mechanism consisting of mitochondrial biogenesis and mitophagy, mitochondrial networking represented by fission and fusion processes involving proteins and metabolites, internal oxidative stress depending on the degree of the metabolic activity of a mitochondrium as well as stochastic external oxidative stress. Additionally, a repairing process was introduced which represents the regain of mtDNA integrity. The original model of Figge et al. included a mitochondrial process called infectious molecular damage which was designed to take into account the spreading of mtDNA mutations during fission and fusion processes. However, there is no evidence in literature that impairing mtDNA mutations are propagated by mitochondrial networking. Although it was observed that after a fission process one daughter mitochondrium establishes a depolarized MMP, this is not connected to the spreading of intramitochondrial damage but to the induction of mitophagy and the corresponding mitochondrial recycling mechanism. [31]

We investigated three mitochondrial quality parameters: The average quality $\overline{q}(t)$ represents the well-being of the mitochondrial network in total. The deviation of quality $\sigma_q(t)$ gives a degree of how equally the overall quality is distributed among mitochondria. The higher $\sigma_q(t)$, the more the qualities in the mitochondrial network are polarized. The third parameter $P(0, t)$ represents the fraction of inactive mitochondria. Mitochondria in this state are not involved in any networking processes of fission and fusion of neither metabolites nor proteins. These mitochondria lie isolated in the cell and wait for either the repair mechanism to restore their integrity or the mitophagy to remove them. Hence, the fraction of inactive mitochondria represents the degree of fragmentation of the mitochondrial network.

Several free parameters such as lifetimes and starting probabilities of mitochondrial processes have to be chosen in advance of the simulations. The values for these parameters can hardly be determined by literature as many publications handle with different cell types which differentiate regarding the velocity of their internal processes. Furthermore, many of these parameters cannot be measured directly. Thus, the free values of the simulations were estimated relatively to each other. Considering this, the model is fertile for qualitative analysis but is of limited use for exact quantifications.

Additionally, it has to be taken into account that there is no evidence regarding a coupling of mitophagy and biogenesis concerning the total mitochondrial mass. In this model the coupling of both processes is necessary in order to maintain the overall probability at a constant value of 1. Actually, contrary to the increasing mitochondrial autophagy there are indications that aging might degenerate the cell's ability to perform mitochondrial biogenesis. [30] In order to perform more exact quantifications of the mitochondrial mass in future, one has to suspend the probabilistic approach from the model and substitute it with absolute values.

Influence of single processes

At first, we investigated the single impact of the individual processes which are defined in the mitochondrial quality model. For most of them their influence on mitochondrial qualities is

rather intuitive. The repair mechanism increases the average mitochondrial quality to the maximum value of 10, implying that all mitochondria establish the highest quality state. For logical reasons the fraction of inactive states and the deviation of quality fall correspondingly to 0. Hence, the repair mechanism leads to a mitochondrial network with a maximum of interconnections and mitochondria of high quality without exception. In contrast, internal oxidative stress due to energy consumption by mitochondria and random external oxidative stress generated by other organelles in the cell lead to an average quality of 0. The decrease of the average quality happens to be faster for internalities than for externalities stress implying that mitochondria are more damaged by themselves than by other cell organelles. Intuitively, both processes increase the fraction of inactive states to 1 and decrease the deviation of quality to 0. Hence, both, internal and external oxidative stress lead to a fully fragmented mitochondrial network consisting only of inactive mitochondria.

Interplay of mitophagy and recycling

Mitophagy and biogenesis are on their own only slightly quality increasing processes in terms of the average quality. After removing all inactive mitochondria from the mitochondrial network mitophagy is not able to remove other mitochondria so that biogenesis can not generate mitochondria with high qualities. In other words: The recycling process stagnates if there are no inactive mitochondria with quality state 0 present in the mitochondrial network. In order to keep the mitochondrial recycling process running mitochondrial fission and fusion generates a significant amount of inactive mitochondria. Investigating networking separately for metabolites and proteins we observe different impacts on mitochondrial quality. Metabolic fission and fusion changes neither the average quality nor the fraction of inactive states but decreases the deviation of quality. This process helps to spread metabolites throughout the cell and increases the corresponding entropy. Fission and fusion of proteins increases moderately the average quality, the deviation of quality and the fraction of inactive states. The interplay of both kinds of fission and fusion prevents the quality increase of proteinaceous networking but only maintains the overall quality level of the starting distribution due to the generation of more inactive mitochondria (0.48 (total) vs 0.28 (proteins) vs 0.09 (metabolites). This effect helps to strongly induce the recycling mechanism of mitophagy and biogenesis without loosing overall quality in the mitochondrial network. Although neither recycling nor networking are on their own quality increasing processes, together they increase the overall mitochondrial quality to the maximum value of 10. Accordingly, the fraction of inactive mitochondria and the deviation of quality fall to 0. This interplay of networking and recycling is proposed in literature. It was observed experimentally that after a fission event there is a high probability that one daughter mitochondrion establishes a depolarized membrane potential accompanied by decreased levels of the fusion protein OPA1 while the other daughter mitochondrion remains metabolically active. As preautophagic mitochondria reduce their membrane potential and OPA1 levels, these results suggest that fission events induce recycling processes.[31] Our simulations support these findings and reveal a connection between two single processes which are not directly connected within the definitions of the mitochondrial quality model.

Mitochondrial quality during aging

Over time all mitochondrial processes together lead to a decrease of the average mitochondrial quality and an increase of both, fragmentation and deviation of quality of the mitochondrial network. An age-related fragmentation of the mitochondrial network was observed *in vitro* recently. It was shown that in muscle cells of nematode C. elegans mitochondrial morphologies fragment with increasing age in terms of smaller mitochondrial volumes.[18] Additionally,

investigations of cultured skin fibroblasts revealed less elongated mitochondria in cells of old volunteers than of young volunteers. [19] Hence, these experimental results validate the presented model.

The simulations indicate that the fragmentation is connected to an increasing number of inactive mitochondria which can not all be recycled by mitophagy and biogenesis. The increasing number of inactive mitochondria also explains the observed perturbations of fission and fusion cycles during aging in various experiments. The original model by Figge et al. suggests that decreased networking among mitochondria prevents the spread of infectious mitochondrial damage. However, so far there is no experimental evidence that mitochondria can infect each other by fusion processes. Instead, fission and fusion induces the recycling mechanism by generating inactive mitochondria. As the number of inactive mitochondria grow during aging due to internal and external oxidative stress the networking mechanism becomes obsolete regarding this point. Therefore decelerated networking prevents the generation of inactive mitochondria which are not necessary to induce mitochondrial recycling in aged cells due to the excessive supply of inactive mitochondria by damaging processes of internal and external oxidative stress. Interestingly, in aged cells the average quality of mitochondria exhibits asymptotic behavior and remains stable at an average quality of about 3 with even a slight increase to higher qualities. As the fraction of inactive mitochondrial states increases monotonously during aging of cells mitochondrial fragmentation does not necessarily correlate to a decrease of the well-being of the mitochondrial network. Hence, fragmentation might be a quality saving process at some point.

The benefit of decreasing mitochondrial repair

The slight but unexpected increase of mitochondrial qualities in aged cells can paradoxically be explained with the decrease of mitochondrial repair during aging. A comparison of the aging process with simulations of stable mitochondrial repair reveals that a non-decreasing repair mechanism is only quality saving until a certain point in time. Afterwards the actual aging process is even superior to stable repair. This paradoxical result is explained by a comparison of the fraction of inactive mitochondria in both simulations. The number of inactive mitochondria is constantly lower for the stable repair process even after having a lower average quality than the actual aging simulation. This indicates that the repair mechanism saves mitochondria from becoming inactive so that they cannot be removed by mitophagic processes and recycled by mitochondrial biogenesis. Thus, in an aged cell a stable repair mechanism thwarts mitochondrial recycling compared to a decreased repair mechanism. This context explains the slight increase of the average mitochondrial quality at the end of the aging simulation. The decreased repair mechanism fails in preventing mitochondria from becoming inactive. Thus, there is a higher probability for mitochondrial recycling to replace the inactive mitochondria with high quality mitochondria that increases the overall quality the mitochondrial network.

Mitochondrial qualities in stressed cells

Environmental circumstances such as high UV radiation or pathogens occasionally require cells to perform high metabolic activities and stimulate the production of reactive oxygen species. These circumstances are simulated by increasing probabilities of external damage and energy consumption. Simulations show that stress leads to degradation of mitochondrial qualities as well as a higher number of isolated mitochondria revealing growing mitochondrial fission states. These results are validated by experimental observations on human lung adenocarcinoma cells. Under the condition of oxidative stress induced by high-fluence low-power laser radiation these cells display a fragmented structure of the mitochondrial network.[39]

Consequently, a stabilization of the production of reactive oxygen species by electron transport chain helps mitochondria to sustain a high quality level and to prevent a high number isolated mitochondria and a fragmented mitochondrial network, respectively. Under this condition we even observe an increase of mitochondrial qualities in aged cells. The reason for this unphysiological behavior might be that in the model so far a coupling of recycling and oxidative stress is not included. It is questionable if the frequency of mitophagy is still increasing in aged cells if oxidative stress is kept at a low level. Therefore, a future expansion of the differential equation in the model should implement a coupling term between recycling and oxidative stress in order to take into account the corresponding feedback.

Sustaining mitochondrial quality in high energy demanding cells

Many active cell types in human tissue of liver, heart or brain require an elevated supply with ATP in order to maintain their functioning. We simulated those cells with high energy demands by increasing their probability of producing internal oxidative stress. Consequently, mitochondria in energy demanding cells harm their own integrity more than cells with a common energy metabolism. This leads to a low quality within the mitochondrial network accompanied by a high fraction of inactive mitochondria that increases during the aging of the cell. As many cells such as hepatocytes or neurons [40], [41] rely on a constant and high-quality supply with energy, mitochondria in these cells have to develop strategies to handle the loss of quality due to their internal oxidative stress. Two processes which appear to be at least partially controlled by mitochondria to sustain their quality are their networking and their recycling. Hence, we modified the free parameters of these processes to identify mechanisms that establish a healthy quality level in mitochondria of energy demanding cells.

Simulations show that isolated single changes in neither starting probability nor the temporal attenuation of networking lead to a distinct increase in the average quality among mitochondria. A combination of an alteration of both parameters results in a moderate increase of average qualities and a corresponding decrease of inactive mitochondria at the beginning of the simulation. This improvement in qualities falls during the aging of cells. Nevertheless it appears to be a valid strategy for mitochondria in energy demanding cells, to increase their probability for fission and fusion and to a stabilize a high level of networking during the aging of the cell in order to keep a high level of quality within the mitochondrial network at least at the beginning of its lifetime. However, this mechanism is accompanied by an increased deviation of quality among mitochondria. This observation suggests that the mechanism helps to generate high quality states of mitochondria at specific locations of high energy demands within the cell but it does not support maintaining a high quality level within the whole mitochondrial network. While a temporal stabilization of the recycling process leads to a drastic decrease of average qualities, an increase of the starting probability for recycling results in a significant increase of the qualities of mitochondria. The improvement is stable during the aging of the cell.

Adding this increase of the probability for recycling to the combined changes in parameters of networking, mitochondria establish an even higher average quality with less deviation in quality and a low fraction of inactive mitochondria. Compared to this strategy, other modifications on networking and recycling are either not significantly quality increasing or have restrictions in terms of their time dependence. Attenuating the temporal change in both processes, networking and recycling as well as an increase in the starting probabilities of both processes increases qualities of mitochondria the beginning of the lifetime of the cell, but this improvement cannot be maintained during aging. Hence, attenuating the decrease of networking processes in addition to a higher starting probabilities of networking and recycling appears to be

the best strategy in order to keep a high, widely spread quality level among mitochondria in energy demanding cells.

Conclusion

In conclusion, we introduced a novel mitochondrial quality model based on the approach of Figge et al in 2012. In the model we transfer the latest findings of experimental research on mitochondrial processes during the aging of cells into explicitly defined biophysical processes. Additionally, we introduce a universal decay and growth law for each mitochondrial process which describes its time-dependence during the aging of cells. Simulations are in coherence with experimental investigations of the mitochondrial network and support current hypotheses about the interplay of distinct mitochondrial processes, revealing new mechanisms that influence mitochondrial qualities during the aging of cells. Our model proposes a fragmentation of the mitochondrial network during aging, suggests a quality increasing coupling of mitochondrial recycling and networking and displays a quality saving mechanism by the decrease of mitochondrial repair functionalities in aged cells. Furthermore, simulations propose that temporal stabilization of networking accompanied by an increase of probabilities in recycling and fission and fusion is a significant quality saving strategy in cells with high energy demands. Overall, the revealed findings give new insights in mitochondrial processes during aging, providing suggestions for further experimental investigations in future.

Supporting Information

S1 Fig. a–c: Interplay of networking and recycling with modified parameters in networking (turquoise, $\rho_{0,\,FF_{m,\,p}} = 0.1$, $\tau_{FF_{m,\,p}} = 100000$) tu and recycling (violet, $\rho_{0,\,mb} = 0.02$, $\tau_{mb} = 100000$) tu. Apart from slight differences at the beginning of each simulation the parameter modifications do not change the qualitative outcome presented in Fig 2d–2f. d–f: Temporal stabilized repair mechanism (dark grey) with modified parameters ($\rho_{0,\,rep} = 0.02$) compared with an unmodified aging process. The point in time at which natural aging is superior to a stabilized repair mechanism is delayed in this simulation to about 100000 tu but the qualitative outcome in Fig 3d–3f is confirmed.
(TIF)

Author Contributions

Conceived and designed the experiments: DM. Performed the experiments: DM. Analyzed the data: DM FF MR SJ HW. Contributed reagents/materials/analysis tools: DM. Wrote the paper: DM FF MR. Designed the model: DM FF MR. Wrote corresponding code in Java: DM.

References

1. Figge MT, Reichert AS, Meyer-Hermann M, Osiewacz HD. Deceleration of fusion-fission cycles improves mitochondrial quality control during aging. PLoS Comput Biol. 2012; 8(6):e1002576. doi: 10.1371/journal.pcbi.1002576 PMID: 22761564

2. Miquel J, Economos AC, Fleming J, Johnson J J E. Mitochondrial role in cell aging. Exp Gerontol. 1980; 15(6):575–91. doi: 10.1016/0531-5565(80)90010-8 PMID: 7009178

3. Balaban RS, Nemoto S, Finkel T. Mitochondria, oxidants, and aging. Cell. 2005; 120(4):483–95. doi: 10.1016/j.cell.2005.02.001 PMID: 15734681

4. Lodish H. Molecular Cell Biology. Freeman, W. H. & Company; 2004.

5. Leyssens A, Nowicky AV, Patterson L, Crompton M, Duchen MR. The relationship between mitochondrial state, ATP hydrolysis, [Mg2+], and [Ca2+](i) studied in isolated rat cardiomyocytes. Journal of Physiology-London. 1996; 496(1):111–128. doi: 10.1113/jphysiol.1996.sp021669

6. Yakes FM, Van Houten B. Mitochondrial DNA damage is more extensive and persists longer than nuclear DNA damage in human cells following oxidative stress. Proc Natl Acad Sci U S A. 1997; 94 (2):514–9. doi: 10.1073/pnas.94.2.514 PMID: 9012815

7. Shokolenko I, Venediktova N, Bochkareva A, Wilson GL, Alexeyev MF. Oxidative stress induces degradation of mitochondrial DNA. Nucleic Acids Res. 2009; 37(8):2539–48. doi: 10.1093/nar/gkp100 PMID: 19264794

8. Lin MT, Beal MF. Mitochondrial dysfunction and oxidative stress in neurodegenerative diseases. Nature. 2006; 443(7113):787–95. doi: 10.1038/nature05292 PMID: 17051205

9. Busch KB, Kowald A, Spelbrink JN. Quality matters: how does mitochondrial network dynamics and quality control impact on mtDNA integrity? Philos Trans R Soc Lond B Biol Sci. 2014; 369 (1646):20130442. PMID: 24864312

10. Nakada K, Inoue K, Ono T, Isobe K, Ogura A, Goto YI, et al. Inter-mitochondrial complementation: Mitochondria-specific system preventing mice from expression of disease phenotypes by mutant mtDNA. Nat Med. 2001; 7(8):934–40. doi: 10.1038/90976 PMID: 11479626

11. Rolland SG, Motori E, Memar N, Hench J, Frank S, Winklhofer KF, et al. Impaired complex IV activity in response to loss of LRPPRC function can be compensated by mitochondrial hyperfusion. Proc Natl Acad Sci U S A. 2013; 110(32):E2967–76. doi: 10.1073/pnas.1303872110 PMID: 23878239

12. Kim I, Rodriguez-Enriquez S, Lemasters JJ. Selective degradation of mitochondria by mitophagy. Arch Biochem Biophys. 2007; 462(2):245–53. doi: 10.1016/j.abb.2007.03.034 PMID: 17475204

13. Jornayvaz FR, Shulman GI. Regulation of mitochondrial biogenesis. Essays Biochem. 2010; 47:69–84. doi: 10.1042/bse0470069 PMID: 20533901

14. Larsen NB, Rasmussen M, Rasmussen LJ. Nuclear and mitochondrial DNA repair: similar pathways? Mitochondrion. 2005; 5(2):89–108. PMID: 16050976

15. Youle RJ, van der Bliek AM. Mitochondrial fission, fusion, and stress. Science. 2012; 337(6098):1062–5. doi: 10.1126/science.1219855 PMID: 22936770

16. Patel PK, Shirihai O, Huang KC. Optimal dynamics for quality control in spatially distributed mitochondrial networks. PLoS Comput Biol. 2013; 9(7):e1003108. doi: 10.1371/journal.pcbi.1003108 PMID: 23874166

17. Mouli PK, Twig G, Shirihai OS. Frequency and selectivity of mitochondrial fusion are key to its quality maintenance function. Biophys J. 2009; 96(9):3509–18. doi: 10.1016/j.bpj.2008.12.3959 PMID: 19413957

18. Regmi SG, Rolland SG, Conradt B. Age-dependent changes in mitochondrial morphology and volume are not predictors of lifespan. Aging (Albany NY). 2014; 6(2):118–30.

19. Sgarbi G, Matarrese P, Pinti M, Lanzarini C, Ascione B, Gibellini L, et al. Mitochondria hyperfusion and elevated autophagic activity are key mechanisms for cellular bioenergetic preservation in centenarians. Aging (Albany NY). 2014; 6(4):296–310.

20. Liu X, Weaver D, Shirihai O, Hajnoczky G. Mitochondrial 'kiss-and-run': interplay between mitochondrial motility and fusion-fission dynamics. EMBO J. 2009; 28(20):3074–89. doi: 10.1038/emboj.2009.255 PMID: 19745815

21. Twig G, Shirihai OS. The interplay between mitochondrial dynamics and mitophagy. Antioxid Redox Signal. 2011; 14(10):1939–51. doi: 10.1089/ars.2010.3779 PMID: 21128700

22. Alexeyev M, Shokolenko I, Wilson G, LeDoux S. The maintenance of mitochondrial DNA integrity—critical analysis and update. Cold Spring Harb Perspect Biol. 2013; 5(5):a012641. doi: 10.1101/cshperspect.a012641 PMID: 23637283

23. Liu Y, Fiskum G, Schubert D. Generation of reactive oxygen species by the mitochondrial electron transport chain. J Neurochem. 2002; 80(5):780–7.

24. Kampen NGv. Stochastic Processes in Physics and Chemistry. 3rd ed. North-Holland Personal Library; 2007.

25. Winter ME. Basic Clinical Pharmacokinetics. 5th ed. Lippincott Williams and Wilkins; 2009.

26. Schwarz TL. Mitochondrial trafficking in neurons. Cold Spring Harb Perspect Biol. 2013; 5(6). doi: 10.1101/cshperspect.a011304 PMID: 23732472

27. van der Bliek AM, Shen Q, Kawajiri S. Mechanisms of mitochondrial fission and fusion. Cold Spring Harb Perspect Biol. 2013; 5(6). doi: 10.1101/cshperspect.a011072 PMID: 23732471

28. Chen H, Vermulst M, Wang YE, Chomyn A, Prolla TA, McCaffery JM, et al. Mitochondrial fusion is required for mtDNA stability in skeletal muscle and tolerance of mtDNA mutations. Cell. 2010; 141 (2):280–9. doi: 10.1016/j.cell.2010.02.026 PMID: 20403324

29. Hill AV. The possible effects of the aggregation of the molecules of haemoglobin on its dissociation curves. The Journal of Physiology. 1910; 40(iv–vii).

PLOS | ONE

30. Seo AY, Joseph AM, Dutta D, Hwang JC, Aris JP, Leeuwenburgh C. New insights into the role of mitochondria in aging: mitochondrial dynamics and more. J Cell Sci. 2010; 123(Pt 15):2533–42. doi: 10.1242/jcs.070490 PMID: 20940129

31. Twig G, Elorza A, Molina AJ, Mohamed H, Wikstrom JD, Walzer G, et al. Fission and selective fusion govern mitochondrial segregation and elimination by autophagy. EMBO J. 2008; 27(2):433–46. doi: 10.1038/sj.emboj.7601963 PMID: 18200046

32. Palikaras K, Tavernarakis N. Mitochondrial homeostasis: the interplay between mitophagy and mitochondrial biogenesis. Exp Gerontol. 2014; 56:182–8. doi: 10.1016/j.exger.2014.01.021 PMID: 24486129

33. Oberley TD, Swanlund JM, Zhang HJ, Kregel KC. Aging results in increased autophagy of mitochondria and protein nitration in rat hepatocytes following heat stress. J Histochem Cytochem. 2008; 56(6):615–27. doi: 10.1369/jhc.2008.950873 PMID: 18379016

34. Wei YH, Lee HC. Oxidative stress, mitochondrial DNA mutation, and impairment of antioxidant enzymes in aging. Exp Biol Med (Maywood). 2002; 227(9):671–82.

35. Brown GC, Borutaite V. There is no evidence that mitochondria are the main source of reactive oxygen species in mammalian cells. Mitochondrion. 2012; 12(1):1–4. doi: 10.1016/j.mito.2011.02.001 PMID: 21303703

36. Lipsky NG, Pedersen PL. Mitochondrial turnover in animal cells. Half-lives of mitochondria and mitochondrial subfractions of rat liver based on [14C]bicarbonate incorporation. J Biol Chem. 1981; 256 (16):8652–7. PMID: 7263675

37. Menzies RA, Gold PH. The turnover of mitochondria in a variety of tissues of young adult and aged rats. J Biol Chem. 1971; 246(8):2425–9. PMID: 5553400

38. Miwa S, Lawless C, von Zglinicki T. Mitochondrial turnover in liver is fast in vivo and is accelerated by dietary restriction: application of a simple dynamic model. Aging Cell. 2008; 7(6):920–3. doi: 10.1111/j.1474-9726.2008.00426.x PMID: 18691181

39. Wu S, Zhou F, Zhang Z, Xing D. Mitochondrial oxidative stress causes mitochondrial fragmentation via differential modulation of mitochondrial fissoin-fusion proteins. FEBS Journal. 2011; 278:941–954. doi: 10.1111/j.1742-4658.2011.08010.x PMID: 21232014

40. Berndt N, Holzhutter HG. The high energy demand of neuronal cells caused by passive leak currents is not a waste of energy. Cell Biochem Biophys. 2013; 67(2):527–35. doi: 10.1007/s12013-013-9538-3 PMID: 23479331

41. Cervinkova Z, Lotkova H, Krivakova P, Rousar T, Kucera O, Tichy L, et al. Evaluation of mitochondrial function in isolated rat hepatocytes and mitochondria during oxidative stress. Altern Lab Anim. 2007; 35 (3):353–61. PMID: 17650955

Chapter 3

Mitochondrial Morphology Model

In chapter 2, the change of mitochondrial qualities during the aging of the cell was simulated in a biophysical model based on the model of Figge et al. [17]. In this chapter, a novel approach is presented, that correlates mitochondrial morphologies with mitochondrial qualities. A computational model was designed, that considers mitochondria as quality-dependent units that undergo biological processes and move within an virtual cell.

3.1   Model

In extremely stressful environments, as, e.g. during electromagnetic radiation, the mitochondrial network dissipates and establishes highly fragmented fission states [43]. Visualizations with electron microscopy reveal, that mitochondrial clusters appear as small bean-like structures. [44] Ramified mitochondrial networks are formed by the merging of many of these small mitochondrial filaments by an interaction of their membranes. [45] Hence, it is reasonable to assume, that highly interconnected mitochondrial networks consist of many small mitochondrial clusters. In the following presentation of the model, these small bean-like structures are called smallest mitochondrial units (SMUs).
Mitochondria move within the cytoplasm of a cell in order to supply energy demanding cell functions and organelles with ATP and to share metabolites and healthy DNA among each other. This behavior was observed within large neurons and is called mitochondrial trafficking. [7] Experimental studies disclose a co-localization of mitochondria and cytoskeletal tubulin fibers. [46] Hence, it is assumed that mitochondria are transported via the tubulin network in the cytoplasm of a cell. [47] Microscopic investigations reveal that the dynamic network of microtubules is largely ramified and covers large spaces within

the cellular body. [48] For that reason, to a large extend the movement of mitochondrial clusters can supposed to be free.

FIGURE 3.1: Scheme of the morphological model
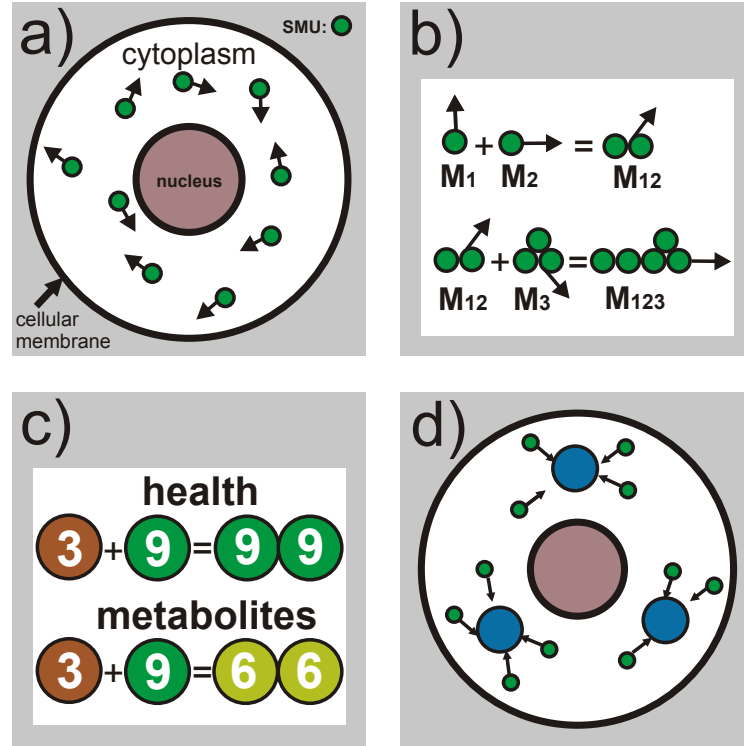
a) Smallest mitochondrial units (SMUs) (green) moving in arbitrary directions (black arrows) within the cytoplasm (white) of the virtual cell. b) Inelastic collisions of SMUs result in larger mitochondrial clusters. c) Change of quality parameters for health and metabolites during a fusion state. The health of the mitochondrial DNA of mitochondria with lower values is raised to the level of their fusion partner. In contrast, metabolites are distributed equally among fusion partners. d) SMUs are attracted by energy demanding ATP consumers (blue).

As a consequence of the described morphological insights on mitochondria, SMUs in the model are designed as units that move freely within the cytoplasm of a two-dimensional virtual cell. This cell is modeled as a circle with a concentric nucleus in the center (Figure 3.1a). Since in reality the cytoplasm in the cell is a viscid fluid [49], the motion of SMUs through the cell's architecture is thwarted. The equation of motion of a single SMU then reads as:

$$\frac{d^2\vec{r}}{dt^2} = -D\frac{d\vec{r}}{dt} \tag{3.1}$$

with $\vec{r}$ being the position of the SMU in lateral dimensions ($\vec{r}$={x,y}) and D being the damping constant of the cytoplasmic medium.

Various proteins and other molecules are attached to cellular and nuclear membranes. [50] Therefore, they do not possess smooth but rough surfaces. For this reason, at the borders of the cell and the nucleus the angle of reflection of SMUs is not equal to the angle of incidence. Instead, SMUs are reflected in random directions and loose an arbitrary amount of energy due to deformation forces upon reflection.

When SMUs or clusters of SMUs meet each other during their way throughout the cytoplasm in the model, they perform an inelastic collision. This mechanism reflects the fusion processes of mitochondrial clusters in reality. [51] During an inelastic collision, the momentum of participating SMUs is conserved (Figure 3.1b):

$$\vec{v}_{12} = \frac{\vec{v}_1 N_1 + \vec{v}_2 N_2}{N_1 + N_2} \qquad (3.2)$$

Here, $\vec{v}_1$ and $\vec{v}_2$ are the velocities of the mitochondrial clusters 1 and 2 prior the collision, while $\vec{v}_{12}$ is the velocity of the resulting cluster. Parameters N_1 and N_2 are the numbers of SMUs in the colliding clusters.

3.1.1 Qualities

In order to correlate mitochondrial morphologies and mitochondrial qualities, each SMU in the model is equipped with a quality q with a discrete value going from 0 to 20. Contrary to the quality model presented in chapter 2, q is separated into two subparameters $q_{\mathrm{h}} \in \{0, 10\}$ and $q_{\mathrm{m}} \in \{0, 10\}$:

$$q = q_{\mathrm{h}} + q_{\mathrm{m}} \qquad (3.3)$$

Here, q_{h} is a health parameter, which represents the integrity of the mitochondrial DNA of the corresponding SMU. A SMU with $q_{\mathrm{h}} = 10$ represents a mitochondrion with completely healthy DNA, while an SMU with a irreversibly harmed DNA has a value of $q_{\mathrm{h}} = 0$. Irreversibly harmed mitochondria are detached from the mitochondrial clusters they belong to by fission processes. [52] In the model, SMUs with a health of $q_{\mathrm{h}} = 0$ perform a fission process and detach from their cluster with a velocity v_{fission} in a random direction. During this process, the total momentum of involved SMUs is conserved. Subsequently, the detached SMU moves isolated in the cytoplasm.

Recent experiments disclosed, that mitochondria share their DNA upon fusion processes in order to compensate for each others failures. [10] In the model, if SMUs perform an

inelastic collision to aggregate to a larger cluster, the health parameter q_h of all involved SMUs is raised to the value of the SMU with the most intact DNA. Hence, sharing parts of DNA in fusion states is a quality raising process in the model. This reflects the fact, that during the fused state all SMUs are able to use each others healthy DNA sequences, in order to produce enzymes and proteins. (Figure 3.1c)

Parameter q_m represents the metabolic supply of a SMU. In addition to the mitochondrial DNA, mitochondria can share metabolites and solvable substances by merging their outer membrane. [9] While a SMU saturated with metabolites has a value of $q_m = 10$, a SMU totally lacking of metabolites establishes $q_m = 0$. If two SMUs meet each other and fuse, it is assumed in the model, that they share their free metabolites in an entropic manner. As a result, after the fusion process all involved SMUs have the same metabolic quality q_m. If their total amount of q_m is not divisible by the number of SMUs, the metabolites are distributed as equal as possible.

3.1.1.1   Quality changing processes

Similar to the quality model, the discrete values of both subparameters q_h and q_m form Markov chains. [53] The probabilities for the alterations between the states' values in 1 time unit (tu) are defined by the biological processes that act on mitochondria. The processes included in the model are described in the following:

- **Oxidative stress:** Over time, mitochondrial DNA and metabolic molecules are harmed by oxidative stress produced by themselves, by other cell organelles [21] and by UV radiation. [29] Hence, in the model this process decreases both quality parameters q_h and q_m by a value of 1 with the probability ρ_{ROS}.

- **Quality regain:** Mitochondria exhibit several processes that repair the integrity of their DNA. [20] Furthermore, they can reproduce and import enzymes and matrix proteins wasted during the production of ATP. [31] In the model, this mechanism is taken into account by increasing quality parameters by 1 with the probability ρ_{rep}.

- **Recycling:** Isolated mitochondria, that are metabolically inactive are removed from the cell by mitophagic processes and replaced by mitochondrial biogenesis. [40] In the model, SMUs that have performed a fission process are removed from the virtual cell by a mitophagic probability ρ_{mito}. In a second step, SMUs can be replaced with a maximum quality of $q = 20$ with a biogenetic probability ρ_{bio}. Thus, in contrast to the quality model (chapter 2), the mitochondrial mass is not constant over time.

3.1.2 Adenosin triphsophate consumers

So far, SMUs in the model form their morphology depending on their own quality. However, the purpose of mitochondrial clusters is to supply the cell with energy as ATP molecules. [5] Therefore, there has to be a coupling between the morphology of the mitochondrial network and the energy demanding cell functions. Experiments revealed, that different localizations in the cell have varying demands for ATP. [54] It is assumed that mitochondrial morphologies are formed by the demands for ATP in the cell. [55] In order to integrate the coupling between cell functions and the mitochondrial network in the model, SMU-attracting Mie potentials are added to the virtual cell, that represent ATP consuming cell sites (Figure 3.1d). These potentials V_C are defined as:

$$V_C = \frac{C_n}{|\vec{r}|^n} - \frac{C_m}{|\vec{r}|^m} \ \text{ with } \ C_n \geq C_m \ \text{ and } \ n \geq m \tag{3.4}$$

The negative term on the right-hand side in equation 3.4 represents the attraction of the Mie potential with attraction parameter C_m, while the positive term is repulsive with repulsion parameter C_n and prevents SMUs from falling into the center of the ATP consumer. This approach relies on the Lennard-Jones potential, which describes the interaction of uncharged and chemically unbound molecules and atoms. [56] In order to establish a long range attraction and a short range repulsion, the exponents in the denominator are set to $n =3$ and $m =2$, respectively. The demand for ATP of cell functions varies over time and ATP levels in cells tend to oscillate. [57] Therefore, the attraction parameter C_m is modeled as an oscillator:

$$C_m = C_{m_0} \sin(ft) + C_{m_0} \tag{3.5}$$

with C_{m_0} being half the maximum amplitude of the oscillator and f being the frequency of the energetic oscillation. With the spatial derivation of the Mie potential (3.4) leading to the acceleration, the equation of motion of a single SMU at $\vec{r}$ in the presence of i ATP consumers at postions $\vec{r_i}$ then reads as:

$$\frac{d^2\vec{r}}{dt^2} = \sum_i \left(-n\frac{C_{n_i}}{|\vec{r_i} - \vec{r}|^{n_i+1}} + m\frac{C_{m_i}}{|\vec{r_i} - \vec{r}|^{m_i+1}} \right) \frac{\vec{r_i} - \vec{r}}{|\vec{r_i} - \vec{r}|} - D\frac{d\vec{r}}{dt} \tag{3.6}$$

3.1.3 Aging

As described in chapter 2, the frequency of biological processes alter over time. This effect is called aging. In order to include an aging mechanism, process probabilities in

the morphology model change their values over time similar to the quality model. Again, the change of biological processes j is described by decay and growth laws:

$$\rho_j = \rho_{j_0}\exp(\pm\frac{t}{\tau}) \tag{3.7}$$

Here, τ represents the lifetime of the processes and ρ_{j_0} the corresponding starting probabilities. The sign of the exponent depends on the aging behavior of the process. Probabilities for mitophagy [42] and mitochondrial DNA repair [32] shrink during aging (negative sign), while both, mitochondrial DNA and production of metabolites get increasingly impaired during aging, so that the corresponding probability for oxidative stress grows (positive sign). [30]

3.2 Validation and results

The morphological model was computationally realized by implementing its mathematical definitions in the programming language Java [33] under usage of the packages *java.util.** [34], *java.io.** [35] and *java.swing.**. [58] All programming scripts are attached to Appendix B. The differential equation (3.6) was numerically solved using Euler's method with minimum time steps of $h = 1$ as in the numerical solution of the differential equation in the quality model (chapter 2). This solution assigns x and y coordinates to the center of each SMU. In following visualizations, the coordinates of the SMUs represent their position in the cytoplasm of the virtual cell. The total quality q of a SMU is given by its color coding going gradually from red (q=0) to green (q=20). In order to examine the characteristics of the model, several quantitative parameters are investigated. As morphological parameters, the total number of all SMUs N per cell, the average distance of all SMUs to the center of the cell $\overline{d}$ in pixels (pxl), the average size of mitochondrial clusters $\overline{n}$ in the number of SMUs they consist of and the average velocity $\overline{v}$ in pixels per time units $\frac{\text{pxl}}{\text{tu}}$ are investigated. Furthermore, as quality parameters the average health $\overline{q}_{\text{h}}$ of all SMUs and spreading of the metabolites given by the standard deviation of the metabolites parameter Δq_{m} among all SMUs are tracked.

The morphological model consists of various free parameters. In Table 3.1 the values of these parameters are defined for all following simulations, if they are not otherwise specified in the text.

Parameters r_{SMU}, r_{cell} and r_{nucleus} represent the radii for the SMUs, cell and the nucleus, while d_{fusion} gives the distance ($d=\sqrt{(x_1 - x_2)^2 + (y_1 - y_2)^2}$) at which two SMUs 1 and 2 recognize each other and perform a fusion process. The velocities v_{fission} and v_{biogen} represent the speed of SMUs after performing a fission process and after being generated

by biogenesis, respectively. The process probabilities for oxidative stress, quality regain by mitochondrial repair, mitophagy and biogenesis are given by ρ_{ROS}, ρ_{rep}, ρ_{mito} and ρ_{bio}. Parameter τ represents the lifetime of all growth and decay laws.

The values of these parameters are discussed in the following sections.

parameter	value
N_{start}	150
r_{cell}	250 pxl
r_{nucleus}	75 pxl
r_{SMU}	6 pxl
d_{fusion}	14 pxl
v_{fission}	$2\,\frac{\mathrm{pxl}}{\mathrm{tu}}$
v_{biogen}	$2\,\frac{\mathrm{pxl}}{\mathrm{tu}}$
ρ_{ROS}	0.01
ρ_{rep}	0.001
ρ_{mito}	0.01
ρ_{bio}	0.01
τ	5000 tu

TABLE 3.1: Free parameters in the morphological model

3.2.1 Starting conditions

Prior to the start of every simulation, to each SMU a random location in the cytoplasm of the virtual cell and a random velocity between $0\frac{\mathrm{pxl}}{\mathrm{tu}}$ and $8\frac{\mathrm{pxl}}{\mathrm{tu}}$ is assigned. In Figure 3.2 investigated parameters are shown over 10000 tu for five different starting distributions with the values for all free parameters as given in Table 3.1. Simulations were performed without considering impacts of the cell on mitochondrial morphologies by ATP consumers and cytoplasmic damping.

Neglecting fluctuations due to the randomness of mitochondrial processes acting on mitochondria, the mitochondrial network establishes a stationary state in all five simulations with the same values for all investigated parameters (average $\pm$ standard deviation): $N = 139.01 \pm 0.28$, $\overline{v} = 0.284 \pm 0.00\,\frac{\mathrm{pxl}}{\mathrm{tu}}$, $\overline{d} = 180.64 \pm 1.74\,\mathrm{pxl}$, $\overline{n} = 9.07 \pm 0.34\,\mathrm{SMUs}$, $\overline{q}_{\mathrm{h}} = 8.63 \pm 0.05$ and $\Delta q_{\mathrm{m}} = 3.42 \pm 0.01$. Hence, the outcomes of the model are not dependent from the starting distributions, that are fed into the algorithm.

3.2.2 Morphological parameters

The morphological appearance of the mitochondrial network in the model can be modified by altering the radii r_{SMU} of the SMUs relatively to the cells dimension and by

FIGURE 3.2: Simulations of morphology model with standard parameter set
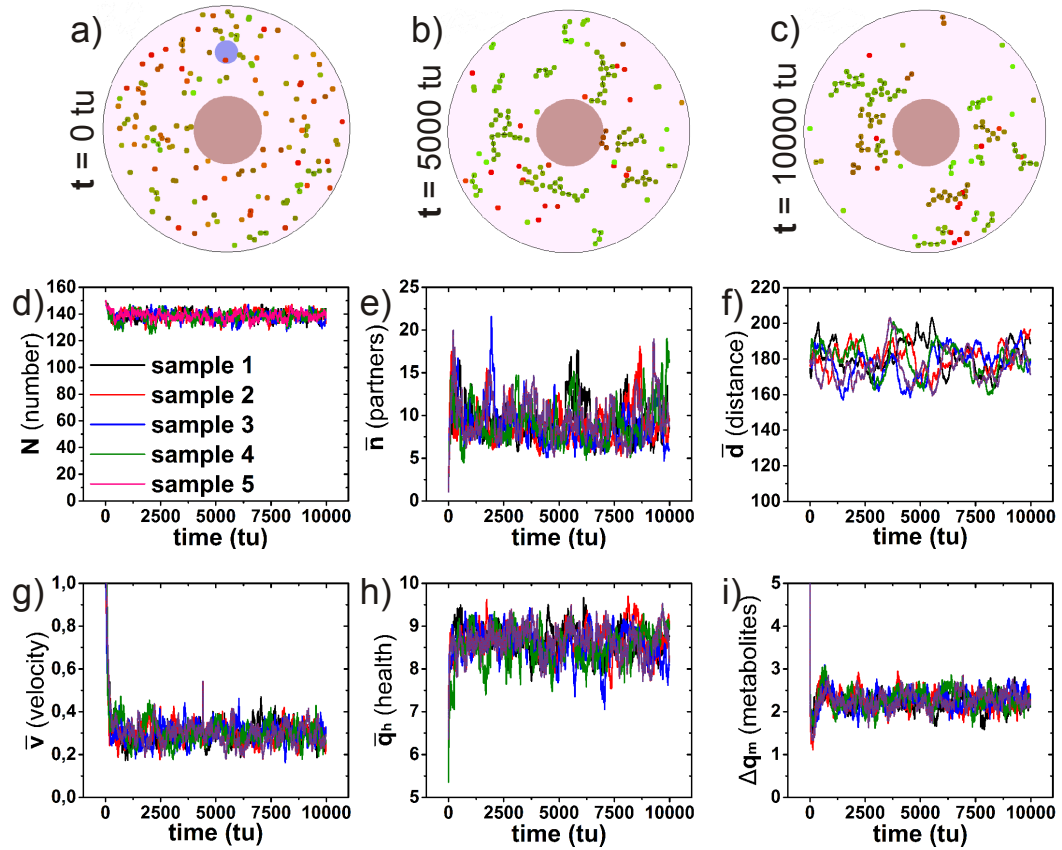
Simulation of mitochondrial network with standard parameter set (Table 3.1) at a) t=0 tu, b) t=5000 tu and c) t=10000 tu. SMUs are depicted in green to red colors according to their quality. The cytoplasm has a beige color, the nucleus is brown. Below, fluctuations of investigated parameters for five simulation samples: d) number of SMUs N representing the mitochondrial mass, e) average number of partners of SMUs $\bar{n}$ representing the mitochondrial cluster size, f) average distance $\bar{d}$ of SMUs to the center of the cell representing the position of mitochondria in the cytoplasm, g) average velocity $\bar{v}$ of SMUs representing mitochondrial motility, h) the average health parameter $\bar{q}_{h}$ representing the integrity of the mitochondrial DNA and i) the deviation of the metabolites parameter Δq_{m} representing the distribution of metabolites among mitochondria.

changing the number of SMUs N_{start}. In the following, consequences of these modifications are presented. Simulations were performed without considering morphological changes due to by ATP consumers and cytoplasmic damping.

3.2.2.1   Number of Smallest Mitochondrial Units

Simulations with $N_{\text{start}} = 50$, $N_{\text{start}} = 100$, $N_{\text{start}} = 150$ and $N_{\text{start}} = 200$ as the starting numbers of SMUs were performed. The rest of the free parameters were set according to Table 3.1. Averages of five simulations for each starting number are presented in Figure 3.3 and Table 3.2.

N_{start}	50	100	150	200
N (SMUs)	46.3 ± 0.2	92.5 ± 0.3	139.0 ± 0.3	185.0 ± 0.4
$\overline{n}$ (SMUs)	3.64 ± 0.18	6.37 ± 0.16	9.07 ± 0.34	11.64 ± 0.39
$\overline{v}$ ($\frac{\text{pxl}}{\text{tu}}$)	0.44 ± 0.01	0.34 ± 0.00	0.28 ± 0.00	0.25 ± 0.00
$\overline{d}$ (pxl)	183.2 ± 2.3	182.5 ± 2.7	180.6 ± 1.7	178.9 ± 2.5
$\overline{q}_{\text{h}}$	7.37 ± 0.06	8.21 ± 0.05	8.63 ± 0.05	8.91 ± 0.03
Δq_{m}	3.43 ± 0.03	3.43 ± 0.02	3.42 ± 0.01	3.42 ± 0.02

TABLE 3.2: Parameter values for different N_{start}

The investigations reveal, that raising the starting number of SMUs increases the average cluster size. A higher density of SMUs in the cytoplasm increases the probability of two SMUs meeting each other. Parallel the average velocity $\overline{v}$ of SMUs decreases with growing starting numbers. This behavior is directly connected to increased cluster sizes $\overline{n}$. The velocity vector of every SMU points in an arbitrary direction. Consequently, if all SMUs in the cell accumulated to a single cluster, the absolute value of the momentum of this large cluster would tend towards zero. Hence, larger clusters of SMUs lead to lower velocities.

These motion dynamics in the model might be related to the behavior of real mitochondria. Apart from being transferred to ATP dependent cell functions, mitochondria move in order to accumulate to efficient network structures. Hence, in mitochondrial networks with many interconnections an extensive mitochondrial motion is not necessary. Biological experiments have to be performed to validate this notion and to correlate the results with the outcomes of the model.

Additionally, higher starting numbers N_{start} lead to a higher average health $\overline{q}_{\text{h}}$ among SMUs. The explanation for an increasing mitochondrial health with N_{start} are larger average cluster sizes $\overline{n}$. The larger the clusters, the more healthy SMUs can share their intact DNA with harmed SMUs. This observation is in agreement with biological experiments showing that mitochondria establish a more interconnected network during phases of high energy demand, as e.g. in moderately stressed cells. [59]

The average distance of the SMUs to the center of the cell $\overline{d}$ and the metabolic variation in the system Δq_{m} are independent from the numbers of SMUs in the simulations. Both parameters establish in average the same levels for all N_{start}.

FIGURE 3.3: Simulations of morphology model with different starting numbers of SMUs
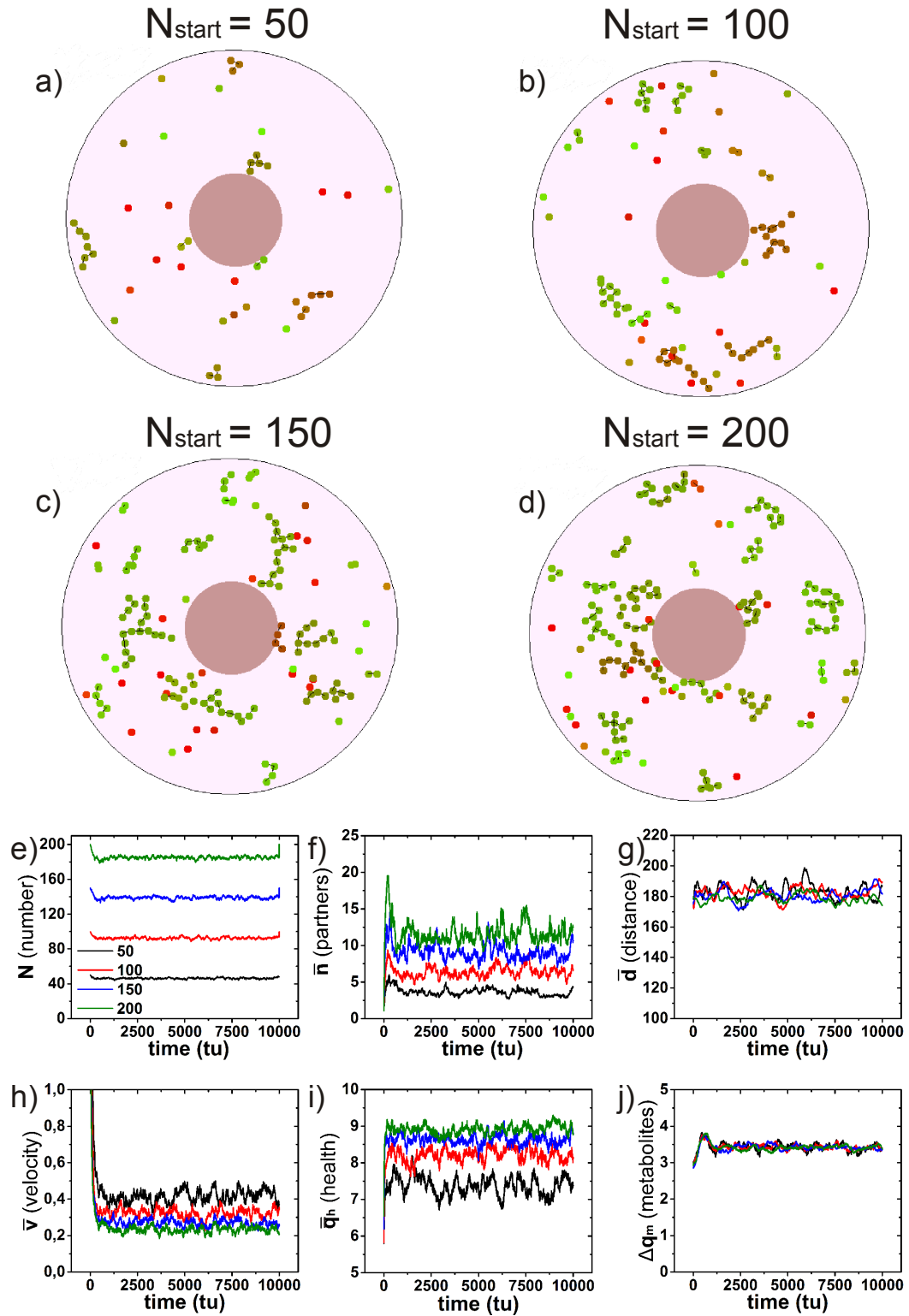
Simulation of mitochondrial network at t=5000 tu for a) $N_{start} = 50$ (black), b) $N_{start} = 100$ (red), c) $N_{start} = 150$ (blue) and d) $N_{start} = 200$ (green). Fluctuations over 10000 tu for e) mitochondrial mass N, f) cluster size $\overline{n}$, g) mitochondrial position $\overline{d}$, h) mitochondrial motility $\overline{v}$, i) health of the mitochondrial DNA $\overline{q}_h$ and j) distribution of metabolites Δq_m.

In reality, the number of mitochondria depends on the cell type and ranges between 80 and 700 units. [6] In order to keep the duration of the simulation at a acceptable level, in following the number of SMUs N is set to 150. In order to simulate mitochondrial behavior in different cell types this number can be varied in future investigations.

3.2.2.2 Size of Smallest Mitochondrial Units

In the following, the radius r_{SMU} and the fusing distance d_{fusion} are altered. The parameter d_{fusion} determines, that two SMUs perform inelastic collisions if they are within a reach of two pixels. This small additional distance to the sum of the radii of two SMUs represents the outreach of corresponding enzymes, which catalyse the fusion process. [8] Simulations with $r_{SMU}=2$ ($d_{fusion} = 6$), 4 (10), 6 (14), 8 (18) and 10 (22) were performed. For the results five simulations were averaged. The averages and standard deviations of all parameters for different r_{SMU} and d_{fusion} are presented in Table (3.3) and Figure 3.4.

r_{SMU} (d_{fusion})	2 (6)	4 (10)	6 (14)	8 (18)	10 (22)
N (SMUs)	138.7 ± 0.2	138.5 ± 0.2	138.6 ± 0.4	138.7 ± 0.3	138.7 ± 0.2
$\overline{n}$ (SMUs)	4.47 ± 0.14	6.55 ± 0.38	9.12 ± 0.27	11.71 ± 0.44	16.01 ± 0.44
$\overline{v}$ ($\frac{pxl}{tu}$)	0.44 ± 0.01	0.36 ± 0.01	0.31 ± 0.00	0.26 ± 0.00	0.24 ± 0.00
$\overline{d}$ (pxl)	186.2 ± 1.0	183.7 ± 1.7	179.3 ± 2.2	176.8 ± 1.7	174.9 ± 1.8
$\overline{q}_h$	7.60 ± 0.03	8.16 ± 0.05	8.62 ± 0.06	8.92 ± 0.04	9.22 ± 0.03
Δq_m	2.67 ± 0.01	2.45 ± 0.03	2.27 ± 0.02	2.07 ± 0.02	1.87 ± 0.04

TABLE 3.3: Parameter values for different r_{SMU} and d_{fusion}

An increased size of SMUs raises the probability of mitochondria to meet each other during their way through the cytoplasm and to perform fusion processes. As a consequence, with growing r_{SMU} and d_{fusion}, respectively, increased average cluster sizes $\overline{n}$ are observed. Similar to higher starting numbers N_{start} growing cluster sizes lead to lower average velocities $\overline{v}$ and a higher average mitochondrial health $\overline{q}_h$. Furtheremore, metabolites are more equally distributed among SMUs and the average distance of SMUs $\overline{d}$ to the center of the cell slightly decreases with growing sizes of SMUs.

In the following simulations, morphological parameters of SMUs are set to $r_{SMU}=6$ pxl and $d_{fusion} = 14$ pxl. According to various measurements mitochondria have a diameter of 0.5 μm to 3 μm. [60, 61] Hence, with this value for r_{SMU} one pixel in the simulations translates to about 0.1 μm in reality. Consequently, in the model mitochondria have a diameter of 2×6 pxl×0.1 $\frac{\mu m}{pxl}$=1.2 μm. As a result, a virtual cell with a radius of 250 pxls represents a large cell in the stratum granulosum of skin with a diameter of 50 μm. The average size of a keratinocyte in the stratum granulosum is about 25 μm to 35 μm.[62]

FIGURE 3.4: Simulations of morphology model with different sizes of SMUs
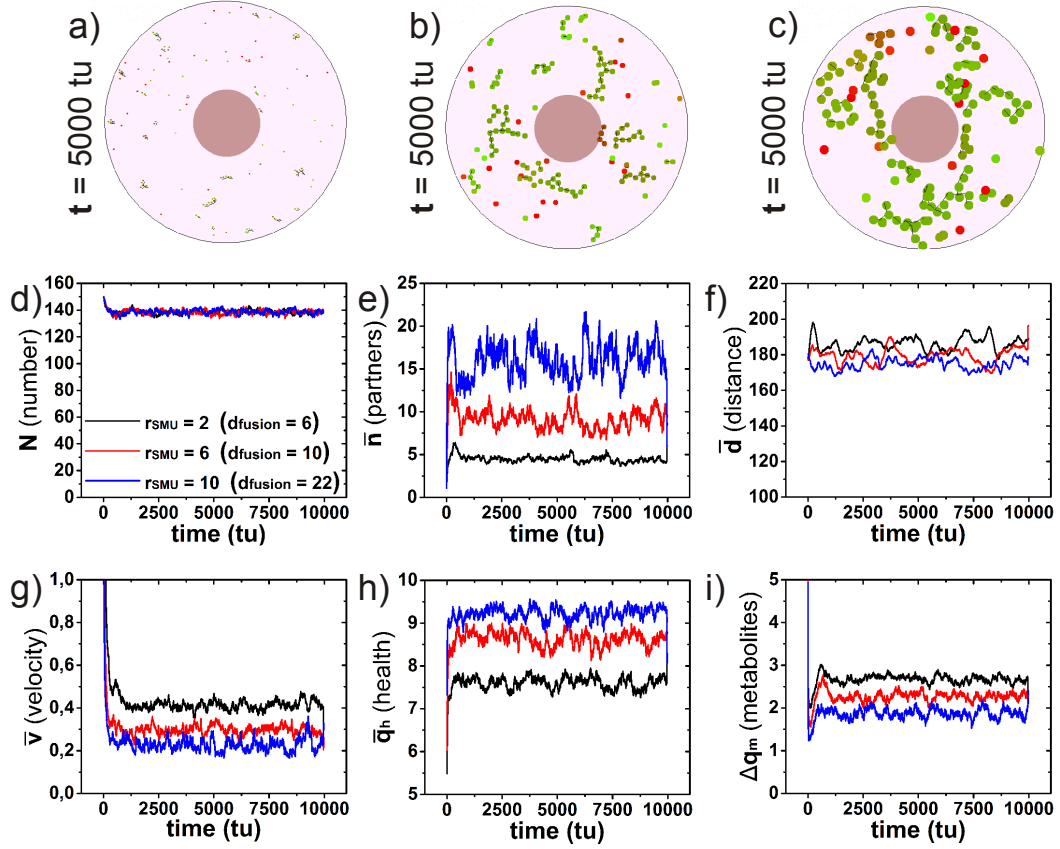
Simulation of mitochondrial network at t=5000 tu for a) r_{SMU}=2 (d_{fusion}=6) (black), b) r_{SMU}=6 (d_{fusion}=14) (red), c) r_{SMU}=10 (d_{fusion}=22) (blue). Fluctuations over 10000 tu for d) mitochondrial mass N, e) cluster size $\overline{n}$, f) mitochondrial position $\overline{d}$, g) mitochondrial motility $\overline{v}$, h) health of the mitochondrial DNA $\overline{q}_{\mathrm{h}}$ and i) distribution of metabolites Δq_{m}.

3.2.2.3 Velocity of Smallest Mitochondrial Units

After performing a fission process and after being produced by biogenesis, new velocities v_{fission} and v_{biogen} are assigned to involved SMUs. Simulations with v_{fission}=2 $\frac{\mathrm{pxl}}{\mathrm{tu}}$, 6 $\frac{\mathrm{pxl}}{\mathrm{tu}}$, 10 $\frac{\mathrm{pxl}}{\mathrm{tu}}$ and v_{biogen}=2 $\frac{\mathrm{pxl}}{\mathrm{tu}}$, 6 $\frac{\mathrm{pxl}}{\mathrm{tu}}$, 10 $\frac{\mathrm{pxl}}{\mathrm{tu}}$ were performed. Results of an average of five simulations for each velocity are presented in Table 3.4 and depicted in Figure 3.5. Simulations reveal, that an increase of both, v_{fission} and v_{biogen}, leads to growing dynamics in the system represented by increased average velocities $\overline{v}$. These dynamics result in larger cluster sizes of SMUs $\overline{n}$ and consequently in a higher average health $\overline{q}_{\mathrm{h}}$ and a better distribution of metabolites with decreasing values for Δq_{m}. Furthermore, the average distance of SMUs to the center $\overline{d}$ slightly decreases. The total amount of

SMUs N is not influenced by a change in v_{fission} and v_{biogen}. In order to avoid an over-valuation of the impact of biogenetic and fission movements on the overall structure of the mitochondrial network, both velocities are set to low values of $v_{\text{fission}} = 2\,\frac{\text{pxl}}{\text{tu}}$ and $v_{\text{biogen}} = 2\,\frac{\text{pxl}}{\text{tu}}$.

v_{fission} / v_{biogen}	$2\,\frac{\text{pxl}}{\text{tu}}$ / $2\,\frac{\text{pxl}}{\text{tu}}$	$6\,\frac{\text{pxl}}{\text{tu}}$ / $6\,\frac{\text{pxl}}{\text{tu}}$	$10\,\frac{\text{pxl}}{\text{tu}}$ / $10\,\frac{\text{pxl}}{\text{tu}}$
N (SMUs)	138.6 ± 0.4	138.8 ± 0.3	138.6 ± 0.3
$\overline{n}$ (SMUs)	9.13 ± 0.27	14.74 ± 0.91	17.94 ± 0.59
$\overline{v}\,\left(\frac{\text{pxl}}{\text{tu}}\right)$	0.31 ± 0.00	0.54 ± 0.01	0.70 ± 0.01
$\overline{d}$ (pxl)	179.3 ± 2.2	177.0 ± 2.1	174.3 ± 1.0
$\overline{q}_{\text{h}}$	8.62 ± 0.06	9.13 ± 0.06	9.31 ± 0.05
Δq_{m}	2.27 ± 0.02	2.01 ± 0.01	1.93 ± 0.02

TABLE 3.4: Parameter values for different velocities v_{fission} and v_{biogen} of Smallest Mitochondrial Units

FIGURE 3.5: Simulations with different values for v_{fission} and v_{biogen}
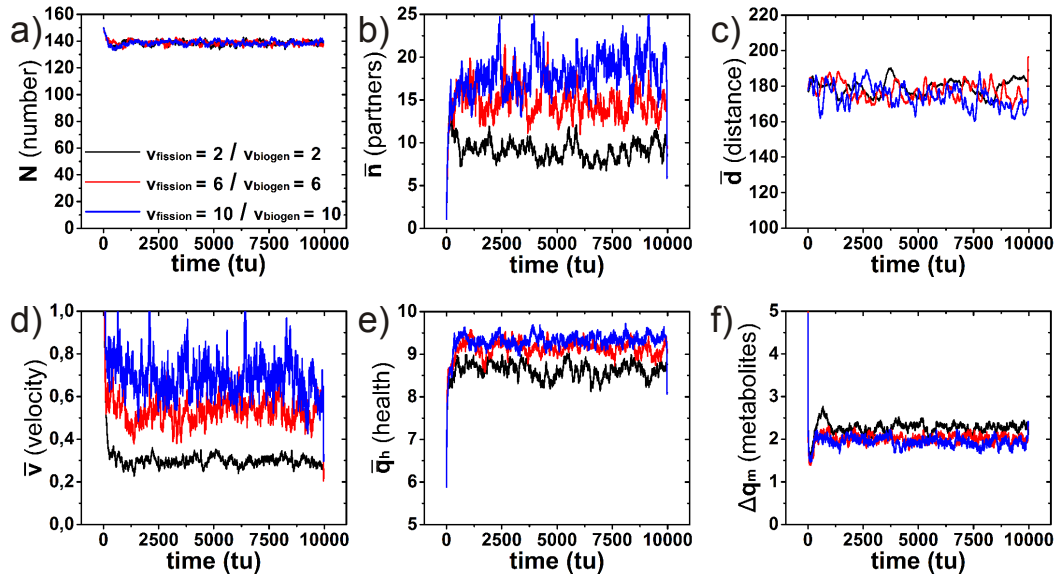
Simulation of mitochondrial network for v_{fission}=2 / v_{biogen}=2 (black), v_{fission}=6 / v_{biogen}=6 (red) and v_{fission}=10 / v_{biogen}=10 (blue). Fluctuations over 10000 tu for a) mitochondrial mass N, b) cluster size $\overline{n}$, c) mitochondrial position $\overline{d}$, d) mitochondrial motility $\overline{v}$, e) health of the mitochondrial DNA $\overline{q}_{\text{h}}$ and f) distribution of metabolites Δq_{m}.

3.2.3 Quality parameters

In the model, the process probabilities ρ_{ROS}, ρ_{rep}, ρ_{mito} and ρ_{bio} are considered as quality parameters, that alter the qualities q_{h} and q_{m} of the SMUs. The values of the probabilities are varied in different simulations presented in Table 3.5. The average of five

simulations for each parameter value is depicted in Figures 3.6, 3.7, 3.8 and 3.9.

Increasing the probability for mitophagic processes ρ_{mito} leads to a more efficient removement of harmed, isolated mitochondria. As a consequence, mitochondrial clusters establish larger cluster sizes $\overline{n}$ with decreased velocities $\overline{v}$. Furthermore, mitochondrial health $\overline{q}_{\text{h}}$ grows to higher values and spreading of metabolites represented by lower values for Δq_{m} is increased. Efficient mitophagy also slightly reduces the number of SMUs N as less irreversibly harmed mitochondria move within the cytoplasm. Similar effects are observed if the probability for biogenesis ρ_{mito} is increased. A strong biogenetic activity maintains the integrity of the mitochondrial network and leads to large clusters $\overline{n}$, high mitochondrial health $\overline{q}_{\text{h}}$ and a equal distribution of metabolites Δq_{m}. Accordingly, low values of ρ_{bio} result in drastically decreased mitochondrial numbers N.

Growing probabilities for mitochondrial repair processes ρ_{repair} actively fights quality losses by oxidative stress. Consequently, a lower amount of isolated irreversibly impaired mitochondria accumulates in the cell. Instead, SMUs aggregate to larger cluster sizes $\overline{n}$ with an increased average health $\overline{q}_{\text{h}}$ and a more equal distribution of metabolites Δq_{m}. Contrary, under growing oxidative stress the integrity of both qualities, mitochondrial health $\overline{q}_{\text{h}}$ and the spreading of metabolites Δq_{m} is impaired. Hence, the number of inactive mitochondria and following fission events is increased. Consequently, cluster sizes $\overline{n}$ shrink to lower values. More mitochondria are removed by mitophagy, so that the number of SMUs N decreases.

In order to quantitatively investigate and compare the influence of modifications in mitophagy, biogenesis, repair and oxidative stress, simulations with small step sizes and more-dimensional variations of ρ_{mito}, ρ_{bio}, ρ_{rep} and ρ_{ROS} should be performed.

setting	N (SMUs)	$\overline{n}$ (SMUs)	$\overline{v}$ ($\frac{\text{pxl}}{\text{tu}}$)	$\overline{d}$ (pxl)	$\overline{q}_{\text{h}}$	Δq_{m}
standard	138.9 ± 0.2	9.02 ± 0.33	0.30 ± 0.01	178.6 ± 2.0	8.60 ± 0.05	2.27 ± 0.01
$\rho_{\text{mito}}{=}0.001$	143.9 ± 0.3	6.65 ± 0.17	0.45 ± 0.01	180.9 ± 3.3	7.64 ± 0.07	2.79 ± 0.02
$\rho_{\text{mito}}{=}0.1$	137.7 ± 0.4	9.41 ± 0.21	0.27 ± 0.01	178.9 ± 0.9	8.73 ± 0.04	2.02 ± 0.02
$\rho_{\text{bio}}{=}0.001$	82.8 ± 1.3	5.46 ± 0.30	0.37 ± 0.01	182.5 ± 1.8	7.91 ± 0.11	2.50 ± 0.04
$\rho_{\text{bio}}{=}0.1$	148.9 ± 0.0	9.63 ± 0.23	0.30 ± 0.01	179.4 ± 0.4	8.71 ± 0.05	2.22 ± 0.01
$\rho_{\text{rep}}{=}0.0001$	137.8 ± 0.5	8.54 ± 0.34	0.32 ± 0.01	179.3 ± 1.3	8.54 ± 0.04	2.31 ± 0.03
$\rho_{\text{rep}}{=}0.01$	147.7 ± 0.2	19.35 ± 1.56	0.15 ± 0.01	174.7 ± 1.8	9.48 ± 0.04	1.37 ± 0.04
$\rho_{\text{ROS}}{=}0.005$	143.5 ± 1.9	12.50 ± 1.75	0.23 ± 0.04	179.4 ± 2.9	9.01 ± 0.19	1.95 ± 0.14
$\rho_{\text{ROS}}{=}0.02$	129.7 ± 0.4	5.44 ± 0.16	0.46 ± 0.00	181.1 ± 1.2	7.91 ± 0.05	2.67 ± 0.02

TABLE 3.5: Parameter values for different probabilities ρ_{mito}, ρ_{bio}, ρ_{rep} and ρ_{ROS}

FIGURE 3.6: Simulations of morphology model with different values for ρ_{mito}
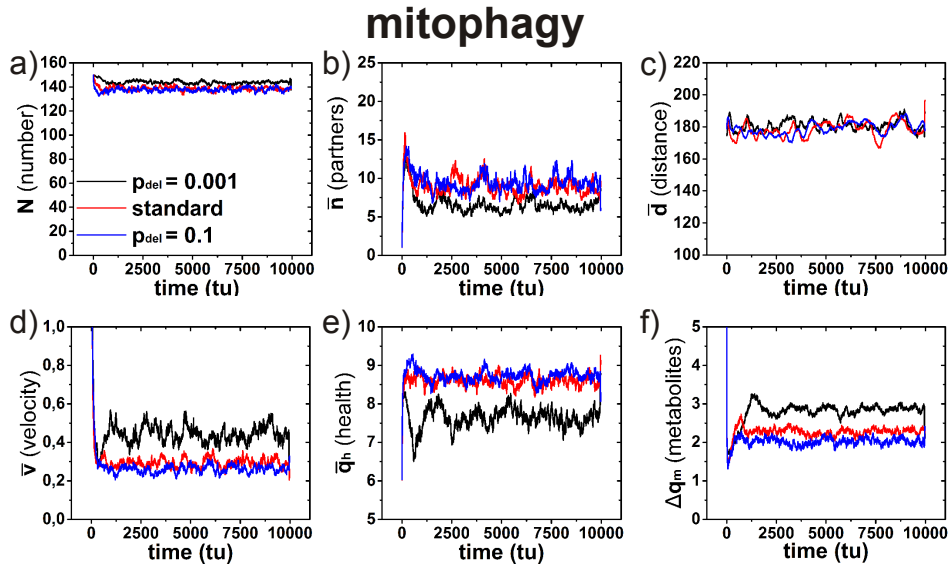
Simulation of mitochondrial network for ρ_{mito}=0.001, the standard parameter setting in Table (3.1) (red) and ρ_{mito}=0.1 (blue) over 10000 tu for a) mitochondrial mass N, b) cluster size $\overline{n}$, c) mitochondrial position $\overline{d}$, d) mitochondrial motility $\overline{v}$, e) health of the mitochondrial DNA $\overline{q}_{\text{h}}$ and f) distribution of metabolites Δq_{m}.

FIGURE 3.7: Simulations of morphology model with different values for ρ_{biogen}
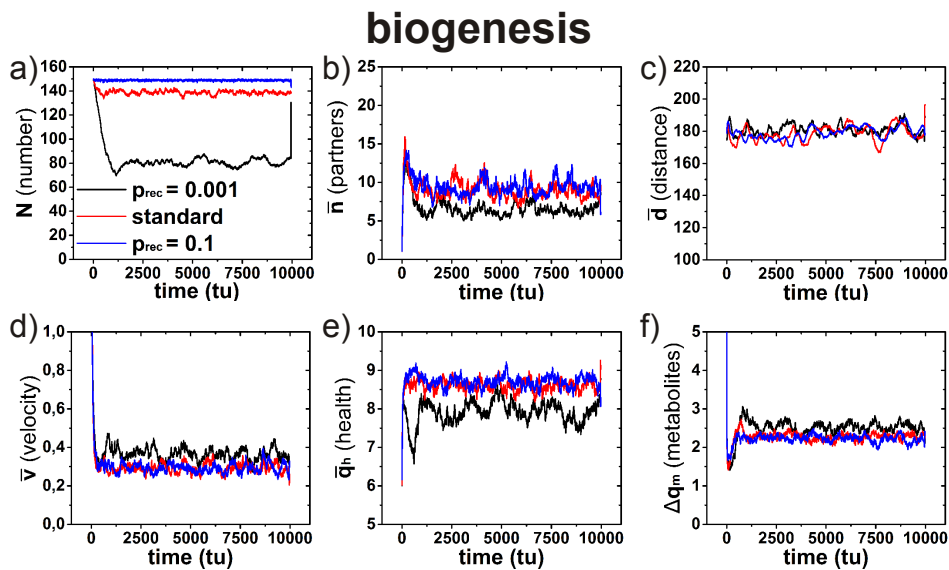
Simulation of mitochondrial network for ρ_{biogen}=0.001, the standard parameter setting in Table (3.1) (red) and ρ_{biogen}=0.1 (blue) over 10000 tu for a) mitochondrial mass N, b) cluster size $\overline{n}$, c) mitochondrial position $\overline{d}$, d) mitochondrial motility $\overline{v}$, e) health of the mitochondrial DNA $\overline{q}_{\text{h}}$ and f) distribution of metabolites Δq_{m}.

FIGURE 3.8: Simulations of morphology model with different values for ρ_{rep}
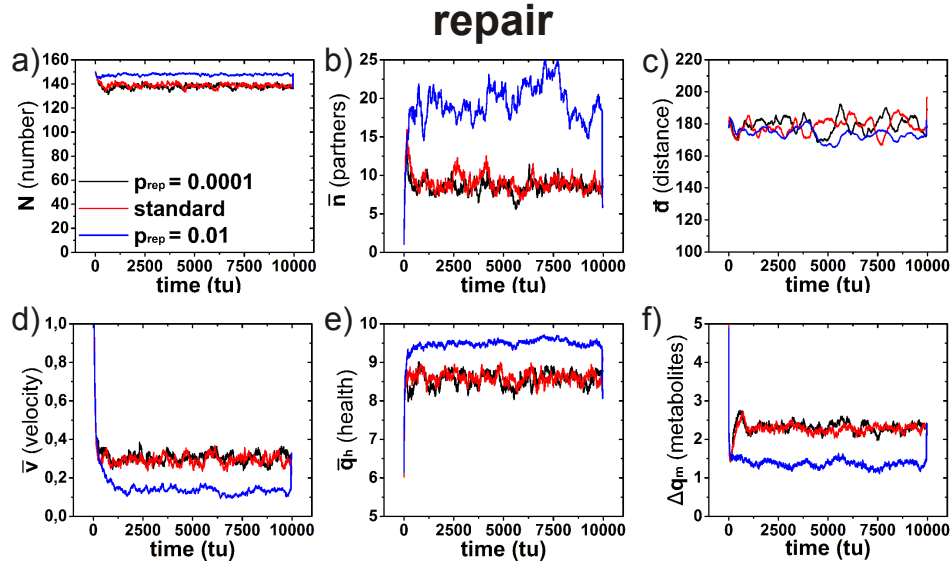
Simulation of mitochondrial network for ρ_{rep}=0.0001, the standard parameter setting in Table (3.1) (red) and ρ_{rep}=0.01 (blue) over 10000 tu for a) mitochondrial mass N, b) cluster size $\overline{n}$, c) mitochondrial position $\overline{d}$, d) mitochondrial motility $\overline{v}$, e) health of the mitochondrial DNA $\overline{q}_{\text{h}}$ and f) distribution of metabolites Δq_{m}.

FIGURE 3.9: Simulations of morphology model with different values for ρ_{ROS}
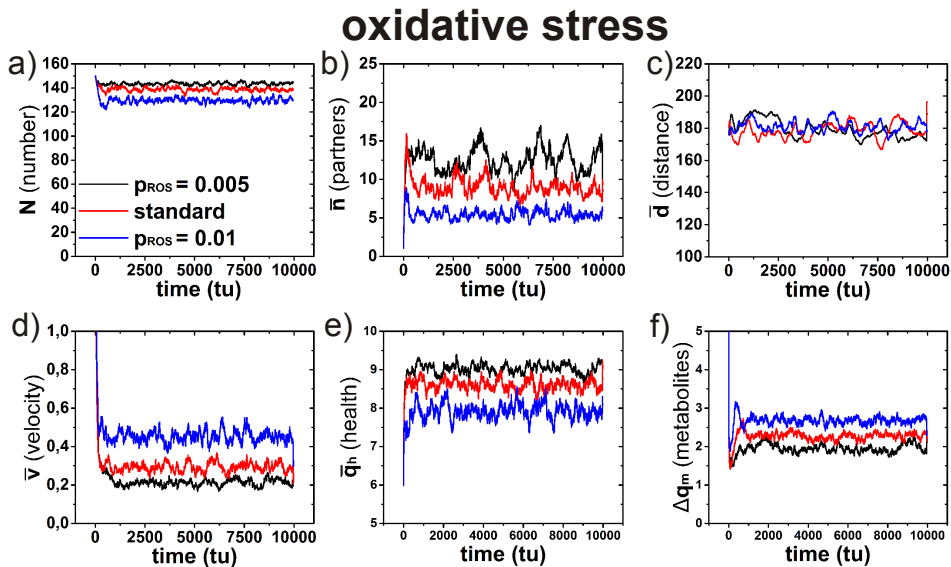
Simulation of mitochondrial network for ρ_{ROS}=0.005, standard parameter setting in Table (3.1) (red) and ρ_{ROS}=0.02 (blue) over 10000 tu for a) mitochondrial mass N, b) cluster size $\overline{n}$, c) mitochondrial position $\overline{d}$, d) mitochondrial motility $\overline{v}$, e) health of the mitochondrial DNA $\overline{q}_{\text{h}}$ and f) distribution of metabolites Δq_{m}.

3.2.4 Adenosin triphosphate consumers

In order to investigate the coupling between the mitochondrial network and the energy demands of a cell, one ATP consumer is placed in the cytoplasm with a distance of 162 pxl to the center of the cell. Damping of the motion of SMUs by friction processes in the cytoplasm was implemented with the damping constant $D = 0.01$.

According to formula (3.4), the behavior of ATP consumers can be modified in two dimensions. Varying the frequency f alters the rate an ATP consumer changes its demand for energy. Modifying the amplitude C_m results in either an increase or a decrease of the power of attraction of the ATP consumer. Thus, it represents the grade of urgency for a supply with ATP molecules by mitochondria. In the following, the influence of variations in both, f and C_m, on mitochondrial morphologies and quality parameters is explored.

3.2.4.1 Oscillation frequency

Simulations were performed with three different oscillation frequencies: $f = 0.001 \frac{1}{\mathrm{tu}}$, $f = 0.003 \frac{1}{\mathrm{tu}}$ and $f = 0.005 \frac{1}{\mathrm{tu}}$. Amplitudes for attraction and repulsion were set to $C_m = 1$ and $C_n = 10$, respectively. With this setting, the repulsion and attraction cancel each other out ($V_C = 0$) at a distance of 10 pxl to the center of the consumer. For all parameters, the results of five simulations were averaged (Figures 3.10, 3.11 and 3.12). Apart from the mitochondrial mass N, morphological and quality parameters couple to all angular frequencies of the oscillations of ATP consumers. There is a small offset of a few time units between oscillations of parameters and the oscillations of consumers for all oscillation frequencies. This delay is considered to be adjustment time for SMUs to the landscape of the Mie potential, e.g. the energetic demand of the ATP consumer. In future experiments it could be of interest to quantify this delay in order to determine the inertia of the mitochondrial system.

Mitochondrial structures alter between the extremes of a free unbound system and the demanding restriction of the energetic architecture created by the ATP consumer. During phases of high energy demand, SMUs localize in the area of the ATP consumer. This results in an decreased average distance $\bar{d}$ to the center of the cell, an aggregation to larger cluster sizes $\bar{n}$ and a decrease of average velocities $\bar{v}$. Furthermore, the average mitochondrial health $\bar{q}_\mathrm{h}$ grows and metabolites are distributed more equally with falling values for Δq_m.

FIGURE 3.10: Simulations with an Adenosin triphosphate consumer with $f = 0.001 \frac{1}{\text{tu}}$
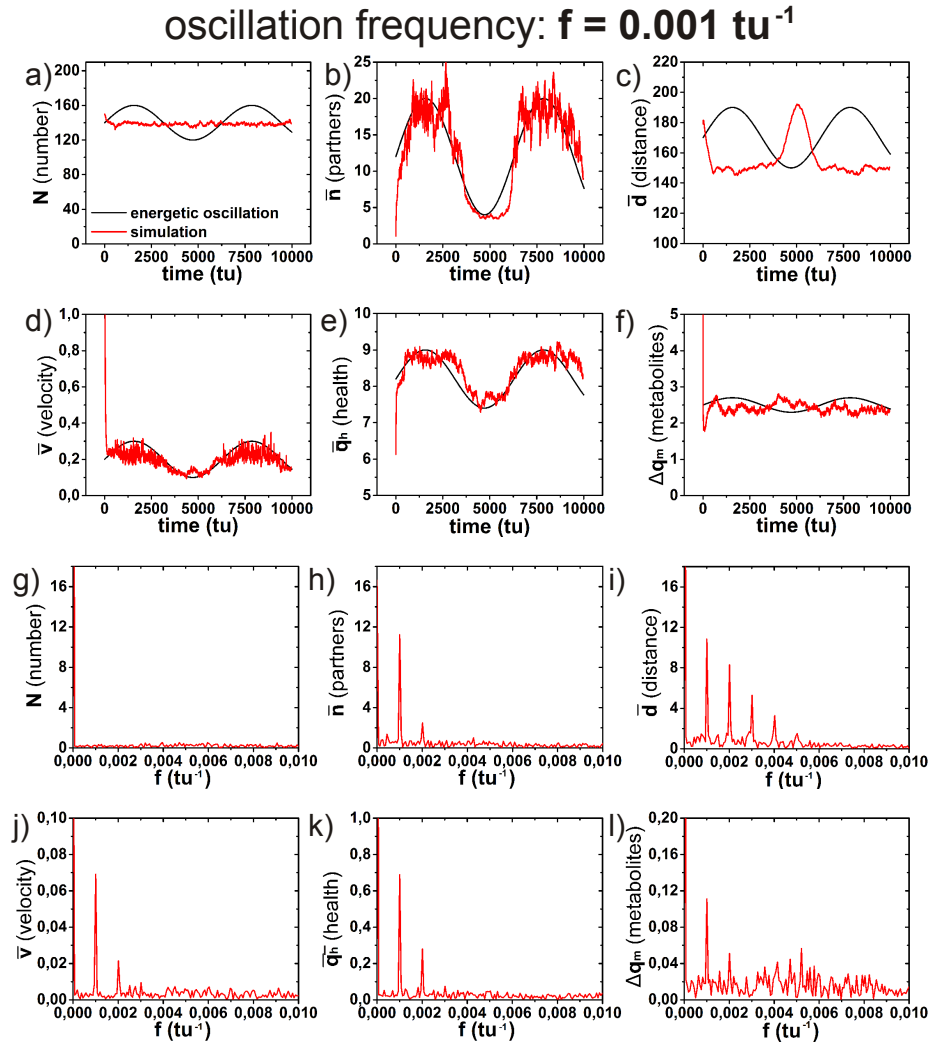
oscillation frequency: **f = 0.001 tu⁻¹**

Simulation of mitochondrial network with ATP consumer with oscillation frequency $f = 0.001 \frac{1}{\text{tu}}$. In black the energetic attraction of the consumer over $10000\,\text{tu}$ is visualized. For the sake of clarity in all plots the oscillation of the ATP consumer between 0 and 2 is scaled to the amplitude of the corresponding parameter. In red the fluctuations for a) mitochondrial mass N, b) cluster size $\bar{n}$, c) mitochondrial position $\bar{d}$, d) mitochondrial motility $\bar{v}$, e) health of the mitochondrial DNA $\bar{q}_{\text{h}}$ and f) distribution of metabolites Δq_{m} are depicted. In g-l) the corresponding Fourier transformation of all parameters are indicated.

FIGURE 3.11: Simulations with an Adenosin triphosphate consumer with $f = 0.003 \frac{1}{tu}$
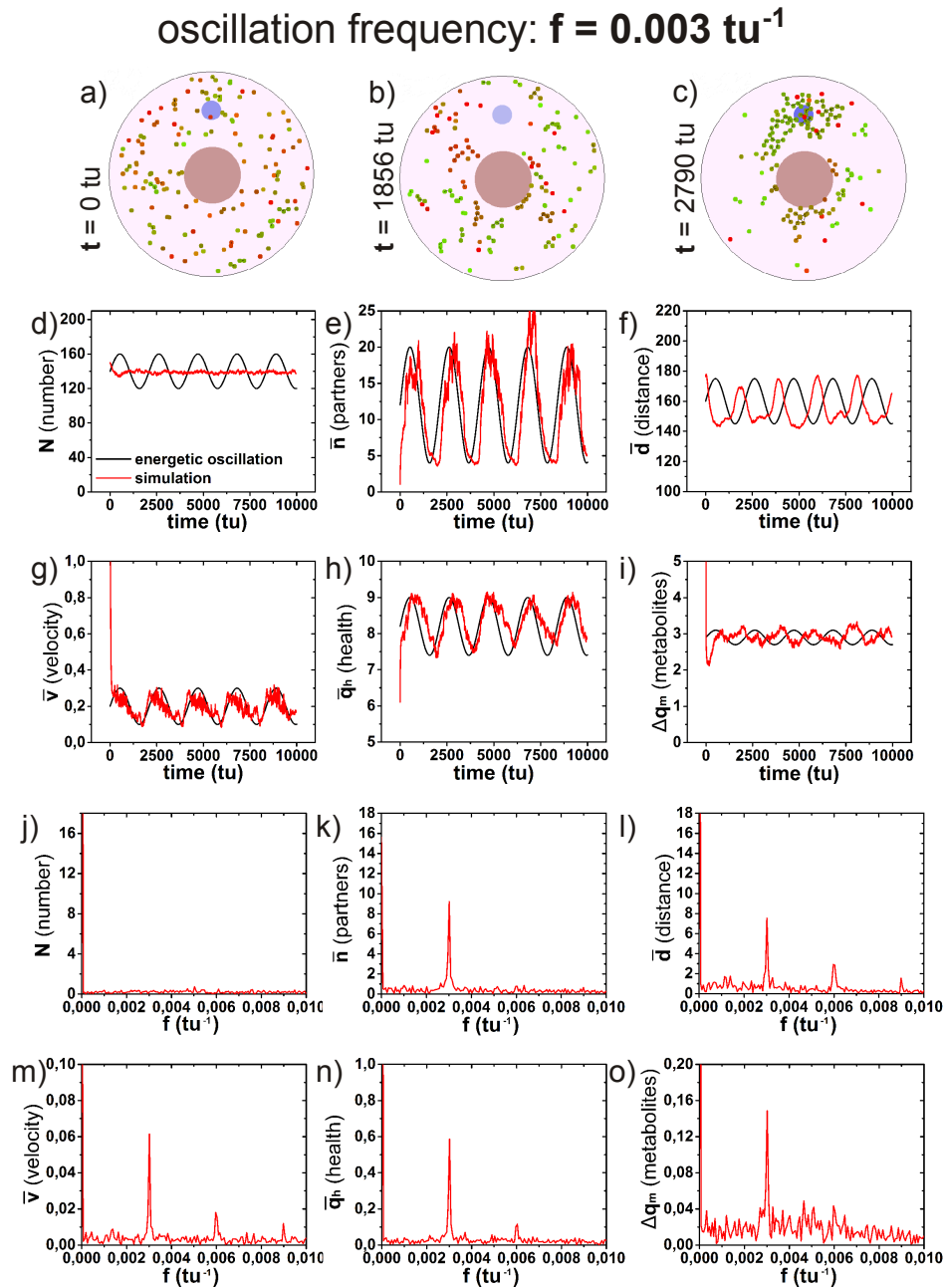
Simulation of mitochondrial network with ATP consumer with oscillation frequency $f = 0.003 \frac{1}{tu}$ at a) 0 tu, b) 1856 tu and c) 2790 tu. In black the energetic attraction of the consumer over 10000 tu is visualized. For the sake of clarity in all plots the oscillation of the ATP consumer between 0 and 2 is scaled to the amplitude of the corresponding parameter. In red the fluctuations for d) mitochondrial mass N, e) cluster size $\overline{n}$, f) mitochondrial position $\overline{d}$, g) mitochondrial motility $\overline{v}$, h) health of the mitochondrial DNA $\overline{q}_h$ and i) distribution of metabolites Δq_m are depicted. In j-o) the corresponding Fourier transformation of all parameters are indicated.

FIGURE 3.12: Simulations with an Adenosin triphosphate consumer with $f = 0.005 \frac{1}{\mathrm{tu}}$
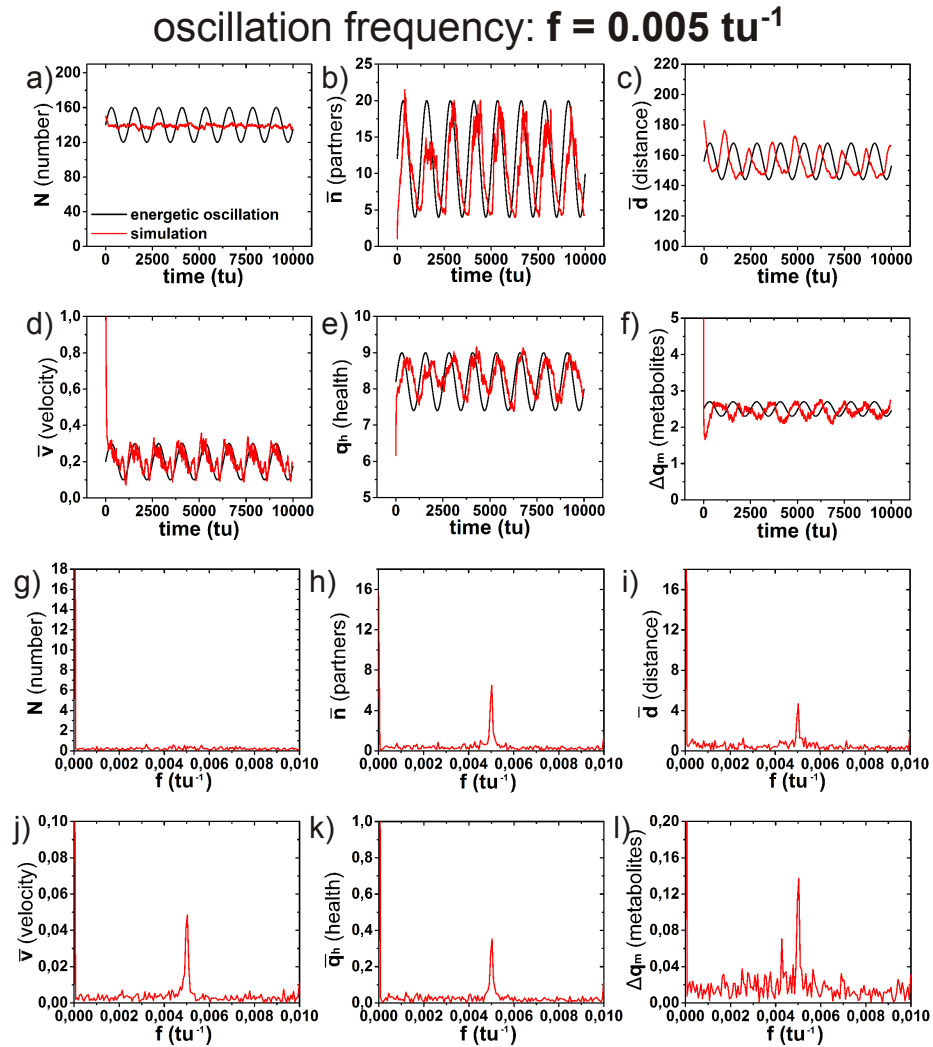
oscillation frequency: **f = 0.005 tu⁻¹**

Simulation of mitochondrial network with ATP consumer with oscillation frequency $f = 0.005 \frac{1}{\mathrm{tu}}$. In black the energetic attraction of the consumer over 10000 tu is visualized. For the sake of clarity in all plots the oscillation of the ATP consumer between 0 and 2 is scaled to the amplitude of the corresponding parameter. In red the fluctuations for a) mitochondrial mass N, b) cluster size $\overline{n}$, c) mitochondrial position $\overline{d}$, d) mitochondrial motility $\overline{v}$, e) health of the mitochondrial DNA $\overline{q}_{\mathrm{h}}$ and f) distribution of metabolites Δq_{m} are depicted. In g-l) the corresponding Fourier transformation of all parameters are indicated.

3.2.4.2 Oscillation amplitude

Simulations were performed with a fixed oscillation frequency of f =0.003 $\frac{1}{\text{tu}}$ and three different attraction amplitudes: C_m =0.5, C_m =1 and C_m =2. For all parameters, the results of five simulations were averaged (Table 3.6, Figure 3.13).

C_m	0.5	1	2
N (SMUs)	138.5 ± 1.7	138.9 ± 1.7	138.8 ± 1.7
$\overline{n}$ (SMUs)	9.74 ± 4.55	11.60 ± 5.88	14.52 ± 7.32
$\overline{v}$ $\left(\frac{\text{pxl}}{\text{tu}}\right)$	0.18 ± 0.11	0.19 ± 0.11	0.23 ± 0.12
$\overline{d}$ (pxl)	157.6 ± 8.3	155.0 ± 9.8	153.2 ± 10.0
$\overline{q}_\text{h}$	8.24 ± 0.43	8.37 ± 0.47	8.56 ± 0.52
Δq_m	2.45 ± 0.17	2.43 ± 0.18	2.36 ± 0.17

TABLE 3.6: Parameter oscillations for different attraction C_m

FIGURE 3.13: Simulations with an Adenosin triphosphate consumer with f =0.003 $\frac{1}{\text{tu}}$ and different C_m
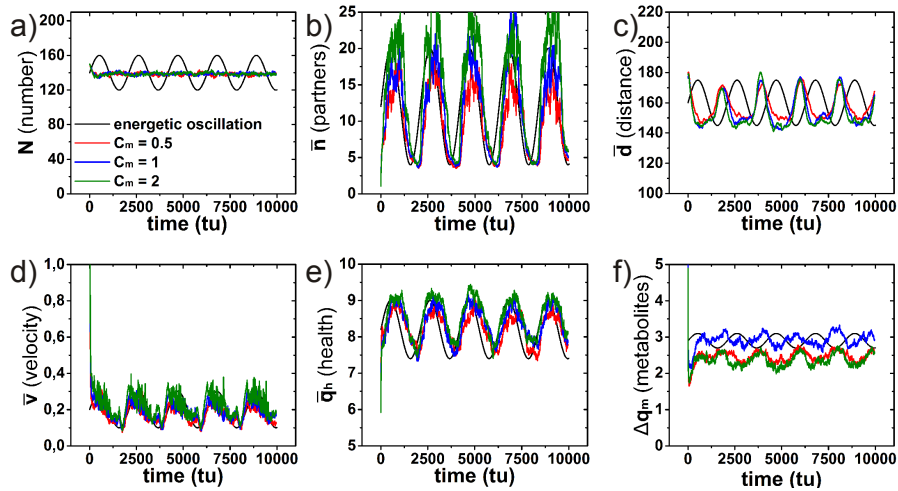
Simulation of mitochondrial network with ATP consumer with oscillation frequency f =0.003 $\frac{1}{\text{tu}}$ and attraction amplitude C_m =0.5 (red), C_m =1 (blue) and C_m =2 (green). In black the energetic attraction of the consumer over 10000 tu is visualized. For the sake of clarity in all plots the oscillation of the ATP consumer between 0 and 2 is scaled to the amplitude of the corresponding parameter. The fluctuations for a) mitochondrial mass N, b) cluster size $\overline{n}$, c) mitochondrial position $\overline{d}$, d) mitochondrial motility $\overline{v}$, e) health of the mitochondrial DNA $\overline{q}_\text{h}$ and f) distribution of metabolites Δq_m are depicted.

With growing attraction parameters C_m of the ATP consumer, SMUs are increasingly accelerated by the Mie potential and establish higher maximum velocities going from $0.18\frac{\text{pxl}}{\text{tu}}$ for C_m=0.5 to $0.23\frac{\text{pxl}}{\text{tu}}$ for C_m=2. This acceleration of mitochondrial dynamics leads to increased cluster sizes in phases of high energy demands growing from about 9.7 SMUs per cluster (C_m=0.5) to about 14.5 SMUs per cluster (C_m=2). Parallel, the

distance of SMUs to the center of the cell falls with growing C_m, as the accumulation of SMUs around the ATP consumer increases. Consequently, parallel to growing cluster sizes the mitochondrial health grows from $\bar{q}_h = 8.24$ to $\bar{q}_h = 8.56$. Additionally, the average deviation of metabolites falls from $\Delta q_m = 2.45$ to $\Delta q_m = 2.36$.

3.2.4.3 Number of Adenosin triphosphate consumers

In order to create a more complex energetic architecture, three ATP consumers are added to the virtual cell. All consumers have a equidistant position to each other of $281\,\text{pxl}$ and a distance of $162\,\text{pxl}$ to the nucleus. The repulsion and attraction parameters for all consumers i are $C_{n_i} = 10$ and $C_{m_i} = 1$. The oscillation frequency differed among the consumers with: $f_1 = 0.001\,\frac{1}{\text{tu}}$, $f_2 = 0.003\,\frac{1}{\text{tu}}$ and $f_3 = 0.005\,\frac{1}{\text{tu}}$. For analysis of all parameters five simulations were averaged and compared with simulations free of consumers. (Figure 3.14)

For all points in time the average distance to the center of the cell in this energetic architecture is lower ($\bar{d} = 139.03 \pm 0.81\,\text{pxl}$) than in consumer free simulations ($\bar{d} = 180.64 \pm 1.74\,\text{pxl}$) and than the distance of ATP consumers of $162\,\text{pxl}$. Apart from fission and biogenetic procedures, movement of SMUs appears basically between ATP consumers. Since Mie potentials force SMUs to move along the shortest possible path between ATP consumers, which would lead through the center of the cell, mitochondria aggregate around the nucleus. In experiments, accumulation of mitochondrial clusters around the nucleus was observed in stressed cells. [63]

Furthermore, the attraction of ATP consumers leads to the accumulation of SMUs to large mitochondrial clusters with $\bar{n} = 15\,\text{SMUs}$ to $\bar{n} = 20\,\text{SMUs}$ in average. Only at two points in time at about $3500\,\text{tu}$ and $6000\,\text{tu}$, the average cluster size falls to the level of a consumer free simulation with about $\bar{n} = 9$. There, all consumers demand a minimum amount of energy, so that SMUs act as a quasi free system. However, this does not result in an increased average distance to the nucleus $\bar{d}$. The reason for this seemingly paradoxical behavior is, that the nucleus partially blocks the free movement of SMUs. As a result, some SMUs stay close to an ATP consumer instead of moving unbound within the cytoplasm. By this mechanism, the nucleus secures the future supply of the energy demands of an ATP consumer.

Due to improved compensation for failures in mitochondrial DNA, the aggregation to bigger clusters leads to an increased mitochondrial health compared to consumer free simulations. ($\bar{q}_{h,\text{consumers}} = 8.90 \pm 0.02$ / $\bar{q}_{h,\text{free}} = 8.63 \pm 0.05$). Moreover, velocities shrink to lower values ($\bar{v}_{\text{consumers}} = 0.22 \pm 0.00$ / $\bar{v}_{\text{free}} = 0.31 \pm 0.00$) as SMUs are most of the time localized at a specific consumer.

FIGURE 3.14: Simulations with three Adenosin triphosphate consumers as energetic architecture
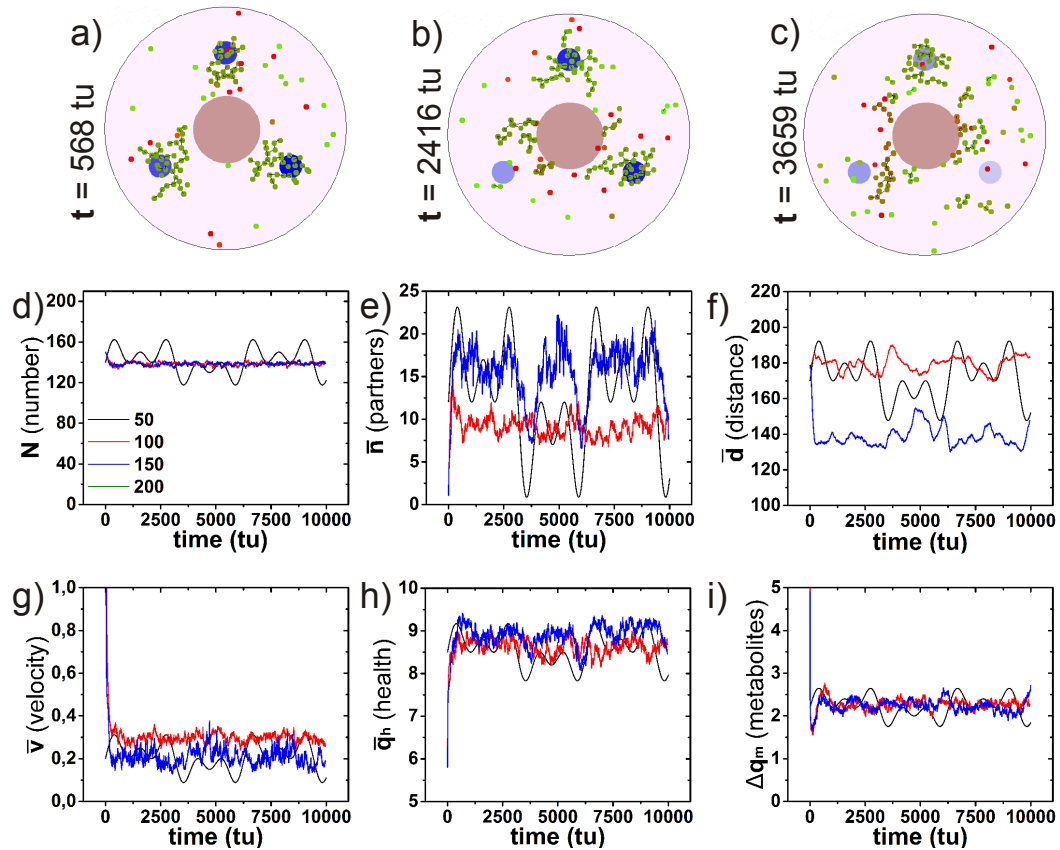
Simulation of mitochondrial network with three ATP consumers at a) 568 tu, b) 2416 tu and c) 3659 tu. In black the energetic attraction of the consumers over 10000 tu is visualized. For the sake of clarity in all plots the oscillation of the ATP consumers between 0 and 2 is scaled to the amplitude of the corresponding parameter. In blue the fluctuations of parameters within the energetic environment, in red without the energetic environment ("free" SMUs) are depicted for d) mitochondrial mass N, e) cluster size $\overline{n}$, f) mitochondrial position $\overline{d}$, g) mitochondrial motility $\overline{v}$, h) health of the mitochondrial DNA $\overline{q}_h$ and i) distribution of metabolites Δq_m are depicted.

A Fourier analysis (Figure 3.15) of all investigated parameters reveals, that the oscillation frequencies f_1, f_2 and f_3 of all three consumers couple to both, the morphological parameters ($\overline{n}$, $\overline{d}$ and $\overline{v}$) and the quality parameters ($\overline{q}_h$, Δq_m). Additionally, oscillations for multiples and superpositions of the ATP consumer frequencies are found. This behavior reveals, that the system of SMUs, e.g. the mitochondrial network, responds to the overall energetic environment of the cell, adapting to various global states of the ATP consuming system. Collectively, mitochondrial structures alter between the extremes of a free and unbound system and the restrictions of an energy demanding architecture in the cell.

FIGURE 3.15: Fourier analysis of simulations with energetic architecture
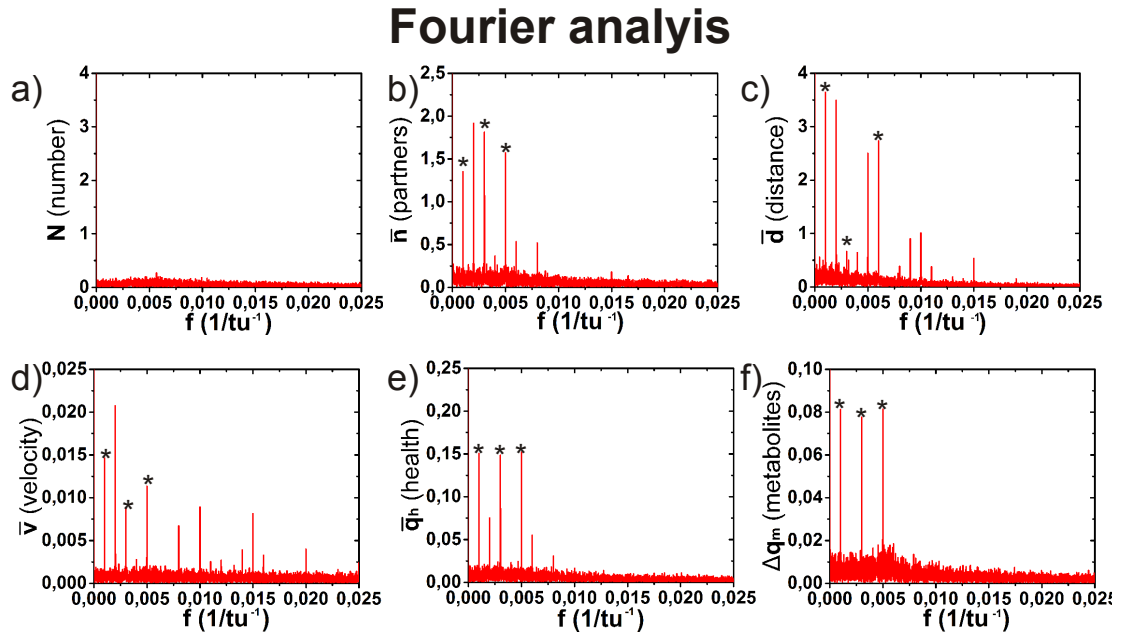
In a-f) the Fourier transformation of all investigated parameters of the energetic architecture are depicted. The oscillation frequencies of the three ATP consumers are asterisked.

3.2.4.4 Aging

In order to implement an aging process in the model, process probabilities are altered in decay laws (mitophagy, mitochondrial repair) and growth laws (ROS) according to equation (3.7). Here, the starting probabilities ρ_{i_0} are given by the general process probabilities of each biological process in Table 3.1. The lifetime of all processes is set to $\tau=5000$ tu. More advanced versions of the model with additional experimental insights on biological processes could include specific lifetimes for all processes. An average of five aging simulations for all investigated parameters in the presence of the energetic architecture with three ATP consumers as presented in the last section is depicted in Figure 3.16.

Simulations disclose shrinking mitochondrial cluster sizes $\overline{n}$ and falling mitochondrial health $\overline{q}_{\mathrm{h}}$ over time due to increased oxidative stress and decreased mitochondrial repair abilities. Since metabolites are distributed less equally in smaller mitochondrial clusters the deviation of the corresponding quality parameter Δq_{m} increases. The total number of mitochondria N slightly decreases. Moreover, due to growing numbers of irreversibly harmed, isolated SMUs, the average velocity of SMUs $\overline{v}$ and their distance to the center $\overline{d}$ increases.

These results lead to the observation of an impaired and fragmented mitochondrial

network in old cells. This conclusion is in line with the results of the quality model in chapter 2.

FIGURE 3.16: Simulations with aging procedure and energetic architecture
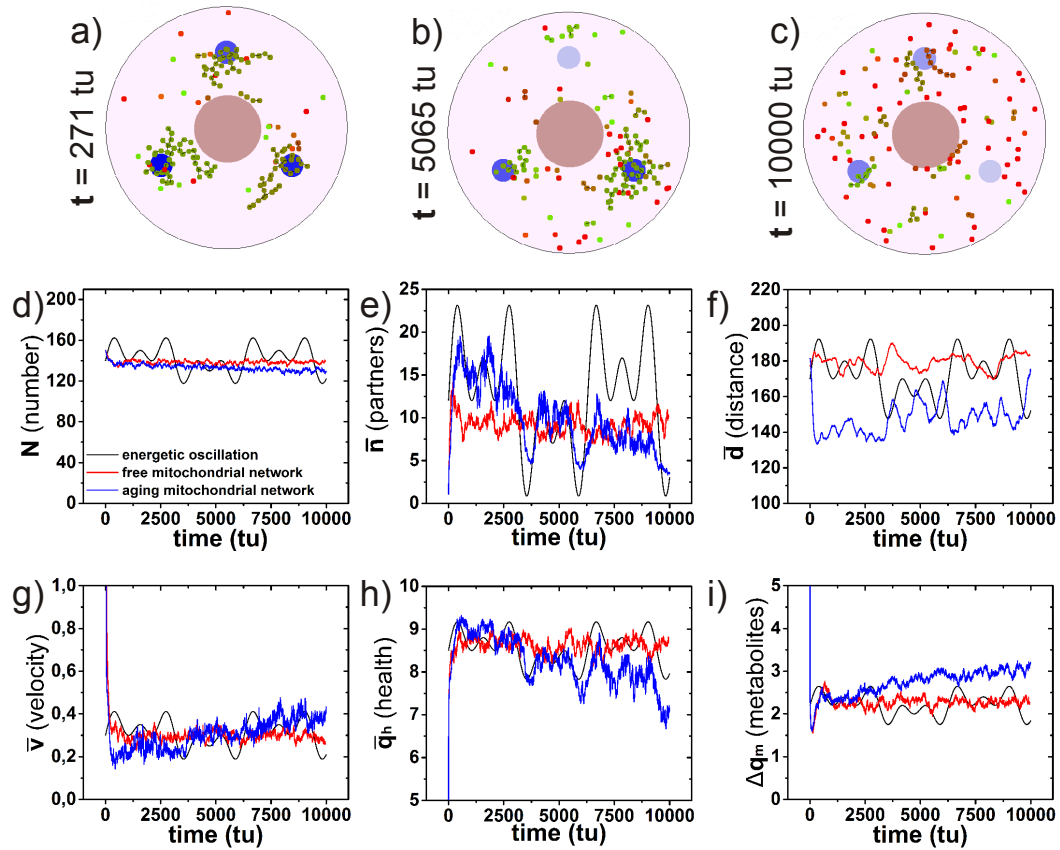
Aging simulation of mitochondrial network with three ATP consumers at a) 271 tu, b) 5065 tu and c) 10000 tu. In black the overall energetic oscillation in the cell over 10000 tu is visualized. In blue the fluctuations of parameters within the energetic environment during aging, in red without the energetic environment and without aging ("free" SMUs) are depicted for d) mitochondrial mass N, e) cluster size $\overline{n}$, f) mitochondrial position $\overline{d}$, g) mitochondrial motility $\overline{v}$, h) health of the mitochondrial DNA $\overline{q}_{\mathrm{h}}$ and i) distribution of metabolites Δq_{m}.

3.3 Discussion

The presented model is able to correlate mitochondrial morphologies with mitochondrial qualities and simulates the interaction between the mitochondrial network and the energy demands of the cell. Simulations reveal a coupling of both, morphological

and quality parameters with the oscillations of the energetic archicture of the cell represented by ATP consumers. During phases of high energy demands mitochondria localize in specific cell areas and accumulate to larger clusters, which improves the compensation for failures in mitochondrial DNA sequences and the distribution of metabolites. Furthermore, in order to shorten paths between energy consuming cell sites, mitochondria condensate around the nucleus. This finding agrees with investigations on stressed cells, where mitochondria also aggregate around the nucleus. [63]

During aging procedures of biological processes, the morphological model reveals an ongoing fragmentation of mitochondrial clusters and falling mitochondrial qualities. This result is in line with the outcomes of the quality model presented in chapter 2. Additionally, a similar behavior was observed in in-vitro experiments. [38, 39]

Moreover, during aging an increased number of mitochondria performing fission processes increases the number of fresh mitochondria generated by mitochondrial biogenesis. As a consequence of enhanced recycling activity, average mitochondrial velocities rise during maturing of the cells in the model. In reality, this mechanism might help mitochondria to aggregate to larger clusters in order to compensate for falling qualities and the fragmentation process caused by aging. However, due to a lack of measurement methods so far there is no experimental data available on the motility of mitochondria. Future experiments should determine the impact of an alteration of mitochondrial velocities on the overall network.

Due to the lack of biological insights some assumptions and definitions of parameter values in the model have to be rather intuitive or simplistic than experimentally determined (see Table 3.1). Results of the model can only qualitatively be compared with experiments but not quantitatively. Similar to the model presented in chapter 2, to date it is not possible to determine the real time scales of the involved biological processes. Instead, their frequency can only be estimated relatively to each other. [17, 37] Additionally, both quality parameters, e.g. the health of mitochondrial DNA and the amount of metabolites present in a mitochondrion, can not be measured directly. Therefore, they can only be compared indirectly with experiments by measuringing, e.g. the mitochondrial membrane potential.

The virtual cell in the model has a two-dimensional design, although in reality all cells exist in three dimensions. Thus, the model applies basically to cells that are quasi two-dimensional systems, as e.g. keratinocytes in the stratum granulosum of the epidermis in human skin. [3] In order to use the model to reconstruct the mitochondrial network in more voluminous cells, as e.g. fibroblasts or myocytes, a third dimension has to be included.

Representing mitochondria, the SMUs in the model move freely within the cytoplasm of the virtual cell. This assumption is only an approximation of the quasi-free motion of mitochondria in reality. Experiments show, that mitochondria are supposed to move

along the widely branched tubulin fibers. [47] In order to include this limited movement capacity, the model has to define fixed paths on which SMUs are allowed to run.

So far, mitochondrial clusters and SMUs in the model always perform a fusion process, if they meet within the cytoplasm, except for SMUs that are irreversibly damaged and have health of $q_h = 0$. Experimentally it is not clear, if two meeting mitochondrial clusters always fuse. A fusion probability based on the qualities of involved SMUs could be included. A similar mechanism is already introduced in the quality model in chapter 2.

Furthermore, in the current version of the model, SMUs share metabolites as equal as possible and compensate for each others DNA failures at a maximum level. Although these basic mechanisms are experimentally proven, to date it remains unclear to which extend mitochondria compensate for each others failures and share metabolites when they merge their inner and outer membranes.

Moreover, it is possible, that, contrary to the current design of the model, in reality fresh mitochondria generated by biogenesis do not carry any metabolites and are useless for ATP production until they either have produced enzymes on their own and proteins or have been supplied by other mitochondria following a fusion process.

So far, in the model the maximum number of SMUs is limited by the starting number N_{start} and the model does not include an aging procedure for biogenesis. Experiments point to increased biogenetic activities and a growing mitochondrial mass in aged cells. [36, 64]. This mechanism could be integrated in the model in future.

The ATP consumers are modeled by Mie potentials, that influence the morphological behavior of SMUs. However, the generation of ATP at energy demanding cell sites also consumes metabolites in mitochondria and harms the mitochondrial health, e.g. by oxidative stress produced during processes of the electron transport chain. [65] Hence, it is reasonable to assume, that the qualities of SMUs are coupled to the proximity to ATP consumers. In a more advanced version of the model, the interaction of mitochondrial qualities and ATP consumers could be integrated by either decreasing the existing quality parameters q_h and q_m or by introducing a third quality parameter q_{atp}, that represents the amount of ATP carried by a SMU. It would be possible to couple this third quality parameter q_{atp} to the grade of integrity of the two existing ones. With this mechanism, a quality-dependent interaction of SMUs and ATP consumers would also take into account a saturation value of ATP for each consumer. Then, the ATP consumer would stop attracting additional SMUs, if the saturation of the consumer is accomplished by the sourrounding SMUs. With these modifications, the energetic cellular architecture could be reconstructed individually for different cell types, such as keratinocytes and fibroblasts. ATP consumers would not only represent general cell functions but could model specific ATP consuming organelles, as e.g. the endoplasmatic reticulum and the Golgi aparatus. [66, 67]

Dependent on the outcomes of more complex versions of the model one might find that the mitochondrial network behaves as a canonical ensemble. The heat bath of the thermodynamic equilibrium would be represented by the cell's environment inducing varying energy demands. Then, the state of the mitochondrial network could be described by a small number of state variables. The velocity of mitochondria could represent a varying temperature and the constant volume would be defined by the shape of the cell. However, in a canonical ensemble, the number of smallest mitochondrial units should be kept at a constant value. Since the mitochondrial mass grows during aging [36], comparison of different mitochondrial networks with canonical states could only be used within a single age group.

Chapter 4

Mitochondrial Network in vivo

The multiphoton microscope Dermaninspect (in-vivo intravital tomograph) developed by Beiersdorf AG (Hamburg, Germany) [68] in collaboration with Jenlab (Jena, Germany) [69] was utilized to perform two in-vivo studies on volunteers in order to investigate the mitochondrial network during epidermal differentiation and skin aging. The fundamental concepts of the experimental setup and the tools of analysis of the investigations are presented in the following chapter.

4.1 Materials and Methods

4.1.1 Non-linear Excitation

Light has two natures. Maxwell's equations (4.1 - 4.4) [70]

$$\nabla \vec{E} = \frac{\rho}{\epsilon_0} \tag{4.1}$$

$$\nabla \vec{B} = 0 \tag{4.2}$$

$$\nabla \times \vec{E} = -\frac{\partial B}{\partial t} \tag{4.3}$$

$$\nabla \times \vec{B} = \mu_0 (\vec{J} + \epsilon \frac{\partial E}{\partial t}) \tag{4.4}$$

with $\vec{E}$ and $\vec{B}$ being the electric field and magnetic field, ρ and $\vec{J}$ being the electric charge density and the electric current density, and with the permeability in the vacuum $\mu_0 = \frac{4\pi}{c}$ and the permittivity in the vacuum $\mu_0 = \frac{1}{4\pi c}$ being universal constants depending on the speed of light $c = 299792458 \frac{m}{s}$, lead in the absence of electrical charge $\rho = 0$ and electrical current $\vec{J} = 0$ to the classical wave equations (4.5-4.6)

$$\nabla^2 \vec{E} = \frac{1}{c^2} \frac{\partial^2 E}{\partial t^2} \tag{4.5}$$

$$\nabla^2 \vec{B} = \frac{1}{c^2} \frac{\partial^2 B}{\partial t^2} \tag{4.6}$$

As a result, light is considered as an electromagnetic wave. The parameter $\lambda = \frac{c}{f}$ (f=frequency) is defined as the wavelength of electromagnetic radiation. The spectrum between $\lambda = 380\,\text{nm}$ (ultraviolett (UV) radiation) and $\lambda = 780\,\text{nm}$ (infrared (IR) radiation) is considered to be visible light.

As light is transported, emitted and absorbed in quantum packages called photons, it can also be esteemed as a particle. [71] The energy E and the momentum $\vec{p}$ of a photon are given by

$$E = \hbar\omega = \frac{hc}{\lambda} \tag{4.7}$$

$$\vec{p} = \hbar\vec{k} \tag{4.8}$$

where $h = 6.626 \cdot 10^{-34} \frac{m^2 kg}{s}$ and $\hbar = \frac{h}{2\pi}$ are Planck's constant and the reduced form of Planck's constant, respectively. The parameter $\omega = 2\pi f$ represents the angular frequency of the photon, while $\vec{k}$ denotes its wave vector with the absolute value $|k| = \frac{2\pi}{\lambda}$. [72]

Quantum systems as, e.g., an atom or a molecule can emit photons spontaneously if they are stimulated to establish an excited state. In excited atoms and molecules, electrons have previously absorbed energy by an interaction with their environment, so that they are pushed out of the orbit of their ground state to higher energy levels. Electrons can release their surplus of energy by emitting a photon and subsequently fall back to their ground state. This process is called spontaneous emission. The emitted light is named fluorescence. The energy of the emitted photon E_{emit} with angular frequency ω_{emit} is given by the difference between the energy levels E_1, E_0 and $E_{\text{non-rad}}$, with E_1 being the excited energy state, E_0 being the ground state and $E_{\text{non-rad}}$ being non-radiative losses:

$$E_{\text{emit}} = E_1 - E_0 - E_{\text{non-rad}} = \hbar\omega_{\text{emit}} \tag{4.9}$$

Atoms or molecules which emit photons upon excitation are called fluorophores. Sources of electromagnetic radiation as, e.g., lasers can be used to stimulate fluorophores to emit fluorescence. Due to the non-radiative energy losses $E_{\text{non-rad}}$ the energy of the absorbed photon is always higher

$$E_{\text{emit}} < E_{\text{abs}} = E_1 - E_0 \tag{4.10}$$

and its wavelength correspondingly shorter than of the emitted photon:

$$\lambda_{\text{emit}} > \lambda_{\text{abs}} \tag{4.11}$$

An electron that absorbs the energy of a photon remains in its excited state for an average lifetime of τ_0. Hence, if a great amount of molecules of a distinct fluorophore is irradiated with a laser light, the number of fluorophores in the excited state N over time t is given by:

$$N = N_0 \cdot \exp(\frac{t}{\tau_0}) \tag{4.12}$$

with N_0 being the number of excited fluorophores at $t = 0$.

During excitation the transition rate R_{10} of the fluorophore between ground state E_0 and excited state E_1 is linearly proportional to the intensity I of the incoming radiation:

$$R_{10,1p} = \sigma_{1p}(\omega_{\text{in}}) \cdot I \tag{4.13}$$

The cross-section σ_{1p} is dependent on the angular frequency ω_{in} of the absorbed photons and is given in units of $\frac{\text{cm}^2\text{s}}{\text{photons}}$. [73]

Instead of exciting an electron by one photon from ground state E_0 to energy level E_1, the electron can absorb two, three or more photons with an energy of E_{abs} in total. [73] In case of a two-photon excitation both photons possess half the energy of the substituted photon: $E_{\text{2p,abs}} = \frac{E_{\text{abs}}}{2}$ (Figure 4.1).

As a consequence, the wavelength of the absorbed photons is twice as long:

$$\lambda_{\text{2p,abs}} = \lambda_{\text{abs}} \cdot 2 \tag{4.14}$$

FIGURE 4.1: Jablonksi diagram for two-photon excitation
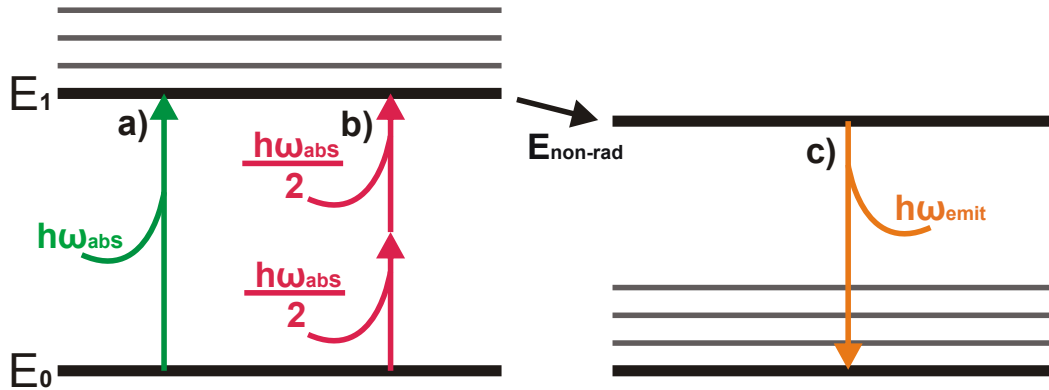
The thick lines represent the main energy levels E_0 and E_1, the thin lines are corresponding rotation and vibration states. a) Linear excitation of an electron from E_0 to E_1 by one photon with frequency ω_{abs}. b) Nonlinear excitation from E_0 to E_1 by parallel absorption of two photons with frequency $\frac{\omega_{\text{abs}}}{2}$. c) The electron falls from E_1 to E_0 by emitting a photon with frequency ω_{emit}.

The non-linear excitation process requires both photons to be absorbed simultaneously by the electron. Hence, there is no intermediate state of the electron between ground-state E_0 and excited state E_1, where the fluorophore has absorbed only one of the two photons. In reality, the photon that is firstly absorbed by the electron has a occupation time of about $0.21\,\text{fs}$ in a virtual state at an excitation wavelength of $800\,\text{nm}$. [74] For a two-photon-effect, the second photon has to meet the electron in that time interval. Contrary to absorption of one photon by an electron, for two-photon excitation the transition rate $R_{10,2p}$ of the fluorophore establishes a quadratic dependence of the intensity of the incoming radiation [75]:

$$R_{10,2p} = \sigma_{2p}(\omega_{\text{in}}^2) \cdot I^2 \tag{4.15}$$

Here, the cross-section σ_{2p} for the transition rate $R_{10,2p}$ is given in measures of GM (Göppert-Mayers), a tribute to the developer of the theory behind two-photon excitation processes, Maria Göppert-Mayer. $1\,\text{GM}$ translates to $10^{-50}\,\frac{\text{cm}^4\text{s}}{\text{photons}^2}$. Correspondingly, σ_{2p} depends on the quadratic of the angular frequency of the incoming radiation ω_{in}.

4.1.1.1 Multiphoton Microscopy

Fluorescence microscopes such as the confocal laser scanning microscope (CLSM) use the emission of light by fluorophores in order to image small structures, as e.g. in biological

systems. In laser scanning microscopy, monochromatic laser light is focused by a lens to the sample. The focal spot probes the surface or a layer within in the sample to excite relevant fluorophores. Their emitted fluorescence propagates back through the lens and is registered by photo-sensitive detectors, such as photo diodes or photomultiplier tubes. By analyzing the detector signals, the fluorescing sample structures are visualized. Imaging different layers in the sample allows to reconstruct it in three dimensions. The spatial resolution of the image is limited by Abbé's Law [76]:

$$d = \frac{\lambda}{2NA} \tag{4.16}$$

According to (4.16), two points in the sample have to have a distance of d in order to image them separately through a lens with a numerical aperture NA using light of a wavelength λ. If self-luminuous structures are investigated as in fluorescence microscopy, two points can be separated if the maximum of the diffractive airy disk of one fluorescing point falls in the minimum of the airy disk of the other point. This leads to Rayleigh's criterion for the resolution of self-luminous structures [77]:

$$d = \frac{0.61\lambda}{NA} \tag{4.17}$$

Practically, this results in a resolution of a few hundred nanometers for images performed with fluorescence laser scanning microscopy.

A multiphoton microscope is a laser scanning microscope, which excites the fluorescence in the sample by nonlinear processes. In two-photon excitation microscopy, due to the quadratic dependence from the intensity of the incoming radiation as given in equation (4.15), focusing of incident laser light through the lens results in a localized excitation of the fluorophore. As a result, the fluorescence in a defined spot in the sample can be imaged with minimized disturbance of stray light of surrounding layers. Therefore, a multiphoton microscope has a better resolution in $x-, y-$ and z-direction than other laser scanning microscopes.

By utilizing the two-photon-effect, the exciting photons of a multiphoton microscope possess half the energy that would be necessary to perform linear excitation. Hence, the wavelength of the laser light is allowed to be twice as long as in one-photon-excitation according to formula (4.14). The elastic scattering of light by structures smaller than the wavelength as in biological samples, shrinks with growing wavelengths according to Rayleigh's law [78]:

$$\sigma_R = \frac{2\pi^5}{3} \frac{d^6}{\lambda^4} \left(\frac{n^2 - 1}{n^2 + 2} \right)^2 \tag{4.18}$$

with σ_R being the average cross-section over all scattering angles of the incident light beam, d representing the diameter of a particle at which the light is scattered, and n being the refractive index of the medium. As a consequence, light with longer wavelengths penetrates deeper into a medium than light with shorter wavelengths. Thus, multiphoton microscopes can image deeper layers in an investigated biological sample than laser scanning microscopes using linear excitation.

Experimental investigations presented in this chapter were performed with the Dermaninspect. This microscope is CE-marked for *in vivo* investigations on skin.

Photons for the excitation of fluorophores are generated by a Ti:sapphire laser (titanium-sapphire laser) called MaiTai (SpectraPhysics, Darmstadt, Germany). [79] Via mode-locking, the MaiTai emits laser pulses with a repetition rate of 80 MHz and a pulse width under 100 fs in the spectral range between $\lambda_{\mathrm{min}} = 710\,\mathrm{nm}$ and $\lambda_{\mathrm{max}} = 920\,\mathrm{nm}$. The photon density in the femtosecond laser pulses is high enough for simultaneous absorption of two or more photons by fluorophores and therefore can be utilized to perform multiphoton excitation. For safety reasons, the maximum power of the laser light is limited to 50 mW.

After passing a polarizer, that is meant to adjust the power input of laser radiaton to the microscope, the laser pulses fall into an objective with a 40x magnification (Zeiss, Oberkochen, Germany). [80] The laser light is focused onto the sample in order to excite fluorophores present in the investigated biological structures. The fluorescence along with the reflected laser light propagates back through the objective and passes a beamsplitter that separates the reflected light and the autofluorescence. Then, optical filters allow to select the wavelength of the autofluorescence that shall be investigated. The Dermaninspect provides optical filters for four different spectral ranges. For measurements in the epidermis and dermis two filters were used: A $548\pm150\,\mathrm{nm}$ filter for autofluorescence and a $410\pm20\,\mathrm{nm}$ filter for second harmonic generation. The filtered fluorescence light finally falls on the detector of a photomultiplier tube (PMT) which amplifies the signal and sends it to a personal computer.

In order to perform three-dimensional investigations, the laser pulses scan the sample. For lateral imaging, the laser light is reflected from a fast moving scanning mirror that guides the laser pulses through the focal layer. The third dimension is visualized by changing the focal layer in vertical direction via a piezo element the moves the objective in z-direction.

The Dermainspect is able to image sections of the sample with a resolution of $512\,\mu\mathrm{m}$ x $512\,\mu\mathrm{m}$, $1024\,\mu\mathrm{m}$ x $1024\,\mu\mathrm{m}$ or $2048\,\mu\mathrm{m}$ x $2048\,\mu\mathrm{m}$. Different zoom steps allow to increase the spatial resolution by parallel reducing the captured section. The point spread function of the microscope leads to a maximum spatial resolution of about $0.4\,\mu\mathrm{m}$ in laterial dimensions and $1.3\,\mu\mathrm{m}$ in vertical direction. [81] The setup allows imaging of dermal layers in depths of about $150\,\mu\mathrm{m}$. Increasing the sampling time from 1 s to a

FIGURE 4.2: Scheme of the setup of the Dermainspect
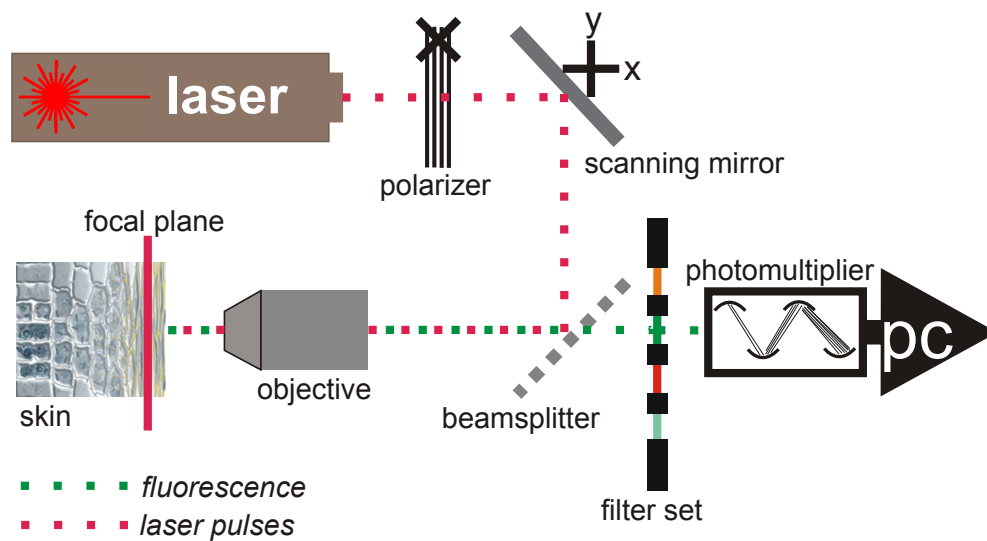
The power of short laser pulses is regulated by a polarizer. A scan mirror guides the pulses through the lateral dimensions (x-y) of the focal plane in the sample. Beforehand pulses are focused by an objective. A piezo element connected to the objective alters the focal plane in z-direction. A beam splitter separates autofluorescence from reflected laser light. The autofluorescence is filtered by one of four optical filters. The signal is emphasized by a photomultiplier tube and eventually analyzed by software on a personal computer.

maximum of about 24 s during the investigation of the sample maximizes the signal-to-noise ratio.

A scheme of the setup is depicted in Figure 4.2.

4.1.2 Endogeneous Fluorophores in Skin

The Dermaninspect is used to image the fluorescence of endogeneous fluorophores in skin. Therefore, no structures in the sample have to be stained. Hence, the investigations are apart from the laser radiation a non-invasive process. Skin consists of three different layers: The epidermis, the dermis and the subcutis (Figure 4.3). The Dermainspect is able to visualize all layers in the epidermis and the upper layers in the dermis *in-vivo*.

FIGURE 4.3: Scheme of the skin
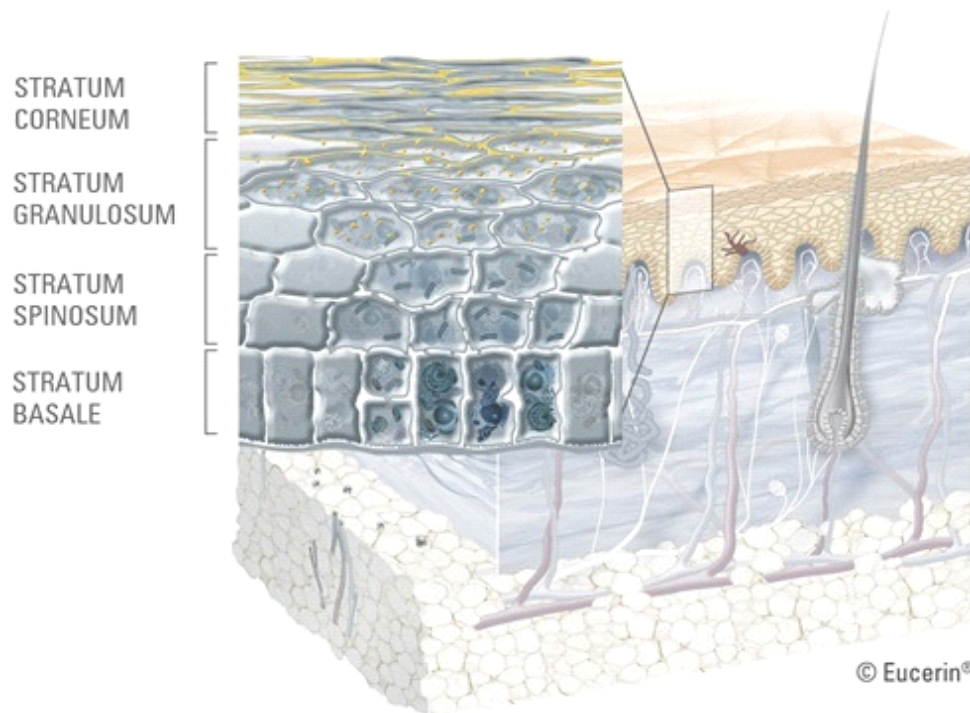
The three main layers of skin are depicted. Beneath the thin epidermis consisting of keratinocytes lies the dermis build of structural proteins such as collagen and elastin. The deepest layer is the subcutis. Die scheme was provided by Eucerin, Beiersdorf.

4.1.2.1 Epidermis

The epidermis is the outer layer of the skin and protects it against microorganisms, loss of water and other external influences as UV radiation as part of the sunlight.
It consists of four sublayers, that represent the differentiation process of keratinocytes. In the undermost layer, the basal layer (stratum basale), proliferation of new keratinocytes via division of stem cells occurs. The new cells move to the upper layers stratum spinosum and stratum granulosum and are transformed to dead corneocytes in the stratum corneum at the end of their differentiation process. During their transition, cells synthesize several keratin proteins that form bundles of keratin filaments. Furthermore, membrane-coating granules release lipids into the intercellular spaces. Meanwhile the shapes of the cells flatten. The last living layer of keratinocytes in the stratum granulosum and the dead corneocytes in the stratum corneum are separated by the stratum lucidum that basically consists of water-resistant lipids and is only visible in palms and foot soles. [3] The stratum corneum forms a hardly penetrable barrier against the intrusion of undesired substances. Corneocytes appear as flattend squames, that are sealed together by lipids and basically consist of the cytoskeleton made of keratin filaments.

[82] The process of differentation from the stratum basale to the stratum corneum is called the epidermal turnover and takes about 40-56 days for one cell layer. [83] The thickness of the epidermis differs between 55 μm to 85 μm. [84]

There are several endogenous fluorophores present in keratinocytes that allow two-photon imaging of epidermal structures. [85] While keratin is basically observed in dead corneocytes, melanin is mostly present in basal cells after being transported from nearby melanocytes via melanosomes. [86] The metabolic activity of keratinocytes can be observed by the autofluorescence of the coenzymes flavin adenine dinucleotide (FAD) and nicotinamide adenine dinucleotide (NADH). [87, 88]

NADH is the most present mitochondrial metabolic fluorophore in the epidermis. [89] It takes part as a coenzyme in the production of adenosine triphosphate (ATP) via glycolysis and oxidative phosphorylation.

In the cytoplasm of a cell, glycolysis decomposes glucose molecules ingested by nutrition into smaller pyruvate molecules and generates two ATP molecules. Additionally, as side products, water, H^+-ions and two NADH molecules are produced. Along with the pyruvate, the NADH molecules are transported to the cell's mitochondria and enter the organelles through their membranes by the Malat-Aspartat shuttle or the glycerol phosphate shuttle. After transforming pyruvate to acetyl-CoA enzymatically during pyruvate decarboxylation, the energy of acetyl-CoA is released by dissolving the energy rich bonds between hydrogen and the rest of the molecule. In this context, three NAD+ molecules are reduced to three NADH molecules per acetyl-CoA. These processes take place in the Krebs cycle within the mitochondrial matrix. Afterwards, the gained energy is transported via the NADH molecules to the matrix protein complexes of the respiratory chain at the inner mitochondrial mebrane. There, NADH hands over an electron to Complex 1 (NADH:ubiquinone oxidoreductase), so that NADH is oxidated again to NAD+. The energy of the electron is gradually released by transferring it from Complex 1 to 2, 3 and 4. The mitochondrion utilizes the released energy to establish a proton motive force along the inner mitochondrial membrane in order to finally transform adenosine diphosphate (ADP) to ATP. [5]

These energy-related processes involving NADH take place within mitochondria. Therefore, apart from NADH produced during glycolysis and being transported to the mitochondrial membrane, cellular NADH is basically located in mitochondrial bodies. Hence, one can assume, that the autofluorescence of NADH represents mitochondrial structures. In order to test this hypothesis, the autofluorescence of NADH was correlated with the fluorescence of stained mitochondria in cultured keratinocytes. For that purpose, neonatal human epidermal keratinocytes were purchased from Lonza Group AG (Basel, Switzerland) [90] and cultured in Dulbecco's Modified Eagle Medium (DMEM) (Life Technologies, Carlsbad, USA) [91], supplemented with 10% fetal calf serum (PAA Laboratories, Pasching, Austria) [92], L-glutamine and penicillin/streptomycin (both:

Life Technologies, Carlsbad, USA). For ideal atmospheric culturing conditions the keratinocytes were maintained in a humidifying incubator with a 5% CO_2 atmosphere at 37°C. Mitochondria in the cells were stained with the fluorescence dye Mito-Tracker Red CMXRos (Life Technologies, Carlsbad, USA) with wavelengths of excitation and emission at 579nm and 599nm, respectively.

Morphological signals of both, the autofluorescence of NADH and the stained mitochondria were compared using a confocal scanning microscope (Leica TCS SP5, Leica Microsystems, Mannheim, Germany) [93] with a 63x objective (HCX PL APO lambda blue 63.0x1.20 WATER UV, Leica). Two lasers excited the autofluorescence of NADH at an optical wavelength of 405 nm and the fluorescence of the Mito-Tracker at 561 nm. Photomultiplier tubes detected the emitted signal of NADH in a spectral range going from 410 nm to 540 nm and of the Mito-Tracker between wavelengths from 570 nm to 650 nm. Bidirectional scans of the samples were performed with an image resolution of 2048 pixels $\times$ 2048 pixels at zoom 3.0, zoom 4.4 and at zoom 7.9. The step size of the focal spot was in every measurement 0.04 μm. The optical resolution of the setup is according to Leica's software about 163 nm in lateral dimensions.

The fluorescence of the Mito-Tracker discloses a near perfect agreement with the autofluorescence of NADH (Figure 4.4). Aberrations are caused by an overstaining of mitochondria with the mitotracker which leads to a merging of separated mitochondrial structures. Additionally, deviations in the metabolic activity of mitochondria leads to discrepancies of intensities in autofluorescence of NADH. Overall, measurements with the confocal scanning microscope confirm the hypothesis, that the autofluorescence of NADH represents the morphological shape of mitochondrial structures.

Excitation and emission spectra of NADH and nicotinamide adenine dinucleotide phosphate (NADPH) are identical. NADPH is a coenzyme that is involved in the pentose phosphate pathway which takes place in the cytoplasm of the cell. [5] Thus, NADPH is not located in mitochondria. Therefore, the overlap of fluorescence spectra of NADPH with NADH might cause a wrong impression of mitochondrial structures. However, experiments revealed, that the concentration of NADH in the cell is about five times higher and the quantum yield of NADH is 1.5 times to 2.5 times greater than of NADPH.[94] Hence, the autofluorescence of NADPH is neglected when analyzing the morphology of the mitochondrial network by the autofluorescence of NADH.

4.1.2.2 Dermis

The dermis is adjacent to the epidermis. It is several hundred micrometers thick and hosts capillaries, hair follicles, sweat glands and sebaceous glands. Moreover, it contains structural proteins such as collagen and elastin, that provide the skin with elasticity

FIGURE 4.4: Autofluorescence of Nicotinamide adenine dinucleotide and stained mitochondria
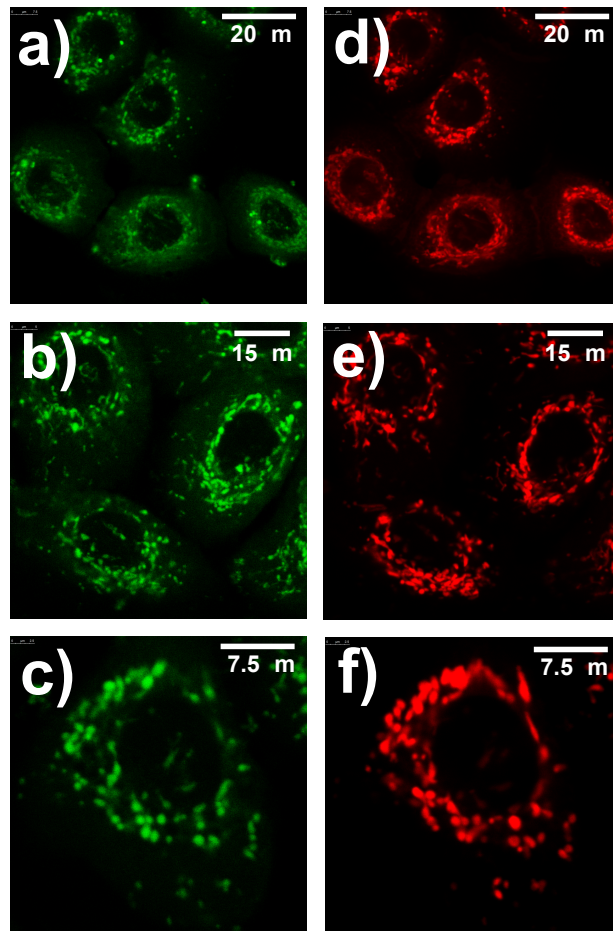
The autofluorescence of NADH (a-c) in comparison with fluorescence of mitochondria stained with MitoTracker (d-f) in cultured keratinocytes with zooming levels 3.0 (a,d), 4.4 (b,e) and 7.9 (c,f)

and firmness. Both of these proteins can be imaged using multiphoton microscopy. While elastic fibers show a characteristic autofluorescence, collagen is imaged by its second harmonic generation (SHG) signal due to the periodic structures of the collagen fibers.[95, 96] As a result, incoming laser radiation with a wavelength of 820 nm gives a defined emission of 410 nm, that can be detected by separating it from the autofluorescence of elastin using a narrow optical bandpass filter. The emitted spectrum in the dermis also contains the autofluorescence of advanced glycation endproducts (AGEs). AGEs are the result of the reaction of dermal proteins with reducing sugars. They are long-living, very stable structures and disturb the elasticity of the dermis by harming structural proteins. AGEs emit light in a broad spectral range. Despite several attempts, so far it is not possible to separate their autofluorescence explicitly from other

fluorophores in skin.[97, 98]

4.1.2.3 Multiphotonic imaging of skin

An image through the epidermis and the upper dermis is shown in Figure 4.5. It was taken at the inner side of the forearm of a 27 year old volunteer. The measurement was performed with the Dermainspect at a two-photonic excitation wavelength of 760 nm for autofluorescence and 820 nm for second harmonic generation.

In the uppermost layer, the stratum corneum, the autofluorescence of keratin depicts the honeycomb structure of corneocytes. Beneath the stratum lucidum that basically consists of transparent lipids and does not fluoresce [3], the stratum granulosum is located. There, keratinocytes establish a very flat shape. The dark spots in the center of the cells are the nuclei, while the very bright patterns in the cytoplasm are caused by the autofluorescence of NADH. These structures represent the morphology of the mitochondrial network. In deeper layers cross-sections of the cells shrink, as keratinocytes are less flat and establish three-dimensional shapes. In the stratum spinosum cell borders of adjacent cells morphologically adapt to each other so that the overall cell layer appears as a mosaic-like structure. In the stratum basale keratinocytes have vertical tube-like shapes. Cross-sections though the cells are so small, that it is not possible to differentiate mitochondrial morphologies from each other. Furthermore, the autofluorescence of melanin, that covers the top of the basal cells as caps, overlaps with emission spectrum of NADH (Figure 4.5). [85]

In the dermis, the autofluorescence signal discloses the structure of elastin fibers. Next to the epidermis, fluorescent elastin appears as vertical elaunin filaments, that are connected to the dermal papillae.[99] In deeper layers, elastin forms broader horizontal fibers. The signal of second harmonic generation reveals the very dense network of collagen fibers. Single filaments bundle to thicker fibers that form a seemingly anarchic system. Collagen fibers are held together by fibroblasts, that connect to the filaments and produce new collagen molecules.[100]

4.1.3 Image Analysis

In the stratum granulosum and the stratum spinosum of skin, multiphoton micrographs show the morphological state of the mitochondrial network based on the autofluorescence of NADH.

In order to analyse the shape and the morphology of mitochondrial clusters in the stratum spinosum and the stratum granulosum, the autofluorescence of NADH has to be

FIGURE 4.5: In-vivo stack through epidermal and dermal layers
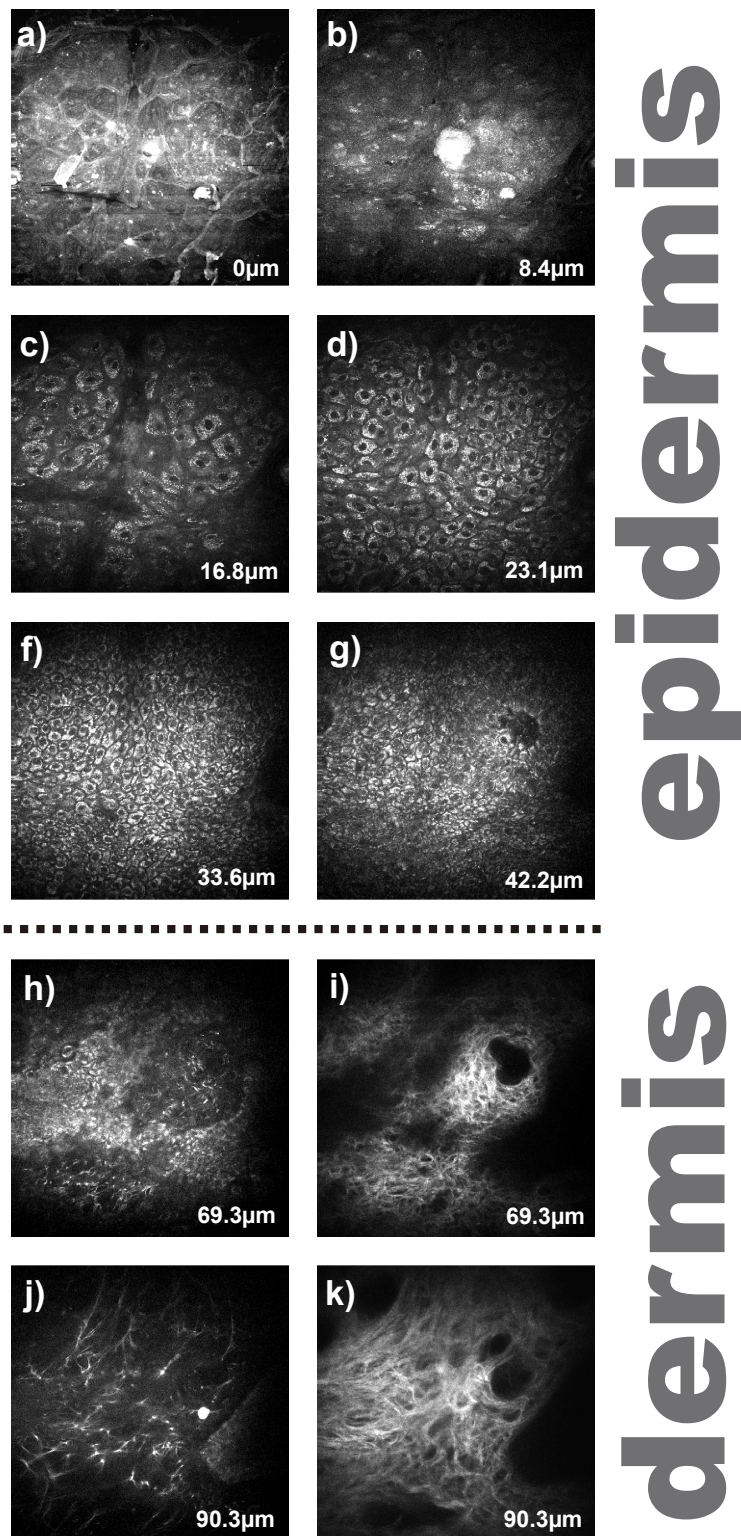
A stack of in-vivo images taken in the epidermis and the upper layers of the dermis of a volunteer. In the epidermis, the stratum corneum (a), the stratum lucidum (b), the stratum granulosum (c), the stratum spinosum (d) and the tube-like basal cells (e, f) are imaged. Dermal structures are revealed by autofluorescence of elastin partially in papillae (h) and then over the whole area of the measurement (j). Parallel measurements of the SHG-Signal disclose the network of collagen fibers (i,k).

extracted from the micrographs. Hence, each pixel in the measurements has to be categorized either as autofluorescence of NADH or as a cytosolic background signal. This separation can be implemented by performing a binarization procedure.

4.1.3.1 Otsu's method

The simplest form of binarization is to apply an arbitrary threshold to the image. Each pixel in the micrograph possesses an individual gray value between 0 and 255 which relates to the intensity of the autofluorescence at this spatial point in the measurement. A global binarization threshold categorizes each pixel either as NADH autofluorescence or as background depending on its gray value. In Figure 4.6 several values for a binarization threshold for the measurements of keratinocytes in the stratum granulosum are tested. The higher the value, the less pixels are classified as NADH. As an alternative for choosing the threshold based on subjective impression, N. Otsu suggested a method for finding an objectively reasonable threshold for binarization.[101] In Otsu's algorithm, binarization is performed without any other a priori knowledge about the studied picture. The algorithm calculates gradually all possible binarizations and selects the one threshold T as optimal that minimizes Otsu's variance:

$$\sigma_{\text{otsu}}^2(T) = \omega_{\text{white}}(T)\sigma_{\text{white}}^2(T) + \omega_{\text{black}}\sigma_{\text{black}}(T)^2 \tag{4.19}$$

with σ_{white}^2 and $\sigma_{\text{black}}^2(T)$ being the variances among gray values of pixels categorized as white (NADH fluorescence) and black (background), respectively. Parameters ω_{white} and ω_{black} are the corresponding weights and represent the probability of a pixel being black or white depending on the chosen threshold T:

$$\omega_{\text{white/black}}(T) = \frac{n_{\text{black/white}}}{N_{\text{total}}} \tag{4.20}$$

where $n_{\text{black/white}}$ represents the number of black and white pixels, respectively and N_{total} represents the total number of pixels in the image. In other words, Otsu's method finds the threshold, in which the gray values among pixels in both classifications, signal and background, are as similar as possible. A global binarization of a keratinocyte with Otsu's method is depicted in Figure 4.6d.

FIGURE 4.6: Binarization procedure of Nicotinamide adenine dinucleotide autofluorescence in keratinocytes
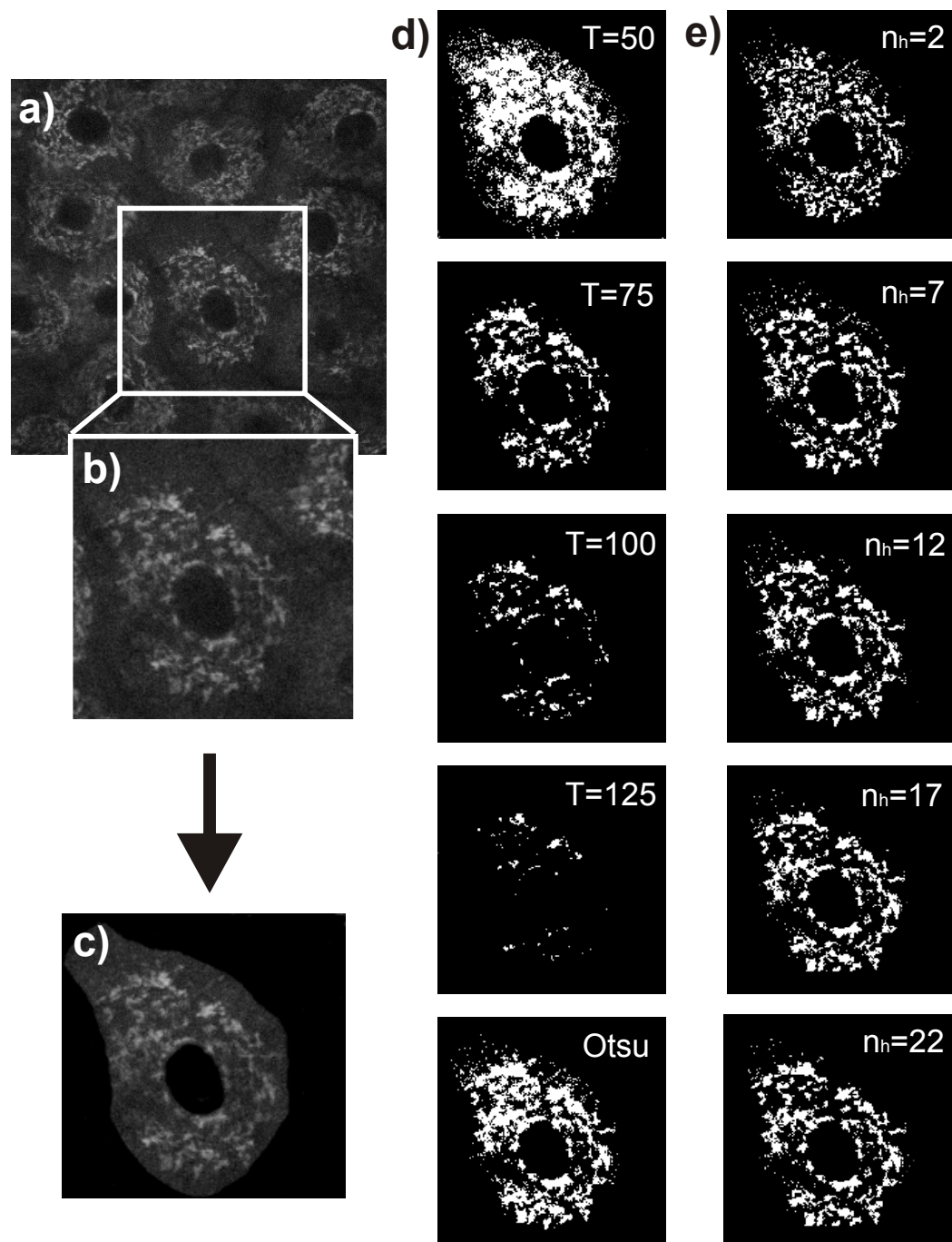
In a measurement (a) the cytoplasm of single keratinocytes (b) is segregated by manually annotating borders of the cell and the nucleus (c). Binarization procedures are performed in the annotated cytoplasms. Different values for a global threshold are compared with the threshold derived by the Otsu method (d). In (e) binarizations with a global and a local Otsu threshold are compared. The size of the local neighbourhood is altered by changing n_h.

4.1.3.2 Local threshold

For various reasons keratinocytes in multiphoton micrographs in the epidermis do not establish a homogeneous intensity over a cell's cross-section. Metabolic variations within the cytoplasm cause fluctuations in the intensity of the autofluorescence of NADH. Furthermore, many cells are not perfectly orientated parallel to the focal plane, so that the autofluorescence in different areas is not excited with the same intensity.

Because a binarization method including a global threshold only does not take into account local intensity disturbances within the image, it falls short in extracting the autofluorescence of NADH in multiphotonic micrographs.

To factor intensity fluctuations in the imaged keratinocyte during the binarization procedure, a local threshold is introduced. This threshold is individual for each pixel in the image and is derived by minimizing Otsu's variance among adjacent pixels. Subsequently, a pixel has to exceed both thresholds, the general global and the individual local threshold, in order to be categorized as autofluorescence of NADH. However, there is no method, to determine a suitable objective value for the size of the area of the pixels' individual neighbourhood. In Figure 4.6e binarizations with different values for the numbers of adjacent pixels regarding the calculation of a local threshold are depicted. The neighbourhood value n_h is an integer, that gives the number of consecutive pixels on an arbitrary edge of the investigated pixel, that are included in deriving the local Otsu threshold. Binarizations with a neighbourhood value of $n_h = 7$ show good results regarding an extraction of the autoflourescence of NADH. With a spatial resolution of $0.4\,\mu$m this is in line with the maximum value of a mitochondria structure of about $3\,\mu$m $(0.4\,\mu\text{m} \times 7 = 2.8\,\mu\text{m})$. [61] Therefore, in all following analysis the neighbourhood value is set to $n_h = 7$.

4.1.3.3 Analysis procedure

All quantitative analysis was performed with the software *SkinTools* from Beiersdorf AG. The Otsu-based algorithm for binarization of multiphoton micrographs was put into practice in the programming language Java [33] under usage of the packages *java.util.** [34] and *java.io.**. [35] Subsequently, the corresponding code was implemented in SkinTools and is attached to this thesis in Appendix C.

In order to perform segregation of autofluorescence from the background in the cytoplasm of keratinocytes, before binarization the borders of the cells and the corresponding nuclei were annotated manually (Figure 4.6c). Afterwards, binarization in the segregated cytoplasm was performed. For quantitative analysis of the morphology of the autofluorescence of NADH, three simple parameters were investigated per keratinocyte. The number of mitochondrial clusters per area of cytoplasm n was determined. Furthermore,

the average cluster size $\overline{A} = \frac{A_f}{n}$ in pixels was calculated by normalizing the fluorescing area A_f to the number of mitochondrial clusters n. In order to take the mitochondrial cluster shape into account for analysis, the average circularity $\overline{C}$ of the clusters was derived. The circularity of C of a single cluster reads:

$$C = \frac{U^2}{4\pi A} \tag{4.21}$$

with U representing the circumference of the fluorescing structure given in edges of pixels and A being the area of the structures in pixels. The circularity has a value of $C = 1$ for a perfect circle. The higher the value of the circularity C is, the less compact and more complex is the investigated structure.

4.2 Results

The Dermainspect was utilized to perform two studies in the skin of volunteers. In both studies the morphology of the mitochondrial network in epidermal keratinocytes was investigated based on the autofluorescence of NADH. All volunteers provided healthy skin of either skin type II or skin type III of Fitzpatrick's phototyping scale. [102] Two weeks before and during the studies volunteers desisted visits of solariums and intensive sun exposure. Furthermore, treatment of both, medical substances and cosmetics, was prohibited during the studies. All volunteers were non-smokers. Both studies were performed in accordance with the recommendations of the current version of the Declaration of Helsinki [103] and the guideline of the International Conference on Harmonization Good Clinical Practice (ICH GCP). [104] Prior the examinations volunteers were provided with fifteen minutes of acclimation to the measurements under standard atmospheric conditions with $23°C \pm 1°C$ and $43\% \pm 2\%$ relative humidity level. All measurements were carried out by trained personnel.

Examinations were performed at the inner side of both forearms of each volunteer. For optical immersion a drop of water was positioned at the investigated spot of the skin. Parallel, by using a magnetic adapter, a thin platelet of glass was placed under the objective with immersion oil between the lens and the glass (Figure 4.7). Following these preparations, the objective approached the skin until the focus reached epidermal and dermal layers. All volunteers in both studies were investigated at two areas of each forearm. Measurements at three different positions in each area were acquired. All measurements had an acquisition time of about $12.5\,\mathrm{s}$ and dimensions of $110\,\mu\mathrm{m} \times 110\,\mu\mathrm{m}$ with $512\,\mathrm{pixels} \times 512\,\mathrm{pixels}$ per image.

FIGURE 4.7: Setup of in-vivo measurements
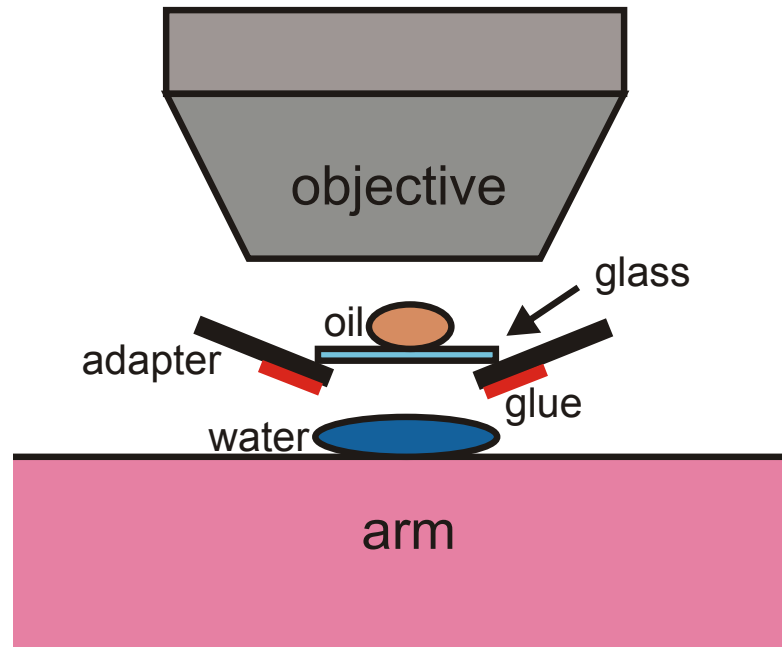
A drop of water is placed on the inner side of the forearm. Immersion oil is placed between the objective and a glass platelet. The three elements are hold together by an magnetic adapter. Then, the objective approaches the arm until the focus of the laser reaches epidermal layers. To prevent movements of the investigated spot relatively to the objective, the skin sticks to the adapter by adhesive tape.

Statistical analysis of morphological parameters was conducted with the software Statistica by StatSoft (Europe) GmbH (Hamburg, Germany). [105] The unpaired samples in the aging study were compared by a Mann-Whitney U test, the paired samples in the differentiation study by a Wilcoxen test. [106] As the p-value for significance the threshold $p =0.05$ was chosen.

In the following subsections the basic results of both studies are presented. Further analysis and discussion are presented in the publication at the end of the chapter.

4.2.1 Aging of Skin

In this study, the morphology of the mitochondrial network in the skin of young and old volunteers was compared. For that purpose, the autofluorescence of keratinocytes in the stratum granulosum was imaged. The study consists of measurements in the epidermis of twelve young (mean $\pm$ SD: 23.75 $\pm$ 1.67 years) and twelve old (mean $\pm$ SD: 72.17 $\pm$ 4.15 years) volunteers.

After experimental examinations and binarization, quantitative analysis of mitochondrial clusters in keratinocytes was performed based on three morphological parameters:

The number of mitochondrial clusters n per area of cytoplasm, the average size of mitochondrial clusters $\overline{A}$ and the average circularity $\overline{C}$. These parameters were analyzed for all mitochondrial clusters in the cytoplasm of keratinocytes and for large mitochondrial clusters. Large mitochondrial clusters are defined as connected fluorescing areas that are larger than the average cluster size in measurements of young volunteers $\overline{A}_{\text{young}} = 9.05$ pixels. Hence, large clusters consist of ten or more pixels. Before statistical comparison between both age groups, the results in each area at the forearms were averaged.

Results for all parameters are presented in Figure 4.8. Analysis disclose that the total amount of autofluorescence of NADH in keratinocytes of cells is significantly higher in old volunteers than in young volunteers ($p \leq 0.001$). Additionally, micrographs show, that cross-sections of single keratinocytes in old volunteers cover greater areas than keratinocytes of young volunteers. [107] Thus, for a relative comparison, the total amount of autofluorescence has to be normalized to the area of the cytoplasm of the cell. Then, a comparison do not reveal any significant differences between young and old skin ($p = 0.826$).

Quantitative analysis of the morphological parameters of all mitochondrial clusters reveals, that the mitochondrial network is more fragmented in old skin than in young skin. There is a significantly higher number n of mitochondrial clusters in keratinocytes of old volunteers than of young volunteers ($p \leq 0.001$). Furthermore, clusters in cells of old skin establish a significantly lower circularity $\overline{C}$ ($p = 0.015$) and a significantly smaller cluster size $\overline{A}$ ($p = 0.035$). Hence, mitochondrial clusters in cells of old volunteers are more compact and smaller than in cells of young volunteers.

A quantitative analysis of the morphology of large mitochondrial clusters discloses a significantly higher number of large mitochondrial clusters n_{large} ($p = 0.039$) in old skin. Additionally, large mitochondrial clusters exhibit higher values for the large cluster size $\overline{A}_{\text{large}}$ ($p = 0.084$) and have a significantly higher circularity $\overline{C}_{\text{large}}$ ($p = 0.002$) in old skin. Thus, large mitochondrial clusters have a tendency to be more complex in the stratum granulosum of old skin.

4.2.2 Epidermal Differentiation

This study was performed in order to investigate alterations in the morphology of the mitochondrial network during the differentiation of keratinocytes in the epidermis. For that purpose keratinocytes at two different states of the differentiation process have to

FIGURE 4.8: Analysis of aging study
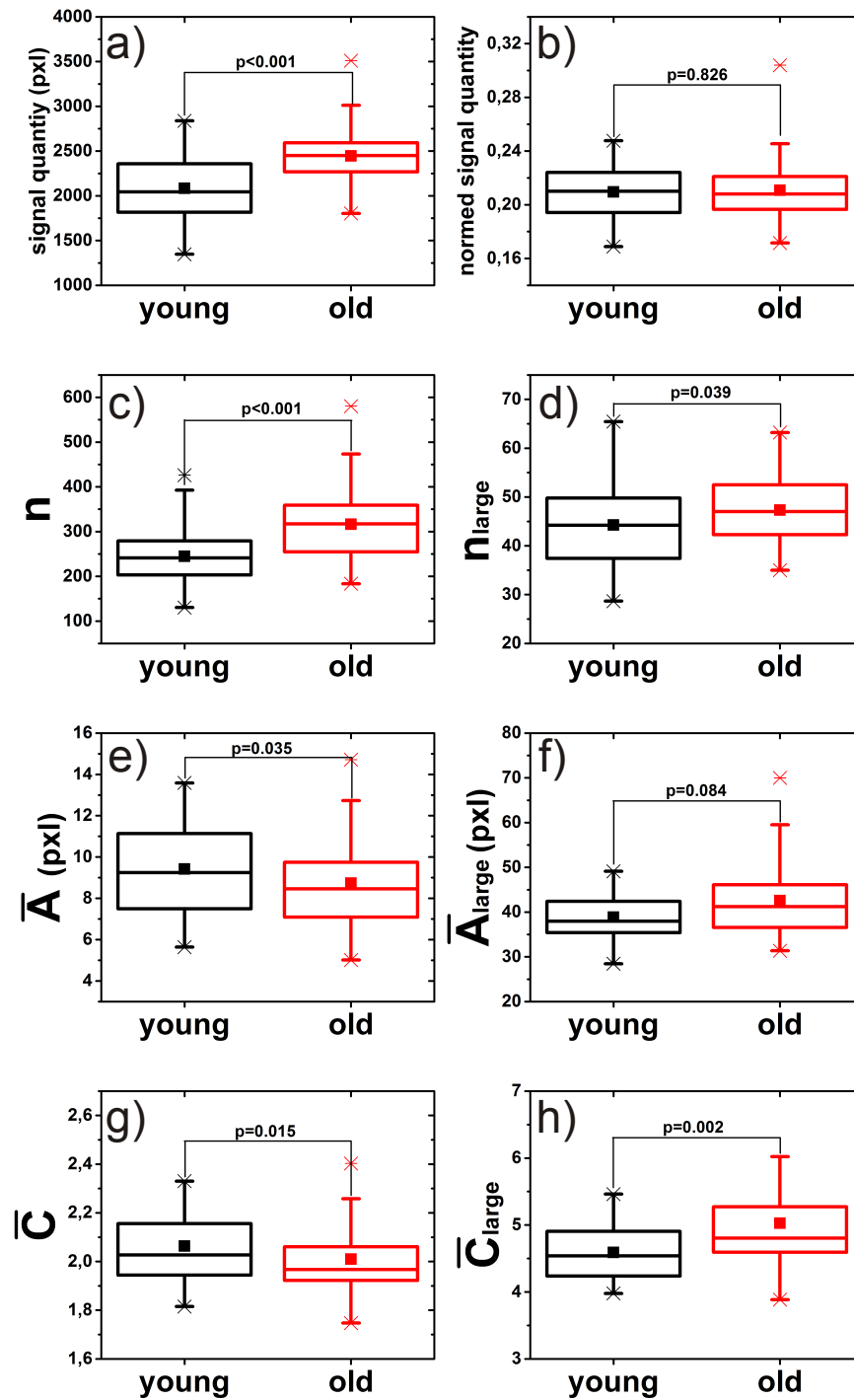
Investigated parameters of the aging study are compared between young and old volunteers by statistical boxplots. The p-value represents the probability if the two compared probability distributions derive from the same population. The square in the box represents the mean value, the horizontal line in the center the median. 25% percent of the measured values are lower than the bottom of the box, 75% of them are lower than the top of the box. The antennas (whiskers) are the corresponding limits for 2.5% and 97.5%. Crosses represent the highest and the lowest value in the distribution.

be imaged. Therefore, examinations in the less differentiated stratum spinosum and in the more differentiated stratum granulosum have been performed. For the study eight volunteers of the same age group (mean $\pm$ SD: 62 ± 1.31 years) were examined. Again, after annotation and binarization procedures the three morphological parameters n, $\overline{A}$ and $\overline{C}$ were investigated for all mitochondrial clusters per cell and for large mitochondrial clusters.

Results for all parameters are presented in Figure 4.9.

As cross-sections of keratinocytes in the stratum spinosum are smaller than in the stratum granulosum, there is less autofluorescence in total in these cells. However, normalizing the amount of autofluorescence to the cell's area discloses a higher density of NADH related signal in the stratum spinosum than in the stratum granulosum.

Quantitative analysis for all clusters reveals a significantly higher number n of mitochondrial clusters in keratinocytes in the stratum granulosum than in the stratum spinosum ($p \leq 0.001$). Moreover, mitochondrial clusters in the stratum spinosum have a significantly higher average size $\overline{A}$ ($p \leq 0.001$) and a significantly higher circularity $\overline{C}$ ($p \leq 0.001$). Hence, mitochondrial clusters in less differentiated keratinocytes in the stratum spinosum establish larger, more complex structures than the more differentiated cells in the stratum granulosum. Thus, during differentiation of keratinocytes the mitochondrial network performs a fragmentation process. Differences between mitochondrial structures of different epidermal layers are similar to the ones of different age groups.

Investigating the same morphological parameters for large mitochondrial clusters reveals a significantly greater average size $\overline{A}_{\text{large}}$ ($p \leq 0.001$) and a significantly higher circularity $\overline{C}_{\text{large}}$ ($p \leq 0.001$) in the stratum spinosum. These findings support the notion of a fragmented mitochondrial network in keratinocytes at the end of their differentiation process in the stratum granulosum. However, analysis of large mitochondrial clusters also discloses a significantly higher number of mitochondrial clusters n_{large} ($p \leq 0.001$) in the stratum granulosum.

4.3 Discussion

Both in-vivo studies demonstrate, that it is possible to image mitochondrial morphologies in the upper epidermis of volunteer's skin based on the autofluorescence of NADH. Therefore, multiphoton microscopy in combination with the Otsu-based binarization algorithm is a valid tool to analyze mitochondrial network structures in vivo.

FIGURE 4.9: Analysis of differentiation study
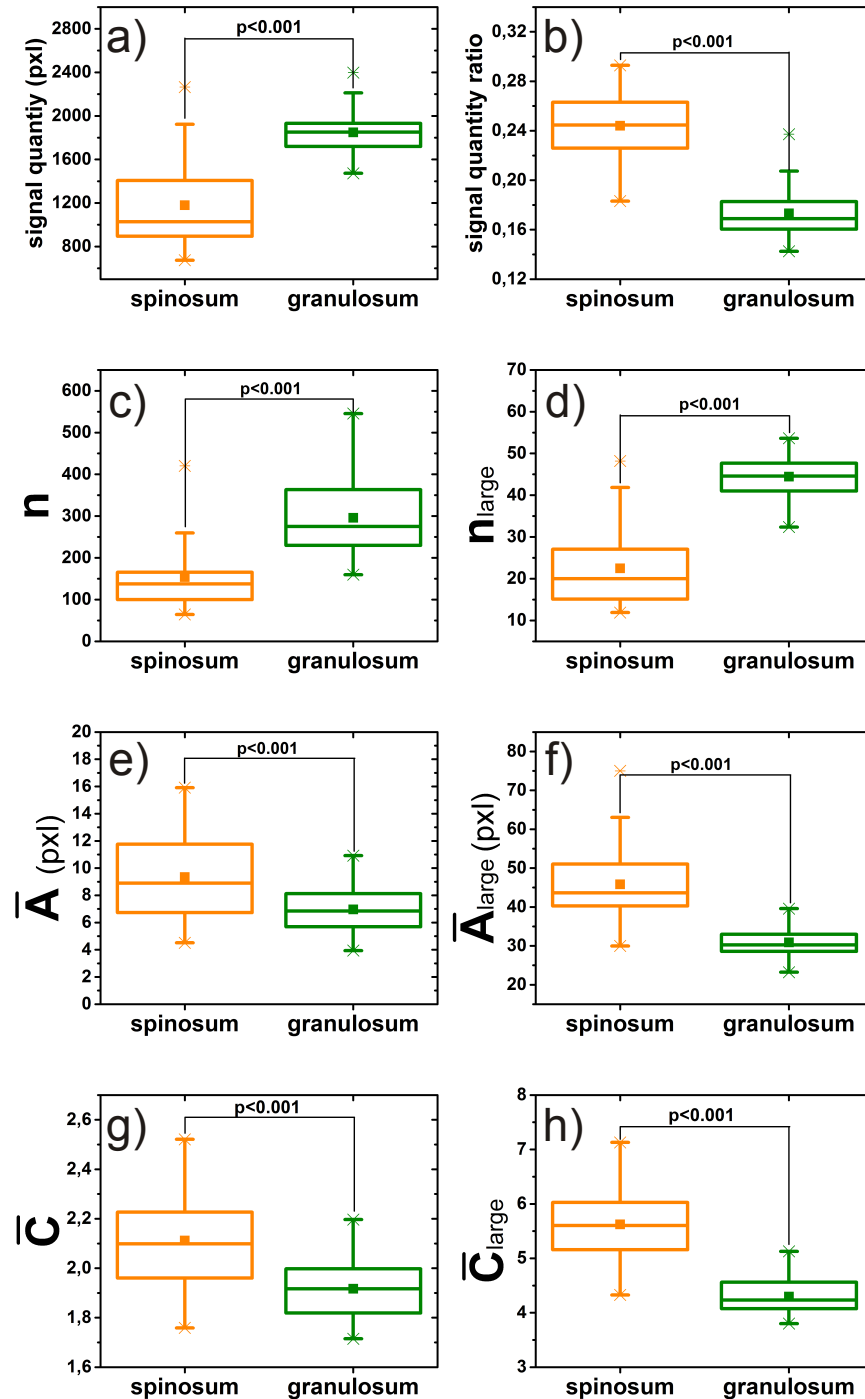
Investigated parameters of the study on differentiation are compared between stratum spinosum and stratum granulosum by statistical boxplots. The p-value represents the probability if two compared probability distributions derive from the same population. The square in the box represents the mean value, the horizontal in the center line the median. 25% percent of the measured values are lower than the bottom of the box, 75% of them are lower than the top of the box. The antennas (whiskers) are the corresponding limits for 2.5% and 97.5%. Crosses represent the highest and the lowest value in the distribution.

4.3.1 Mitochondrial fragmentation

The comparison of the mitochondrial network in the stratum granulosum of different age groups and the investigation of the network during the differentiation of keratinocytes in the epidermis reveal a fragmentation process. During aging and differentiation, mitochondrial morphologies decompose to a higher number of shrinking, compact clusters. The observed fragmentation processes in both studies are in line with the outcomes of the quality model in chapter 2 and the morphological model in chapter 3. Furthermore, smaller mitochondrial clusters in old cells were also observed in recent in-vitro experiments. [38, 39]

Aging and differentiation share different processes that are possibly responsible for mitochondrial fragmentation:

- During aging, the generation of reactive oxygen species (ROS) in skin increases due to production by other cell organelles or by mitochondria themselves. [65] Moreover, continuous UV radiation from the sun produces oxidative stress. [29] ROS harm mitochondrial structures, as e.g. the mitochondrial DNA and cause mitochondrial fission states. [22, 52] Various publications reveal, that oxidative stress also participates in differentiation of keratinocytes and might even be utilized to catalyze several differentiation procedures. [4]

- Over time, cells lose their ability of removing irreversibly harmed mitochondria from the cytoplasm by mitophagic processes. [28] As a result, damaged mitochondria, that do not take part in any fission and fusion processes, remain isolated in the cytoplasm and form a more fragmented mitochondrial network. The involvement of autophagic procedures in differentiation [108] might point in a similar direction for the fragmentation of the mitochondrial network during the epidermal turnover.

- Several aging processes as the decrease of mitochondrial protein synthesis due to damaged mitochondrial DNA sequences [109] lead to a regression of the metabolic activity of mitochondria. Hence, the mitochondrial membrane potential (MMP) which represents the activity of ATP production, declines during aging. [110] Recent experiments revealed, that the reduction of the MMP is also observed during the epidermal differentiation of keratinocytes. [111] As metabolically inactive mitochondria are removed the mitochondrial network [18], the decay of the MMP could result in mitochondrial fragmentation during both, aging and differentiation.

- Experiments on cultured keratinocytes of young and old donors revealed that the composition of the energy metabolism alters during aging. An increased lactate

production in keratinocytes of old donors points to enhanced glycolytic procedures in aged cells. [112] Accordingly, a study on keratinocytes revealed a respiratory uncoupling during differentiation procedures. [113] Publications on mitochondrial morphologies disclose, that increased fermentation and declined oxidative phosphorylation in cells lead to a fragmentation of the mitochondrial network. [114]

However, in each of the two studies investigated parameters for large mitochondrial clusters partially disagree significantly with the impression of a fragmentation of the mitochondrial network.

Comparing granular keratinocytes during aging reveals significantly more complex ($\overline{C}_{\mathrm{large}}$) and greater large clusters ($\overline{A}_{\mathrm{large}}$) in the cells of old skin than of young skin. An explanation for this contradictory observation is provided by the fact, that elongated mitochondria are spared from autophagy. [115] Hence, accumulation of mitochondria to large clusters in cells of old skin might be a mechanism to save healthy mitochondria from being removed by mitophagic processes.

According to the analysis, keratinocytes in the stratum granulosum establish a higher number of large mitochondrial clusters n_{large} than keratinocytes in the stratum spinosum. This contradicts the idea of a fragmented mitochondrial network in more differentiated cells. However, this paradoxical finding is explained by the enormous sizes of the mitochondrial clusters in the stratum spinosum. In this layer the clusters are nearly twice as large as in the stratum granulosum. Instead of forming various large clusters, mitochondria aggregate to few very large structures. Consequently, the number of large clusters is not an adequate parameter to compare the widespread networking morphologies in the stratum spinosum with the more isolated clusters in the stratum granulosum.

4.3.2 Methodical improvements

Although the introduced methods can be considered as a successful approach to analyze the mitochondrial network in human skin in vivo, there is potential for improvements. Due to the altering thickness of the epidermis depending on the volunteer, neither the stratum granulosum nor the stratum spinosum can be imaged in well-defined depths. In the studies, examiners perform a vertical scan from the stratum corneum down to the dermis and define the depths of the stratum granulosum and the stratum spinosum individually for each volunteer. The definitions are made based on the morphological appearance and the experience of the investigators. For future studies, morphological parameters for each layer have to be defined as detailed as possible, as e.g. an average diameter of keratinocytes or an average distance between cell borders.

Not only mitochondrial NADH appears as autofluorescence in the measurements, but also some cytosolic NADH and melanin that penetrates in small doses from the stratum basale to upper epidermal layers. Due to the overlap of excitation and emission spectra, both of these disruptive factors can not be filtered by only measuring the intensity of autofluorescence. However, additionally examining fluorescence lifetimes with a high spatial resolution could assist separating mitochondrial NADH from cytosolic NADH and melanin. Mitochondrial protein-bound NADH has fluorescence lifetimes of about 2.0 ns, while lifetimes of free NADH in the cytosol are about 0.3 ns long. [116] Fluorescence lifetimes of melanin are relatively short with 100 ps. [117] Thus, all three components can be distinguished by their individual lifetime.

In order to track the morphological structure of the mitochondrial network through the whole differentiation process, mitochondrial clusters in the stratum basale have to be investigated. The autofluorescence of NADH could be separated from the fluorescing melanin caps by measuring fluorescence lifetimes. Another solution is an improvement of the resolution in z-direction in order to reconstruct a three-dimensional image of the mitochondrial network in basal cells.

The results of all simulations are presented and discussed in detail in the following manuscript submitted to PLoS ONE.

4.4 Publication

RESEARCH ARTICLE

Fragmentation of the mitochondrial network in skin *in vivo*

Daniel Mellem[1,2], Martin Sattler[2], Sonja Pagel-Wolff[2], Sören Jaspers[2], Horst Wenck[2], Michael Alexander Rübhausen[1], Frank Fischer[2]*

1 Center for Free-Electron Laser Science (CFEL), University of Hamburg, Hamburg, Germany, **2** Beiersdorf AG, Applied Biophysics, Hamburg, Germany

* frank.fischer@beiersdorf.com

Abstract

Mitochondria form dynamic networks which adapt to the environmental requirements of the cell. We investigated the aging process of these networks in human skin cells *in vivo* by multiphoton microscopy. A study on the age-dependency of the mitochondrial network in young and old volunteers revealed that keratinocytes in old skin establish a significantly more fragmented network with smaller and more compact mitochondrial clusters than keratinocytes in young skin. Furthermore, we investigated the mitochondrial network during differentiation processes of keratinocytes within the epidermis of volunteers. We observe a fragmentation similar to the age-dependent study in almost all parameters. These parallels raise questions about the dynamics of biophysical network structures during aging processes.

Introduction

Cells in human tissue produce their energy in form of adenosine triphosphate (ATP) basically by oxidative phosphorylation. This process takes place in mitochondria, that form highly dynamic networks adapting fast to the cells' environment and their metabolic requirements. [1] In recent years, numerous experiments have been performed to investigate correlations between mitochondrial network states and corresponding metabolic processes within cells. Cancer cells lacking of a glycolytic medium establish fusion states of the mitochondrial network correlating with a change in energy production going from glycolysis to oxidative phosphorylation. [2] In contrast, a transfer from respiratory to glycolytic conditions leads to a fragmentation of the mitochondrial network. [3] During moderate stress mitochondrial networks form hyperfusion states which coincide with increased ATP production. [4] On the contrary, high stress levels induce to a fragmentation of networks. [5] Mitochondrial fission and fusion states are considered to be quality saving mechanisms of the cell. Fission states support repelling of heavily damaged mitochondria from the network, e.g. during autophagy and mitophagy. [6, 7] In contrast, fusion states help to compensate for defect protein complexes or rare metabolites among mitochondria. [8, 9] Recently, a fragmentation of the mitochondrial network with age was observed *in vitro*. [10] The interplay of mitochondrial dynamics was simulated biophysically in a probabilistic quality model which also revealed a significant fragmentation of the mitochondrial network during aging. [11]

In this paper, we present investigations of mitochondrial morphologies during aging and differentiation of keratinocytes in human skin *in vivo*. We performed two studies: The first study explored variations of the mitochondrial network in epidermal keratinocytes of young and old volunteers. The second study extended the results by investigating the role of the mitochondrial network during the epidermal turnover.

Materials and methods

Tissue can be investigated non-invasively *in vivo* by imaging endogenous fluorophores using multiphoton microscopy. [12–14] An important metabolic fluorophore in the epidermis is nicotinamide adenine dinucleotide (NADH) [15, 16] which serves as an electron carrier from the Krebs cycle to respiratory chain. Thus, NADH is almost exclusively located in mitochondria. We tested this premise by *in vitro* investigations using a confocal scanning microscope (Leica TCS SP5, Leica Microsystems, Mannheim, Germany). Neonatal human epidermal keratinocytes were purchased from Lonza Group AG (Basel, Switzerland) and cultured in Dulbecco's Modified Eagle Medium (DMEM) (Life Technologies, Carlsbad, USA), supplemented with 10% fetal calf serum (PAA Laboratories, Pasching, Austria), L-glutamine and penicillin/streptomycin (both: Life Technologies, Carlsbad, USA). During culturing cells were maintained in a humidifying incubator with a 5% CO_2 atmosphere at 37°C. Mitochondria in the cells were marked with MitoTracker Red CMXRos (Life Technologies, Carlsbad, USA). We correlated the fluorescence of the dye from 570nm to 650nm to the autofluorescence of keratinocytes in the NADH emission spectrum from 410 nm to 540 nm (Fig 1). The measurements were performed with a 63x objective (HCX PL APO lambda blue 63.0x1.20 WATER UV, Leica). Single images of 2048*2048 pixels were generated with a bidirectional scan either at zoom 3.0 (82μm x 82 μm, step size: 0.04 μm) with scanning rate of 100Hz or at zoom 7.9 (31.2μm x 31.2μm, step size: 0.04μm) with scanning rate of 200Hz.

We found a nearly perfect agreement of morphologies of stained mitochondria with the autofluorescence signal of NADH. Aberrations are possibly caused by an overstaining of the dye, leading to very high intensities and consequently to agglomerations of mitochondrial morphologies in the micrograph. Intensity deviations among autofluorescent mitochondrial structures are assumed to be fluctuations in the metabolic activity. Previous studies indicate that the concentration of NADH is five times higher [17] and the quantum yield is 1.5 to 2.5 greater than of coenzyme NADPH [18] that is fluorescing in the same spectral range. So, potential interference of NADH with the coenzyme NADPH can be neglected.
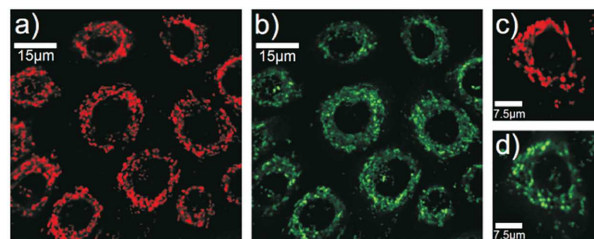
Fig 1. Fluorescence of dyed mitochondria (a) and autofluorescence of NADH (b) in keratinocytes (zoom 3.0). Fluorescence of dyed mitochondria (c) and autofluorescence of NADH (d) in a single keratinocyte (zoom 7.9).

https://doi.org/10.1371/journal.pone.0174469.g001

Imaging mitochondrial network morphologies *in vivo* by the autofluorescence of NADH was performed with a multiphoton microscope (Dermainspect, developed by Jenlab GmbH (Jena, Germany) in collaboration with Beiersdorf AG (Hamburg, Germany) (S1 Fig). The device includes a femtosecond laser with a repetition rate of 80MHz and a pulse width of 150fs. Laser pulses excite the autofluorescence of NADH in the epidermis at a wavelength of 750nm. The autofluorescence is separated from the laser light by a 548nm ± 150nm band-pass filter (HQ 548/305m-2P, Schott AG, Mainz, Germany) and detected by a photomultiplier tube (PMT). In order to image a single cell layer in the epidermis, the focus of the laser through an objective (40x magnification, 1.3 numerical aperture) is scanned parallel to the surface of the skin with an image acquisition time of about 12,5s. During the measurement the z-position is controlled by a piezo element. To prevent disturbance in the images by the movement of the volunteer, the objectives adheres to the skin of the volunteers. Each image has the dimensions of 110μm x 110μm and a resolution of 512pixels x 512pixels. In all measurements the laser power after the objective was set to 20 mW. For the quantitative analyses of mitochondrial morphologies we developed an image binarization algorithm that extracted mitochondrial structures from multiphotonic measurements: Firstly, the cytoplasm of each keratinocyte was taken from the measurements by manually annotating the cell borders and the corresponding nuclei in all images. Then, an Otsu-based [19] image algorithm extracted mitochondrial morphologies using binarization (S1 Fig). A pixel in one annotations had to exceed two thresholds in order to be categorized as NADH-autofluorescence during the binarization process: A global threshold which factors the gray values of all pixels in the annotation and a local threshold which is defined by the gray value of the surrounding pixels. Both of these thresholds were calculated via the Otsu-method. The algorithm calculates gradually all possible binarizations and selects the gray value as the optimal threshold that minimizes the Otsu variance:

$$\sigma_\omega(T) = \omega_{\text{white}}(T)\sigma^2_{\text{white}}(T) + \omega_{\text{black}}(T)\sigma^2_{\text{black}}(T) \qquad (1)$$

In the Eq (1) T represents the threshold of the gray value for the binarization, $\sigma_\omega(T)$ its Otsu variance, $\sigma^2_i(T)$ the variances of the gray values of black and white pixels and $\omega_i(T)$ their corresponding weights. After binarization procedures, the algorithm assigns all signal related pixels to common signal clusters, so that they fulfill the definition of 4-neighbor-connectivity. The number of pixels per cluster defines its area A, the number of edges which border on black pixels (the background of the measurement) defines its circumference U and the parameter $C = U^2/4\pi A$ defines its circularity. A represents the volume of a mitochondrial structure, C its circularity. Mann-Whitney-Tests were used for statistical analysis (p$\leq$0.05:*; p$\leq$0.01:**; p$\leq$0.001:***). The analysis was performed with the software "Statistica" by StatSoft (Europe) GmbH (Hamburg, Germany). All corresponding plots were depicted with the software Origi-nPro 8 (OriginLab Corporation, Northampton, USA).

Two clinical *in vivo* studies were performed. Written informed consent was obtained from each volunteer in both studies. All volunteers provided skin without pathologies and possessed skin types II and III of the Fitzpatrick phototyping scale. [20] Prior and during the studies all volunteers were required to desist from visits of solariums and intensive sun exposure. Treatment of skin in the investigated areas with cosmetic substances and medicals was prohibited during the studies. Measurements in four areas at the inner side of the forearm were performed. In each area multiphotonic images were acquired at three positions. The results of all positions were averaged in each area. The examinations were performed by trained personnel at standard atmospheric conditions (23˚C ± 1˚C and 43% ± 2% relative humidity). All volunteers were provided with fifteen minutes of acclimatization prior to the measurements. The studies were conducted according to the recommendations of the

current version of the Declaration of Helsinki and the Guideline of the International Conference on Harmonization Good Clinical Practice, (ICH GCP). In addition, this study was approved and cleared by the institutional ethics review board (Beiersdorf AG, Hamburg, Germany). Written informed consent was obtained from each volunteer in both studies.

Results

In the first study the mitochondrial morphology in epidermal keratinocytes of twelve young (mean ± SD: 23.75 ± 1.67 years) and twelve old (72.17 ± 4.15 years) volunteers was analysed by statistically comparing 48 areas in each age group. We analysed the number, area and circularity of the mitochondrial clusters per keratinocyte in the stratum granulosum in a depth of about 15 μm. The results of all examined parameters were averaged in each area before statistical comparison. Mitochondrial clusters in the stratum granulosum of young volunteers are significantly larger (p = 0.029) and have a significantly higher circularity (p = 0.014) (Fig 2). In contrast, the number of mitochondrial clusters normalized to the size of each keratinocyte is significantly higher (p = 0.006) in old skin (S2 Fig).

In the second study the morphology of the mitochondrial networks in keratinocytes of the stratum spinosum (depth of about 25 μm) and the stratum granulosum (depth of about 15 μm) were analysed by statistically comparing 32 areas in each layer. For determination of the layers, a prescan through the epidermis was performed during which the mosaic structure of the spinolar cells and the larger and rounder granular cells were identified by trained personnel. All eight volunteers were of the same age group (62 ± 1.31 years). Again, investigated parameters were averaged in each area. The average size per mitochondrial cluster is significantly larger (p ≤ 0,001) and its circularity significantly higher (p ≤ 0,001) in the stratum spinosum (Fig 3). Contrary, the number of mitochondrial clusters normalized to the cell size tends to be higher (p ≤ 0,086) in the stratum granulosum (S3 Fig).

Discussion

Our study of the mitochondrial network during aging reveals, that granular epidermal keratinocytes in young skin have less clusters in total than keratinocytes in old skin. Additionally, clusters in granular keratinocytes of young volunteers are bigger in size and less circular in shape. These findings reveal a high connectivity among mitochondria in the stratum granulosum in young skin and a fragmented mitochondrial network in the stratum granulosum of old skin. Granular keratinocytes of young volunteers seem to prefer a fusion state of the mitochondrial network which is not maintained during aging.

In our second study we investigated the changes of mitochondrial morphologies during epidermal differentiation. At the beginning of the epidermal turnover proliferation of keratinocytes occurs in the deepest layer of the epidermis, the stratum basale. During their differentation process keratinocytes migrate to upper layers, i.e. the stratum spinosum and the stratum granulosum, and finally transform into dead corneocytes in the stratum corneum. [21] For an analysis of mitochondrial network states during differentiation, we performed examinations in two layers above the stratum basale: in the stratum spinosum and the stratum granulosum. The stratum spinosum is the layer next to the stratum basale, so that keratinocytes in the stratum spinosum are less differentiated than in the stratum granulosum which is the last living epidermal layer before cornification occurs. We observed that the number of mitochondrial clusters tends to increase during differentiation. Additionally, clusters significantly shrink to smaller volumes and more compact shapes. These parameters indicate that mitochondrial networks in the stratum spinosum establish fused states which fragment during differentiation processes.
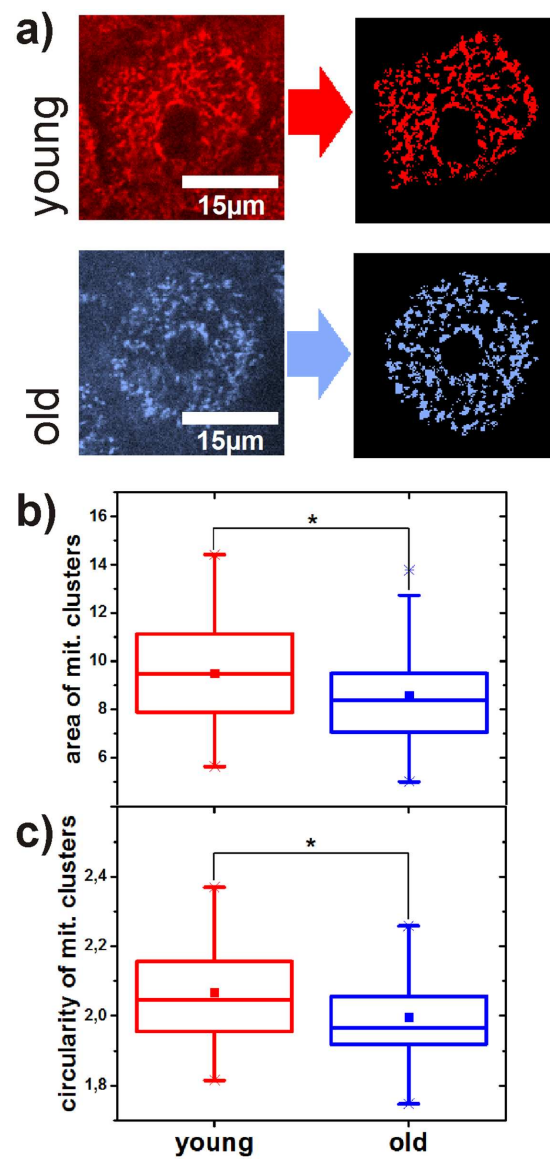
Fig 2. (a) Comparison of mitochondrial networks in young volunteers and old volunteers before and after binarization. Age-related comparison of size (b) and circularity (c) of mitochondrial clusters in keratinocytes. The p-value represents the probability if the two compared probability distributions derive from the same population. The square in the box represents the mean value, the horizontal line in the center the median. 25% percent of the measured values are lower than the bottom of the box, 75% of them are lower than the top of the box. The antennas (whiskers) are the corresponding limits for 2.5% and 97.5%. Crosses represent the highest and the lowest value in the distribution.

https://doi.org/10.1371/journal.pone.0174469.g002
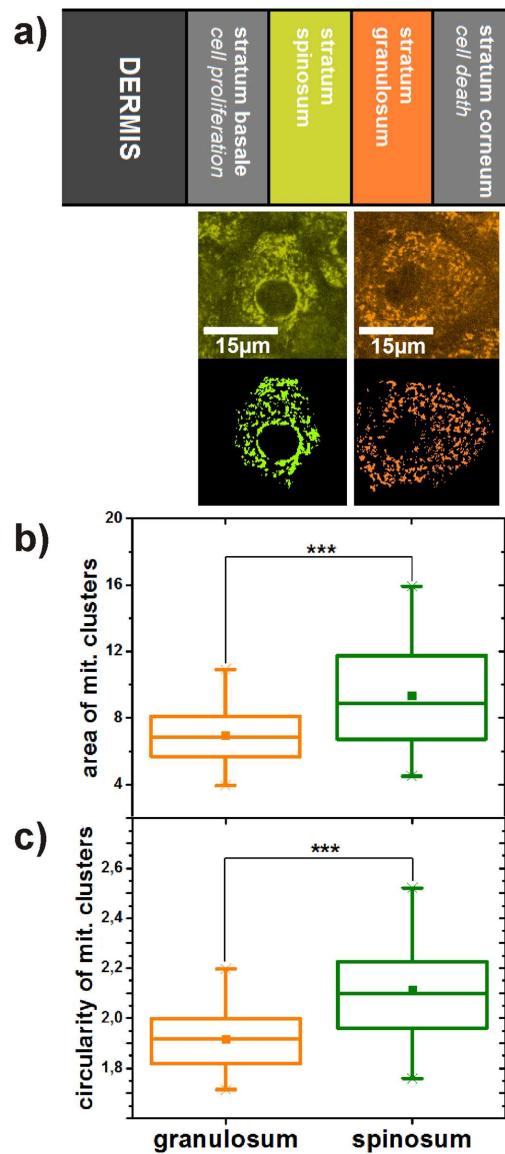
Fig 3. (a) Comparison of mitochondrial networks in stratum spinosum and stratum granulosum representing different states during the differentiation process of keratinocytes. Differentiation-related comparison of size (b) and circularity (c) of mitochondrial clusters in keratinocytes. The p-value represents the probability if the two compared probability distributions derive from the same population. The square in the box represents the mean value, the horizontal line in the center the median. 25% percent of the measured values are lower than the bottom of the box, 75% of them are lower than the top of the box. The antennas (whiskers) are the corresponding limits for 2.5% and 97.5%. Crosses represent the highest and the lowest value in the distribution.

https://doi.org/10.1371/journal.pone.0174469.g003

Comparing the results of the two studies the dynamics in mitochondrial network morphologies during differentiation agree well with changes during skin aging in volunteers. In the following we refer to several processes which play a role in the fragmentation of the mitochondrial network.

Reactive oxygen species (ROS) are produced due to long-term solar UV radiation [22] as well as intrinsic generation by mitochondria and other cell organelles. [23] Oxidative stress causes long-term damage to intramitochondrial structures [24] and leads to mitochondrial fission states during aging. [25] Numerous experiments point to the importance of oxidative stress for differentiation processes of keratinocytes. [26] The exclusion of heavily ROS-damaged mitochondria from the mitochondrial network could thereby lead to a fragmentation of the network's morphology during aging and differentiation.

Mitochondrial aging processes lead to a quality decay of mitochondria [27] which correlates with an age-related decrease of mitochondrial membrane potentials (MMP). [28] The decrease of the MMP also plays a role during the differentiation of keratinocytes. [21] Experiments revealed that mitochondria with low MMPs are excluded from the network by autophagic processes. [29]

Mitophagic and autophagic processes exclude heavily damaged mitochondria from the network. Mitochondrial autophagy increases during the aging of cells [30], thereby fragmenting intermitochondrial connections. Autophagic activity is similarly involved in the differentiation of keratinocytes. [31]

In cultivated keratinocytes an increased glycolytic activity in old volunteers was observed. [32] This shift from oxidative phosphorylation to glycolysis during aging correlates with a fragmentation of the mitochondrial network. Recent publications disclose the change of mitochondrial metabolisms during the differentiation process. [33]

There are several alternatives to explain the similarities of mitochondrial morphologies during aging and differentiation. For instance, keratinocytes could exploit natural aging processes to catalyze differentiation procedures which consequently leads to a fragmentation of the mitochondrial network. Another possible explanation is that mitochondrial morphologies are independent from differentiation and purely influenced by aging processes during the epidermal turnover. Further investigations are necessary to clarify the physiological connections between aging and differentiation regarding mitochondrial morphologies in cells. The influence of aging processes on mitochondrial quality was investigated in computational quality models. [11, 34] A fragmentation of the mitochondrial network during aging of cells and a deceleration of fission and fusion cycles as a quality saving process were observed. The models reveal quality saving mechanisms for mitochondria such as the interplay of mitochondrial networking and recycling and the quality saving benefit of a decreased mitochondrial repair ability in old cells. Hence, our findings are qualitatively in good agreement with the model.

Conclusion

In conclusion, we have measured and analyzed the morphology of mitochondrial networks in human skin *in vivo* for the first time. We found a significant fragmentation of mitochondrial morphologies in granular keratinocytes during aging. Our results are qualitatively in good agreement with age-dependent investigations *in vitro* and with simulations of biophysical models. Moreover, we observed a fragmentation of the network during the differentiation process of keratinocytes in the epidermis. The parallels of both studies raise questions about the linkage of aging and differentiation concerning mitochondrial morphologies.

Supporting information

S1 Fig. (a) setup of multiphoton microscope (b) measurement of autofluorescence of NADH in stratum granulosum (c) binarization of measured keratinocyte with otsu algorithm.
(TIF)

S2 Fig. Comparison of number of mitochondrial clusters in young and old volunteers normed to the size of keratinocytes.
(TIF)

S3 Fig. Comparison of number of mitochondrial clusters in stratum spinosum and stratum granulosum normed to the size of keratinocytes.
(TIF)

S1 Dataset. The .csv-file provides the data of mitochondrial cluster numbers, cluster size and cluster circularity in all 40 areas that were investigated in the skin of young and old volunteers and in the stratum spinosum and the stratum granulosum.
(CSV)

Author Contributions

Conceptualization: FF DM.

Data curation: DM SPW MS FF.

Formal analysis: DM SPW MS FF.

Investigation: DM SPW MS.

Methodology: DM MS SPW FF.

Project administration: FF.

Resources: DM SPW MS FF.

Software: DM.

Supervision: FF HW SJ MR.

Validation: DM SPW MS FF.

Visualization: DM.

Writing – original draft: DM.

Writing – review & editing: DM FF MR HW SJ.

References

1. Youle RJ, van der Bliek AM. Mitochondrial fission, fusion, and stress. Science. 2012; 337(6098):1062–5. https://doi.org/10.1126/science.1219855 PMID: 22936770

2. Rossignol R, Gilkerson R, Aggeler R, Yamagata K, Remington SJ, Capaldi RA. Energy substrate modulates mitochondrial structure and oxidative capacity in cancer cells. Cancer Res. 2004; 64(3):985–93. https://doi.org/10.1158/0008-5472.CAN-03-1101 PMID: 14871829

3. Jakobs S, Martini N, Schauss AC, Egner A, Westermann B, Hell SW. Spatial and temporal dynamics of budding yeast mitochondria lacking the division component Fis1p. J Cell Sci. 2003; 116(Pt 10):2005–14. https://doi.org/10.1242/jcs.00423 PMID: 12679388

Fragmentation of the mitochondrial network in skin *in vivo*

4. Tondera D, Grandemange S, Jourdain A, Karbowski M, Mattenberger Y, Herzig S, et al. SLP-2 is required for stress-induced mitochondrial hyperfusion. EMBO J. 2009; 28(11):1589–600. https://doi.org/10.1038/emboj.2009.89 PMID: 19360003

5. van der Bliek AM, Shen Q, Kawajiri S. Mechanisms of mitochondrial fission and fusion. Cold Spring Harb Perspect Biol. 2013; 5(6). https://doi.org/10.1101/cshperspect.a011072 PMID: 23732471

6. Singh SB, Ornatowski W, Vergne I, Naylor J, Delgado M, Roberts E, et al. Human IRGM regulates autophagy and cell-autonomous immunity functions through mitochondria. Nat Cell Biol. 2010; 12 (12):1154–65. https://doi.org/10.1038/ncb2119 PMID: 21102437

7. Kim I, Rodriguez-Enriquez S, Lemasters JJ. Selective degradation of mitochondria by mitophagy. Arch Biochem Biophys. 2007; 462(2):245–53. https://doi.org/10.1016/j.abb.2007.03.034 PMID: 17475204

8. Nakada K, Inoue K, Ono T, Isobe K, Ogura A, Goto YI, et al. Inter-mitochondrial complementation: Mito-chondria-specific system preventing mice from expression of disease phenotypes by mutant mtDNA. Nat Med. 2001; 7(8):934–40. https://doi.org/10.1038/90976 PMID: 11479626

9. Rolland SG, Motori E, Memar N, Hench J, Frank S, Winklhofer KF, et al. Impaired complex IV activity in response to loss of LRPPRC function can be compensated by mitochondrial hyperfusion. Proc Natl Acad Sci U S A. 2013; 110(32):E2967–76. https://doi.org/10.1073/pnas.1303872110 PMID: 23878239

10. Regmi SG, Rolland SG, Conradt B. Age-dependent changes in mitochondrial morphology and volume are not predictors of lifespan. Aging (Albany NY). 2014; 6(2):118–30. https://doi.org/10.18632/aging.100639 PMID: 24642473

11. Figge MT, Reichert AS, Meyer-Hermann M, Osiewacz HD. Deceleration of fusion-fission cycles improves mitochondrial quality control during aging. PLoS Comput Biol. 2012; 8(6):e1002576. https://doi.org/10.1371/journal.pcbi.1002576 PMID: 22761564

12. Lakowicz JR, Szmacinski H, Nowaczyk K, Johnson ML. Fluorescence lifetime imaging of free and pro-tein-bound NADH. Proc Natl Acad Sci U S A. 1992; 89(4):1271–5. https://doi.org/10.1073/pnas.89.4.1271 PMID: 1741380

13. Skala MC, Riching KM, Gendron-Fitzpatrick A, Eickhoff J, Eliceiri KW, White JG, et al. In vivo multipho-ton microscopy of NADH and FAD redox states, fluorescence lifetimes, and cellular morphology in pre-cancerous epithelia. Proc Natl Acad Sci U S A. 2007; 104(49):19494–9. https://doi.org/10.1073/pnas.0708425104 PMID: 18042710

14. Puschmann S, Rahn CD, Wenck H, Gallinat S, Fischer F. Approach to quantify human dermal skin aging using multiphoton laser scanning microscopy. J Biomed Opt. 2012; 17(3):036005. https://doi.org/10.1117/1.JBO.17.3.036005 PMID: 22502563

15. Mayevsky A, Rogatsky GG. Mitochondrial function in vivo evaluated by NADH fluorescence: from ani-mal models to human studies. Am J Physiol Cell Physiol. 2007; 292(2):C615–40. https://doi.org/10.1152/ajpcell.00249.2006 PMID: 16943239

16. Balu M, Mazhar A, Hayakawa CK, Mittal R, Krasieva RB. In vivo multiphoton NADH fluorescence reveals depth-dependent keratinocyte metabolism in human skin. Biophys J. 2013; 104(1):258–67. https://doi.org/10.1016/j.bpj.2012.11.3809 PMID: 23332078

17. Klaidman LK, Leung AC, Adams J J D. High-performance liquid chromatography analysis of oxidized and reduced pyridine dinucleotides in specific brain regions. Anal Biochem. 1995; 228(2):312–7. https://doi.org/10.1006/abio.1995.1356 PMID: 8572312

18. Avi-Dor Y, Olson JM, Doherty MD, Kaplan NO. Fluorescence of Pyridine Nucleotides in Mitochondria. J Biol Chem. 1962; 237:2377–2383.

19. Otsu N. A Threshold Selection Method from Gray-Level Histograms. Systems, Man and Cybernetics, IEEE Transactions. 1979; 9(1):5. https://doi.org/10.1109/TSMC.1979.4310076

20. Fitzpatrick TB. Soleil et peau. Journal de Médecine Esthétique. 1975; 2:2.

21. Allombert-Blaise C, Tamiji S, Mortier L, Fauvel H, Tual M, Delaporte E, et al. Terminal differentiation of human epidermal keratinocytes involves mitochondria- and caspase-dependent cell death pathway. Cell Death Differ. 2003; 10(7):850–2. https://doi.org/10.1038/sj.cdd.4401245 PMID: 12815468

22. D'Orazio J, Jarrett S, Amaro-Ortiz A, Scott T. UV Radiation and the Skin. Int J Mol Sci. 2013; 14 (6):12222–48. https://doi.org/10.3390/ijms140612222 PMID: 23749111

23. Brown GC, Borutaite V. There is no evidence that mitochondria are the main source of reactive oxygen species in mammalian cells. Mitochondrion. 2012; 12(1):1–4. https://doi.org/10.1016/j.mito.2011.02.001 PMID: 21303703

24. Yakes FM, Van Houten B. Mitochondrial DNA damage is more extensive and persists longer than nuclear DNA damage in human cells following oxidative stress. Proc Natl Acad Sci U S A. 1997; 94 (2):514–9. https://doi.org/10.1073/pnas.94.2.514 PMID: 9012815

25. Wu S, Zhou F, Zhang Z, Xing D. Mitochondrial oxidative stress causes mitochondrial fragmentation via differential modulation of mitochondrial fission-fusion proteins. FEBS J. 2011; 278(6):941–54. https://doi.org/10.1111/j.1742-4658.2011.08010.x PMID: 21232014

26. Hamanaka RB, Chandel NS. Mitochondrial metabolism as a regulator of keratinocyte differentiation. Cell Logist. 2013; 3(1):e25456. https://doi.org/10.4161/cl.25456 PMID: 24475371

27. Rooyackers OE, Adey DB, Ades PA, Nair KS. Effect of age on in vivo rates of mitochondrial protein synthesis in human skeletal muscle. Proc Natl Acad Sci U S A. 1996; 93(26):15364–9. https://doi.org/10.1073/pnas.93.26.15364 PMID: 8986817

28. Hagen TM, Yowe DL, Bartholomew JC, Wehr CM, Do KL, Park JY, et al. Mitochondrial decay in hepatocytes from old rats: membrane potential declines, heterogeneity and oxidants increase. Proc Natl Acad Sci U S A. 1997; 94(7):3064–9. https://doi.org/10.1073/pnas.94.7.3064 PMID: 9096346

29. Twig G, Shirihai OS. The interplay between mitochondrial dynamics and mitophagy. Antioxid Redox Signal. 2011; 14(10):1939–51. https://doi.org/10.1089/ars.2010.3779 PMID: 21128700

30. Oberley TD, Swanlund JM, Zhang HJ, Kregel KC. Aging results in increased autophagy of mitochondria and protein nitration in rat hepatocytes following heat stress. J Histochem Cytochem. 2008; 56(6):615–27. https://doi.org/10.1369/jhc.2008.950873 PMID: 18379016

31. Aymard E, Barruche V, Naves T, Bordes S, Closs B, Verdier M, et al. Autophagy in human keratinocytes: an early step of the differentiation? Exp Dermatol. 2011; 20(3):263–8. https://doi.org/10.1111/j.1600-0625.2010.01157.x PMID: 21166723

32. Prahl S, Kueper T, Biernoth T, Wohrmann Y, Munster A, Furstenau M, et al. Aging skin is functionally anaerobic: importance of coenzyme Q10 for anti aging skin care. Biofactors. 2008; 32(1–4):245–55. https://doi.org/10.1002/biof.5520320129 PMID: 19096122

33. Hamanaka RB, Glasauer A, Hoover P, Yang S, Blatt H, Mullen AR, et al. Mitochondrial reactive oxygen species promote epidermal differentiation and hair follicle development. Sci Signal. 2013; 6(261):ra8. https://doi.org/10.1126/scisignal.2003638 PMID: 23386745

34. Mellem D, Jaspers S, Wenck H, Rübhausen MA, Fischer F. Quality Saving Mechanisms of Mitochondria during Aging in a Fully Time-Dependent Computational Biophysical Model. PLoS ONE. 2016; 11(1):1–22. https://doi.org/10.1371/journal.pone.0146973 PMID: 26771181

Chapter 5

Summary and Outlook

This thesis deals with different in silico and in vivo methods, that investigate the morphological and qualitative dynamics of the mitochondrial network.

Based on the approach by Figge et. al in 2012 [17] a novel computational model was created, that simulates the change of mitochondrial qualities over time. A superposition of biological processes, such as networking dynamics, recycling procedures, oxidative stress and repair mechanisms act on mitochondria and alter the probabilities of quality states q. A change of the frequencies over time of each biological process allows to simulate an aging process of the mitochondrial network.

Simulations reveal a fragmentation of mitochondrial network structures and growing amounts of inactive, isolated mitochondria during aging. Additionally, a quality increasing benefit of the coupling of networking dynamics and recycling processes is revealed. This finding confirms experiments that indicate that mitochondrial fission processes induce mitophagy. [18] Moreover, simulations disclose a novel quality saving mechanism during aging due to decreasing mitochondrial repair abilities.

In order to correlate mitochondrial qualities with mitochondrial morphologies and to investigate the interactions between the mitochondrial network and the energy demands of the cell, a second model was designed. Here, mitochondria move as small units (Smallest Mitochondrial Units (SMUs)) within a two-dimensional, virtual cell. Inelastic collisions of mitochondria lead to the aggregation of larger mitochondrial clusters, forming a complex network structure. Growing mitochondrial cluster sizes lead to growing mitochondrial health, an equal distribution of metabolites and a decrease in average motilities of mitochondria. This effect can be amplified by an increase of the mitochondrial mass in the virtual cell and by growing velocities of fission and biogenetic procedures.

The energy demand of the cell is represented by adenosintriphosphate (ATP) consumers that stand for the various energy consuming organelles and other ATP demanding cell functions in the cytoplasm. ATP consumers are modeled by oscillating Mie potentials, that attract SMUs and mitochondrial clusters. Simulations show a coupling of the oscillations of ATP consumers and the morphology and quality parameters of the mitochondrial network. It is revealed, that mitochondrial structures adapt to the energetic demand within the cell. In phases of high energy demand mitochondrial clusters aggregate at the locations of ATP consumers and condensate around the nucleus. The latter was also observed experimentally in stressed cells. [63] Contrary, during low energy demands of ATP consumers, i.e. a low attraction of Mie potentials, mitochondria move freely within the cytoplasm of the virtual cell.

In an experimental approach, mitochondrial structures were imaged in vivo in epidermal keratinocytes of volunteers using multiphoton microscopy. The autofluorescence of the coenzyme nicotinamide adenine dinucleotide (NADH) was excited by femtosecond laser pulses with high photon densities. Since NADH is basically located within the mitochondrial matrix, its autofluorescence represents the structure of the mitochondrial network. A binarization algorithm based on the Otsu method was developed in order to analyse the NADH autofluorescence in multiphoton micrographs and to examine the morphology of mitochondrial clusters.

Two studies very performed. The mitochondrial network in keratinocytes in the stratum granulosum was compared between a young and an old age group. Furthermore, the change of mitochondrial morphologies during the differentiation process of keratinocytes within the epidermal turnover was investigated. For that, the mitochondrial network was imaged in two different epidermal layers, the less differentiated stratum spinosum and the more differentiated stratum granulosum. Experiments reveal mitochondrial fragmentation in both studies, during aging and during differentiation, respectively.

Simulations and experiments in this thesis open up diverse options for further investigations on the mitochondrial network. For an in-depth validation of the computational models, Monte-Carlo simulations should be performed in order to test a broader range of input parameters. Additionally, possible couplings of free parameters in the model should be revealed by a parallel, multidimensional variation of their values. As a next step, corresponding in-vitro experiments should be performed. For that purpose, the fluorescence of mitochondrial network structures and the measurement of mitochondrial membrane potentials should be correlated with morphology and quality parameters. This would help to verify quality saving mechanisms and morphological behavior revealed in the presented computational models. Hence, the models are tools to suggest experiments in order to understand the overall behavior of mitochondrial networks.

Moreover, the time scales of the various biological processes included in both models should be measured in experiments. Thus, the models would not only be of qualitative, but also of quantitative use. They could provide quantitative time-related predictions of mitochondrial behavior and could be directly compared with experiments.

In the morphology model, the velocity of mitochondria and mitochondrial clusters is tracked. To date, their are no methods presented to measure mitochondrial motility in biological experiments. Including mitochondrial velocities in investigations on mitochondrial networks would add a new dimension to the analysis of mitochondrial network morphologies and would help to compare the morphology model with biological experiments.

Overall, computational models and in-vivo experiments disclose a fragmentation process of mitochondrial networks over time as observed in recent publications on in-vitro experiments. [38, 39] Simulations explain increased fission processes due to a growing amount of harmed mitochondria with oxidative stress, causing mitochondrial fragmentation. This phenomenon is accelerated by the loosing ability of the cell to remove harmed, isolated mitochondria by mitophagic processes. Coupling of networking and recycling processes, mitochondrial clustering and decreasing mitochondrial repair abilities support a preservation of the integrity of the mitochondrial network.

Future investigations of biophysical experiments and enhanced computational models will provide further insights on the complex dynamics of mitochondrial networks.

Appendix A

Appendix Quality Model

FileData.java

```java
import java.io.*;
import java.util.*;

public class FileData {
    public static void main(String[] args) throws IOException {
        //Festlegung von Parametern
        String file_import = "verteilung.asc"; //Eingelesene Verteilung
        String file_export = "Ergebnis.asc"; //Simulationsergebnis
        int state_resolution = 11; //Aufloesung der Messung
        int time_resolution = 10;
        int end_of_time = 100000;

        //Aufrufen der Simulationsdaten
        EditFile measure = new EditFile();
        double states_in_time[][] = measure.EditMatrix(file_import,
state_resolution, time_resolution, end_of_time);

        //Export der Simulationsdaten
        int i,j;
        WriteFile data = new WriteFile(file_export, true);
        data.open();
        for(j=0;j<end_of_time/time_resolution;j++){
            for(i=0; i<state_resolution+2; i++){
                double wert = states_in_time[i][j];
                String value = Double.toString(wert);
                data.writeToFile(value + "; ");
            }
            data.writeToFile("%n");
        }
        data.close();
        System.out.println("Simsalabim.\nAusgabedateien geschrieben.");
    }
}
```

ReadFile.java

```java
import java.io.*;
import java.util.*;

public class ReadFile {

    private String path;

    public ReadFile(String file_path) {
        path = file_path;
    }

    int readNumbers() throws IOException {
        FileReader file_to_read = new FileReader(path);
        BufferedReader bf = new BufferedReader(file_to_read);
        Scanner preScan = new Scanner(bf);

        double anumber;
        int numberOfDoubles = 0;

        while ((anumber = preScan.nextDouble() )!= 1){
            numberOfDoubles++;
        }
        bf.close();
        return numberOfDoubles;
    }

    public double[] OpenFile(int resolution) throws IOException {

        FileReader fr = new FileReader(path);
        BufferedReader nReader = new BufferedReader(fr);
        Scanner scan = new Scanner(nReader);
        int stop = resolution*resolution;

        double[] data = new double[resolution];

        int i;

            for (i=0; i < resolution; i++) {
                data[i] = scan.nextDouble();
            }

            nReader.close();
            return data;
    }
}
```

WriteFile.java

```java
import java.io.*;


public class WriteFile {

private String path;
private boolean append_to_file = false;

public WriteFile(String file_path) {
    path = file_path;
}

public WriteFile(String file_path, boolean append_value){
    path = file_path;
    append_to_file = append_value;
}


PrintWriter print_line;
FileWriter write;

public void open() throws IOException {
    write = new FileWriter(path, append_to_file);
    print_line = new PrintWriter(write);
}

public void close() throws IOException {
    print_line.close();
    write.close();
}

public void writeToFile(String number) throws IOException{
    print_line.printf(number);
}
}
```

EditFile.java

```java
import java.io.*;

public class EditFile {


    public EditFile() {
}
    public double[][] EditMatrix(String file_path, int state_resolution,
        int time_resolution, int end_of_time) throws IOException {

          //Lese Zustand
          ReadFile messung = new ReadFile(file_path);
          double[] matrix = messung.OpenFile(state_resolution);

          //Erstelle Zustandsmatrix
          int i,j,k,l,m,q,q0,t;
          double[] edit_matrix = new double[state_resolution+1];
          for(i=0; i<state_resolution; i++){
              edit_matrix[i] = matrix[i];
          }
          edit_matrix[state_resolution]=0;



          //----------Parameter und Variablen fuer Zeitschleife------------

          //Allgemeines
          double zeitschritt = 1;
          double euler = 2.718281828459045;
          double average_quality = 0;
          double standard_deviation_quality=0;
          int array_counter = 0;
          double[][] daten_array =
new double[state_resolution+2][end_of_time/time_resolution];
          //================================================================

          //Mitophagy und Biogenese
           double p_mp = 0.01;
           double tau_mp = 50000;
           double mp_threshold = 0.5;
           //double p_dec_bio=0.1;
           //double tau_dec_bio=35000;
          //================================================================

          //Reparatur
          double p_rep = 0.01;
          double tau_rep = 50000;
          //================================================================

          //Erstelle Quality Decay
          double p_qd = 0.01;
          double tau_qd = 50000;
          //================================================================

          //Fission und Fusion
```

```
        double fis_fus_1 = 3;
        double fis_fus_2 = 2;
        double p_ff_met = 0.05;
        double p_fus_pro = 0.05;
        double p_fis_pro = 0.05;
        double tau_ff_met = 50000;
        double tau_fus_pro = 50000;
        double tau_fis_pro = 50000;


        //================================================================

        //ROS
        double p_moc_dam = 0.005;
        double tau_moc_dam = 50000;
        double moc_dam = 0.3;
        //================================================================

    //===================Z E I T S C H L E I F E====================
        for(t=0; t<end_of_time; t++){

        /*for(i=0;i<state_resolution;i++){
                System.out.print("Wahrscheinlichkeit fuer Zustand "+i+
": "+edit_matrix[i]+"\n");
            }*/

        double p_sum = 0;
        for(i=0; i<state_resolution; i++){
            p_sum = p_sum + edit_matrix[i];
        }

        System.out.print("Wahrscheinlichkeitsumme: "+p_sum+"\n");

        //M I T O P H A G Y  %  B I O G E N E S E
        double[] mitophagy_biogenesis_rate = new double[state_resolution];
        //double dec_bio = p_dec_bio*Math.pow(euler,(t/tau_dec_bio));
        //int decay_biogenesis= (int) Math.round(dec_bio);
        //System.out.print("Verlust Biogenesequalitaet: "+decay_biogenesis+"\n");

        for(q0=0;q0<state_resolution;q0++){
            if(q0<mp_threshold){
                double delta_mitbio = Math.pow(p_mp*Math.pow(euler,(t/tau_mp))
,(q0+1))*edit_matrix[q0];
                //System.out.print("Aenderung MitBio: "+delta_mitbio+"\n");
                mitophagy_biogenesis_rate[q0]=-delta_mitbio;

                mitophagy_biogenesis_rate[state_resolution-1]=
mitophagy_biogenesis_rate
[state_resolution-1]+delta_mitbio;
            }
        }
        //================================================================

        //R O S S C H A D E N
        int[] random_matrix = new int[state_resolution];
        int inter_value, random_value_int, random_value_int2;
```

```
        double p_random_damages , random_value_double , damage ;

         double moc_dam_rate = p_moc_dam*Math.pow(euler ,(t/tau_moc_dam));
         //Berechne Molekularschaden
         p_random_damages = zeitschritt*moc_dam_rate ;

         for(i=0; i<state_resolution; i++){
             random_matrix [i]=i;
         }
         for(i=1; i<state_resolution; i++){
             inter_value = random_matrix [i];
             random_value_int = (int) (Math.random()*state_resolution);
             random_matrix [i] = random_matrix [random_value_int ];
             random_matrix [random_value_int ] = inter_value ;
         }
         for(j=0; j<state_resolution; j++){
             i=random_matrix [j];
             random_value_double = (double) (Math.random()*1.0);
             if(random_value_double < p_random_damages ){
                 random_value_int2 = (int) (Math.random()*(i-1));
                 damage = (double) (Math.random()*moc_dam)*edit_matrix [i];
                 edit_matrix [i]=edit_matrix [i]-damage ;
                 edit_matrix [random_value_int2]=
edit_matrix [random_value_int2]+damage ;
             }
         }
         //===============================================================

         //F I S S I O N & F U S I O N   A L L G E M E I N
         double[][] fis_fus_met = new double[state_resolution][state_resolution];
         double[][] fus_prot = new double[state_resolution][state_resolution];
         double[][] fis_prot = new double[state_resolution][state_resolution];

         double list_ff_q_pos =0;
         double list_ff_q_neg =0;
         double[] fis_fus_matrix_met = new double[state_resolution];

         for(i=0;i<state_resolution;i++){
             for(j=0;j<state_resolution;j++){
                 fis_fus_met [i][j]=p_ff_met*Math.pow(euler ,(-t/tau_ff_met ))
*(Math.pow(Math.abs((i-j)),fis_fus_1)/(Math.pow(fis_fus_2 ,fis_fus_1)+
Math.pow(Math.abs((i-j)),fis_fus_1)));
                 }
         }

         for(i=0;i<state_resolution;i++){
             for(j=0;j<state_resolution;j++){
                 fus_prot [i][j]=p_fus_pro*Math.pow(euler ,(-t/tau_fus_pro))
*(Math.pow(Math.abs((i-j)),fis_fus_1)/(Math.pow(fis_fus_2 ,fis_fus_1)+
Math.pow(Math.abs((i-j)),fis_fus_1)));
                 }
         }

         for(i=0;i<state_resolution;i++){
             for(j=0;j<state_resolution;j++){
```

```
                        fis_prot[i][j]=p_fis_pro*Math.pow(euler,(t/tau_fis_pro))
*(Math.pow(Math.abs((state_resolution-1-i)),fis_fus_1)/
(Math.pow(fis_fus_2,fis_fus_1)+Math.pow(Math.abs((state_resolution-1-i)),fis_fus_1)));
                }
        }
        //===============================================================

        //F I S S I O N & F U S I O N   M E T A B O L I T E
        for(q0=0;q0<state_resolution;q0++){
            for(i=0; i<state_resolution; i++){
                for(j=0; j<state_resolution; j++){
                    for(k=0; k<state_resolution; k++){
                        for(l=0; l<state_resolution; l++){
                            //if((i+j)%2==0){
                                if((i+j) == (k+l) && i<j && k==l
&& i>mp_threshold && k>mp_threshold){
                                    if((i==q0 || j==q0)){
                                        list_ff_q_neg = list_ff_q_neg +
fis_fus_met[i][j]*edit_matrix[i]*edit_matrix[j];
                                        if(i==q0 && j==q0){
                                            list_ff_q_neg = list_ff_q_neg +
fis_fus_met[i][j]*edit_matrix[i]*edit_matrix[j];
                                        }
                                    }
                                    if((k==q0 || l==q0)){
                                        list_ff_q_pos = list_ff_q_pos +
fis_fus_met[i][j]*edit_matrix[i]*edit_matrix[j];
                                        if(k==q0 && l==q0){
                                            list_ff_q_pos = list_ff_q_pos +
fis_fus_met[i][j]*edit_matrix[i]*edit_matrix[j];
                                        }
                                    }
                                }
                            //}
                            /*if((i+j)%2==1){
                                if((i+j) == (k+l) && i<j && (k==l+1 || k+1==l) &&
i>mp_threshold && k>mp_threshold){
                                    if((i==q0 || j==q0)){
                                        list_ff_q_neg = list_ff_q_neg +
fis_fus_met[i][j]*edit_matrix[i]*edit_matrix[j];
                                        if(i==q0 && j==q0){
                                            list_ff_q_neg = list_ff_q_neg +
fis_fus_met[i][j]*edit_matrix[i]*edit_matrix[j];
                                        }
                                    }
                                    if((k==q0 || l==q0)){
                                        list_ff_q_pos = list_ff_q_pos +
fis_fus_met[i][j]*edit_matrix[i]*edit_matrix[j];
                                        if(k==q0 && l==q0){
                                            list_ff_q_pos = list_ff_q_pos +
fis_fus_met[i][j]*edit_matrix[i]*edit_matrix[j];
                                        }
                                    }
                                }
                            }*/
```

```
                    }
                  }
                }
              }
          fis_fus_matrix_met[q0] = -list_ff_q_neg+list_ff_q_pos;

          list_ff_q_neg = 0;
          list_ff_q_pos = 0;
        }
        //==============================================================

        //F U S I O N   P R O T E I N E
        double list_fusprot_q_pos=0;
        double list_fusprot_q_neg=0;
        double list_fisprot_q_pos=0;
        double list_fisprot_q_neg=0;
        double[] fus_matrix_prot = new double[state_resolution];
        double[] fis_matrix_prot = new double[state_resolution];

        /*for(q0=0;q0<state_resolution;q0++){
          for(i=0; i<state_resolution; i++){
            for(j=0; j<state_resolution; j++){
              for(k=0; k<state_resolution; k++){
                for(l=0; l<state_resolution; l++){
                  if(i>mp_threshold && i<j && j==l && k==l){
                    if((i==q0 || j==q0)){
                      list_fusprot_q_neg = list_fusprot_q_neg +
fus_prot[i][j]*edit_matrix[i]*edit_matrix[j];
                    }
                    if((k==q0 && l==q0)){
                      list_fusprot_q_pos = list_fusprot_q_pos +
2*fus_prot[i][j]*edit_matrix[i]*edit_matrix[j];
                    }
                  }
                }
              }
            }
          }
          fus_matrix_prot[q0] = -list_fusprot_q_neg+list_fusprot_q_pos;

          list_fusprot_q_neg = 0;
          list_fusprot_q_pos = 0;
        }*/
        //==============================================================

        //F I S S I O N   P R O T E I N E
        for(q0=0;q0<state_resolution;q0++){
          for(i=0; i<state_resolution; i++){
            for(j=0; j<state_resolution; j++){
              for(k=0; k<state_resolution; k++){
                for(l=0; l<state_resolution; l++){
                  if(i==j && i>mp_threshold && j==l && k<mp_threshold){
                    if((i==q0 && j==q0)){
                      list_fisprot_q_neg = list_fisprot_q_neg +
2*fis_prot[i][j]*edit_matrix[i]*edit_matrix[j];
```

```
                    }
                    if((k==q0 || l==q0)){
                        list_fisprot_q_pos = list_fisprot_q_pos +
fis_prot[i][j]*edit_matrix[i]*edit_matrix[j];
                    }
                }
            }
        }
    }
}
fis_matrix_prot[q0] = -list_fisprot_q_neg+list_fisprot_q_pos;

list_fisprot_q_neg = 0;
list_fisprot_q_pos = 0;
}
//==============================================================

// Q U A L I T Y   D E C A Y
double[] quality_decay_rate = new double[state_resolution];

for(q0=0; q0<state_resolution; q0++){
double qd_prob_sum=0;

    for(k=(q0+1); k<(state_resolution); k++){
        double bin_coeff1;
        int faculty_n1 = 1;
        int faculty_k1 = 1;
        int faculty_nk1 = 1;

        for(j=1;j<=(k);j++){
            faculty_n1=faculty_n1*j;
        }
        for(j=1;j<=(k-q0);j++){
            faculty_k1=faculty_k1*j;
        }
        for(j=1;j<=(q0);j++){
            faculty_nk1=faculty_nk1*j;
        }

        bin_coeff1=(faculty_n1)/(faculty_k1*faculty_nk1);
        qd_prob_sum = qd_prob_sum+bin_coeff1*
Math.pow(p_qd*Math.pow(euler,(t/tau_qd)),(k-q0))*
Math.pow((1-p_qd*Math.pow(euler,(t/tau_qd))),q0)*edit_matrix[k];
        }

    for(i=0; i<q0; i++){
        double bin_coeff2;
        int faculty_n2 = 1;
        int faculty_k2 = 1;
        int faculty_nk2 = 1;

        for(j=1;j<=q0;j++){
            faculty_n2=faculty_n2*j;
        }
        for(j=1;j<=(q0-i);j++){
```

```
                    faculty_k2=faculty_k2*j;
                }
                for(j=1;j<=i;j++){
                    faculty_nk2=faculty_nk2*j;
                }

                bin_coeff2=(faculty_n2)/(faculty_k2*faculty_nk2);
                qd_prob_sum = qd_prob_sum-bin_coeff2*Math.pow(p_qd*
Math.pow(euler,(t/tau_qd)),(q0-i))*Math.pow((1-p_qd*
Math.pow(euler,(t/tau_qd))),(i))*edit_matrix[q0];
            }

             quality_decay_rate[q0]= qd_prob_sum;

        }
        //==============================================================

        //R E P A R A T U R
        double[] repair_rate = new double[state_resolution];

        for(q0=0; q0<state_resolution; q0++){
        double rep_prob_sum=0;

            //Verlorene Wahrscheinlichkeitsmasse fuer Qualitaetszustand q0
            for(k=(q0+1); k<(state_resolution); k++){
                double bin_coeff1_rep;
                int faculty_n1_rep = 1;
                int faculty_k1_rep = 1;
                int faculty_nk1_rep = 1;

                for(j=1;j<=(state_resolution-1-q0);j++){
                    faculty_n1_rep=faculty_n1_rep*j;
                }
                for(j=1;j<=(k-q0);j++){
                    faculty_k1_rep=faculty_k1_rep*j;
                }
                for(j=1;j<=(state_resolution-1-k);j++){
                    faculty_nk1_rep=faculty_nk1_rep*j;
                }

                bin_coeff1_rep=(faculty_n1_rep)/(faculty_k1_rep*faculty_nk1_rep);
                rep_prob_sum = rep_prob_sum-bin_coeff1_rep*
Math.pow(p_rep*Math.pow(euler,(-t/tau_rep)),(k-q0))*
Math.pow((1-p_rep*Math.pow(euler,(-t/tau_rep))),(state_resolution-1-k))*
edit_matrix[q0];
                }

            //Gewonne Wahrscheinlichkeitsmasse fuer Qualitaetszustand q0
            for(i=0; i<q0; i++){
                double bin_coeff2_rep;
                int faculty_n2_rep = 1;
                int faculty_k2_rep = 1;
                int faculty_nk2_rep = 1;

                for(j=1;j<=(state_resolution-1-i);j++){
```

```
                        faculty_n2_rep=faculty_n2_rep*j;
                }
                for(j=1;j<=(q0-i);j++){
                        faculty_k2_rep=faculty_k2_rep*j;
                }
                for(j=1;j<=(state_resolution-1-q0);j++){
                        faculty_nk2_rep=faculty_nk2_rep*j;
                }
                bin_coeff2_rep=(faculty_n2_rep)/(faculty_k2_rep*faculty_nk2_rep);
                rep_prob_sum = rep_prob_sum+bin_coeff2_rep*
Math.pow(p_rep*Math.pow(euler,(-t/tau_rep)),(q0-i))*
Math.pow((1-p_rep*Math.pow(euler,(-t/tau_rep))),(state_resolution-1-q0))*
edit_matrix[i];
            }

            repair_rate[q0]= rep_prob_sum;
        }
        //==============================================================


        // W A H R S C H E I N L I C H K E I T E N
        for(q=0; q<state_resolution; q++){

            //System.out.print("ZUSTAND: "+q+"\n");
             edit_matrix[q] =   edit_matrix[q]+
                                zeitschritt*(
                                mitophagy_biogenesis_rate[q]+
                                quality_decay_rate[q]+
                                fis_fus_matrix_met[q]+
                                fus_matrix_prot[q]+fis_matrix_prot[q]+
                                repair_rate[q]);

        }
        array_counter = array_counter + 1;

        if(array_counter == time_resolution){
            for(m=1;m<state_resolution+1;m++){
                daten_array[m][t/time_resolution]=edit_matrix[m-1];
                average_quality = average_quality + (m-1)*(edit_matrix[m-1]);
            }
            for(i=0;i<state_resolution;i++){
                standard_deviation_quality=standard_deviation_quality+
Math.sqrt(Math.pow((i-average_quality),2))*daten_array[i+1][t/time_resolution];
            }
            daten_array[0][t/time_resolution]=average_quality;
            daten_array[state_resolution+1][t/time_resolution]=
standard_deviation_quality;

            standard_deviation_quality=0;
            average_quality =0;
            array_counter = 0;
        }
    }
```

```
        return daten_array;

    }

}
```

Appendix B

Appendix Morphological model

FileData.java

```java
import javax.swing.*;
import java.awt.*;
import java.io.*;

public class MitoMorph extends JFrame{

    //GLOBALE VARIABLEN
    public int time; //Laufvariable Zeit
    public int max_time=100000; //Simulationsdauer
    public int mito_number=150; //Menge Mitochondrien
    double[][] mito_data = new double[max_time+2][17]; //Datensicherung
    public double sum_mass, distance_center, distance_center_fct,
average_velocity, average_health_real, average_health,
average_metabolics, deviation_metabolics, deviation_metabolics_real,
                    mitochondria_fct, average_health_real_fct, average_health_fct,
average_metabolics_fct, deviation_metabolics_fct, deviation_metabolics_fct_real,
average_partners, sum_partners, average_partners_fct,
sum_partners_fct; //gesicherte Parameter
    public int mspf=1; //Verzoegerung zwischen zwei Zeitschritten
    public int cell_rad=250; //Zellradius
    public int nuc_rad=75; //Kernradius
    public int edge=50; //Rand
    public double consumer_1_x = 300;
    public double consumer_1_y = 138;
    public double consumer_2_x = 441;
    public double consumer_2_y = 381;
    public double consumer_3_x = 159;
    public double consumer_3_y = 381;
    public double consumer_rad = 50;


    //ERZEUGE MITOCHONDRIEN AUS DEVELOPMITO
    DevelopMito locs = new DevelopMito();
    public double[][][] mito_locs = locs.MitoStart(mito_number,
cell_rad, nuc_rad, edge);
```

```
//HAUPTPROGRAMM
public static void main(String[] args) throws IOException{
    MitoMorph fenster = new MitoMorph();
    double[][]mito_data=fenster.startMyGraphics();

    //Speichere Daten in Textdatei
    int i,j;
    Print data = new Print("mito_data.txt", true);
    data.open();
    for(j=0;j<100002;j++){
        for(i=0;i<17;i++){
            double wert = mito_data[j][i];
            String value = Double.toString(wert);
            data.writeToFile(value + "; ");
        }
        data.writeToFile("%n");
    }
    data.close();
}

//ERZEUGE FENSTER
public MitoMorph(){
setDefaultCloseOperation(JFrame.EXIT_ON_CLOSE);
    setTitle("Mitochondriales Netzwerk");
    setSize(600, 600);
    setVisible(true);
}

//ERZEUGE ANIMATION
public double[][] startMyGraphics(){
    int i,y;

    //Zeitschleife
    for(time=0;time<max_time;time++){

        //Datensicherung
        sum_mass=0;
        distance_center=0;
        sum_partners=0;
        average_partners=0;
        average_health_real=0;
        average_health=0;
        average_metabolics=0;
        mitochondria_fct=0;
        distance_center_fct=0;
        average_velocity=0;
        sum_partners_fct=0;
        average_partners_fct=0;
        average_health_real_fct=0;
        average_health_fct=0;
        average_metabolics_fct=0;
        deviation_metabolics=0;
        deviation_metabolics_fct=0;
        deviation_metabolics_real=0;
```

```
                      deviation_metabolics_fct_real=0;

                      for(y=0;y<mito_number;y++){
                          if(mito_locs[y][6][0]<0.5){
                              sum_mass=sum_mass+1;
                              distance_center=distance_center+
Math.sqrt(Math.pow(300-mito_locs[y][0][0],2)+Math.pow(300-mito_locs[y][0][1],2));
                              for(i=0;i<mito_number;i++){
                                  if(mito_locs[y][1][i]==1){
                                      sum_partners=sum_partners+1;
                                  }
                              }
                              average_partners=average_partners+sum_partners;
                              sum_partners=0;
                              average_health=average_health+mito_locs[y][5][0];
                              average_health_real=average_health_real+mito_locs[y][5][1];
                              average_metabolics=average_metabolics+mito_locs[y][4][0];
                          }

                          if(mito_locs[y][5][0]>0 && mito_locs[y][6][0]<0.5){
                              mitochondria_fct=mitochondria_fct+1;
                              distance_center_fct=distance_center_fct+
Math.sqrt(Math.pow(300-mito_locs[y][0][0],2)+Math.pow(300-mito_locs[y][0][1],2));
                              average_velocity=average_velocity+
Math.sqrt(Math.pow(mito_locs[y][0][2],2)+Math.pow(mito_locs[y][0][3],2));
                              for(i=0;i<mito_number;i++){
                                  if(mito_locs[y][1][i]==1){
                                      sum_partners_fct=sum_partners_fct+1;
                                  }
                              }
                              average_partners_fct=average_partners+sum_partners;
                              sum_partners_fct=0;
                              average_health_fct=average_health_fct+mito_locs[y][5][0];
                              average_health_real_fct=average_health_real_fct+mito_locs[y][5][1];
                              average_metabolics_fct=average_metabolics_fct+mito_locs[y][4][0];
                          }
                      }
                      mito_data[time][0]=sum_mass;
                      mito_data[time][1]=distance_center/sum_mass;
                      mito_data[time][2]=average_partners/sum_mass;
                      mito_data[time][3]=average_health/sum_mass;
                      mito_data[time][4]=average_health_real/sum_mass;
                      mito_data[time][5]=average_metabolics/sum_mass;
                      mito_data[time][6]=mitochondria_fct;
                      mito_data[time][7]=distance_center_fct/mitochondria_fct;
                      mito_data[time][8]=average_partners_fct/mitochondria_fct;
                      mito_data[time][9]=average_health_fct/mitochondria_fct;
                      mito_data[time][10]=average_health_real_fct/mitochondria_fct;
                      mito_data[time][11]=average_metabolics_fct/mitochondria_fct;

                      for(i=0;i<mito_number;i++){
                          if(mito_locs[i][6][0]<0.5){
                              deviation_metabolics=deviation_metabolics+
Math.pow((mito_locs[i][4][1]-average_metabolics/sum_mass),2);
                              deviation_metabolics_real=deviation_metabolics_real+
```

```
Math.pow((mito_locs[i][4][0]-average_metabolics/sum_mass),2);
                }
                if(mito_locs[i][5][0]>0.5 && mito_locs[i][6][0]<0.5){
                    deviation_metabolics_fct=deviation_metabolics_fct+
Math.pow((mito_locs[i][4][1]-average_metabolics_fct/mitochondria_fct),2);
                    deviation_metabolics_fct_real=deviation_metabolics_fct_real+
Math.pow((mito_locs[i][4][0]-average_metabolics_fct/mitochondria_fct),2);
                }
            }
            mito_data[time][12]=Math.sqrt(deviation_metabolics
/(sum_mass-1));
            mito_data[time][13]=Math.sqrt(deviation_metabolics_fct
/(mitochondria_fct-1));
            mito_data[time][14]=Math.sqrt(deviation_metabolics_real
/(sum_mass-1));
            mito_data[time][15]=Math.sqrt(deviation_metabolics_fct_real
/(mitochondria_fct-1));
            mito_data[time][16]=average_velocity/mitochondria_fct;

            mito_locs = locs.MitoLogs(mito_locs, cell_rad, nuc_rad, mito_number,
edge, consumer_1_x, consumer_1_y, consumer_2_x, consumer_2_y,
consumer_3_x, consumer_3_y,time);

            //Erzeuge naechstes Bild
            repaint();
            try{
                Thread.sleep(mspf);
            }
            catch (InterruptedException e) {
            }
        }
        return mito_data;
    }


    //ZEICHNE ZELLE UND MITOCHONDRIEN
    @Override public void paint(Graphics g){
        int i,j;

        //Double Buffering
        Image offscreenImage;
        Graphics offscreenGraphics;
        offscreenImage = createImage(900,600);
        offscreenGraphics=offscreenImage.getGraphics();
        Insets insets = getInsets();
        int originX = insets.left;
        int originY = insets.top;
        int breite  = getSize().width  - insets.left - insets.right;
        int hoehe   = getSize().height - insets.top  - insets.bottom;

        //Grafikelemente
        offscreenGraphics.clearRect(originX, originY, breite-1, hoehe-1);
        Color CellColor = new Color(255,240,255);
        offscreenGraphics.setColor(CellColor);
        offscreenGraphics.fillOval(40,40,520,520);
        offscreenGraphics.setColor(Color.BLACK);
```

```
        offscreenGraphics.drawOval(40,40,520,520);
        Color NucColor = new Color(200,150,150);
        offscreenGraphics.setColor(NucColor);
        offscreenGraphics.fillOval(230,230,145,145);
        Color ConsumerColor_weak = new Color(200-(int),
(100*mito_locs[1][8][0]),200-(int),(100*mito_locs[1][8][0]),240);
        offscreenGraphics.setColor(ConsumerColor_weak);
        offscreenGraphics.fillOval((int)(consumer_1_x-consumer_rad/2),
(int)(consumer_1_y-consumer_rad/2),(int)consumer_rad,(int)consumer_rad);
        Color ConsumerColor_medium = new Color(200-(int),
(100*mito_locs[1][8][1]),200-(int),(100*mito_locs[1][8][1]),240);
        offscreenGraphics.setColor(ConsumerColor_medium);
        offscreenGraphics.fillOval((int)(consumer_2_x-consumer_rad/2),
(int)(consumer_2_y-consumer_rad/2),(int)consumer_rad,(int)consumer_rad);
        Color ConsumerColor_strong = new Color(200-(int),
(100*mito_locs[1][8][2]),200-(int),(100*mito_locs[1][8][2]),240);
        offscreenGraphics.setColor(ConsumerColor_strong);
        offscreenGraphics.fillOval((int)(consumer_3_x-consumer_rad/2),
(int)(consumer_3_y-consumer_rad/2),(int)consumer_rad,(int)consumer_rad);
        offscreenGraphics.setColor(Color.BLACK);
        offscreenGraphics.setFont(new Font("TimesRoman",Font.BOLD,24));
        offscreenGraphics.drawString("Time: "+Integer.toString(time), 30, 70);
        offscreenGraphics.drawString("fps: "+Integer.toString(1000/mspf),
30,70+2*cell_rad);
        offscreenGraphics.setFont(new Font("TimesRoman",Font.BOLD,20));
        offscreenGraphics.drawString("Alle Mitochondrien",2*cell_rad+100,70);
        offscreenGraphics.drawLine(2*cell_rad+95, 75, 2*cell_rad+380, 75);
        offscreenGraphics.setFont(new Font("TimesRoman",Font.PLAIN,20));
        offscreenGraphics.drawString("Mass: "+Double.toString(
Math.round(mito_data[time][0]*10)/10.0),2*cell_rad+100,100);
        offscreenGraphics.drawString("Kernnaehe: "+Double.toString(
Math.round(mito_data[time][1]*10)/10.0),2*cell_rad+100,125);
        offscreenGraphics.drawString("Partnermenge: "+Double.toString(
Math.round(mito_data[time][2]*10)/10.0),2*cell_rad+100,150);
        offscreenGraphics.drawString("Qualitaet: "+Double.toString(
Math.round(mito_data[time][4]*10+mito_data[time][5]*10)/10.0)+
" ("+Double.toString(Math.round(mito_data[time][3]*10+
mito_data[time][5]*10)/10.0)+")",2*cell_rad+100,175);
        offscreenGraphics.drawString("Gesundheit: "+Double.toString(
Math.round(mito_data[time][4]*10)/10.0)+" ("+Double.toString(
Math.round(mito_data[time][3]*10)/10.0)+")",2*cell_rad+100,200);
        offscreenGraphics.drawString("Metabolite: "+Double.toString(
Math.round(mito_data[time][5]*10)/10.0),2*cell_rad+100,225);
        offscreenGraphics.drawString("SD Metabolite: "+Double.toString(
Math.round(mito_data[time][12]*10)/10.0)+" ("+Double.toString(
Math.round(mito_data[time][14]*10)/10.0)+")",2*cell_rad+100,250);
        offscreenGraphics.setFont(new Font("TimesRoman",Font.BOLD,20));
        offscreenGraphics.drawString("Funktionale Mitochondrien",
2*cell_rad+100,295);
        offscreenGraphics.drawLine(2*cell_rad+95,
300, 2*cell_rad+380, 300);
        offscreenGraphics.setFont(new Font("TimesRoman",Font.PLAIN,20));
        offscreenGraphics.drawString("Mass: "+Double.toString(
Math.round(mito_data[time][6]*10)/10.0),2*cell_rad+100,325);
        offscreenGraphics.drawString("Kernnaehe: "+Double.toString(
```

```
Math.round(mito_data[time][7]*10)/10.0),2*cell_rad+100,350);
        offscreenGraphics.drawString("Partnermenge: "+Double.toString(
Math.round(mito_data[time][8]*10)/10.0),2*cell_rad+100,375);
        offscreenGraphics.drawString("Qualitaet: "+Double.toString(
Math.round(mito_data[time][10]*10+mito_data[time][11]*10)/10.0)+" (
"+Double.toString(Math.round(mito_data[time][9]*10+
mito_data[time][11]*10)/10.0)+")",2*cell_rad+100,400);
        offscreenGraphics.drawString("Gesundheit: "+Double.toString(
Math.round(mito_data[time][10]*10)/10.0)+" ("+Double.toString(
Math.round(mito_data[time][9]*10)/10.0)+")",2*cell_rad+100,425);
        offscreenGraphics.drawString("Metabolite: "+Double.toString(
Math.round(mito_data[time][11]*10)/10.0),2*cell_rad+100,450);
        offscreenGraphics.drawString("SD Metabolite: "+Double.toString(
Math.round(mito_data[time][13]*10)/10.0)+" ("+Double.toString(
Math.round(mito_data[time][15]*10)/10.0)+")",2*cell_rad+100,475);
        for(i=0;i<mito_number;i++){
            offscreenGraphics.setColor(Color.BLACK);
            for(j=0;j<mito_number;j++){
                if(mito_locs[i][2][j]>0.5){
                    offscreenGraphics.drawLine((int) Math.round(
mito_locs[i][0][0]), (int) Math.round(mito_locs[i][0][1]),
(int) Math.round(mito_locs[j][0][0]), (int) Math.round(mito_locs[j][0][1]));
                }
            }
            Color MitoColor = new Color (240-(((int)
Math.round(mito_locs[i][4][1])+(int) Math.round(mito_locs[i][5][1])*12)),
(int) Math.round((mito_locs[i][4][1])+(int) Math.round(mito_locs[i][5][1]))*12,0);
            //offscreenGraphics.drawString(Integer.toString(Math.round(i)),
(int) Math.round(mito_locs[i][0][0])-5, (int) Math.round(mito_locs[i][0][1])-5);
            offscreenGraphics.setColor(MitoColor);
            offscreenGraphics.fillOval((int) Math.round(
mito_locs[i][0][0])-5, (int) Math.round(mito_locs[i][0][1])-5, 12, 12);
        }
        g.drawImage(offscreenImage, 0, 0, this);
    }

    //AKTUALISIERE UPDATE METHODE
    @Override public void update(Graphics g){
        paint(g);
    }
}
```

DevelopMito.java

```java
public class DevelopMito {

    public DevelopMito(){

}
    public double[][][] MitoStart(int mito_number, int cell_rad,
int nuc_rad, int edge){

        int y;
        int start_velocity=8; //Maximale Vektorlaenge in x oder y

        double[][][] mito_start = new double[mito_number][10][400];
        /* C O D I E R U N G
        [0][0] X-Position
        [0][1] Y-Position
        [0][2] X-Geschwindigkeit
        [0][3] y-Geschwindigkeit
        [1][i] Fusionen
        [2][i] First Contact
        [3][i] Blacklist
        [4][0] Metabolite
        [5][0] Gesundheit
        [6][0] Exil
        [7][0] Abstandsueberpruefung nur nach Fission
        [8][0] Consumers
        [9][0] */

        for(y=0;y<mito_number;y++){
            mito_start[y][0][0]=cell_rad+edge;
            mito_start[y][0][1]=cell_rad+edge;
            while((mito_start[y][0][1]>cell_rad+edge-
Math.sqrt(Math.pow(nuc_rad,2)-Math.pow(edge+cell_rad-mito_start[y][0][0], 2))
&& mito_start[y][0][1]<cell_rad+edge+Math.sqrt(Math.pow(nuc_rad,2)-
Math.pow(edge+cell_rad-mito_start[y][0][0], 2)) && mito_start[y][0][0]>
cell_rad-nuc_rad+edge && mito_start[y][0][0]<cell_rad+nuc_rad+edge) ||
mito_start[y][0][1]<edge+cell_rad-Math.sqrt(Math.pow(cell_rad,2)-
Math.pow(edge+cell_rad-mito_start[y][0][0],2)) || mito_start[y][0][1]>edge+
cell_rad+Math.sqrt(Math.pow(cell_rad,2)-Math.pow(edge+cell_rad-
mito_start[y][0][0],2))){
                mito_start[y][0][0]= (Math.random()*2*cell_rad+edge);
                mito_start[y][0][1]= (Math.random()*2*cell_rad+edge);
            }
            mito_start[y][0][2]=(Math.random()*start_velocity-
(Math.random()*start_velocity));
            mito_start[y][0][3]=(Math.random()*start_velocity-
(Math.random()*start_velocity));
            mito_start[y][1][y]=1;
            mito_start[y][4][0]= Math.round(Math.random()*10);
            mito_start[y][5][0]= Math.round(Math.random()*10);
        }

        return mito_start;
    }
```

```
    public double[][][] MitoLogs(double[][][] mito_locs, int cell_rad, int nuc_rad,
int mito_number, int edge, double consumer_1_x, double consumer_1_y,
double consumer_2_x, double consumer_2_y,double consumer_3_x,
double consumer_3_y, int time){

        //KONSTANTEN UND VARIABLEN
        //Konstanten
        int fission_velocity=2; //Maximale Vektorlaenge nach Fission
        int recycling_velocity=2; //Maximale Vektorlaenge nach Recycling
        int black_duration=-10000; //Dauer der Isoliertheit
        int fusion_gap=14;//Abstand, ab dem eine Fusion geschieht
        int max_gap = 16;//Maximaler Abstand vor Trennung
        double damping = 0.99;//Daempfung
        double lifetime = 10000;
        double euler = 2.718281828459045;//Eulersche Zahl

        //Wahrscheinlichkeiten
        double fusion_prob = 0; //Fusion
        double fission_prob = 0.5; //Fission
        double delete_prob_start = 0.01; //Ausloeschung
        double recycling_prob_start = 0.01;//Regenerierung
        double supply_decay_prob_start = 0.01;//Verlust Metabolite
        double health_decay_prob_start = 0.01;//Verlust Gesundheit
        double supply_gain_prob_start = 0.001;//Gewinn Metabolite
        double health_gain_prob_start = 0.001;//Gewinn Gesundheit

        double delete_prob;
        double recycling_prob;
        double supply_decay_prob;
        double health_decay_prob;
        double supply_gain_prob;
        double health_gain_prob;

        //Hilfsvariablen
        double vel_x_new, vel_y_new;//Streuung
        int partner_cntr_j;//Fusion
        int partner_number;//Fission
        double sum_metabolites;//Qualitaetsausgleich
        int fusion_partners;//Qualitaetsausgleich
        double max_health;//Qualitaetsausgleich
        double average_metabolites;//Qualitaetsausgleich
        int connection_check;//Abstandstrennung
        int[] connected_mitos= new int[mito_number];//Abstandstrennung

        //Laufvariablen
        int i,j,k,l,m;
        int mito_counter;

        //AENDERUNG VON PROZESSWAHRSCHEINLICHKEITEN
        delete_prob=delete_prob_start;//*
Math.pow(euler,(-((double)time)/lifetime));
        recycling_prob=recycling_prob_start;//*
Math.pow(euler,(-((double)time)/lifetime));
        supply_decay_prob=supply_decay_prob_start;//*
Math.pow(euler,(((double)time)/lifetime));
```

```
        health_decay_prob=health_decay_prob_start;//*
Math.pow(euler,(((double)time)/lifetime));
        supply_gain_prob=supply_gain_prob_start;//*
Math.pow(-euler,(((double)time)/lifetime));
        health_gain_prob=health_gain_prob_start;//*
Math.pow(-euler,(((double)time)/lifetime));

        //DURCHLAUF DER MITOCHONDRIEN
        for(mito_counter=0;mito_counter<mito_number;mito_counter++){

            //MENGE DER CLUSTERPARTNER BERECHNEN
            partner_number=0;
            for(k=0;k<mito_number;k++){
                if(mito_locs[mito_counter][1][k]>0.5 ||
mito_locs[k][1][mito_counter]>0.5){
                    partner_number=partner_number+1;
                }
            }

            //BEWEGUNGSGLEICHUNGEN
            mito_locs[mito_counter][0][0]= mito_locs[mito_counter][0][0]+
mito_locs[mito_counter][0][2];
            mito_locs[mito_counter][0][1]= mito_locs[mito_counter][0][1]+
mito_locs[mito_counter][0][3];

            //Streuung Zellrand
            if(mito_locs[mito_counter][0][0]<edge+cell_rad-
(int) Math.round(Math.sqrt(Math.pow(cell_rad,2)-
Math.pow(Math.abs(mito_locs[mito_counter][0][1]-edge-cell_rad),2)))){
                vel_x_new = Math.random()*Math.sqrt(Math.pow(
mito_locs[mito_counter][0][2],2)+Math.pow(mito_locs[mito_counter][0][3],2));
                vel_y_new = Math.random()*Math.sqrt(Math.pow(
mito_locs[mito_counter][0][2],2)+Math.pow(mito_locs[mito_counter][0][3],2)-
Math.pow(vel_x_new,2))-Math.random()*Math.sqrt(Math.pow(
mito_locs[mito_counter][0][2],2)+Math.pow(mito_locs[mito_counter][0][3],2)-
Math.pow(vel_x_new,2));
                for(k=0;k<mito_number;k++){
                    if(mito_locs[mito_counter][1][k]==1){
                        mito_locs[k][0][0]=mito_locs[k][0][0]-
mito_locs[mito_counter][0][2];
                        mito_locs[k][0][1]=mito_locs[k][0][1]-
mito_locs[mito_counter][0][3];
                        mito_locs[k][0][2]=vel_x_new;
                        mito_locs[k][0][3]=vel_y_new;
                    }
                }
            }
            if(mito_locs[mito_counter][0][0]>edge+cell_rad+(int)
Math.round(Math.sqrt(Math.pow(cell_rad,2)-Math.pow(Math.abs(
mito_locs[mito_counter][0][1]-edge-cell_rad),2)))){
                vel_x_new = -(Math.random()*Math.sqrt(Math.pow(
mito_locs[mito_counter][0][2],2)+Math.pow(mito_locs[mito_counter][0][3],2)));
                vel_y_new = (Math.random()*Math.sqrt(Math.pow(
mito_locs[mito_counter][0][2],2)+Math.pow(mito_locs[mito_counter][0][3],2)-
Math.pow(vel_x_new,2))-Math.random()*Math.sqrt(Math.pow(
```

```
mito_locs[mito_counter][0][2],2)+Math.pow(mito_locs[mito_counter][0][3],2)-
Math.pow(vel_x_new,2)));
                for(k=0;k<mito_number;k++){
                    if(mito_locs[mito_counter][1][k]==1){
                        mito_locs[k][0][0]=mito_locs[k][0][0]-
mito_locs[mito_counter][0][2];
                        mito_locs[k][0][1]=mito_locs[k][0][1]-
mito_locs[mito_counter][0][3];
                        mito_locs[k][0][2]=vel_x_new;
                        mito_locs[k][0][3]=vel_y_new;
                    }
                }
            }
            if(mito_locs[mito_counter][0][1]<edge+cell_rad-(int) Math.round(
Math.sqrt(Math.pow(cell_rad,2)-Math.pow(Math.abs(mito_locs[mito_counter][0][0]-
edge-cell_rad),2)))){
                vel_y_new = (Math.random()*Math.sqrt(Math.pow(
mito_locs[mito_counter][0][2],2)+Math.pow(mito_locs[mito_counter][0][3],2)));
                vel_x_new = (Math.random()*Math.sqrt(Math.pow(
mito_locs[mito_counter][0][2],2)+Math.pow(mito_locs[mito_counter][0][3],2)-
Math.pow(vel_y_new,2))-Math.random()*Math.sqrt(Math.pow(
mito_locs[mito_counter][0][2],2)+Math.pow(mito_locs[mito_counter][0][3],2)-
Math.pow(vel_y_new,2)));
                for(k=0;k<mito_number;k++){
                    if(mito_locs[mito_counter][1][k]==1){
                        mito_locs[k][0][0]=mito_locs[k][0][0]-
mito_locs[mito_counter][0][2];
                        mito_locs[k][0][1]=mito_locs[k][0][1]-
mito_locs[mito_counter][0][3];
                        mito_locs[k][0][2]=vel_x_new;
                        mito_locs[k][0][3]=vel_y_new;
                    }
                }
            }
            if(mito_locs[mito_counter][0][1]>edge+cell_rad+(int) Math.round(
Math.sqrt(Math.pow(cell_rad,2)-Math.pow(Math.abs(
mito_locs[mito_counter][0][0]-edge-cell_rad),2)))){
                vel_y_new = -(Math.random()*Math.sqrt(Math.pow(
mito_locs[mito_counter][0][2],2)+Math.pow(mito_locs[mito_counter][0][3],2)));
                vel_x_new = (Math.random()*Math.sqrt(Math.pow(
mito_locs[mito_counter][0][2],2)+Math.pow(mito_locs[mito_counter][0][3],2)-
Math.pow(vel_y_new,2))-Math.random()*Math.sqrt(Math.pow(
mito_locs[mito_counter][0][2],2)+Math.pow(mito_locs[mito_counter][0][3],2)-
Math.pow(vel_y_new,2)));
                for(k=0;k<mito_number;k++){
                    if(mito_locs[mito_counter][1][k]==1){
                        mito_locs[k][0][0]=mito_locs[k][0][0]-
mito_locs[mito_counter][0][2];
                        mito_locs[k][0][1]=mito_locs[k][0][1]-
mito_locs[mito_counter][0][3];
                        mito_locs[k][0][2]=vel_x_new;
                        mito_locs[k][0][3]=vel_y_new;
                    }
                }
            }
```

```
            //Streuung Kerngrenzen
            if(mito_locs[mito_counter][0][1]>edge+cell_rad-nuc_rad &&
mito_locs[mito_counter][0][1]<edge+cell_rad+nuc_rad &&
mito_locs[mito_counter][0][0]> cell_rad+edge-Math.sqrt(Math.pow(nuc_rad,2)-
Math.pow(edge+cell_rad-mito_locs[mito_counter][0][1],2)) &&
 mito_locs[mito_counter][0][0]<edge+cell_rad){
                vel_x_new = -(Math.random()*Math.sqrt(Math.pow(
mito_locs[mito_counter][0][2],2)+Math.pow(mito_locs[mito_counter][0][3],2)));
                vel_y_new = (Math.random()*Math.sqrt(Math.pow(
mito_locs[mito_counter][0][2],2)+Math.pow(mito_locs[mito_counter][0][3],2)-
Math.pow(vel_x_new,2))-Math.random()*
Math.sqrt(Math.pow(mito_locs[mito_counter][0][2],2)
+Math.pow(mito_locs[mito_counter][0][3],2)-Math.pow(vel_x_new,2)));
                for(k=0;k<mito_number;k++){
                    if(mito_locs[mito_counter][1][k]==1){
                        mito_locs[k][0][0]=mito_locs[k][0][0]-
mito_locs[mito_counter][0][2];
                        mito_locs[k][0][1]=mito_locs[k][0][1]-
mito_locs[mito_counter][0][3];
                        mito_locs[k][0][2]=vel_x_new;
                        mito_locs[k][0][3]=vel_y_new;
                    }
                }
            }
            if(mito_locs[mito_counter][0][1]>edge+cell_rad-nuc_rad &&
mito_locs[mito_counter][0][1]<edge+cell_rad+nuc_rad && mito_locs[mito_counter][0][0]<
cell_rad+edge+Math.sqrt(Math.pow(nuc_rad,2)-Math.pow(edge+cell_rad-
mito_locs[mito_counter][0][1],2)) && mito_locs[mito_counter][0][0]>
edge+cell_rad){
                vel_x_new = (Math.random()*Math.sqrt(Math.pow(
mito_locs[mito_counter][0][2],2)+Math.pow(mito_locs[mito_counter][0][3],2)));
                vel_y_new = (Math.random()*Math.sqrt(Math.pow(
mito_locs[mito_counter][0][2],2)+Math.pow(mito_locs[mito_counter][0][3],2)-
Math.pow(vel_x_new,2))-Math.random()*Math.sqrt(Math.pow(
mito_locs[mito_counter][0][2],2)+Math.pow(mito_locs[mito_counter][0][3],2)-
Math.pow(vel_x_new,2)));
                for(k=0;k<mito_number;k++){
                    if(mito_locs[mito_counter][1][k]==1){
                        mito_locs[k][0][0]=mito_locs[k][0][0]-
mito_locs[mito_counter][0][2];
                        mito_locs[k][0][1]=mito_locs[k][0][1]-
mito_locs[mito_counter][0][3];
                        mito_locs[k][0][2]=vel_x_new;
                        mito_locs[k][0][3]=vel_y_new;
                    }
                }
            }
            if(mito_locs[mito_counter][0][0]>edge+cell_rad-nuc_rad &&
mito_locs[mito_counter][0][0]<edge+cell_rad+nuc_rad && mito_locs[mito_counter][0][1]>
cell_rad+edge-Math.sqrt(Math.pow(nuc_rad,2)-Math.pow(edge+cell_rad-
mito_locs[mito_counter][0][0],2)) && mito_locs[mito_counter][0][1]<
edge+cell_rad){
                vel_y_new = -(Math.random()*
Math.sqrt(Math.pow(mito_locs[mito_counter][0][2],2)
+Math.pow(mito_locs[mito_counter][0][3],2)));
```

```
            vel_x_new = (Math.random()*
Math.sqrt(Math.pow(mito_locs[mito_counter][0][2],2)
+Math.pow(mito_locs[mito_counter][0][3],2)-Math.pow(vel_y_new,2))-
Math.random()*Math.sqrt(Math.pow(mito_locs[mito_counter][0][2],2)+
Math.pow(mito_locs[mito_counter][0][3],2)-Math.pow(vel_y_new,2)));
                for(k=0;k<mito_number;k++){
                    if(mito_locs[mito_counter][1][k]==1){
                        mito_locs[k][0][0]=mito_locs[k][0][0]-
mito_locs[mito_counter][0][2];
                        mito_locs[k][0][1]=mito_locs[k][0][1]-
mito_locs[mito_counter][0][3];
                        mito_locs[k][0][2]=vel_x_new;
                        mito_locs[k][0][3]=vel_y_new;
                    }
                }
            }
            if(mito_locs[mito_counter][0][0]>edge+cell_rad-nuc_rad &&
mito_locs[mito_counter][0][0]<edge+cell_rad+nuc_rad && mito_locs[mito_counter][0][1]<
cell_rad+edge+Math.sqrt(Math.pow(nuc_rad,2)-Math.pow(edge+cell_rad-
mito_locs[mito_counter][0][0],2)) && mito_locs[mito_counter][0][1]>
edge+cell_rad){
                vel_y_new = (Math.random()*Math.sqrt(Math.pow(
mito_locs[mito_counter][0][2],2)+Math.pow(mito_locs[mito_counter][0][3],2)));
                vel_x_new = (Math.random()*Math.sqrt(
Math.pow(mito_locs[mito_counter][0][2],2)+
Math.pow(mito_locs[mito_counter][0][3],2)-
Math.pow(vel_y_new,2))-Math.random()*
Math.sqrt(Math.pow(mito_locs[mito_counter][0][2],2)+
Math.pow(mito_locs[mito_counter][0][3],2)-Math.pow(vel_y_new,2)));
                for(k=0;k<mito_number;k++){
                    if(mito_locs[mito_counter][1][k]==1){
                        mito_locs[k][0][0]=mito_locs[k][0][0]-
mito_locs[mito_counter][0][2];
                        mito_locs[k][0][1]=mito_locs[k][0][1]-
mito_locs[mito_counter][0][3];
                        mito_locs[k][0][2]=vel_x_new;
                        mito_locs[k][0][3]=vel_y_new;
                    }
                }
            }

            //RESTDAUER DER ISOLATION BERECHNEN
            for(j=0;j<mito_number;j++){
                if(mito_locs[mito_counter][3][j]!=0){
                    mito_locs[mito_counter][3][j]=mito_locs[mito_counter][3][j]+1;
                }
            }

            //RECYCLING
            //Ausloeschung
            if(Math.random()>1-delete_prob && partner_number<1.5 &&
mito_locs[mito_counter][5][0]<0.5){
                mito_locs[mito_counter][6][0]=1;
                mito_locs[mito_counter][0][0]=0;
                mito_locs[mito_counter][0][1]=0;
```

```
                mito_locs[mito_counter][0][2]=0;
                mito_locs[mito_counter][0][3]=0;
                }
        //Wiederbelebung
        if(Math.random()>1-recycling_prob && mito_locs[mito_counter][6][0]>0.5){
                mito_locs[mito_counter][6][0]=0;
                mito_locs[mito_counter][4][0]=10;
                mito_locs[mito_counter][5][0]=10;
                mito_locs[mito_counter][0][0]= cell_rad+edge;
                mito_locs[mito_counter][0][1]= cell_rad+edge;
                while((mito_locs[mito_counter][0][1]>cell_rad+
edge-Math.sqrt(Math.pow(nuc_rad,2)-Math.pow(edge+cell_rad-
mito_locs[mito_counter][0][0], 2)) && mito_locs[mito_counter][0][1]<
cell_rad+edge+Math.sqrt(Math.pow(nuc_rad,2)-Math.pow(edge+cell_rad-
mito_locs[mito_counter][0][0], 2)) && mito_locs[mito_counter][0][0]>
cell_rad-nuc_rad+edge && mito_locs[mito_counter][0][0]<cell_rad+nuc_rad+edge)
|| mito_locs[mito_counter][0][1]<edge+cell_rad-Math.sqrt(Math.pow(cell_rad,2)-
Math.pow(edge+cell_rad-mito_locs[mito_counter][0][0],2)) ||
mito_locs[mito_counter][0][1]>edge+cell_rad+Math.sqrt(Math.pow(cell_rad,2)-
Math.pow(edge+cell_rad-mito_locs[mito_counter][0][0],2))){
                        mito_locs[mito_counter][0][0]=Math.random()*2*cell_rad+edge;
                        mito_locs[mito_counter][0][1]=Math.random()*2*cell_rad+edge;
                }
                mito_locs[mito_counter][0][2]=Math.random()*recycling_velocity-
(Math.random()*recycling_velocity);
                mito_locs[mito_counter][0][3]=Math.random()*recycling_velocity-
(Math.random()*recycling_velocity);
                for(j=0;j<mito_number;j++){
                    if(j!=mito_counter && mito_locs[j][6][0]<0.5){
                        mito_locs[mito_counter][3][j]=0;
                        mito_locs[j][3][mito_counter]=0;
                        }
                }
            }


        //QUALITAETSAENDERUNG
        //Qualitaetsverlust
        if(Math.random()>1-supply_decay_prob &&
mito_locs[mito_counter][4][0]>0.5){
                mito_locs[mito_counter][4][0]=mito_locs[mito_counter][4][0]-1;
            }
        if(Math.random()>1-health_decay_prob &&
mito_locs[mito_counter][5][0]>0.5){
                mito_locs[mito_counter][5][0]=mito_locs[mito_counter][5][0]-1;
            }
        //Qualitaetsgewinn
        if(Math.random()>1-supply_gain_prob &&
mito_locs[mito_counter][4][0]<9.5 && mito_locs[mito_counter][6][0]<0.5){
                mito_locs[mito_counter][4][0]=mito_locs[mito_counter][4][0]+1;
            }
        if(Math.random()>1-health_gain_prob &&
mito_locs[mito_counter][5][0]<9.5 && mito_locs[mito_counter][6][0]<0.5){
                mito_locs[mito_counter][5][0]=mito_locs[mito_counter][5][0]+1;
            }
```

```
            //FUSION
            for(j=0;j<mito_number;j++){
                if(Math.random()>fusion_prob && mito_counter!=j &&
mito_locs[j][6][0]<0.5 && Math.sqrt(Math.pow(Math.abs(
mito_locs[mito_counter][0][0]-mito_locs[j][0][0]),2)+Math.pow(Math.abs(
mito_locs[mito_counter][0][1]-mito_locs[j][0][1]),2))<fusion_gap && (
mito_locs[j][3][mito_counter]==0 && mito_locs[mito_counter][3][j]==0)){
                    mito_locs[mito_counter][2][j]=1;

                    partner_cntr_j=0;
                    for(k=0;k<mito_number;k++){
                        if(mito_locs[j][1][k]>0.5){
                            partner_cntr_j=partner_cntr_j+1;
                        }
                    }
                    mito_locs[j][0][2] = (mito_locs[j][0][2]*
partner_cntr_j+mito_locs[mito_counter][0][2]*partner_number)/
(partner_cntr_j+partner_number);
                    mito_locs[j][0][3] = (mito_locs[j][0][3]*
partner_cntr_j+mito_locs[mito_counter][0][3]*partner_number)/
(partner_cntr_j+partner_number);

                    for(k=0;k<mito_number;k++){
                        if(mito_locs[j][1][k]>0.5 || mito_locs[k][1][j]>0.5){
                            mito_locs[mito_counter][1][k]=1;
                            mito_locs[k][1][mito_counter]=1;
                            mito_locs[k][0][2] = mito_locs[j][0][2];
                            mito_locs[k][0][3] = mito_locs[j][0][3];
                        }
                        if(mito_locs[mito_counter][1][k]>0.5 ||
mito_locs[k][1][mito_counter]>0.5){
                            mito_locs[j][1][k]=1;
                            mito_locs[k][1][j]=1;
                            mito_locs[k][0][2] = mito_locs[j][0][2];
                            mito_locs[k][0][3] = mito_locs[j][0][3];
                        }
                    }
                }
            }

            //FISSION
            if(Math.random()>fission_prob && partner_number>1.5 &&
(mito_locs[mito_counter][5][0]<0.5)){
                double fis_rel_x=Math.random()*fission_velocity;
                double fis_rel_y=Math.random()*fission_velocity;
                double sign_x_prob=1*Math.random();
                double sign_y_prob=1*Math.random();
                double sign_x=1;
                double sign_y=1;

                if(sign_x_prob>0.5){
                    sign_x=-1;
                }
                if(sign_y_prob>0.5){
                    sign_y=-1;
```

```
                }

                double vel_x_neu_fis= fis_rel_x*sign_x;
                double vel_y_neu_fis= fis_rel_y*sign_y;

                double vel_x_neu_clu=((partner_number-1)*
mito_locs[mito_counter][0][2]-vel_x_neu_fis)/(partner_number-1);
                double vel_y_neu_clu=((partner_number-1)*
mito_locs[mito_counter][0][3]-vel_y_neu_fis)/(partner_number-1);
                mito_locs[mito_counter][0][2]=vel_x_neu_fis;
                mito_locs[mito_counter][0][3]=vel_y_neu_fis;

                for(l=0;l<mito_number;l++){
                    if(l!=mito_counter){
                        if(mito_locs[mito_counter][1][l]>0.5){
                            mito_locs[l][7][0]=1;
                            mito_locs[l][0][2]=vel_x_neu_clu;
                            mito_locs[l][0][3]=vel_y_neu_clu;
                        }
                        mito_locs[l][3][mito_counter]=black_duration;
                        mito_locs[l][2][mito_counter]=0;
                        mito_locs[l][1][mito_counter]=0;
                        mito_locs[mito_counter][3][l]=black_duration;
                        mito_locs[mito_counter][2][l]=0;
                        mito_locs[mito_counter][1][l]=0;
                    }
                }
            }

            //TRENNUNG BEI ABSTANDSVERGROESSERUNG NACH FISSION
            if(mito_locs[mito_counter][7][0]>0.5){
                connection_check=0;
                for(k=0;k<mito_number;k++){
                    if(k==mito_counter){
                        connected_mitos[k]=1;
                    }
                    else{
                        connected_mitos[k]=0;
                    }
                }
                for(j=0;j<mito_number;j++){
                    if(j!=mito_counter && mito_locs[mito_counter][1][j]>0.5 &&
(Math.abs(mito_locs[mito_counter][0][0]-mito_locs[j][0][0])>max_gap ||
Math.abs(mito_locs[mito_counter][0][1]-mito_locs[j][0][1])>max_gap)){
                        for(k=0;k<mito_number;k++){
                            for(i=0;i<mito_number;i++){
                                if(k!=j && mito_locs[k][1][i]>0.5 &&
connection_check==0 && connected_mitos[i]==1 && connected_mitos[k]==0){
                                    if(Math.abs(mito_locs[k][0][0]-mito_locs[i][0][0])
<max_gap && Math.abs(mito_locs[k][0][1]-mito_locs[i][0][1])<max_gap){
                                        if(Math.abs(mito_locs[k][0][0]-
mito_locs[j][0][0])<max_gap && Math.abs(mito_locs[k][0][1]-
mito_locs[j][0][1])<max_gap){
                                            connection_check=1;
                                            i=mito_number;
```

```
                                        k=mito_number;
                                    }
                                    else{
                                        connected_mitos[k]=1;
                                        i=mito_number;
                                        k=0;
                                    }
                                }
                            }
                        }
                    }
                    if(connection_check==0){
                        for(l=0;l<mito_number;l++){
                            if(connected_mitos[l]==1){
                                for(m=0;m<mito_number;m++){
                                    if(connected_mitos[m]==0 &&
mito_locs[l][1][m]>0.5){
                                        mito_locs[l][1][m]=0;
                                        mito_locs[m][1][l]=0;
                                        mito_locs[l][2][m]=0;
                                        mito_locs[m][2][l]=0;
                                    }
                                }
                            }
                        }
                    }
                }
                mito_locs[mito_counter][7][0]=0;
            }

            //QUALITaeTSAUSGLEICH
            sum_metabolites=0;
            fusion_partners=0;
            max_health=0;
            for(i=0;i<mito_number;i++){
                if(mito_locs[mito_counter][1][i]>0.5 ||
mito_locs[i][1][mito_counter]>0.5){
                    sum_metabolites=sum_metabolites+mito_locs[i][4][0];
                    fusion_partners = fusion_partners+1;
                    if(mito_locs[i][5][0]>max_health){
                        max_health=mito_locs[i][5][0];
                    }
                }
            }
            average_metabolites = Math.round(sum_metabolites/fusion_partners);

            for(i=0;i<mito_number;i++){
                if(mito_locs[mito_counter][1][i]>0.5 ||
mito_locs[i][1][mito_counter]>0.5){
                    mito_locs[i][4][1]=average_metabolites;
                    mito_locs[i][5][1]=max_health;
                }
            }
```

```
//ENERGIEZENTREN
if(mito_locs[mito_counter][5][0]>0.5 && mito_locs[mito_counter][6][0]<0.5){
    int consumer_number=3;
    //Consumer definieren
    double[][] consumers = new double[consumer_number][4];
    consumers[0][0]=consumer_1_x;
    consumers[0][1]=consumer_1_y;
    consumers[0][2]=1*Math.sin(0.005*time)+1;
    mito_locs[1][8][0]=consumers[0][2];
    consumers[0][3]=10;
    consumers[1][0]=consumer_2_x;
    consumers[1][1]=consumer_2_y;
    consumers[1][2]=0;//1*Math.sin(0.003*time)+1;
    mito_locs[1][8][1]=consumers[1][2];
    consumers[1][3]=0;//10;
    consumers[2][0]=consumer_3_x;
    consumers[2][1]=consumer_3_y;
    consumers[2][2]=0;//1*Math.sin(0.005*time)+1;
    mito_locs[1][8][2]=consumers[2][2];
    consumers[2][3]=0;//10;

    double con_dist, dist_x, dist_y, dist_ratio,con_vel_x_att,
con_vel_y_att, con_vel_ges_att, con_vel_x_dis,con_vel_y_dis, con_vel_ges_dis;

    double energy_acceleration_x=0;
    double energy_acceleration_y=0;

    for(j=0;j<mito_number;j++){
        if(mito_locs[mito_counter][1][j]>0.5){
            for(i=0;i<3;i++){
                dist_x=mito_locs[j][0][0]-consumers[i][0];
                dist_y=mito_locs[j][0][1]-consumers[i][1];
                con_dist=Math.sqrt(Math.pow(dist_x,2)+Math.pow(dist_y,2));
                dist_ratio=Math.abs(dist_x)/Math.abs(dist_y);

                con_vel_ges_att=consumers[i][2]/Math.pow(con_dist,2);
                con_vel_ges_dis=consumers[i][3]/Math.pow(con_dist,3);


                con_vel_y_att=Math.sqrt((con_vel_ges_att)/
(1+Math.pow(dist_ratio,2)));
                con_vel_x_att=dist_ratio*con_vel_y_att;
                con_vel_y_dis=Math.sqrt((con_vel_ges_dis)/
(1+Math.pow(dist_ratio,2)));
                con_vel_x_dis=dist_ratio*con_vel_y_dis;

                if(mito_locs[j][0][0]>consumers[i][0]){
                    energy_acceleration_x=energy_acceleration_x-
con_vel_x_att+con_vel_x_dis;
                }
                else{
                    energy_acceleration_x=energy_acceleration_x+
con_vel_x_att-con_vel_x_dis;
                }
                if(mito_locs[j][0][1]>consumers[i][1]){
```

```
                              energy_acceleration_y=energy_acceleration_y-
con_vel_y_att+con_vel_y_dis;
                          }
                          else{
                              energy_acceleration_y=energy_acceleration_y+
con_vel_y_att-con_vel_y_dis;
                          }
                     }
                 }
             }

             //Neue Geschwindigkeit mit Daempfungskonstante
             for(j=0;j<mito_number;j++){
                 if(mito_locs[mito_counter][1][j]>0.5){
                     mito_locs[j][0][2]=mito_locs[j][0][2]*
damping+energy_acceleration_x/partner_number;
                     mito_locs[j][0][3]=mito_locs[j][0][3]*
damping+energy_acceleration_y/partner_number;
                 }
             }
         }
     }

     return mito_locs;
 }

}
```

Appendix C

Appendix Otsu algorithm

FileData.java

```java
import java.io.*;
import java.util.*;

public class FileData {

    public static void main(String[] args) throws IOException {
        //Festlegung von Parametern
        String file_import = "beispiel.txt"; //Eingelesene Messung
        String file_export = "beispiel_bina.txt"; //Editierte Messung
        String file_analyses = "beispiel_daten.txt"; //Analyse-Daten
        int resolution = 128; //Aufloesung der Messung
        int nexts = 0; //Anzahl verglichener Nachbarn in alle Richtungen

        //Binearisierung der Messung
        EditFile measure = new EditFile();
        int[][] mesmatrix = measure.EditMatrix(file_import, resolution, nexts);

        //Analyse der Binearisierung
        AnalyseFile analyse = new AnalyseFile();
        double quantification[] = analyse.SignalQuant(mesmatrix, resolution);
        ArrayList cluster = analyse.ClusterQuant(mesmatrix, resolution);
        System.out.print("Die Messung ist: "+quantification[0]+" Pixel gross.");
        System.out.print(" Die Signalmenge betraegt: "+quantification[1]+".");
        System.out.print(" Das ist ein prozentualer Anteil von "
+quantification[2]+"%.\n");

        //Analyse der Signalcluster
        Cluster cluster_analysis = new Cluster();
        double cluster_data[][] = cluster_analysis.Cluster_quantification(cluster);

        int i;
        for(i=0; i<cluster_data.length; i++){
        System.out.print("Clustergroesse: "+cluster_data[i][1]+"\n");
        }
```

```
//Speicherung des binearisierten Bilds
WriteFile data = new WriteFile(file_export, true);
data.open();
int k, l;
for(l=0; l<resolution; l++){
   for(k=0; k<resolution; k++){
      int wert = mesmatrix[k][l];
      String value = Integer.toString(wert);
      data.writeToFile(value + " ");
   }
   data.writeToFile("%n");
}
data.close();

//Speicherung der Cluster-Analyse
int j;
WriteFile analyses = new WriteFile(file_analyses, true);
analyses.open();
for(i=0; i<cluster_data.length; i++){
   for(j=0; j<3; j++){
         analyses.writeToFile(cluster_data[i][j]+ " ");
   }
   analyses.writeToFile("%n");
}
analyses.close();

System.out.println("Simsalabim.\nAusgabedateien geschrieben.");
   }

}
```

ReadFile.java

```java
import java.io.*;
import java.util.*;

public class ReadFile {

    private String path;

    public ReadFile(String file_path) {
        path = file_path;
    }

    int readNumbers() throws IOException {
        FileReader file_to_read = new FileReader(path);
        BufferedReader bf = new BufferedReader(file_to_read);
        Scanner preScan = new Scanner(bf);

        int anumber;
        int numberOfInts = 0;

        while ((anumber = preScan.nextInt() )!= 1){
            numberOfInts++;
        }
        bf.close();
        return numberOfInts;
    }

    public int[][] OpenFile(int resolution) throws IOException {

        FileReader fr = new FileReader(path);
        BufferedReader nReader = new BufferedReader(fr);
        Scanner scan = new Scanner(nReader);
        int stop = resolution*resolution;

        int[][] data = new int[resolution][resolution];

        int i, j;

        for (j=0; j < resolution; j++) {
            for (i=0; i < resolution; i++) {
                data[i][j] = scan.nextInt();
            }
        }

            nReader.close();
            return data;
    }
}
```

WriteFile.java

```java
package textfiles;
import java.io.*;


public class WriteFile {

private String path;
private boolean append_to_file = false;

public WriteFile(String file_path) {
    path = file_path;
}


public WriteFile(String file_path, boolean append_value){
    path = file_path;
    append_to_file = append_value;
}


PrintWriter print_line;
FileWriter write;

public void open() throws IOException {
    write = new FileWriter(path, append_to_file);
    print_line = new PrintWriter(write);
}

public void close() throws IOException {
    print_line.close();
    write.close();
}

public void writeToFile(String number) throws IOException{
    print_line.printf(number);
}
}
```

EditFile.java

```java
package textfiles;
import java.io.*;
import java.util.*;


public class EditFile {


    public EditFile() {
}
    public int[][] EditMatrix(String file_path, int resolution, int nexts)
                throws IOException {


            //Lese Messmatrix
            ReadFile messung = new ReadFile(file_path);
            int[][] matrix = messung.OpenFile(resolution);
            int[][] matrix_edit = new int[resolution][resolution];
            int i,j,k,l,m,n;

            double sum = 0;
            double average_nexts;

            double sum_value = 0;
            double sum_edges = 0;
            double sum_edges_std = 0;

            //---O T S U - S C H W E L L W E R T---//

            //Ermittle maximalen Grauwert
            double max=0;
            for(i=0;i<resolution;i++){
                for(j=0;j<resolution;j++){
                    if(matrix[i][j] > max){
                        max = matrix[i][j];
                    }
                }
            }

            double otsu=1000000000;
            double otsu_temp;
            double otsu_threshold=0;
            double w1;
            double w2;
            double sum_my1=0;
            double sum_my2=0;
            double my1;
            double my2;
            double sum_var1=0;
            double sum_var2=0;
            double var1;
            double var2;
            ArrayList bin1 = new ArrayList();
            ArrayList bin2 = new ArrayList();
```

```
//Finde Otsu-Schwellwert
for(i=1;i<max;i++){
    for(j=0;j<resolution;j++){
        for(k=0;k<resolution;k++){
            if(matrix[j][k]<i){
                bin1.add(matrix[j][k]);
            }
            else{
                bin2.add(matrix[j][k]);
            }
        }
    }
    double bin1size = bin1.size();
    double bin2size = bin2.size();

    for(j=0;j<bin1.size();j++){
        sum_my1 = sum_my1 + (int) bin1.get(j);
    }
    my1 = sum_my1 / bin1size;

    for(j=0;j<bin2.size();j++){
        sum_my2 = sum_my2 + (int) bin2.get(j);
    }
    my2 = sum_my2 / bin2size;

    for(j=0;j<bin1.size();j++){
        sum_var1 = sum_var1 + (my1-(int) bin1.get(j))*
(my1-(int) bin1.get(j));
    }
    var1 = sum_var1 / bin1size;

    for(j=0;j<bin2.size();j++){
        sum_var2 = sum_var2 + (my2-(int) bin2.get(j))*
(my2-(int) bin2.get(j));
    }
    var2 = sum_var2 / bin1size;

    otsu_temp = (bin1size/(resolution*resolution))*var1 +
(bin2size/(resolution*resolution))*var2;
    if(otsu_temp < otsu){
        otsu = otsu_temp;
        otsu_threshold = i;
    }
    sum_my1 = 0;
    sum_my2 = 0;
    sum_var1 = 0;
    sum_var2 = 0;
    bin1.clear();
    bin2.clear();
}

//Berechne mittlere Intensitaet fuer die Messung
for(i=0; i<resolution; i++){
    for(j=0; j<resolution; j++){
        sum_value = sum_value + matrix[i][j];
```

```
            }
        }
        double average_value = sum_value/(resolution*resolution);

        //Berechne Standardabweichung der Intensitaet fuer die Messung
        double sum_std = 0;
        for(i=0; i<resolution; i++){
            for(j=0; j<resolution; j++){
                sum_std = sum_std + (matrix[i][j]-average_value)*
(matrix[i][j]-average_value);
            }
        }
        double std_gen = Math.sqrt(sum_std/(resolution*resolution-1));

        //Berechne mittleren Gradienten fuer die Messung
        for(i=0; i<(resolution); i++){
            for(j=0; j<(resolution-1); j++){
                sum_edges = sum_edges + Math.abs(matrix[i][j]-matrix[i][j+1])+
Math.abs(matrix[j][i]-matrix[j+1][i]);
            }
        }
        double average_gradient = sum_edges/((resolution-1)*resolution*2);

        //Berechne Standardabweichung des Gradienten fuer die Messung
        for(i=0; i<(resolution); i++){
            for(j=0; j<(resolution-1); j++){
                sum_edges_std = sum_edges_std + Math.abs(average_gradient
-Math.abs(matrix[i][j]-matrix[i][j+1])
+Math.abs(average_gradient-Math.abs(matrix[j][i]-matrix[j+1][i])));
            }
        }
        double std_gradient = sum_edges_std/((resolution-1)*resolution*2-1);

        System.out.print("Mittlerer Gradient: "+average_gradient+"\n");
        System.out.print("Standardabweichung Gradient: "+std_gradient+"\n");

    //Unterer Schwellwert der Poisson-Verteilung
    double p_summe = 0;
    int untere_signifikanz = 0;

    for(i=1; p_summe < 0.95 ;i++){
        p_summe = p_summe + (Math.exp(i*(1.0+
Math.log(average_value/i))-average_value))/
(Math.sqrt(2.0*Math.PI*(i+1.0/6.0)));
        untere_signifikanz = untere_signifikanz+1;
    }
    System.out.print("Untere Signifikanz: "+untere_signifikanz+"\n");

    //Berechne Binarisierung Nachbarn
    ArrayList neighbours = new ArrayList();
    for(i=0; i<resolution; i++){
        for(j=0; j<resolution; j++){
            if(i>nexts && i<(resolution-nexts) && j>nexts &&
j<(resolution-nexts)) {
                for(k=0; k<(2*nexts+1); k++){
```

```
                 for(l=0; l<(2*nexts+1); l++){
                     neighbours.add(matrix[i+k-nexts][j+l-nexts]);
                     sum = sum + matrix[i+k-nexts][j+l-nexts];
                 }
             }

             //Ermittle den mittleren Grauwert der Nachbarschaft
             average_nexts = sum/((nexts*2+1)*(nexts*2+1));

             //Ermittle die Standardabweichung des Grauwerts der Nachbarschaft
             for(k=0; k<(2*nexts+1); k++){
                 for(l=0; l<(2*nexts+1); l++){
                     sum_std = sum_std +
(matrix[i+k-nexts][j+l-nexts]-average_nexts)*
(matrix[i+k-nexts][j+l-nexts]-average_nexts);
                 }
             }
             double std_nexts = Math.sqrt(sum_std/((nexts*2+1)*(nexts*2+1)-1));
             sum = 0;
             sum_std=0;

             //Ermittle maximalen Grauwert der Nachbarschaft
             int n_max=0;
             for(m=0; m<neighbours.size(); m++){
                if((int) neighbours.get(m) > n_max){
                  n_max = (int) neighbours.get(m);
                }
             }

             //Finde Otsu-Schwellwert der Nachbarschaft
             double n_otsu=1000000000;
             double n_otsu_temp;
             double n_otsu_threshold=0;
             double n_sum_my1=0;
             double n_sum_my2=0;
             double n_my1;
             double n_my2;
             double n_sum_var1=0;
             double n_sum_var2=0;
             double n_var1;
             double n_var2;
             ArrayList n_bin1 = new ArrayList();
             ArrayList n_bin2 = new ArrayList();

             for(m=1;m<n_max;m++){
                for(n=0; n<neighbours.size(); n++){
                   if((int) neighbours.get(n) < m){
                      n_bin1.add(neighbours.get(n));
                   }
                   else{
                      n_bin2.add(neighbours.get(n));
                   }
                }

                double n_bin1size = n_bin1.size();
```

```
                          double n_bin2size = n_bin2.size();

                          for(n=0; n<n_bin1.size(); n++){
                          n_sum_my1 = n_sum_my1 + (int) n_bin1.get(n);
                          }
                          n_my1 = n_sum_my1 / n_bin1size;

                          for(n=0; n<n_bin2.size(); n++){
                              n_sum_my2 = n_sum_my2 + (int) n_bin2.get(n);
                          }
                          n_my2 = n_sum_my2 / n_bin2size;

                          for(n=0; n<n_bin1.size(); n++){
                              n_sum_var1 = n_sum_var1 + (n_my1-(int) n_bin1.get(n))
*(n_my1-(int) n_bin1.get(n));
                          }
                          n_var1 = n_sum_var1 / n_bin1size;

                          for(n=0; n<n_bin2.size(); n++){
                              n_sum_var2 = n_sum_var2 + (n_my2-(int) n_bin2.get(n))
*(n_my2-(int) n_bin2.get(n));
                          }
                          n_var2 = n_sum_var2 / n_bin2size;

                          n_otsu_temp = (n_bin1size/((nexts+1)*2))*n_var1
+ (n_bin2size/((nexts+1)*2))*n_var2;
                          if(n_otsu_temp < n_otsu){
                            n_otsu = n_otsu_temp;
                            n_otsu_threshold = m;
                          }

                          n_sum_my1 = 0;
                          n_sum_my2 = 0;
                          n_sum_var1 = 0;
                          n_sum_var2 = 0;
                          n_bin1.clear();
                          n_bin2.clear();
                      }

                      if(matrix[i][j]>n_otsu_threshold && matrix[i][j]>otsu_threshold){
                           matrix_edit[i][j]=1;
                      }
                      else{
                          matrix_edit[i][j]=0;
                      }
                  }
                  else{
                      matrix_edit[i][j]=0;
                  }
                  neighbours.clear();
              }
          }
      return matrix_edit;
    }
}
```

AnalyseFile.java

```java
import java.io.*;
import java.util.*;

public class AnalyseFile {

    public AnalyseFile() {
    }

    public double[] SignalQuant(int[][] matrix_analyse, int resolution)
throws IOException  {

        double sum_pixel = 0;
        double sum_signal = 0;
        double[] signalQuant = new double[3];

        int i, j;
        for(i=0; i<resolution; i++){
            for(j=0; j<resolution; j++){
                sum_pixel=sum_pixel+1;
                if (matrix_analyse[i][j] == 1) {
                    sum_signal = sum_signal + 1;
                }
            }
        }

        signalQuant[0] = sum_pixel;
        signalQuant[1] = sum_signal;
        signalQuant[2] = sum_signal/sum_pixel*100;

        return signalQuant;
    }

    public ArrayList ClusterQuant(int[][] matrix_analyse, int resolution)
throws IOException {

        //Zaehle Signalpixel
        int i, j;
        int signal_pxl = 0;
        for(i=0; i<resolution; i++){
            for(j=0; j<resolution; j++){
                if (matrix_analyse[i][j] == 1) {
                    signal_pxl = signal_pxl + 1;
                }
            }
        }

        //Weise Pixel zeilweise Koordinaten zu
        int k,l;
        int zaehler_column = 0;
        int[][] coords_column = new int[signal_pxl][2];
        for(k=0; k<resolution; k++){
            for(l=0; l<resolution; l++){
                if(matrix_analyse[k][l]==1){
                    coords_column[zaehler_column][0]= k;
```

```
                    coords_column[zaehler_column][1]= l;
                    zaehler_column = zaehler_column + 1;
                }
            }
        }


        //Weise Pixel spaltenweise Koordinaten zu
        int zaehler_line = 0;
        int[][] coords_line = new int[signal_pxl][2];
        for(k=0; k<resolution; k++){
            for(l=0; l<resolution; l++){
                if(matrix_analyse[l][k]==1){
                    coords_line[zaehler_line][0]= k;
                    coords_line[zaehler_line][1]= l;
                    zaehler_line = zaehler_line + 1;
                }
            }
        }


        //Fasse Pixel zeilenweise zusammen//


        //Zaehle Zeilen-Vektorlaenge
        int t;
        int m = 0;
        int line_cluster_no = 0;
        while(m<signal_pxl){
                for(t=0; (m+t<signal_pxl) && ((coords_line[m][0])==
(coords_line[m+t][0]))
&& ((coords_line[m][1]+t)==(coords_line[m+t][1])); t++){
                }
                m=m+t;
                line_cluster_no=line_cluster_no+1;
        }


        //Weise Zeilen-Vektor Daten zu
        int[][] line_vector = new int[line_cluster_no][3];
        int u;
        int n = 0;
        int line_no = 0;

        while(n<signal_pxl){
                for(u=0; (n+u<signal_pxl) && ((coords_line[n][0])==
(coords_line[n+u][0]))
&& ((coords_line[n][1]+u)==(coords_line[n+u][1])); u++){
                    line_vector[line_no][0]=coords_line[n][0];
                    line_vector[line_no][1]=coords_line[n][1];
                    line_vector[line_no][2]=coords_line[n+u][1];
                }
                n=n+u;
                line_no=line_no+1;
        }


        int[][] unite_line = new int[line_cluster_no][3];
        n = 0;
        line_no = 0;
```

```
        while(n<signal_pxl){
                for(u=0; (n+u<signal_pxl) && ((coords_line[n][0])==
(coords_line[n+u][0]))
&& ((coords_line[n][1]+u)==(coords_line[n+u][1])); u++){
                        unite_line[line_no][0]=coords_line[n][0];
                        unite_line[line_no][1]=coords_line[n][1];
                        unite_line[line_no][2]=coords_line[n+u][1];
                }
                n=n+u;
                line_no=line_no+1;
        }


        //Fasse Pixel spaltenweise zusammen

        //Zaehle Spalten-Vektorlaenge
        int column_cluster_no = 0;
        m=0;
        while(m<signal_pxl){
                for(t=0; (m+t<signal_pxl) && ((coords_column[m][0])==
(coords_column[m+t][0]))
&& ((coords_column[m][1]+t)==(coords_column[m+t][1])); t++){
                }
                m=m+t;
                column_cluster_no=column_cluster_no+1;
        }


        //Weise Spalten-Vektor Daten zu
        int[][] column_vector = new int[column_cluster_no][3];
        int column_no = 0;
        n=0;
        while(n<signal_pxl){
                for(u=0; (n+u<signal_pxl) && ((coords_column[n][0])==
(coords_column[n+u][0]))
&& ((coords_column[n][1]+u)==(coords_column[n+u][1])); u++){
                        column_vector[column_no][0]=coords_column[n][0];
                        column_vector[column_no][1]=coords_column[n][1];
                        column_vector[column_no][2]=coords_column[n+u][1];
                }
                n=n+u;
                column_no=column_no+1;
        }


        int[][] unite_col = new int[column_cluster_no][3];
        column_no = 0;
        n=0;
        while(n<signal_pxl){
                for(u=0; (n+u<signal_pxl) && ((coords_column[n][0])==
(coords_column[n+u][0]))
&& ((coords_column[n][1]+u)==(coords_column[n+u][1])); u++){
                        unite_col[column_no][0]=coords_column[n][0];
                        unite_col[column_no][1]=coords_column[n][1];
                        unite_col[column_no][2]=coords_column[n+u][1];
                }
                n=n+u;
                column_no=column_no+1;
```

```
        }

        //Baue Cluster
        ArrayList cluster = new ArrayList();
        ArrayList single_cluster = new ArrayList();
        ArrayList raster_line = new ArrayList();
        ArrayList raster_col = new ArrayList();

        int[] temp_line = new int[3];
        int[] temp_col = new int[3];
        int[] space = {0,0,0};
        int[] debug = new int[3];

        int count, line, col, raster, clusters;
        int schalter = 0;
        int count_sc = 0;
        int count_rl = 0;
        int count_rc = 0;

        for(clusters=0; clusters<column_vector.length; clusters++){

        schalter = 0;

        if(unite_col[clusters][0]!=0 && unite_col[clusters][1]!=0
&& unite_col[clusters][2]!=0){
        raster_col.add(column_vector[clusters]);
            unite_col[clusters][0]=0;
            unite_col[clusters][1]=0;
            unite_col[clusters][2]=0;

        for(count=0; schalter !=3; count++){

            if(schalter == 0){

              for(raster=0; raster<raster_col.size(); raster++){
                temp_line = (int[]) raster_col.get(raster);

                for(line=0; line<unite_line.length; line++){

                    if((temp_line[0]>=unite_line[line][1] &&
temp_line[0]<=unite_line[line][2]) &&
                            (unite_line[line][0]>=temp_line[1] &&
unite_line[line][0]<=temp_line[2])){

                        single_cluster.add(count_sc, line_vector[line]);
                        raster_line.add(count_rl, line_vector[line]);

                        unite_line[line][0]=0;
                        unite_line[line][1]=0;
                        unite_line[line][2]=0;

                        count_sc = count_sc+1;
                        count_rl = count_rl+1;
                    }
                }
```

```
                    }
                    if(raster_line.isEmpty()){
                        schalter = 2;
                            raster_line.clear();
                        raster_col.clear();
                        count_rc = 0;
                        count_rl = 0;
                    }
                    else{
                        schalter = 1;
                        raster_col.clear();
                        count_rc = 0;
                    }
            }

            else if(schalter == 1){
                for(raster=0; raster<raster_line.size(); raster++){
                    temp_col = (int[]) raster_line.get(raster);

                    for(col=0; col<unite_col.length; col++){
                        if((temp_col[0]>=unite_col[col][1] &&
temp_col[0]<=unite_col[col][2]) &&
                            (unite_col[col][0]>=temp_col[1] &&
unite_col[col][0]<=temp_col[2])){

                            raster_col.add(count_rc, column_vector[col]);

                            unite_col[col][0]=0;
                            unite_col[col][1]=0;
                            unite_col[col][2]=0;

                            count_rc = count_rc+1;
                        }
                        }
                        }
                    if(raster_col.isEmpty()){
                        schalter = 2;
                            raster_line.clear();
                        raster_line.clear();
                        count_rc = 0;
                        count_rl = 0;
                    }
                    else{
                        schalter = 0;
                        raster_line.clear();
                        count_rl=0;
                    }
            }

            else if(schalter == 2){
                single_cluster.add(count_sc,space);
                count_sc = count_sc + 1;
                raster_line.clear();
                raster_col.clear();
                count_rc = 0;
```

```
                count_rl = 0;

                schalter = 3;
            }
        }
        }
        }

        return single_cluster;

    }
}
```

ClusterFile.java

```java
import java.io.*;
import java.util.*;
import java.math.*;


public class Cluster {

    public Cluster(){
    }

    public double[][] Cluster_quantification(ArrayList clusterlist){

        //ANZAHL DER CLUSTER ZAEHLEN
        int[] temp = new int[3];
        int cluster_number = 0;
        int i;

        for(i=0; i<clusterlist.size(); i++){

            temp = (int[]) clusterlist.get(i);
            if(temp[0]==0 && temp[1]==0 && temp[2]==0){
                cluster_number = cluster_number + 1;
            }
        }

        System.out.print("Die Anzahl der Cluster ist: "+cluster_number+"\n");

        //UMFANG UND AREAL DER CLUSTER BESTIMMEN
        double[][] cluster_data = new double[cluster_number][3];
        int count=0;
        int temp_count=0;
        int count_add=0;
        int schalter;
        int schalter2 = 0;
        int k;
        int[] temp_line = new int[3];
        int[] per_temp_line = new int[3];
        int j, start, end;

        for(i=0; i<cluster_number; i++){

            schalter = 0;

            for(count=count_add; schalter == 0 && count_add <
clusterlist.size();count++){

                temp_line = (int[]) clusterlist.get(count);

                if(temp_line[0]!=0 && temp_line[1]!=0 && temp_line[2]!=0){

                    schalter2 = 0;
                    count_add = count_add+1;
                    cluster_data[i][0] = cluster_data[i][0]+temp_line[2]-
temp_line[1]+1;
```

```
                    cluster_data[i][1] = cluster_data[i][1]+2+2*(temp_line[2]-
temp_line[1]+1);

                    for(j=temp_count; schalter2 == 0; j++){

                        per_temp_line = (int[]) clusterlist.get(j);

                        if(per_temp_line[0]!=0 && per_temp_line[1]!=0 &&
per_temp_line[2]!=0){
                            if((per_temp_line[0]+1 == temp_line[0]) ||
(per_temp_line[0]-1 == temp_line[0])){
                                start = per_temp_line[1];
                                end = per_temp_line[2];
                                for(k=start; k <= end; k++){
                                    if(k >= temp_line[1] && k <= temp_line[2]){
                                        cluster_data[i][1] = cluster_data[i][1]-1;
                                    }
                                }
                            }
                        }

                        else{
                            schalter2 = 1;
                        }

                    }
                }
                else{
                    schalter = 1;
                    count_add = count_add+1;
                    temp_count = count_add;

                }
            }
        }

        //FORMFAKTOR DER CLUSTER BERECHNEN
        double pi = 3.14159265358979;

        for(i=0; i<cluster_number; i++){
            cluster_data[i][2] = (cluster_data[i][1]*cluster_data[i][1])/
(4*pi*cluster_data[i][0]);
        }

        //AUSGABEWERTE BESTIMMEN
        double[] cluster_values = new double[21];

        cluster_values[0] = cluster_number;

        double clusterarea_mean = 0;
        double clusterperi_mean = 0;
        double clustershape_mean = 0;
        double clusterarea_stad = 0;
        double clusterperi_stad = 0;
        double clustershape_stad = 0;
```

```
        double clusterarea_sum = 0;
        double clusterperi_sum = 0;
        double clustershape_sum = 0;
        double nopxl_clusterarea_mean = 0;
        double nopxl_clusterperi_mean = 0;
        double nopxl_clustershape_mean = 0;
        double nopxl_clusterarea_stad = 0;
        double nopxl_clusterperi_stad = 0;
        double nopxl_clustershape_stad = 0;
        double nopxl_clusterarea_sum = 0;
        double nopxl_clusterperi_sum = 0;
        double nopxl_clustershape_sum = 0;
        double large_clusterarea_mean = 0;
        double large_clusterperi_mean = 0;
        double large_clustershape_mean = 0;
        double large_clusterarea_stad = 0;
        double large_clusterperi_stad = 0;
        double large_clustershape_stad = 0;
        double large_clusterarea_sum = 0;
        double large_clusterperi_sum = 0;
        double large_clustershape_sum = 0;

        //Mittelwerte
        for(i=0; i<cluster_number; i++){
            clusterarea_sum = clusterarea_sum + cluster_data[i][0];
            clusterperi_sum = clusterperi_sum + cluster_data[i][1];
            clustershape_sum = clustershape_sum + cluster_data[i][2];
        }
        clusterarea_mean = (clusterarea_sum/cluster_number);
        clusterperi_mean = (clusterperi_sum/cluster_number);
        clustershape_mean = (clustershape_sum/cluster_number);

        //Standardabweichungen
        for(i=0; i<cluster_number; i++){
            clusterarea_stad = clusterarea_stad +
(cluster_data[i][0]-clusterarea_mean)*
(cluster_data[i][0]-clusterarea_mean);
            clusterperi_stad = clusterperi_stad +
(cluster_data[i][1]-clusterperi_mean)*
(cluster_data[i][1]-clusterperi_mean);
            clustershape_stad = clustershape_stad +
(cluster_data[i][2]-clustershape_mean)*
(cluster_data[i][2]-clustershape_mean);
        }

        //Anzahl Cluster ohne Einzelpixel
        int nopxl_cluster_number = 0;
        for(i=0; i<cluster_number; i++){
            if(cluster_data[i][0] != 1 && cluster_data[i][0] != 0){
                nopxl_cluster_number = nopxl_cluster_number + 1;
            }
        }

        //Mittelwerte ohne Einzelpixel
        for(i=0; i<cluster_number; i++){
```

```
                if(cluster_data[i][0] != 1 && cluster_data[i][0] != 0){
                    nopxl_clusterarea_sum = nopxl_clusterarea_sum + cluster_data[i][0];
                    nopxl_clusterperi_sum = nopxl_clusterperi_sum + cluster_data[i][1];
                    nopxl_clustershape_sum = nopxl_clustershape_sum + cluster_data[i][2];
                }
            }
            nopxl_clusterarea_mean = (nopxl_clusterarea_sum/nopxl_cluster_number);
            nopxl_clusterperi_mean = (nopxl_clusterperi_sum/nopxl_cluster_number);
            nopxl_clustershape_mean = (nopxl_clustershape_sum/nopxl_cluster_number);

            //Standardabweichungen ohne Einzelpixel
            for(i=0; i<cluster_number; i++){
                if(cluster_data[i][0] != 1 && cluster_data[i][0] != 0){
                    nopxl_clusterarea_stad = nopxl_clusterarea_stad +
(cluster_data[i][0]-nopxl_clusterarea_mean)*
(cluster_data[i][0]-nopxl_clusterarea_mean);
                    nopxl_clusterperi_stad = nopxl_clusterperi_stad +
(cluster_data[i][1]-nopxl_clusterperi_mean)*
(cluster_data[i][1]-nopxl_clusterperi_mean);
                    nopxl_clustershape_stad = nopxl_clustershape_stad +
(cluster_data[i][2]-nopxl_clustershape_mean)*
(cluster_data[i][2]-nopxl_clustershape_mean);
                }
            }

            //Anzahl grosse Cluster
            int large_cluster_number = 0;
            for(i=0; i<cluster_number; i++){
                if(cluster_data[i][0] >= 10){
                    large_cluster_number = large_cluster_number + 1;
                }
            }

            //Mittelwerte grosse Cluster
            for(i=0; i<cluster_number; i++){
                if(cluster_data[i][0] >= 10){
                    large_clusterarea_sum = large_clusterarea_sum + cluster_data[i][0];
                    large_clusterperi_sum = large_clusterperi_sum + cluster_data[i][1];
                    large_clustershape_sum = large_clustershape_sum + cluster_data[i][2];
                }
            }
            large_clusterarea_mean = (large_clusterarea_sum/large_cluster_number);
            large_clusterperi_mean = (large_clusterperi_sum/large_cluster_number);
            large_clustershape_mean = (large_clustershape_sum/large_cluster_number);

            //Standardabweichungen grosse Cluster
            for(i=0; i<cluster_number; i++){
                if(cluster_data[i][0] >= 10){
                    large_clusterarea_stad = large_clusterarea_stad +
(cluster_data[i][0]-large_clusterarea_mean)*
(cluster_data[i][0]-large_clusterarea_mean);
                    large_clusterperi_stad = large_clusterperi_stad +
(cluster_data[i][1]-large_clusterperi_mean)*
(cluster_data[i][1]-large_clusterperi_mean);
                    large_clustershape_stad = large_clustershape_stad +
```

```
( cluster_data [i ][2] - large_clustershape_mean )*
( cluster_data [i ][2] - large_clustershape_mean );
            }
        }

        cluster_values [1] = clusterarea_mean ;
        cluster_values [2] = Math . sqrt ( clusterarea_stad /( cluster_number -1));
        cluster_values [3] = clusterperi_mean ;
        cluster_values [4] = Math . sqrt ( clusterperi_stad /( cluster_number -1));
        cluster_values [5] = clustershape_mean ;
        cluster_values [6] = Math . sqrt ( clustershape_stad /( cluster_number -1));
        cluster_values [7] = nopxl_cluster_number ;
        cluster_values [8] = nopxl_clusterarea_mean ;
        cluster_values [9] = Math . sqrt ( nopxl_clusterarea_stad /
( nopxl_cluster_number -1));
        cluster_values [10] = nopxl_clusterperi_mean ;
        cluster_values [11] = Math . sqrt ( nopxl_clusterperi_stad /
( nopxl_cluster_number -1));
        cluster_values [12] = nopxl_clustershape_mean ;
        cluster_values [13] = Math . sqrt ( nopxl_clustershape_stad /
( nopxl_cluster_number -1));
        cluster_values [14] = large_cluster_number ;
        cluster_values [15] = large_clusterarea_mean ;
        cluster_values [16] = Math . sqrt ( large_clusterarea_stad /
( large_cluster_number -1));
        cluster_values [17] = large_clusterperi_mean ;
        cluster_values [18] = Math . sqrt ( large_clusterperi_stad /
( large_cluster_number -1));
        cluster_values [19] = large_clustershape_mean ;
        cluster_values [20] = Math . sqrt ( large_clustershape_stad /
( large_cluster_number -1));

        return cluster_data ;
    }
}
```

List of Publications

- D. Mellem, F. Fischer, S. Jaspers, H. Wenck, M. Rübhausen, *Quality Saving Mechanisms of Mitochondria during Aging in a Fully Time-Dependent Computational Biophysical Model*, PLoS ONE **11(1)**, 2016

- D. Mellem, M. Sattler, S. Pagel-Wolff, S. Jaspers, H. Wenck, M. Rübhausen, F. Fischer, *Fragmentation of the Mitochondrial Network in Skin in vivo*, PLoS ONE **12(6)**, 2017

Bibliography

[1] M.A. Farage, K.W. Miller, P. Elsner, and H.I. Maibach. Mitochondrial dysfunction in aging: Much progress but many unresolved questions. *Int J Cosmet Sci*, 30: 87–95, 2008.

[2] R. Kohen. Skin antioxidants: their role in aging and in oxidative stress–new approaches for their evaluation. *Biomed Pharmacother*, 53(4):181–92, 1999.

[3] W. Montagna. *The Structure and Function of Skin*. Academic Press Inc., 1956.

[4] R. B. Hamanaka and N. S. Chandel. Mitochondrial metabolism as a regulator of keratinocyte differentiation. *Cell Logist*, 3(1):e25456, 2013.

[5] H. Lodish, A. Berk, C. A. Kaiser, M. Krieger, M. P. Scott, and A. Bretscher. Molecular cell biology, 2004.

[6] E. D. Robin and R. Wong. Mitochondrial dna molecules and virtual number of mitochondria per cell in mammalian cells. *J Cell Physiol*, 136(3):507–13, 1988.

[7] T. L. Schwarz. Mitochondrial trafficking in neurons. *Cold Spring Harb Perspect Biol*, 5(6), 2013.

[8] A. M. van der Bliek, Q. Shen, and S. Kawajiri. Mechanisms of mitochondrial fission and fusion. *Cold Spring Harb Perspect Biol*, 5(6), 2013.

[9] X. Liu, D. Weaver, O. Shirihai, and G. Hajnoczky. Mitochondrial 'kiss-and-run': interplay between mitochondrial motility and fusion-fission dynamics. *EMBO J*, 28(20):3074–89, 2009.

[10] H. Chen, M. Vermulst, Y. E. Wang, A. Chomyn, T. A. Prolla, J. M. McCaffery, and D. C. Chan. Mitochondrial fusion is required for mtdna stability in skeletal muscle and tolerance of mtdna mutations. *Cell*, 141(2):280–9, 2010.

[11] D. Lee, K. Y. Kim, M. S. Shim, S. Y. Kim, M. H. Ellisman, R. N. Weinreb, and W. K. Ju. Coenzyme q10 ameliorates oxidative stress and prevents mitochondrial alteration in ischemic retinal injury. *Apoptosis*, 19(4):603–14, 2014.

[12] B.A.I. Payne and P.F. Cinnery. Mitochondrial dysfunction in aging: Much progress but many unresolved questions. *Biochimica et Biophysica Acta*, 1847:1347–53, 2015.

[13] M. Klingenberg. The adp and atp transport in mitochondria and its carrier. *Biochim Biophys Acta*, 1778(10):1978–2021, 2008.

[14] I. J. Holt, A. E. Harding, and J. A. Morgan-Hughes. Deletions of muscle mitochondrial dna in patients with mitochondrial myopathies. *Nature*, 331(6158): 717–9, 1988.

[15] D. C. Wallace, G. Singh, M. T. Lott, J. A. Hodge, T. G. Schurr, A. M. Lezza, L. J. Elsas, and E. K. Nikoskelainen. Mitochondrial dna mutation associated with leber's hereditary optic neuropathy. *Science*, 242(4884):1427–30, 1988.

[16] M. Mimaki, X. Wang, M. McKenzie, D. R. Thorburn, and M. T. Ryan. Understanding mitochondrial complex 1 assembly in health and disease. *Biochim Biophys Acta*, 1817(6):851–62, 2012.

[17] M. T. Figge, A. S. Reichert, M. Meyer-Hermann, and H. D. Osiewacz. Deceleration of fusion-fission cycles improves mitochondrial quality control during aging. *PLoS Comput Biol*, 8(6):e1002576, 2012.

[18] G. Twig, A. Elorza, A. J. Molina, H. Mohamed, J. D. Wikstrom, G. Walzer, L. Stiles, S. E. Haigh, S. Katz, G. Las, J. Alroy, M. Wu, B. F. Py, J. Yuan, J. T. Deeney, B. E. Corkey, and O. S. Shirihai. Fission and selective fusion govern mitochondrial segregation and elimination by autophagy. *EMBO J*, 27(2):433–46, 2008.

[19] K. Palikaras and N. Tavernarakis. Mitochondrial homeostasis: the interplay between mitophagy and mitochondrial biogenesis. *Exp Gerontol*, 56:182–8, 2014.

[20] N. B. Larsen, M. Rasmussen, and L. J. Rasmussen. Nuclear and mitochondrial dna repair: similar pathways? *Mitochondrion*, 5(2):89–108, 2005.

[21] Y. H. Wei and H. C. Lee. Oxidative stress, mitochondrial dna mutation, and impairment of antioxidant enzymes in aging. *Exp Biol Med (Maywood)*, 227(9): 671–82, 2002.

[22] I. Shokolenko, N. Venediktova, A. Bochkareva, G. L. Wilson, and M. F. Alexeyev. Oxidative stress induces degradation of mitochondrial dna. *Nucleic Acids Res*, 37 (8):2539–48, 2009.

[23] G. C. Brown and V. Borutaite. There is no evidence that mitochondria are the main source of reactive oxygen species in mammalian cells. *Mitochondrion*, 12(1): 1–4, 2012.

[24] M.E. Winter. Basic clinical pharmacokinetics, 2004.

[25] G.L. Bretthorst E.T. Jaynes. *Probability Theory: The Logic of Science*. Cambridge University Prewss, 2003.

[26] Archibald V. Hill. The possible effects of the aggregation of the molecules of haemoglobin on its dissociation curves. *The Journal of Physiology*, 40(iv-vii), 1910.

[27] A. Y. Seo, A. M. Joseph, D. Dutta, J. C. Hwang, J. P. Aris, and C. Leeuwenburgh. New insights into the role of mitochondria in aging: mitochondrial dynamics and more. *J Cell Sci*, 123(Pt 15):2533–42, 2010.

[28] T. D. Oberley, J. M. Swanlund, H. J. Zhang, and K. C. Kregel. Aging results in increased autophagy of mitochondria and protein nitration in rat hepatocytes following heat stress. *J Histochem Cytochem*, 56(6):615–27, 2008.

[29] M. A. Birch-Machin and H. Swalwell. How mitochondria record the effects of uv exposure and oxidative stress using human skin as a model tissue. *Mutagenesis*, 25(2):101–7, 2010.

[30] A. D. Romano, G. Serviddio, A. de Matthaeis, F. Bellanti, and G. Vendemiale. Oxidative stress and aging. *J Nephrol*, 23 Suppl 15:S29–36, 2010.

[31] T. D. Fox. Mitochondrial protein synthesis, import, and assembly. *Genetics*, 192 (4):1203–34, 2012.

[32] V. Gorbunova, A. Seluanov, Z. Mao, and C. Hine. Changes in dna repair during aging. *Nucleic Acids Res*, 35(22):7466–74, 2007.

[33] Java SE at a glance. `http://www.oracle.com/technetwork/java/javase/overview/index.html`, 2016.

[34] java.util Package. `https://docs.oracle.com/javase/7/docs/api/java/util/package-summary.html`, 2016.

[35] java.io Package. `https://docs.oracle.com/javase/7/docs/api/java/io/package-summary.html`, 2016.

[36] H. C. Lee, P. H. Yin, C. W. Chi, and Y. H. Wei. Increase in mitochondrial mass in human fibroblasts under oxidative stress and during replicative cell senescence. *J Biomed Sci*, 9(6 Pt 1):517–26, 2002.

[37] D. Mellem, F. Fischer, S. Jaspers, H. Wenck, and M. Rubhausen. Quality saving mechanisms of mitochondria during aging in a fully time-dependent computational biophysical model. *PLoS One*, 11(1):e0146973, 2016.

[38] S. G. Regmi, S. G. Rolland, and B. Conradt. Age-dependent changes in mitochondrial morphology and volume are not predictors of lifespan. *Aging (Albany NY)*, 6(2):118–30, 2014.

[39] G. Sgarbi, P. Matarrese, M. Pinti, C. Lanzarini, B. Ascione, L. Gibellini, E. Dika, A. Patrizi, C. Tommasino, M. Capri, A. Cossarizza, A. Baracca, G. Lenaz, G. Solaini, C. Franceschi, W. Malorni, and S. Salvioli. Mitochondria hyperfusion and elevated autophagic activity are key mechanisms for cellular bioenergetic preservation in centenarians. *Aging (Albany NY)*, 6(4):296–310, 2014.

[40] G. Twig and O. S. Shirihai. The interplay between mitochondrial dynamics and mitophagy. *Antioxid Redox Signal*, 14(10):1939–51, 2011.

[41] G. Lopez-Lluch, P. M. Irusta, P. Navas, and R. de Cabo. Mitochondrial biogenesis and healthy aging. *Exp Gerontol*, 43(9):813–9, 2008.

[42] G. Cavallini, A. Donati, M. Taddei, and E. Bergamini. Evidence for selective mitochondrial autophagy and failure in aging. *Autophagy*, 3(1):26–7, 2007.

[43] S. Wu, F. Zhou, Z. Zhang, and D. Xing. Mitochondrial oxidative stress causes mitochondrial fragmentation via differential modulation of mitochondrial fission-fusion proteins. *FEBS J*, 278(6):941–54, 2011.

[44] M. Picard, K. White, and D. M. Turnbull. Mitochondrial morphology, topology, and membrane interactions in skeletal muscle: a quantitative three-dimensional electron microscopy study. *J Appl Physiol (1985)*, 114(2):161–71, 2013.

[45] R. J. Youle and A. M. van der Bliek. Mitochondrial fission, fusion, and stress. *Science*, 337(6098):1062–5, 2012.

[46] W. M. Saxton and P. J. Hollenbeck. The axonal transport of mitochondria. *J Cell Sci*, 125(Pt 9):2095–104, 2012.

[47] V. Anesti and L. Scorrano. The relationship between mitochondrial shape and function and the cytoskeleton. *Biochim Biophys Acta*, 1757(5-6):692–9, 2006.

[48] C. M. Waterman-Storer. Microtubules and microscopes: how the development of light microscopic imaging technologies has contributed to discoveries about microtubule dynamics in living cells. *Mol Biol Cell*, 9(12):3263–71, 1998.

[49] A. M. Mastro, M. A. Babich, W. D. Taylor, and A. D. Keith. Diffusion of a small molecule in the cytoplasm of mammalian cells. *Proc Natl Acad Sci U S A*, 81(11): 3414–8, 1984.

[50] G. M. Cooper. *The Cell - A Molecular Approach*. Sinauer Associates, 2000.

[51] S. B. Berman, F. J. Pineda, and J. M. Hardwick. Mitochondrial fission and fusion dynamics: the long and short of it. *Cell Death Differ*, 15(7):1147–52, 2008.

[52] M. Frank, S. Duvezin-Caubet, S. Koob, A. Occhipinti, R. Jagasia, A. Petcherski, M. O. Ruonala, M. Priault, B. Salin, and A. S. Reichert. Mitophagy is triggered by mild oxidative stress in a mitochondrial fission dependent manner. *Biochim Biophys Acta*, 1823(12):2297–310, 2012.

[53] A. A. Markov. Rasprostranenie zakona bol'shih chisel na velichiny, zavisyaschie drug ot druga. *Izvestiya Fiziko-matematicheskogoobschestva pri Kazanskom universitete*, 15:22, 1906.

[54] H. Imamura, K. P. Nhat, H. Togawa, K. Saito, R. Iino, Y. Kato-Yamada, T. Nagai, and H. Noji. Visualization of atp levels inside single living cells with fluorescence resonance energy transfer-based genetically encoded indicators. *Proc Natl Acad Sci U S A*, 106(37):15651–6, 2009.

[55] M. Liesa and O. S. Shirihai. Mitochondrial dynamics in the regulation of nutrient utilization and energy expenditure. *Cell Metab*, 17(4):491–506, 2013.

[56] J.E. Lennard-Jones. On the determination of molecular fields. *Proc R Soc Lond*, 106(738):15, 1924.

[57] E. K. Ainscow and G. A. Rutter. Glucose-stimulated oscillations in free cytosolic atp concentration imaged in single islet beta-cells: evidence for a ca2+-dependent mechanism. *Diabetes*, 51 Suppl 1:S162–70, 2002.

[58] Java Swing Package. `https://docs.oracle.com/javase/7/docs/api/javax/swing/package-summary.html`, 2016.

[59] D. Tondera, S. Grandemange, A. Jourdain, M. Karbowski, Y. Mattenberger, S. Herzig, S. Da Cruz, P. Clerc, I. Raschke, C. Merkwirth, S. Ehses, F. Krause, D. C. Chan, C. Alexander, C. Bauer, R. Youle, T. Langer, and J. C. Martinou. Slp-2 is required for stress-induced mitochondrial hyperfusion. *EMBO J*, 28(11): 1589–600, 2009.

[60] L. Wiemerslage and D. Lee. Quantification of mitochondrial morphology in neurites of dopaminergic neurons using multiple parameters. *J Neurosci Methods*, 262: 56–65, 2016.

[61] J. Lewis B. Alberts, A. Johnson. *Molecular Biology of the Cell*. Garland Science, 2002.

[62] M. Iftimia, W.R. Brugge, and D.X. Hammer. *Advances in Optical Imaging for Clinical Medicine*. Wiley, 2011.

[63] A. B. Al-Mehdi, V. M. Pastukh, B. M. Swiger, D. J. Reed, M. R. Patel, G. C. Bardwell, V. V. Pastukh, M. F. Alexeyev, and M. N. Gillespie. Perinuclear mitochondrial clustering creates an oxidant-rich nuclear domain required for hypoxia-induced transcription. *Sci Signal*, 5(231):ra47, 2012.

[64] I. Bratic and A. Trifunovic. Mitochondrial energy metabolism and ageing. *Biochimica et Biophysica Acta*, 1797:961–967, 2010.

[65] C. Garcia-Ruiz, A. Colell, A. Morales, N. Kaplowitz, and J. C. Fernandez-Checa. Role of oxidative stress generated from the mitochondrial electron transport chain and mitochondrial glutathione status in loss of mitochondrial function and activation of transcription factor nuclear factor-kappa b: studies with isolated mitochondria and rat hepatocytes. *Mol Pharmacol*, 48(5):825–34, 1995.

[66] N. Vishnu, M. Jadoon Khan, F. Karsten, L. N. Groschner, M. Waldeck-Weiermair, R. Rost, S. Hallstrom, H. Imamura, W. F. Graier, and R. Malli. Atp increases within the lumen of the endoplasmic reticulum upon intracellular ca2+ release. *Mol Biol Cell*, 25(3):368–79, 2014.

[67] M. J. Bingham, T. J. Ong, W. J. Ingledew, and H. J. McArdle. Atp-dependent copper transporter, in the golgi apparatus of rat hepatocytes, transports cu(ii) not cu(i). *Am J Physiol*, 271(5 Pt 1):G741–6, 1996.

[68] Beiersdorf AG. `www.beiersdorf.com`, 2016.

[69] JenLab GmbH. `http://www.jenlab.de/`, 2016.

[70] J. C. Maxwell. A dynamical theory of the electromagnetic field. *Philosophical Transactions of the Royal Society of London*, 155:54, 1865.

[71] A. Einstein. Über einen die erzeugung und verwandlung des lichtes betreffenden heuristischen gesichtspunkt. *Annalen der Physik*, 322(6), 1905.

[72] H. Paul. *Photonen: Eine Einführung In Die Quantenoptik*. Teubner Studienbücher Physik. Teubner Verlag, 1999.

[73] J.R. Lakowicz. *Principles of Fluorescence Spectroscopy*. Springer, 2006.

[74] D.L. Andrews. *Fundamentals of Photonics and Physics*. Photonics Volume 1. Wiley, 2015.

[75] B. R. Masters and P. T. C. So. *Handbook for Biomedical Nonlinear Optical Microscopy.* Oxford University Press, 2008.

[76] E. Abbe. Beiträge zur theorie des mikroskops und der mikroskopischen wahrnehmung. *Archiv für mikroskopische Anatomie*, 9(1):6, 1873.

[77] F.R.S. Lord Rayleigh. Investigations in optics, with special reference to the spectroscope. *Philosophical magazine*, 8(49):14, 1879.

[78] F.R.S. Lord Rayleigh. On the light from the sky, its polarization and colour, on the scattering of light by small particles, on the electromagnetic theory of light, on the transmission of light through an atmosphere containing small particles in suspension, and on the origin of the blue of the sky. *Philosophical Magazine*, 1871, 1881, 1899.

[79] Spectra-Physics AG. `http://www.spectra-physics.com/`, 2016.

[80] Carl Zeiss AG. `http://www.zeiss.de/corporate/de_de/home.html`, 2016.

[81] F. Fischer, K. König, and S. Puschmann. Characterization of multiphoton laser scanning device optical parameters for image restoration. In *Proc. SPIE 5463, Femtosecond Laser Applications in Biology*, volume 140, 2004.

[82] R. L. Eckert and E. A. Rorke. Molecular biology of keratinocyte differentiation. *Environ Health Perspect*, 80:109–16, 1989.

[83] M. I. Koster. Making an epidermis. *Ann N Y Acad Sci*, 1170:7–10, 2009.

[84] J. Sandby-Moller, T. Poulsen, and H. C. Wulf. Epidermal thickness at different body sites: relationship to age, gender, pigmentation, blood content, skin type and smoking habits. *Acta Derm Venereol*, 83(6):410–3, 2003.

[85] Y. Yu, A. M. Lee, H. Wang, S. Tang, J. Zhao, H. Lui, and H. Zeng. Imaging-guided two-photon excitation-emission-matrix measurements of human skin tissues. *J Biomed Opt*, 17(7):077004, 2012.

[86] G. E. Costin and V. J. Hearing. Human skin pigmentation: melanocytes modulate skin color in response to stress. *FASEB J*, 21(4):976–94, 2007.

[87] M. C. Skala, K. M. Riching, A. Gendron-Fitzpatrick, J. Eickhoff, K. W. Eliceiri, J. G. White, and N. Ramanujam. In vivo multiphoton microscopy of nadh and fad redox states, fluorescence lifetimes, and cellular morphology in precancerous epithelia. *Proc Natl Acad Sci U S A*, 104(49):19494–9, 2007.

[88] W. Y. Sanchez, C. Obispo, E. Ryan, J. E. Grice, and M. S. Roberts. Changes in the redox state and endogenous fluorescence of in vivo human skin due to intrinsic and photo-aging, measured by multiphoton tomography with fluorescence lifetime imaging. *J Biomed Opt*, 18(6):061217, 2013.

[89] A. Mayevsky and G. G. Rogatsky. Mitochondrial function in vivo evaluated by nadh fluorescence: from animal models to human studies. *Am J Physiol Cell Physiol*, 292(2):C615–40, 2007.

[90] Lonza Group AG. `www.lonza.com`, 2016.

[91] Life Technologies AG. `https://www.thermofisher.com/de/de/home.html`, 2016.

[92] PAA Laboratories GmbH. `http://www.gelifesciences.com/webapp/wcs/stores/servlet/catalog/en/GELifeSciences-de/products/AlternativeProductStructure_16873/`, 2016.

[93] Leica Microsystems Holdings GmbH. `http://www.leica-microsystems.com/de/startseite/`, 2016.

[94] M. C. Skala, K. M. Riching, D. K. Bird, A. Gendron-Fitzpatrick, J. Eickhoff, K. W. Eliceiri, P. J. Keely, and N. Ramanujam. In vivo multiphoton fluorescence lifetime imaging of proteinbound and free nadh in normal and pre-cancerous epithelia. *J Biomed Opt*, 12(2), 2007.

[95] S. J. Lin, Jr. Wu, R., H. Y. Tan, W. Lo, W. C. Lin, T. H. Young, C. J. Hsu, J. S. Chen, S. H. Jee, and C. Y. Dong. Evaluating cutaneous photoaging by use of multiphoton fluorescence and second-harmonic generation microscopy. *Opt Lett*, 30(17):2275–7, 2005.

[96] S. Puschmann, C. D. Rahn, H. Wenck, S. Gallinat, and F. Fischer. Approach to quantify human dermal skin aging using multiphoton laser scanning microscopy. *J Biomed Opt*, 17(3):036005, 2012.

[97] J. Y. Tseng, A. A. Ghazaryan, W. Lo, Y. F. Chen, V. Hovhannisyan, S. J. Chen, H. Y. Tan, and C. Y. Dong. Multiphoton spectral microscopy for imaging and quantification of tissue glycation. *Biomed Opt Express*, 2(2):218–30, 2010.

[98] A. A. Ghazaryan, P. S. Hu, S. J. Chen, H. Y. Tan, and C. Y. Dong. Spatial and temporal analysis of skin glycation by the use of multiphoton microscopy and spectroscopy. *J Dermatol Sci*, 65(3):189–95, 2012.

[99] G. Cotta-Pereira, F. Guerra Rodrigo, and S. Bittencourt-Sampaio. Oxytalan, elaunin, and elastic fibers in the human skin. *J Invest Dermatol*, 66(3):143–8, 1976.

[100] G. J. Fisher, J. Varani, and J. J. Voorhees. Looking older: fibroblast collapse and therapeutic implications. *Arch Dermatol*, 144(5):666–72, 2008.

[101] N. Otsu. A threshold selection method from gray-lebel histograms. *IEEE Transactions on Systems, Man, and Cybernetics*, 9(1):5, 1979.

[102] Thomas B. Fitzpatrick. Soleil et peau. *Journal de Médecine Esthétique*, 2:2, 1975.

[103] Declaration of Helsinki. `http://www.wma.net/en/30publications/10policies/b3/`, 2016.

[104] ICH Good Clinical Practice. `http://www.ich.org/products/guidelines/efficacy/efficacy-single/article/good-clinical-practice.html`, 2016.

[105] Statsoft GmbH. `http://www.statsoft.de/`, 2016.

[106] D.R. Whitney H.B. Mann. On a test of whether one of two random variables is stochastically larger than the other. *The Annals of Mathematical Statistics*, 18(1): 11, 1947.

[107] V. Lutz, C. D. Rahn, and S. Puschmann. Determination of skin aging in vivo using multi photon laser scanning microscopy (mplsm) in the stratum granulosum. In *European Society for Dermatological Research*, 2010.

[108] E. Aymard, V. Barruche, T. Naves, S. Bordes, B. Closs, M. Verdier, and M. H. Ratinaud. Autophagy in human keratinocytes: an early step of the differentiation? *Exp Dermatol*, 20(3):263–8, 2011.

[109] O. E. Rooyackers, D. B. Adey, P. A. Ades, and K. S. Nair. Effect of age on in vivo rates of mitochondrial protein synthesis in human skeletal muscle. *Proc Natl Acad Sci U S A*, 93(26):15364–9, 1996.

[110] T. M. Hagen, D. L. Yowe, J. C. Bartholomew, C. M. Wehr, K. L. Do, J. Y. Park, and B. N. Ames. Mitochondrial decay in hepatocytes from old rats: membrane potential declines, heterogeneity and oxidants increase. *Proc Natl Acad Sci U S A*, 94(7):3064–9, 1997.

[111] C. Allombert-Blaise, S. Tamiji, L. Mortier, H. Fauvel, M. Tual, E. Delaporte, F. Piette, E. M. DeLassale, P. Formstecher, P. Marchetti, and R. Polakowska. Terminal differentiation of human epidermal keratinocytes involves mitochondria- and caspase-dependent cell death pathway. *Cell Death Differ*, 10(7):850–2, 2003.

[112] S. Prahl, T. Kueper, T. Biernoth, Y. Wohrmann, A. Munster, M. Furstenau, M. Schmidt, C. Schulze, K. P. Wittern, H. Wenck, G. M. Muhr, and T. Blatt. Aging skin is functionally anaerobic: importance of coenzyme q10 for anti aging skin care. *Biofactors*, 32(1-4):245–55, 2008.

[113] R. B. Hamanaka, A. Glasauer, P. Hoover, S. Yang, H. Blatt, A. R. Mullen, S. Getsios, C. J. Gottardi, R. J. DeBerardinis, R. M. Lavker, and N. S. Chandel. Mitochondrial reactive oxygen species promote epidermal differentiation and hair follicle development. *Sci Signal*, 6(261):ra8, 2013.

[114] R. Rossignol, R. Gilkerson, R. Aggeler, K. Yamagata, S. J. Remington, and R. A. Capaldi. Energy substrate modulates mitochondrial structure and oxidative capacity in cancer cells. *Cancer Res*, 64(3):985–93, 2004.

[115] L. C. Gomes, G. Di Benedetto, and L. Scorrano. During autophagy mitochondria elongate, are spared from degradation and sustain cell viability. *Nat Cell Biol*, 13 (5):589–98, 2011.

[116] J. R. Lakowicz, H. Szmacinski, K. Nowaczyk, and M. L. Johnson. Fluorescence lifetime imaging of free and protein-bound nadh. *Proc Natl Acad Sci U S A*, 89 (4):1271–5, 1992.

[117] M. J. Simpson, J. W. Wilson, M. A. Phipps, F. E. Robles, M. A. Selim, and W. S. Warren. Nonlinear microscopy of eumelanin and pheomelanin with subcellular resolution. *J Invest Dermatol*, 133(7):1822–6, 2013.

Acknowledgements

Mein besonderer Dank gilt...

- Dr. Frank Fischer für die hervorragende Betreuung meiner Doktorarbeit, die angenehme Zusammenarbeit im Labor und darüber hinaus, sowie die Offenheit und Neugier gegenüber neuen Ideen

- Prof. Dr. Michael Rübhausen für die Übernahme des Erstgutachtens, die ideenreichen Diskussionen und Anregungen, sowie die wertvollen Tipps für unsere Publikationen

- dem Mikroskopie-Labor mit Sonja Pagel-Wolf, Martin Sattler, Erwin Gärtner und Meike Halm für Fitnessbanddiskussionen, Goldzugforschung, Fußballdebatten und Zwiebelkuchen

- Sören Jaspers und Dr. Horst Wenck für die Möglichkeit, meine Promotion bei der Beiersdorf AG zu absolvieren

- allen Mitarbeitern der Front End Innovation und speziell der Biophysik für kollegiale Arbeitsatmosphäre und offene Ohren

- der Stiftung der deutschen Wirtschaft für die ideelle und finanzielle Unterstützung meiner Arbeit

- Achim, Fabian, Malte, Markus für "Theorie, räudig wie nie", "Achtung, die Kurve" und gute Zeiten

- meinen Freunden für alles, was nichts mit Physik zu tun hat

- meinen Großeltern, meinen Geschwistern und besonders meinen Eltern für immerwährende Unterstützung